EXPERIMENTAL AND ANALYTICAL STUDY OF INTERNAL BEAM TO COLUMN CONNECTIONS SUBJECTED TO REVERSED CYCLIC LOADING

by

Ahmad Jan Durrani

James K. Wight

A Report on Research Sponsored by
National Science Foundation
Grant No. PFR 78-24556

Report UMEE 82R3
Department of Civil Engineering
The University of Michigan
Ann Arbor, MI 48109

July 1982

MR0423

ABSTRACT

EXPERIMENTAL AND ANALYTICAL STUDY OF INTERNAL BEAM TO COLUMN CONNECTIONS SUBJECTED TO REVERSED CYCLIC LOADING

by

Ahmad Jan Durrani

Chairman: James K. Wight

In a reinforced concrete building subjected to earthquake type loading the beam to column connections constitute one of the critical regions and they must be designed and detailed to dissipate large amounts of energy without a significant loss of stiffness or strength.

In the experimental part of this study, six full size interior beam-column subassemblages were tested under quasi-static loading which was intended to simulate earthquake input. All specimens were designed following the accepted design philosophy of strong column-weak beam approach. The three variables selected for this investigation included the percentage of transverse hoop reinforcement in the joint (ρ_t=0.75% to 1.15%), the joint shear stress level ($10\sqrt{f_c'}$ to $15\sqrt{f_c'}$) and the presence of transverse beams and slab on half of the specimens.

On the basis of test results it was concluded that the joint shear stress level was critical for the

satisfactory performance of beam to column connections without transverse beams and slab. For connections with transverse beams and slab, a well confined joint core was essential for the effective participation of the transverse beams in resisting joint shear. For the evaluation and design of joints, a joint performance index is proposed which integrates the effect of pertinent variables influencing the joint behavior. For detailing, an odd number of layers of hoops in the joint is recommended with a minimum of three layers.

In the analytical part of this study, a hysteretic model for beam-column subassemblages is developed from the hysteretic behavior of specimens observed during testing. The proposed model accounted for pinching of hysteresis loops, stiffness degradation, reduced unloading stiffness and fixed end rotations due to the slippage of bars through the joint. A simple analytical model for computing the maximum story displacements for regular frames is proposed. This model idealizes a building frame as an elastic column with rotational restraints at the floor levels. Three building frames of five, seven and ten stories were analyzed using the SIMPLE program developed specifically for this model. The maximum story level displacements were found to be in good agreement with those obtained from more complex models.

ACKNOWLEDGEMENTS

This report was submitted by Ahmad Jan Durrani in partial fulfillment of the requirements for the degree of Doctor of Philosophy (Civil Engineering) at The University of Michigan. Dr. Durrani wishes to express his profound gratitude to Professor James K. Wight, chairman of his doctoral committee, for providing invaluable guidance, encouragement, and financial support throughout this research without which this report could not have been possible. The authors would like to thank professors Glen V. Berg, Robert D. Hanson, Subhash C. Goel and Richard A. Scott (members of the doctoral committee) for reviewing the report and offering helpful suggestions.

This investigation was part of the research project directed by Professor James K. Wight and sponsored by the National Science Foundation through grant PFR 78-24556. The conclusions and opinions expressed in this dissertation are solely those of the authors and do not necessarily represent the views of the sponsors.

The authors would also like to express their appreciation of the excellent computing and plotting facility offered by The Computing Center of The University of Michigan. Thanks are also to a number of graduate and undergraduate students who helped in the testing program at various stages.

PREFACE

The subject matter reported in this dissertation is divided into two parts. The first part deals with the experimental study of beam to column connections subjected to earthquake type loading. The second part consists of an analytical study based on the behavior beam-column subassemblages observed during the experimental research.

The first chapter defines the objective and scope of this research and gives a detailed review of the previous research related to this study. Chapters II, III and IV are devoted entirely to the experimental study. The analytical study is reported in Chapters V and VI.

It is suggested that the reader select appropriate chapters depending on his/her interest and depth of knowledge. A general understanding of the experimental research can be obtained by reading appropriate parts of Chapter I and Chapter VII. Those interested in details of specimen fabrication, test set up and instrumentation are referred to Chapeter II. A detailed account of the behavior of individual specimens observed during testing is contained in Chapter III. Because of the depth of information contained in this chapter, it is recommended that only the most interested reader consider this chapter. Those interested in the effects of various parameters on the performance of beam to column connections and in the details

of the proposed joint performance index may wish to read Chapter IV only.

Details of the hysteretic and the analytical model for the nonlinear dynamic analysis of reinforced concrete frame are provided in Chapter V. Results of the analytical study are reported in Chapter VI. For a general understanding of the analytical study, Chapter VI and the appropriate parts of Chapter VII should suffice.

Further details of the experimental as well as analytical study are provided in Appendices A through G. It may be added for clarity that the term 'beam to column connection' used frequently in the text refers to the joint at beam to column intersection and the term 'beam-column subassemblage' implies the test subassembly. The terms 'column load' and 'column load point displacement' represent the column lateral load and column lateral displacement respectively.

TABLE OF CONTENTS

LIST OF TABLES

LIST OF FIGURES

LIST OF APPENDICES

Appendix

NOTATION

A_s = Area of Bottom Reinforcement of Beam

A_s' = Area of Top Reinforcement of Beam

A_{sj} = Area of Joint Hoop Reinforcement

b_{col} = Width of Column

d = Effective Depth of Beam

d' = Depth of Beam to Top Steel

d_{col} = Effective Depth of Column

D = Undeformed Length of Joint Diagonal

D_y = Displacement at Yield

D_{max} = Maximum Displacement in Loading Direction

E_c = Modulus of Elasticity of Concrete

E_s = Modulus of Elasticity of Steel

E_{sh} = Strain Hardening Modulus of Steel

E_i = Energy Dissipated in the ith Cycle

E_y = Energy Dissipated During the Yield Cycle

f_c' = Ultimate Compressive Strength of Concrete

f_{su} = Ultimate Strength of Steel

f_t = Tensile Strength of Concrete

f_y = Nominal Yield Strength of Steel

f_{ya} = Actual Yield Strength of Steel

h = Depth of Column

I_{cr}^{+} = Cracked Moment of Inertia for Positive Bending

I_{cr}^{-} = Cracked Moment of Inertia for Negative Bending

K_i = Stiffness of ith Branch of Hysteresis Model

L = Length of Element

LVDT = Linear Variable Displacement Transducer

m_i = Mass Associated with ith Degree of Freedom

M^+ = Positive Moment Capacity of Beam

M^- = Negative Moment Capacity of Beam

M_{pos} = Psitive Moment Capacity

M_{neg} = Negative Moment Capcity

n = Number of Layers of Hoops in the Joint

N = Element Axial Force

V_j = Joint Shear

V_{col} = Shear in Column

v_j = Joint Shear Stress

X = Displacement of Mass Relative to Base

$\dot{X}$ = Velocity of Mass Relative to Base

$\ddot{X}$ = Acceleration of Mass Relative to Base

[C] = Damping Matrix

[I] = Identity Matrix

[k] = Element Stiffness Matrix

$[k_g]$ = Element Geometric Stiffness

$[k_e]$ = Effective Element Stiffness

$[K_s]$ = Elastic System Stiffness Matrix

$[K_{sp}]$ = Rotational Spring Stiffness Matrix

$[\bar{K}]$ = Reduced System Stiffness Matrix

{P} = Force Vector

[M] = Mass Matrix

$\{\Delta R\}$ = Incremental Rotation

ΔF = Incremental Force

Δt = Time Increment

ΔX = Incremental Relative Displacement Vector

$\Delta \dot{X}$ = Incremental Relative Velocity Vector

$\Delta \ddot{X}$ = Incremental Relative Acceleration Vector

$\Delta \ddot{X}_g$ = Incremental Base Acceleration

$\hat{\Delta} X$ = Incremental Displacement over Extended Time Interval

$\hat{\Delta} \dot{X}$ = Incremental Velocity over Extended Time Interval

$\hat{\Delta} \ddot{X}$ = Incremental Accel. over Extended Time Interval

$\hat{\Delta} F$ = Incremental Force over Extended Time Interval

α = Percentage of Joint Hoop Reinforcement

β = Exponential Constant

γ = Shear Deformation of Joint

δ_i = Maximum Top Column Displacement in ith Cycle

δ_y = Maximum Top Column Displacement in Yield Cycle

$\{\delta\}$ = Displacement Vector

ε_0 = Concrete Strain at Maximum Compressive Stress

ε_u = Ultimate Strain of Concrete

ε_y = Yield Strain of Steel

ε_{sh} = Strain at Beginning of Strain Hardening

ε_{su} = Strain at Ultimate Strength of Steel

ζ_n = Modal Damping Ratio for nth Mode

η = Factor for the effect of Transverse Beams and Slab

θ = Angle Between Joint Diagonal and Horizontal Axis

θ = Factor for Extended Time Interval

θ_{cr} = Rotation Corresponding to Cracking Moment on Elastic Branch

θ_{max} = Maximum Rotation Attained During Loading

θ'_y = Rotation of Joint due to Yielding of Beams

θ_{slip} = Rotation of Joint due to Slippage of Bars

θ_y = Total Rotation of Joint at Yield Level

θ_r = Rotation at Change in Sign of Joint Rotation

λ = Coefficient of Normalized Shear Stress

μ = Displacement Ductility

ρ_t = Percentage of Joint Hoop Reinforcement

τ = Extended Time Interval

ϕ = Ratio of Energy Dissipated during ith Cycle to Energy Dissipated during Yield Cycle

ϕ_{bar} = Reinforcing Bar Diameter

$\{\phi\}_n$ = nth Mode Shape

ω_n = Natural Frequency for nth Mode

Ω = Joint Performance Index

CHAPTER I

INTRODUCTION

1.1 General

Observations of the behavior of several reinforced concrete buildings subjected to strong earthquakes has demonstrated that it is possible to design reinforced concrete buildings to withstand earthquakes of severe intensity without collapse. While this signifies the adequacy of the current design philosophy, it has also raised some new questions. The laboratory experiments and the analytical investigations in recent years have helped answer some of these questions. However, there are still a large number of uncertainties which need further investigations.

The current state of knowledge allows us to design a building for a certain type of behavior and predict its seismic response with a certain degree of confidence. The results of experimental investigations on the behavior of reinforced concrete members and connections, along with the sophisticated modelling techniques made possible by high speed computers, have provided us with the tools for a rational design which is implied in all the current seismic codes. The efforts directed towards predicting the dynamic

response of a building as realistically as possible has achieved a modest amount of success. However, the use of sophisticated modelling techniques in the design of a building is severely limited.

Experience has shown that buildings designed according to the prevalent design practice have invariably been deformed beyond their elastic limit to absorb and dissipate energy when subjected to moderate or strong earthquakes. The structure, therefore, has to be designed and detailed to meet the high ductility demands and at the same time prevent sudden collapse. Investigations of the behavior of structural elements which may cause sudden collapse have led to many improvements in the design and detailing procedure. However, there are certain areas which need further investigation. One such area is the beam to column connection. Such subassemblages, when subjected to large load reversals in laboratory testing, have been observed to undergo considerable degradation in stiffness and strength. While such observations have been directly used by ASCE-ACI Committee 352 (11) to improve the seismic design provisions, considerable improvement is still desired.

A second area which needs further attention is the inelastic dynamic response of reinforced concrete structures. The variables involved in the analysis and their interaction are generally so complex that the overall response of a structure can only be evaluated through the

use of an appropriate mathematical model. The inelastic behavior is introduced in the analysis through a hysteretic model based on the laboratory tests of the elements expected to undergo inelastic deformations. A number of such models based on experimental investigations have been proposed to predict the response observed in the field and measured during the tests. Some of these models are overly simple and do not account for the nonlinear response mechanism, while others are too complicated to use in a dynamic analysis. The degree of sophistication required for the analytical model of a building depends on the purpose of response analysis and the complexity of structure. A discrete finite element model of a structure is more realistic and desirable, but the cost of computation becomes prohibitive. Particularly, for preliminary design purposes, a simpler yet reasonably realistic model is extremely desirable.

1.2 Objective and Scope

This investigation is a part of the research program to study the behavior of beam to column connections under earthquake type loading and deals specifically with the interior joints of a reinforced concrete moment resisting frame buildings. The principal objectives of this study included three distinct parts:

1) To investigate experimentally, the behavior of beam to column connections which were designed to to test the limits of current design practice

(11). In this experimental study, the effect of the level of shear stress in the joint and the effect of confinement of the joint on satisfactory performance of the subassembly were investigated. The confinement was provided by hoop reinforcement in the joint and by the presence of lateral beams and slab. The study is intended to evaluate joints with reinforcement less than that recommended by the ACI-ASCE Committee 352 Recommendations (11) and to suggest improved recommendations for the design of connections.

2) To observe the hysteretic behavior of beam-column subassemblages under cyclic loading and then develop a representative hysteretic model. This model was to be relatively simple, yet realistic.

3) To develop a simplified analytical model of a moment resisting reinforced concrete frame building. Because this model is to be used primarily for design, data input should be easy and convenient and the parameters needed in a preliminary design of a building should be quickly and cheaply obtained.

To achieve these objectives, six interior beam-column subassemblages were designed and constructed according to the provisions of Appendix A of ACI Code (14). The ratio of flexural capacities of columns to that of beams was kept constant at 1.5 in all the specimens. Three of the

specimens had lateral beams and slab to study the effect of confinement as provided in a real structure. The other three specimens were 'bare' connections. The other two parameters varied in the specimen included the amount of joint reinforcement (ρ_t=0.75% to 1.15%) and the magnitude of joint shear stress ($10\sqrt{f'_c}$ to $15\sqrt{f'_c}$, psi units). These test specimens were subjected to laboratory loading routines intended to simulate earthquake loading.

The observed hysteretic behavior was used to develop a hysteretic model. Three reinforced concrete moment resisting frames with five, seven and ten stories were designed using the current UBC code (44). The frames were modelled using the proposed analytical and hysteresis models. A special purpose computer program for nonlinear dynamic analysis using the proposed model was developed and used to study the time-history response of frames for El Centro 1940 NS base acceleration input. The response was compared to the response obtained using the 'LARZ' program (37).

1.3 Review of Previous Research

The behavior of beam to column connections under seismic loading has been studied by several researchers over the last two decades. The areas investigated varied from design procedure and connection details to analytical modelling of beam-column subassemblages and frames. Some of the conclusions drawn from these studies form the basis for current design philosophy while others need further

investigation. Since this study has two parts, consisting of an experimental and an analytical investigation, the previous research in these areas are presented separately.

1.3.1 Experimental Research

In one of the earlier investigations of beam to column connections, Hanson and Conner(1) observed that the presence of transverse beams framing into the joint improved the behavior and stressed the importance of proper detailing of the joint. They also pointed out that although the requirement for shear reinforcement and confinement hoops within the joint were not directly related, they were somewhat interdependent. Higashi and Ohwada (2) investigated the behavior of beam to column connections subjected to lateral loads. They observed the appearance of cracks in the connection panel during the first loading cycle at a shear stress of twelve to fourteen percent of ultimate strength of concrete. For specimens which experienced an early bond failure and slippage of bars, the specimens had less joint cracking. They also observed an improved rigidity and strength of connections due to the presence of transverse beams.

Megget (3) studied the anchorage of beam reinforcement in seismic resistance of reinforced concrete frames and recommended that the joint reinforcement be designed to resist the shear entirely within their elastic limit. Townsend and Hanson (4) in their investigation of inelastic behavior of connections observed that a large

number of cycles of inelastic loading at a relatively low amplitudes did not significantly reduce the strength of connections. Renton (5) from his tests of beam to column joints under cyclic loading, concluded that the unsupported length of ties could affect the confinement of the joint core and suggested the use of cross ties. He also emphasized the need for an upper limit for the unrestrained length of joint hoops.

Patton (6) investigated the use of anchorage blocks welded to the beam reinforcement to prevent their slippage through the joint core. He recommended the use of anchorage blocks and suggested the use of sufficient joint hoop reinforcement to compensate for any loss of confinement due to outward bowing of hoops. Smith (7) noted that the hoops placed close to the top and bottom reinforcement of beams were not effective joint shear reinforcement. He also concluded that the yielding of joint hoops caused disintegration of core concrete and resulted in the formation of a hinge within the joint. This, according to Smith, prevented the formation of compression strut and severely reduced the load carrying capacity.

Uzumeri and Seckin (8) found that the loading history did not affect the strength, but seriously affected the stiffness of the beam to column subassemblies. They also considered the use of joint reinforcement with flat yield plateau undesirable for confinement. In their opinion, the joint shear reinforcement contributed to the shear strength

in some proportion other than the one established for flexural members and recommended that the joint stirrups be extended above and below the beam reinforcement at same spacing as in the joint. An investigation by Jirsa et al. (9) indicated that large variations in axial load and increases in transverse reinforcement above certain amounts had very little effect on the ultimate strength of the joint. Lee et al. (10) observed that strength and energy dissipation capacity of beam to column connections degraded after every cycle of loading at the same displacement and degradation was found to be less for specimens containing more transverse reinforcement. They also questioned the use of truss analogy for joint design.

Meinheit and Jirsa (12) studied the shear strength of reinforced concrete beam to column connections. They concluded that an increase in the percentage of transverse joint hoops increased the shear strength, but the increase was not proportional to the yield strength of the hoops. They also attributed the post cracking shear strength of joint concrete to a combination of aggregate interlock and confinement. Fenwick and Irvine (13) recommended the use of diagonal strut action instead of panel truss action for joint design. Their tests indicated a higher sustained strength and better ductile performance for joints with bond plates than the more conventional details, in spite of the fact that they used a very low joint reinforcement.

Birss (15) in his investigation of the elastic

behavior of joints, emphasized the importance of vertical as well as horizontal shear and stressed the need for using vertical shear reinforcement. Paulay et al. (16) proposed that the total joint shear force applied to a joint core be apportioned between that carried by the concrete diagonal strut and that carried by a truss mechanism consisting of horizontal stirrups, vertical stirrups and intermediate column bars. They also suggested a limit on the beam bar diameter to avoid bond failure and excessive slippage.

Scribner and Wight (17) observed that intermediate longitudinal reinforcement in beams with maximum shear stress greater than $3\sqrt{f'_c}$, significantly increased both the total energy dissipation and stability of hysteretic response of beam-column subassemblies. Soleimani et al. (18) observed from their tests of two half-scale beam-column subassemblages that after the loss of bond of the main bars in a joint, the inelastic deformations were concentrated at the fixed ends and stressed the importance of fixed end rotations in analysis.

Buckingsale et al. (19) found that the joint core of beam-column subassemblages carrying heavy column axial load performed much better than those subassemblies which had low axial load. They also observed that the test specimens with small axial load displayed slippage of reinforcing bars through the joint core.

Zhang and Jirsa (20) analysed the data of beam to column connections tested by various researchers and

recommended the use of the compression strut mechanism to calculate joint shear strength. They found the use of welded and closely meshed reinforcement in both directions within the joint to be most effective.

Other research related to the behavior of beam to column joints, include the investigation by Celebi and Penzien (27) of critical regions of reinforced concrete components, as influenced by moment and shear. They reported no significant influence of dynamic loading on the stiffness degradation and energy absorption properties of specimens tested within a deflection ductility range of 1 to 4. However, the dynamic loading appeared to increase the yield strength by as much as 20%. Hawkins et al. (40) studied the bond deterioration in external beam to column connections under cyclic loading. They observed that under cyclic loading, bond failed at a much lower slip level than for monotonic loading. They also concluded that the compressive strength of concrete and the bar loading history significantly affected the bond failure and slip.

Kaar, Fiorato et al. (41) investigated the limiting strain of concrete confined by rectangular hoops. They observed the limiting concrete strain for confined concrete to be of the order of four to five times the assumed ultimate strain. They recommended the use of smaller size hoops at smaller spacing to improve energy dissipation through higher ductilities.

1.3.2 Analytical Research

In one of the earlier investigations on the behavior of structures during earthquake, Housner (21) recommended the design of structures with sufficient energy absorbing capacity and damping for safety against collapse in the event of an extremely strong earthquake. Clough (22) demonstrated that the response of a single degree of freedom structure with degrading stiffness behaved distinctly different from an equivalent system with ordinary idealized elasto-plastic property. He noted that the properties of the degrading system were affected permanently by yielding and changed proportionately. He further concluded that large ductility factors were developed in short period structures and much less ductility factor was required in flexible, long period structures.

Takeda et al. (23) investigated the hysteretic behavior of small scale connections under simulated earthquake loading and observed a rapid change in the stiffness and energy absorbing capacity of specimens during the test. He proposed a hysteretic model that was capable of handling different possibilities of loading and unloading at different levels of deformation. Several researchers have verified satisfactory agreement between Takeda's Model and measured response of model frames.

Gates (24) studied the performance of instrumented high rise buildings in the San Fernando earthquake of Feb. 9, 1971. Earthquake motions recorded at the base of

the buildings were used as the forcing functions to the mathematical models of the buildings. Three of the buildings experienced inelastic deformations in the beam to column connections. Each one of them exhibited lengthening of building period and the story shear forces actually experienced by the buildings far exceeded the design forces. His study also indicated that the structures which had been dynamically analyzed and designed to withstand a potential earthquake, had a higher margin of earthquake safety than those buildings designed to minimum code standards.

Otani and Sozen (25) tested small scale one bay-three story frames for base motions simulating earthquake records. In the nonlinear dynamic analyses of these frames, they considered the joint cores to be infinitely rigid and included the effect of fixed end rotations due to bond slip by placing bilinear rotational springs at member ends. The analytical model predicted the response of test frames satisfactorily for large amplitudes.

McKevitt, Anderson et al. (26) studied the use of simple energy methods for seismic design of structures wherein they considered the total required energy capacity and its distribution over various dissipative mechanisms. They concluded that the ratio of energy dissipated by viscous damping to hysteretic damping increased with the increase in damping ratio. They also observed that the stiffness degrading systems dissipated more energy in

hysteretic behavior than the non-degrading systems. Celebi and Penzien (27) attributed the nonlinear behavior of force-deformation hysteresis loops to a combination of Bauschinger effect and shear deformation, the latter causing the pinching of the hysteresis loops. They questioned the use of elasto-plastic, Ramberg-Osgood or Clough's degrading stiffness model to predict the force deformation relationships, particularly when shear influence was significant. They stressed the need for including the pinching effect in the hysteresis model.

Chopra and Kan (28) extended the study by Clough (22) to multi-degree of freedom systems. They used a shear building idealization with a Clough hysteresis system for defining the relation between story shear and drift. The post-yield stiffness was considered as one-tenth of the initial elastic stiffness and the damping ratio assumed as five percent for all the modes. Their results reaffirmed the previous findings for a single degree of freedom system wherein it was concluded that stiffness degradation had little influence on the ductility requirements for flexible buildings.

Since some form of numerical solution is always an integral part of nonlinear dynamic analysis, a convenient solution technique is very essential. Wilson et al.(29) proposed an unconditionally stable scheme with the assumption that the linearization over the time increment was adequate. This technique allows a much larger time step

as it is chosen with regard to accuracy only and not with regard to stability of the solution. Hart and Vasudevan (30) investigated the damping aspect of seismic design of buildings. They developed a procedure for estimation of modal damping for elastic and inelastic building response and recommended the use of the same value of modal damping for all the modes.

Gulkan and Sozen (31) observed that inelastic response of reinforced concrete elements could be represented by a linear response model which incorporated the effects of inelastic energy dissipation. Shibata and Sozen (32) proposed a substitute structure method which extended the above procedure to multi-degree of freedom systems.

Luyties III et al. concluded from their study on the inelastic dynamic analysis of frames that the single component or dual component representation of the inelastic behavior of a member gave results within the desired accuracy, given the uncertainty of the expected ground motion characteristics.

Anderson and Townsend (34) compared different models for reinforced concrete frames with degrading stiffness. They represented the nonlinear behavior in beam and column elements by two component elements with finite joint width acting as rigid segments. They observed that a reduction in the stiffness of reinforced concrete following loading into the inelastic range and the hysteresis modelling can have

significant effect on the dynamic response.

Viwathanatepa et al. (35) examined the behavior of interior beam-column subassemblages and verified that the elasto-plastic model was unsuitable for predicting the behavior of reinforced concrete members under seismic loading, particularly when full or partial reversal of lateral displacement was likely to occur. For cyclic loading, they emphasized the need to account for bar pull-out in the joint. Iwan and Gates (36) compared the accuracy of approximate methods in which the nonlinear systems were replaced by equivalent linear systems. The linear system response only approximated the response of hysteretic system.

Saiidi and Sozen (37) studied the influence of hysteresis models on the calculated response of reinforced concrete structures. He proposed modified versions of the Takeda model and the bilinear model and called them the Sina model and the Q-Hyst model, respectively. He also studied an equivalent nonlinear single degree of freedom system consisting of a mass, a viscous damper and a rotational spring. The results from these analytical models were in good agreement with the experimental results from small-scale ten story frames tested on a shaking table.

Moehle and Sozen (38) investigated the earthquake response of reinforced concrete structures with stiffness interruptions. Their study indicated that: (1) significant inelastic behavior could be expected in frame joints, (2)

effective stiffness decreased with new maxima of displacement and (3) moment rotation curves for both interior and exterior joints had significant pinching. They also noted that due to: (1) more pronounced pinching for interior joints, (2) the similarity between displacement and rotation curves and (3) concentration of cracks in beams rather than in columns, the majority of inelastic action occurred in beams. They suggested that the column behavior could be represented satisfactorily by linear elements with stiffness based on fully cracked section.

Bannon, Biggs et al. (39) studied the seismic damage in reinforced concrete frames and compared the performance of a dual component model, fibre model and finite element model, for inelastic dynamic analysis. They used the single component model with each member represented by an elastic beam element with inelastic springs at the ends. Shear and slippage was accounted for by an additional pair of springs at the ends. They analyzed a set of quasi-static cyclic load tests of connections and concluded that the single component model was sufficiently accurate in reproducing the inelastic cyclic behavior of reinforced concrete members.

CHAPTER II

EXPERIMENTAL INVESTIGATION

2.1 General

The primary purpose of the experimental portion of this study was to investigate the confinement requirements for an interior joint at different values of joint shear stress. Confinement of concrete in the joint depends on the amount of transverse hoop reinforcement and the configuration of framing members.

2.2 Design of Test Specimens

In a reinforced concrete moment resisting ductile frame, the lateral force moments due to an earthquake are observed to be much larger than the gravity load moments, particularly in the lower and intermediate stories. The effect of moments due to gravity loads on the location of inflection points in the beams could therefore be neglected. Assuming a point of zero moment at the column mid-height and beam mid-span, a suitable testing arrangement for a beam to column connection will is as shown in Fig. 2.1. The deformed shape of the subassembly and the critical combination of forces acting on the joint are shown in Fig. 2.2 and Fig. 2.3 respectively.

Consistent with the accepted design philosophy of

strong columns and weak beams, the ratio of the sum of the flexural strength of the columns to that of the beams was kept constant at 1.5 for this investigation. The primary variables of the testing program were: (1) the percentage of transverse reinforcement within the joint (ρ_t=0.75% to 1.15%), (2) the joint shear stress ($10\sqrt{f'_c}$ to $15\sqrt{f'_c}$,psi units) and (3) the presence of transverse beams and slab. All the subassemblies were designed in accordance with Appendix A of ACI 318-77 (14). The joint hoop reinforcement was kept at a minimum for ease of construction. The joint reinforcement ratio in all the specimens was considerably lower than the Recommendations of ACI-ASCE Committee 352 (11).

2.3 Description of Test Specimens

Six interior beam-column subassemblages were tested during the experimental investigation. These specimens are divided into two groups of three specimens each. The group which had transverse beams and slab was designated as the S-series and the other group, without transverse beams and slab, was designated as the X-series. A numeral following the letter designation, e.g. X2, represents the specimen number in that series. As mentioned previously, the flexural strength ratio of columns to beams was kept constant at 1.5 for all the specimens in both the series. The column to beam flexural strength ratios, amount of joint hoop reinforcement and the magnitude of joint shear stress in the X-series and S-series specimens are given in Table

2.1. The overall specimen size, beam cross sections and the column cross sections were kept the same for all the specimens and only the main reinforcement was varied to achieve different joint shear levels while keeping the flexural strength ratio constant.

TABLE 2.1 PARAMETRIC DETAILS

Specimen	Moment Ratio	Joint Reinforcement ρ_t* %	Joint Shear Stress Coeff. α†	with/ without Slab
X1	1.25	0.76	13.2	w/o slab
X2	1.37	1.15	13.5	w/o slab
X3	1.22	0.76	10.4	w/o slab
S1	1.22	0.76	13.2	w/ slab
S2	1.21	1.15	15.3	w/ slab
S3	1.32	0.76	12.5	w/ slab

* $\rho_t = A_{sj}/b_{col}(d-d')$

† $\alpha = V_{joint}/((bh)_{col}\sqrt{f'_c})$

The joint hoop reinforcement ratio, ρ_t, was varied between 0.75% to 1.5%. The joint reinforcement consisted of a diamond and a square hoop of Grade 40 steel in each layer(Fig. A.5). Specimens X2 and S2 had three layers of hoops (ρ_t=1.15%) while the other specimens had two layers of hoops each (ρ_t=0.75%). The main beam width in all the specimens was 3 in. smaller than the column width. The slab width in the S-series specimens was 39-1/2 in., the maximum

permitted by the testing frame dimensions. The overall dimensions of a typical specimen and the cross sectional details of beams, columns and slab are shown in Figs. 2.4 and 2.5 respectively. The dimensions and the reinforcement details of all the specimens are given in Table 2.2. The ultimate flexural capacities of beams and columns and the column to beam flexural strength ratios of all the subassemblages is given in Table 2.3. A more complete description of design and reinforcement details of all the subassemblages is provided in Appendix A.

2.4 Material Properties

An average concrete compressive strength of 4000 psi was specified for all the specimens. The X-series specimens and the columns of the S-series specimens were cast using hand mixed concrete prepared in the laboratory. The slab and beam portion of S-series specimens needed a larger volume of concrete and were cast using ready mixed concrete of the same specified strength. The concrete mix was designed using Type I portland cement and a well graded gravel with one inch maximum aggregate size. The water-cement ratio was selected to result in an average slump of 5 in. in order to facilitate proper compaction. Because all the specimens were cast in three different stages, and sometimes with more than one batch of mix for a particular casting stage, a sufficient number of 6in. x 12in. cylinders were cast for each batch to determine the concrete compressive strength at 28 days and at the time the

TABLE 2.2 BEAM AND COLUMN DIMENSIONS

Specimen	Beam		Column		Slab		Transverse Beam	
	Size (in.)	Reinforcement	Size (in.)	Reinforcement	Size	Reinforcement	Size (in.)	Reinforcement
X1	11x16.5	Top =4-#7 Bot.=4-#6	14.25x14.25	8-#8	-	-	-	-
X2	11x16.5	Top =4-#7 Bot.=4-#6	14.25x14.25	8-#8	-	-	-	-
X3	11x16.5	Top =3-#7 Bot.=3-#6	14.25x14.25	4-#7 4-#6	-	-	-	-
S1	11x16.5	Top =2-#7 6-#4 Bot.=4-#6	14.25x14.25	8-#8	4x39.5	#4@4in. c/c #4@6in. c/c	11x15	Top =4-#6 Bot.=4-#6
S2	11x16.5	Top =2-#7 6-#4 Bot.=4-#6	14.25x14.25	8-#8	4x39.5	#4@4in. c/c #4@6in. c/c	11x15	Top =4-#6 Bot.=4-#6
S3	11x16.5	Top =2-#7 4-#4 Bot.=3-#6	14.25x14.25	8-#7	4x39.5	#4@4in. c/c #4@6in. c/c	11x15	Top =3-#6 Bot.=3-#6

TABLE 2.3 FLEXURAL STRENGTH OF BEAMS AND COLUMNS

Specimen	Column Load (Kip)	Beam/Slab		Column Moment (Kip-in.)	$\frac{\sum M_{cols.}}{\sum M_{beams}}$
		M_{pos} (K-in.)	M_{neg} (K-in.)		
X1	55.0	1501	2023	2203	1.25
X2	55.0	1494	1766	2235	1.37
X3	48.2	1140	1522	1620	1.22
S1	70.0	1661	2024	2248	1.22
S2	70.0	1633	2035	2215	1.21
S3	54.0	1240	2033	2164	1.32

specimens were tested. Cylinders (4in. x 8in.) were also cast for each batch to determine stress vs. strain properties of concrete. Average concrete compressive strengths are given in Table 2.4 and a typical stress vs. strain curve for the concrete is shown in Fig. 2.6. Details of the concrete mix design are provided in Appendix B

Grade 40 No.6 and No.7 bars were used for the main reinforcement in the beams. The main reinforcement in the columns was Grade 60, No.8 bars. The stirrup ties used in the beams were fabricated with No.3 Grade 40 bars. The column shear reinforcement was fabricated from No.4 Grade 40 bars. Steel coupons for all the bar sizes were tested for strength and stress vs. strain properties. Average steel properties are given in Table 2.5 and a typical stress

TABLE 2.4 AVERAGE ULTIMATE CONCRETE STRENGTH

Specimen	Beam / Slab (psi)	Top Column (psi)	Bottom Column (psi)
X1	4980	4715	4245
X2	4880	5235	4475
X3	4500	3910	4790
S1	6030	4323	4320
S2	4460	3600	4100
S3	4100	3700	4230

vs. strain curve for Grade 40 and Grade 60 steel are shown in Fig. 2.7.

TABLE 2.5 PROPERTIES OF REINFORCING STEEL

Bar Size	Grade	E_s*	f_y*	ε_y†	ε_{sh}†	E_{sh}*	ε_{su}†	f_{su}*
#3	40	28.7	48.8	1.70	12.5	0.98	180	73.0
#4	40	28.5	51.0	1.79	13.1	1.05	172	78.1
#6	40	27.9	50.0	1.79	12.8	1.04	195	82.0
#7	40	28.4	48.0	1.69	11.2	0.97	185	80.3
#8	60	29.2	60.0	2.05	5.1	1.63	135	102.0

* $(ksi)x10^3$

† $(in./in.)x10^{-3}$

2.5 Fabrication of Specimens

Each specimen was constructed in three stages in a

vertical position, to simulate construction phases in a building. After attaching all the strain gages at appropriate locations on the reinforcement of specimen, the column reinforcing cage was assembled and placed vertically in the formwork for the bottom portion of the column. Hand mixed concrete was then placed up to a few inches below the joint. During the next two days, beam and slab reinforcement was placed in position and two steel pipes were inserted near the beam ends to facilitate a pin connection (Fig. C.1). The beam and slab portion of the specimen was then cast with ready mixed concrete for the S-series specimens and with hand mixed concrete for the X-series specimens. The concrete was placed up to approximately two inches above the top of the main beams. Two or three days later, formwork was erected for the top column and the final stage of casting concrete was completed. The specimens were stripped of formwork about one week after casting and cured for another week under wet burlap.

2.6 Test Set Up

The testing frame consisted of an outer reaction frame and an inner four hinge frame. A 250 kip actuator mounted on the outer frame displaced the top beam of the inner frame horizontally by 11 inches in its tension stroke and by 5 inches in its compression stroke. The reaction frame was diagonally braced to minimize any deformations. A schematic drawing of the test set up is shown in Fig. 2.8.

The specimen was mounted in a vertical position with the the column ends held to the top and bottom beams through a system of end plates, rollers and brackets, which were intended to simulate a hinged support. The inflection points in beams were simulated by inserting a pin near the beam ends. It was assumed that the beam inflection points moved only horizontally under any lateral load. Therefore, the beam ends were tied to the bottom beam through a pair of force links which had hinges at both of their ends to simulate a roller support action. An X-series specimen in the testing frame is shown in Fig. 2.9. For S-series specimens, the slab was stiffened by a pair of steel channels (Fig. D.1) to prevent any premature failure of the slab either at the beam and slab interface or along any other oblique direction. The deformations induced in the reaction frame at the peak lateral load were found to be negligible.

2.7 Instrumentation

Three different types of transducers were used to monitor the applied loads and displacements and the resulting strains and deformations in the specimens. The horizontal shear applied through the actuator was measured with a load cell attached to the piston of the actuator. The lateral displacement of the column was recorded through two independent sources. Besides the actuator LVDT (linear variable displacement transducer), a cable LVDT was attached to the column at 4 inches from its top at the roller

location. It was then fixed to a bracket external to the testing frame to observe displacements, independent of any frame deformations. Both the transducers were calibrated before testing began and checked for linearity.

The beam force links not only produced a roller support action at the beam ends, but also acted as load cells to measure the shear in the beams. Each force link had two sets of strain gage bridges for this purpose. These force links were calibrated with a 50 kip actuator and a calibrated load cell.

The strains in the reinforcing bars were measured through a set of strain gages bonded to the reinforcement in and around the joint area. On average, each specimen had thirty strain gages. Figure 2.10 shows the location of strain gages for a S-series specimen. A detailed location of these gages for each specimen is given in Appendix E. For the X-series specimens, the joint shear deformation was also measured by a pair of diagonally placed displacement transducers. This was not possible for the S-series specimens due to the presence of transverse beams.

2.8 Loading and Data Acquisition

All the specimens were tested under controlled deformation and subjected to quasi-static cyclic loading to simulate earthquake forces. The lateral displacements applied at the top of the column were controlled in terms of displacement ductilities. The displacement ductility for this purpose was defined as the ratio of column load point

displacement at any stage during the test to the corresponding displacement at initial yield of beam longitudinal reinforcement. A typical loading routine is given in Fig. 2.11. Before the first cycle to yield point, the specimens were subjected to a preliminary load cycle of half the expected yield load. This ensured proper connections and checked the data recording devices for proper functioning. The column axial load was applied at the bottom using a compact hydraulic jack. This load was applied one day prior to the test to eliminate any immediate creep effect.

Column shear load and the load point displacements were continuously plotted on an X-Y plotter. The displacement ductilities applied to the specimens were based on the actual yield displacement observed from the load-displacement curves. For every new cycle, the displacement was incremented by half the yield displacement. A typical test sequence consisted of seven cycles and reached a displacement ductility of four.

All the electrical resistance strain gages and transducers were read by a scanner unit during pauses in the loading sequence. These pauses were called load points and were selected to correspond to significant changes of the slope of the load vs. displacement hysteresis loops. The data read by the scanner was printed and punched on a paper tape as the test progressed.

CHAPTER III

EXPERIMENTAL RESULTS

3.1 General

The data recorded during each test can be grouped into the following categories:

(1) a record of crack development in the specimen corresponding to each change in lateral load on the column,

(2) a continuous plot of load vs. displacement that determined the load history during the test and

(3) a record of strain at each gage location in the specimen corresponding to each load point.

In addition to that, joint deformations in the X-series specimens and the shear in the main beams of all specimens were also recorded. Each type of data individually reflects on certain aspects of the behavior of a test specimen and collectively determine the influence of a particular variable on the overall behavior of the subassemblage. The significance of each type of data as related to the behavior of the joint along with some general observations will be discussed separately, followed by a discussion of individual specimen behavior.

3.2 Crack Development

During each test the cracking pattern, location and size of cracks, provide a first hand insight into the behavior of a specimen. The failure mode is also partly determined by the extent of cracking at the critical regions of the subassemblage. Because all the specimens for this study were designed with strong column-weak beam philosophy, only minor cracking was expected in the columns. Except for a few hair line flexural cracks in a region close to the joint, no substantial column cracking was observed in any of the specimens. Although the cracking was insignificant, the columns of the S-series specimens had more cracks by the end of a test than the columns of the X-series specimens.

Flexural cracks in the beams appeared as soon as the specimens were loaded. These cracks later joined flexural-shear cracks and formed a grid of inclined cracks during the cyclic load reversals. Most of the cracking was confined to a region close to the joint on either side of it. In the X-series specimens, the extent of cracking in the beams was very much dependent on the performance of the joint. For specimens with excessive cracking and shear deformation of the joint, the main beams suffered relatively fewer cracks, and most of the cracking was confined within a distance equal to the depth of the beam on either side of the joint. The width of the cracks progressively reduced with the distance away from the joint. The beam-column interface in the S-series specimens had a major flexural crack at the

bottom of the beam extending towards the slab. The cracking pattern in the beams of all the specimens in S-series was similar and extended the same distance away from the column face.

The slabs of the S-series specimens had flexural cracks extending across their entire width and roughly parallel to each other. These cracks were evenly spaced at a distance equal to the depth of the slab and spread throughout the length of the slab. The first crack at the junction of slab and column was the widest and their width progressively reduced away from the column.

In the X-series specimens, the cracks in the joint were readily detectable visually. The presence of transverse beams in the S-series specimens obscured the observation of cracks in the joint. The diagonal cracks in the joint of the X-series specimens appeared during the first cycle. During successive cycles, the number of cracks in the joint increased and their severity depended on the joint shear stress level and the confinement of the core. A typical cracking pattern in the X-series specimens is shown in Fig. 3.1. For specimens with transverse beams and slab, the only sign of joint cracking was the spalling of concrete at the intersection of main and transverse beams.

The transverse beams in the S-series specimens had minimal cracking. Inclined torsional cracks were observed in the transverse beams of all S-series specimens. Most of such cracking occurred close to the joint. Depending upon

the shear stiffness of the joint, the transverse beams also experienced diagonal shear cracks in its cross section. A few flexural cracks in the side of these beams parallel to its axis were also observed. Figure 3.2 illustrates typical cracks in transverse beams of S-series specimens.

3.3 Strength and Stiffness of Joint

The degradation of load carrying capacity and stiffness is easily seen from the applied column load vs. column load point displacement hysteresis curves. The hysteresis loops of all the specimens are shown in Figs. 3.3(a) through 3.3(f). Hysteresis loops of specimens X3 and S3 are plotted on a different scale and therefore, cannot be readily compared with the rest of the specimens. The hysteresis loops represent a combined behavior of joint, beams and the columns. Most of the inelastic action occurred in beams. However, if the joint deteriorated before any significant damage occurred in beams, the hysteresis represented the behavior of the joint.

Comparing the response of the X-series specimens, as shown in Figs. 3.3(a) through 3.3(c), it can be seen that the load carrying capacity of specimen X1 began to deteriorate soon after the first two load cycles while specimen X2 had no decay in strength for the first four cycles. Specimen X3 had a stable load carrying capacity through the first six load cycles. None of the S-series specimens exhibited any reduction in strength with increased displacement ductility. However, the specimens carried a

lower load during a repeat cycle at particular ductility level (Figs. 3.3(d) to 3.3(f)).

All the specimens experienced a loss of stiffness as indicated by the pinching at mid-cycle of the load vs. displacement hysteresis loops . The degree of pinching in each specimen varied slightly, depending upon the values of the variables used. Pinching is caused mainly by: (1) shear deformation of the joint (2) wide flexural cracks in the hinging zone of the beams (3) slippage of beam and column bars through the joint and (4) some looseness in the test set up. A slight amount of relative movement between the specimen and the frame at the load application point can cause significant softening of the reloading stiffness.

A careful examination of the hysteresis loops in Figs. 3.3(a) to 3.3(c) indicates that specimen X2 had less pinching than specimen X1. Pinching of the hysteresis loops for specimen X3 can not be directly compared with the pinching of hysteresis loops for the specimens X1 and X2 due to the different scale of hysteresis plots.

The stiffness degradation of the S-series specimens could not be readily determined from the hysteresis loops due to the following reasons: (1) the specimens with the slab did not have a well defined yield load and therefore, a consistent loading history could not be maintained in specimen S1, (2) repeat cycles, which were introduced for analytical modeling, further made the comparison difficult, (3) the S-series specimens had larger yield displacements

and therefore, fewer loading cycles could be accomplished within the displacement limits of the test set up and (4) joint shear deformation could not be measured due to the presence of transverse beams.

After taking into account the variation in loading history and the scale effect, the column load vs. displacement hysteresis curves for specimen S2 appear to have less pinching than those for specimens S1 and S3. Slab specimen S1 had a more rapid degradation of stiffness than specimen S3. These conclusions are confirmed by considering the total energy dissipation capabilities of specimens.

A well designed and detailed specimen is expected to maintain its strength as well as its stiffness under cyclic loading within a reasonable limit of displacement ductilities. Comparing all the specimens in the X-series as well as the S-series, it may be concluded that the S-series specimens showed better strength and stiffness characteristics than the X-series specimens.

Shear deformation in the joint provides another measure of joint stiffness. The two LVDTs placed diagonally across the corners of the joint panel measured the elongation and shortening of the diagonals for each loading situation. The shear deformation of the joint panel was computed using the model suggested by Buckingsale et al. (19) and shown in Fig. 3.4. The total shear deformation consists of two components, namely,

$$\gamma_1 = (0.5\ \Delta_1\ \text{Sin}\ \theta + 0.5\ \Delta_2\ \text{Sin}\ \theta)/(D\ \text{Cos}\ \theta) \quad (3.1)$$

and

$$\gamma_2 = (0.5\ \Delta_1\ \text{Sin}\ \theta + 0.5\ \Delta_2\ \text{Sin}\ \theta)/(D\ \text{Sin}\ \theta) \quad (3.2)$$

where D is the undeformed length of the joint diagonal and θ is its inclination with the horizontal. The total shear deformation is then given by

$$\gamma = (\Delta_1+\Delta_2)/(D\ \text{Sin}2\theta) \quad (3.3)$$

where Δ_1 and Δ_2 are the changes in the lengths of the diagonals. This information was obtained only for the X-series specimens. The displacement vs. shear deformation plots of these specimens are shown in Figs. 3.5(a) to 3.5(c). A comparison of the shear deformation of the joint in the X-series specimens for the same lateral displacement, shows that the shear deformation progressively reduced from specimen X1 to X3 and that the corresponding shear stiffness for the later cycles substantially improved in the same order. Specimen X3, with the lowest level of the joint shear stress, had the least joint shear deformation and loss of stiffness. Specimen X1, which had the least joint confining reinforcement along with a higher level of joint shear stress, showed excessive shear deformation and stiffness degradation in the joint. This is in agreement with the larger pinching of hysteresis loops for specimen X1 than for specimens X2 and X3.

3.4 Energy Dissipation

The column load vs. column load point displacement curves, referred to as hysteresis loops, are the single most important source of information for load and stiffness degradation and for the energy characteristics of a subassemblage. The area within the loops for each cycle of loading is proportional to the energy dissipated during that cycle. Energy dissipated during each cycle for all the specimens is given in Table 3.1. Because the yield load and yield displacements were not the same for all the specimens, a more realistic comparison of energy dissipation for each specimen could be made by considering the normalized energy dissipation with the corresponding displacement ductilities. Table 3.2 gives the energy dissipated, normalized with respect to the yield cycle energy dissipation, for different levels of displacement ductilities. A plot of normalized energy dissipation vs. displacement ductilities is shown in Fig. 3.6.

A sufficient amount of energy dissipation without substantial loss of strength and stiffness constitutes a desirable behavior for a beam-column subassemblage under cyclic loading. Excessive pinching of the hysteresis loops, due to the severe damage either in the joint or in the adjoining areas, indicates a reduced energy dissipation capacity. Any significant crack in the elements of the subassemblage in effect contributes to the softening of the reloading stiffness. As shown in Figs. 3.3(a) to 3.3(f),

TABLE 3.1 ENERGY DISSIPATION DURING EACH LOAD CYCLE (K-in.)

Specimen	Yield Cycle	2nd. Cycle	3rd. Cycle	4th. Cycle	5th. Cycle	6th. Cycle	7th. Cycle
X1	63.9	80.0	115.3	169.5	205.8	222.8	236.9
X2	59.0	91.9	142.3	179.6	219.2	244.8	260.0
X3	28.3	41.0	77.1	106.6	131.2	165.4	175.2
S1	75.7	149.9	240.3	164.7 *	258.3	202.2 *	-
S2	51.8	73.2	98.1	143.6	191.1	273.1	211.6
S3	43.6	61.3	90.3	114.5	139.0	171.9	188.7

* Repeat cycle

TABLE 3.2 NORMALIZED ENERGY DISSIPATION

Specimen	μ^+	$\phi\dagger$	μ	ϕ	μ	ϕ	μ	ϕ	μ	ϕ	μ	ϕ	μ	ϕ
X1	1.25	1.25	1.50	1.80	-	-	2.10	2.65	2.50	3.22	2.90	3.49	3.40	3.71
X2	1.30	1.55	-	-	1.80	2.41	2.20	3.04	2.70	3.72	3.10	4.15	3.60	4.41
X3	1.40	1.45	-	-	1.90	2.72	2.40	3.77	2.80	4.64	3.30	5.84	3.90	6.19
S1	....	....	1.45	1.98	1.95	3.17* (2.18)	2.40	3.41* (2.67)	-	-	-	-	-	-
S2	1.35	1.41	1.60	1.89	1.90	2.77	2.25	3.69	2.70	5.27	-	-	-	-
S3	1.30	1.40	1.60	2.07	1.90	2.62	2.20	3.19	2.60	3.94	2.90	4.32	-	-

$^+$ $\mu = \delta_i/\delta_y$

$\dagger$ $\phi = E_i/E_y$

* Energy dissipated during repeat cycle in parentheses

the loops get more pinched as higher displacements are imposed on the specimens. Every additional displacement initiated more cracks in beams and in the joints, and widened the existing cracks, causing more pinching of the loops. The energy dissipation, however, is also dependent upon the load carrying capacity of a specimen. For the X-series specimens, the energy dissipation consistently improved for all ductility levels from specimen X1 through specimen X3, as shown in Table 3.2. A maximum ductility level of four was achieved in this series.

For the S-series specimens, however, the hysteretic behavior could not be compared as readily because of the reasons explained in the last section. All of these specimens sustained their maximum load capacity through most of the loading cycles. Specimen S1 was subjected to larger displacements during each cycle and the third and fourth cycles were repeated at the same ductility level. An average of seventy percent of the energy for a new loading cycle was dissipated during the repeat cycle. Although specimen S1 was loaded through a displacement ductility of only 2.4, it dissipated significantly higher energy than the other S-series specimens, for the same ductility levels. This is attributed to the higher strength of concrete used in this particular specimen and is explained in detail in Chapter 4.

Specimen S2 had a lower energy dissipation during the first three cycles than specimen S3. During the later

cycles, however, specimen S2 dissipated significantly higher energy than specimen S3 for equivalent ductility levels. This comparison is further borne out in the normalized energy dissipation vs. ductility plot shown in Fig. 3.6. Specimen S1 had no increase in energy dissipation after a displacement ductility of 2.0 while specimen S2 showed a steady increase in its energy dissipation capacity.

3.5 Individual Specimen Behavior

In this section, the behavior of each specimen is examined in detail. Particular attention is given to the cracking history, severity of damage, energy dissipation, stiffness degradation, decay of strength, slippage of bars and any other behavior peculiar to the specimen. Certain aspects of behavior were, however, common to all the specimens. Because the columns were flexurally stronger than the beams in all the specimens, most of the cracking occurred in the beams in a region close to the joint. The columns had a few hair line flexural cracks in some of the specimens and remained essentially in the cracked-elastic range. The hysteresis loops for all the specimens showed a varying degree of pinching, but in general, were of similar shape.

The variables for each of the specimen are given in Table 2.1 and the pertinent parameters for the individual specimens to assist in behavior identification. Data from strain gages attached to the reinforcement bars will be used to explain any peculiarities. The variables given for each

specimen are; α, the coefficient of joint shear stress normalized with respect to the square root of the concrete compressive strength ; λ, the coefficient of normalized shear stress in beams; ρ_t, the percentage of joint transverse reinforcement; and f'_c, the compressive strength of concrete used in the beams and joint.

Specimen X1 (α=13.2, ρ_t=0.76%, λ=3.07, f'_c=4980 psi)

This specimen had two layers of hoops in the joint, each consisting of a square hoop and a diamond shape hoop. The hoops were placed at a distance of 3 in. vertically on either side from the center of the joint. The specimen was loaded through seven cycles with a maximum displacement ductility of 3.4. During the first cycle, diagonal cracks of varying length appeared in the joint. The center of the joint core began to deteriorate rapidly in the fourth cycle. In the subsequent cycles no further cracking occurred in the beams and most of the inelastic action was concentrated in the joint area. Concrete between the two layers of hoops in the joint spalled off at the end of the seventh cycle and wide cracks extended from the hollow core area towards the corners of the joint. The cracks in the specimen and the extensive damage in the joint core are shown in Figs. 3.7 and 3.8, respectively.

The load carrying capacity of the specimen began to drop rapidly after the third cycle and the hysteresis loops showed increased pinching with each additional cycle as shown in Fig. 3.3(a). The increase in energy dissipation

with any additional displacement reduced considerably after the fifth cycle, which had a ductility of 2.5, as shown in Fig. 3.6. The shear deformation in the joint significantly increased after the first two loading cycles and the shear stiffness deteriorated rapidly as is indicated by the displacement vs. shear deformation plot of Fig. 3.5(a). The maximum observed shear stress in the beams was $3.07\sqrt{f'_c}$ (psi units) and did not cause any extensive cracking or slip type movement across the flexural cracks.

All the main reinforcement bars of the beams yielded at a location close to the face of the column during the first cycle. As the joint core began to crack, the main beam bars tended to slip through the core. As shown in Fig. 3.9, the main beam bar yielded in tension at the gage location WB4 during the positive half of the first loading cycle. As the load is reversed, the tensile strain in the bar decreased from point A to point B shown on the plot. While loading in the negative direction, it is expected that reinforcing bar would be subjected to compression at this location and tension at the corresponding location on the other side of the joint. At point B on the plot, however, this expected trend changed and consequently, the strain in the bar, instead of continuously decreasing along BC, began to increase along BD. It was assumed that this indicated the propogation of tensile stress through the core from the other side of joint and marked the beginning of slippage. Such a reversal of strain in the reinforcing bar was also

observed in the subsequent cycles. After the fourth cycle, there was no further increase in the cyclic strain and the bar appeared to pull freely through the joint.

At a distance d/2 (d = effective depth of beam) from the face of column, the main bars experienced both tensile and compressive strains, indicating very little slip. The plot of strain variation at this location (gage WB1) is shown in Fig. 3.10. The strain in the bar varied over a narrow range between tension and compression during the first three cycles. Yielding of the bar at this location occurred during the fourth cycle as indicated by a sudden increase in strain along line AB on the plot. However, there was still no reversal of strain during the opposite half cycle of loading which would indicate any significant slippage. During the sixth loading cycle, the change of slope at point C on the plot showed a slight tendency to slip. The strain at this location was approximately 1/5th of the strain in the main bar at the face of the column. The damage in the beams was clearly confined within a very small region close to the joint.

Typical column bar behavior for an edge bar and a middle bar is shown in Figs. 3.11 and 3.12 respectively. The middle column bar experienced tensile strain only (Fig. 3.12) because these bars remained on the tension side of the neutral axis whatever the loading direction. The column bars did not experience any yielding, but the slippage of edge bars through the joint began from the very

first loading cycle. In Fig. 3.11, the change of slope at point B from AB to BC indicates the beginning of slippage in the edge bar.

The edge column bars showed a very peculiar strain behavior. During the positive half of each loading cycle the bar at gage location TC1 slipped and went into tension instead of compression (point B in Fig. 3.11). Also, the increase in strain for each additional cycle was much higher during the positive loading than during the negative loading. There are two possible explanations. During the positive loading direction, the diagonal crack in the joint crosses the column bar at the gage location. With the increased size of the existing crack and the introduction of new cracks with each additional loading cycle, the strain in the bar increaseddrelatively faster than when the crack opens in the other diagonal direction during the negative half of loading cycle. A second explanation is based on the progressive shift of peak bond stress with the slippage of the bar. As shown in Fig. 3.13, with every new loading cycle resulting in additional slippage of the bar, the peak bond stress profile moves away from the tension end of the bar. As the peak value crosses the strain gage location during the loading cycles accompanied by slippage, an increasing amount of stress was carried by the bar and hence, the rapid increase in strain.

All the transverse reinforcement hoops in the joint yielded. The square hoops yielded during the first cycle

while the diamond shaped hoops yielded in the third cycle. Typical load vs. strain plots for the two type of hoops are shown in Figs. 3.14 and 3.15. Yield of the transverse reinforcement and a reduction in the magnitude of cyclic strain indicates a loss of confinement.

Specimen X2 (α=13.5, ρ_t=1.15%, λ=3.67, f'_c=4880 psi)

Because of the higher percentage of joint transverse hoop reinforcement, this specimen exhibited relatively less damage in the joint than specimen X1. The joint reinforcement consisted of three layers of hoops placed at a spacing of 3 inches. As in the case of specimen X1, the first cycle of loading to yield level caused diagonal cracks in the joint and flexural cracks in the beams which extended one beam depth away from the joint. With an increasing number of cycles, more cracks appeared in the beams and the joint. The flexural and shear cracks in the beams joined across the depth of the beam to form a typical criss-cross pattern spread over a distance of approximately twice the effective depth of beam on either side of the joint. During the sixth cycle, at a ductility level of 3.1, the concrete cover of the joint core started to spall off. However, the joint core remained well confined by the hoops and the damage was forced over a larger region in the beams. The condition of the specimen at the end of the seventh cycle is shown in Fig. 3.16.

The load carrying capacity of this specimen remained stable through the first four cycles of loading. In the

subsequent cycles, the strength and stiffness dropped and the hysteresis loops became more pinched, as can be seen in Fig. 3.3(b). As shown in Fig. 3.5(b), the joint in this specimen displayed a smaller degree of shear deformation for the same displacement than specimen X1. The hysteretic behavior of this specimen was a marked improvement over specimen X1. The energy dissipated by the specimen increased with each additional displacement. Energy dissipated, normalized with respect to the yield cycle energy and corresponding to various ductility levels, is shown in Fig. 3.6 and the total energy dissipated during each cycle is given in Table 3.1.

Main reinforcement in the beams yielded during the first cycle at a location close to the face of the column. A typical load vs. strain plot for a gage at this location is shown in Fig. 3.17. During the first loading cycle, a reversal in the direction of strain occurs at point A, as shown on the plot. Because there is no continuation of such tendency in the subsequent cycles, this indicates a localized slip. However, in the fifth cycle the compressive stress in the bar changes to tensile stress at point B in Fig. 3.17 and a reversal of slope on the strain plot continues through the last two cycles. However, this specimen experienced very little slippage in the beam main reinforcement.

Strain variation at a distance of half the effective depth of beam away from the face of the column for the same

bar is indicated in Fig. 3.18. For the first three cycles, the bar alternated through tension and compression, depending upon the direction of loading. Yielding occurred during the fourth cycle and thereafter, the strain level dropped as the strength of the specimen decayed.

The column bars remained elastic through all the loading cycles. The behavior of the middle bar was essentially the same as in the specimen X1. Two distinctly different behaviors of the outer column bars are shown in Figs. 3.19 and 3.20. The column bar with the gage BC1 shown in Fig. 3.19, indicates typical excursions into tension and compression without any slip. A column bar behavior similar to that observed in the specimen X1, is shown in Fig. 3.20. The reasons for slip and the accompanying increasing tensile strain during the negative half of loading cycle have been explained previously in the behavior of specimen X1. In specimen X1 both the edge column bars slipped through the joint while in specimen X2 only one edge bar with gage BC3 slipped through the joint. There is no apparent reason for such a disparity in the behavior.

The rectangular hoops in the joint in all the layers, yielded a few cycles earlier than the diamond shape hoops. On the average, the square hoops yielded in the second cycle while the diamond shaped hoops yielded in the third cycle. A typical behavior of a square and a diamond shape hoop is shown in Fig. 3.21 and 3.22, respectively. The gages on the hoops were located close to a corner of the joint. Strains

were, therefore, higher for the direction of loading which caused diagonal joint cracks which passed through the corner where the gages were located. The gages indicated lower strains when the direction of loading caused cracks to open along the other diagonal. The resulting bias in the yielding of these hoops can be seen in these plots.

The hoops kept the joint core well confined and no visible deterioration of the core was noticed through the end of the test. Due to the well confined core, there was only minor slippage of beam bars and consequently, no open cracks at the beam column interface. The shear stress level in the beam was low (λ=3.67) and did not cause any deterioration of the hinging region in the beams.

Specimen X3 (α=10.4, ρ_t=0.76%, λ=2.74, f'_c=4500 psi)

Specimen X3 had a lower shear stress in the joint and also had a lower amount of joint hoop reinforcement. As in the case of specimen X1, this specimen had two layers of joint hoop reinforcement, each placed approximately 3 in. away from the center of the joint. In the absence of a confining hoop at the mid-height of the joint, a softer core developed at the intersection of the diagonal cracks in the joint. Due to the lower shear stress level in the joint, damage to the core, which was comparable to that of specimen X1, was delayed upto the seventh cycle.

Diagonal cracks in the joint did not appear until the second cycle. However, the beams experienced extensive flexural cracking over a length of approximately twice the

effective depth of beams on either side of the joint as early as the first cycle. The specimen at the end of second cycle is shown in Fig. 3.23(a). Cracking occurred mostly in beams until the sixth cycle when the joint core at the junction of the diagonal cracks began to soften and disintegrate considerably. In the last two cycles, the joint core had the same appearance of extensive damage as in the case of specimen X1. The large size of the diagonal cracks divided the joint core into four triangular wedges and each moved as an integral part of the connecting elements relative to the other wedges. Figure 3.24 shows the damage in the core and the beams at the end of the seventh cycle.

The specimen displayed a sustained load carrying capacity for the first five cycles. During the last two cycles, the load capacity reduced by a very small amount, as indicated in Fig. 3.3(c). Because of the different scale of the hysteresis loops for this specimen, it was difficult to compare the stiffness degradation and pinching of the loops with the other X-series specimens. However, a comparison of the shear deformation of the joints, provides an additional unbiased evidence. Comparing the shear deformations for the same displacement level in Figs. 3.5(a), (b) and (c), specimen X3 shows a higher shear stiffness and a smaller shear deformation than specimens X1 and X2. A further evidence of better behavior is provided by the energy dissipated during each cycle. As is seen from the Fig. 3.6,

specimen X3 dissipated a higher amount of energy during each cycle than the other two specimens in X-series. Once the joint became sufficiently disintegrated by the seventh cycle, the energy dissipation reduced conspicuously.

The main reinforcing bars of the beams showed no slippage until the sixth cycle, when the joint core became increasingly fractured. A typical propagation of yield in the main bars is shown in Figs. 3.25 and 3.26. The inner set of gages on the main bars were located close to the face of the column (e.g. WB2 in Fig. 3.25) and the outer set of gages were placed at a distance of half the effective depth of beam from the column face (e.g. WB1 in Fig. 3.26). On the average, the bars at inner gage locations yielded in the second cycle while at the outer gage locations, the bars yielded in the third cycle. The gages WB1 and WB2, attached to the main beam bar as shown in Figs. 3.25 and 3.26 respectively, confirm the spread of flexural mechanism away from the column face. The reversal of strain in gage WB2 during the sixth loading cycle indicates the slippage of main beam bar at the face of column.

The column bars remained elastic during all the loading cycles. Their behavior was essentially identical to that observed in the specimens X1 and X2. The middle column bars, as explained previously, usually are on the tension side of the neutral axis and hence remain in tension for most of the loading situation except when the loads are very small. Figures 3.27(a), 3.27(b) and 3.27(c) show the strain

history of the middle bar at the top, center and bottom of the joint. The gage CJ in Fig. 3.27(b) indicates a strain twice as large as shown by the gages at the top and bottom of the joint. This is probably due to the fact that the middle bar within the joint also resists the vertical component of shear in the joint.

The joint hoop reinforcement of this specimen yielded in the fifth cycle. The square hoops effectively carried the joint shear stress through most of the loading cycles in the elastic range. The load vs. strain plot of Fig. 3.28(a) shows a gradual increase in the tensile strain for each loading direction. Both types of hoops appear to have yielded simultaneously in the fifth cycle between the points A and B. The joint reinforcement provided adequate confinement to the core for most of the loading cycles.

Specimen S1 (α=13.2, ρ_t=0.76%, λ=4.65, f'_c=6030 psi)

This specimen had a higher strength concrete than all the other specimens. Cracks in the joint core could not be examined visually due to the presence of transverse beams. The slab and the beams experienced flexural cracks beginning in the first cycle. Most of the flexural cracking was confined to a distance along the beam equal to its effective depth on either side of the column. The first crack in the slab occurred at the slab-column junction running across the full width of the slab. With each cycle, more cracks appeared in the slab at a regular spacing approximately equal to the depth of the slab. Figure 3.29

shows such parallel cracks in the slab at the end of the fourth cycle. The width of the cracks progressively decreased with the distance from the column. Inclined flexural-shear cracks in the beams in the vicinity of column became increasingly wider with each cycle. A major crack at the beam-column junction opened to a width of one-half inch by the end of the test and extended through three-quarters of the beam depth. The column also showed some flexural cracking close to the joint. The cracking pattern at the end of the fifth cycle, which was the last cycle in this particular test, is shown in Fig. 3.30. The transverse beams did not suffer any visible damage except for a horizontal crack at the junction of the web and slab during the fourth cycle.

Unlike the X-series specimens, the S-series specimens did not have a well defined yield point. The slab bars became increasingly effective with every additional cycle and the load carrying capacity increased accordingly. This specimen was cycled through two elastic cycles before a truly yield cycle was identified on the load vs. displacement curve. The third and fourth cycles were repeated to observe any deterioration of stiffness and loss of energy dissipation capacity. As indicated by the hysteresis loops of this specimen in Fig. 3.3(d), the specimen resisted higher load with each additional displacement as more bars in the slab yielded and the ones which had already yielded began to strain harden. The

stiffness degraded considerably during the repeat cycles and on the average, the load dropped by ten percent and the energy dissipation dropped by as much as thirty percent. For a new displacement cycle, the load increased irrespective of the repeat cycle, but the stiffness degradation caused additional pinching of the hysteresis loops and a reduction of energy dissipation capacity, as can be seen in Fig. 3.6.

The main beam bars did not show any slippage. Figures 3.31 and 3.32 show the strain history of the bar at the inner and outer gage locations respectively. During the first two elastic load cycles, the bar underwent both tensile and compressive strains. All bars yielded at both gage locations during the third cycle. As can be seen from these figures, the bars strained as much as ten times the yield strain, causing wide flexural-shear cracks in the region adjacent to the column. The slab bars closer to the column yielded simultaneously with the main beam bars during the first yield cycle. The slab bars away from the column appear to have yielded later during subsequent cycles. The strain-history of slab bar at gage location S1 is shown in Fig. 3.33. The slippage of the bar observed in this plot is due to the high tensile strain in the bar which caused a split in the slab at the reinforcement level as can be seen in Fig. 3.30.

In the column three gages were attached to the middle bar at locations shown in Fig. E2. The strains at these

locations indicate column behavior identical to the column of specimen X1. Strains in the column bar remained below the yield level for all the loading cycles. As in the specimen X1, the strain in the column bar at mid-depth of the joint was larger than at the top and bottom of the joint.

Figures 3.34 and 3.35 illustrate the behavior of joint hoop reinforcement. The rectangular hoops yielded in the second load cycle, indicating some loss of confinement during the second and third cycles. First yielding of diamond shape hoops (Fig. 3.35) occurred in the second cycle. On the average, joint hoops experienced maximum strains of 0.019.

Transverse beams of the specimen were loaded indirectly through the slab. During the loading cycle, the slab applied direct tensile force on one side of the transverse beam with a simultaneous compressive force on the other side. The transverse beams resisted such a load through a combination of shear, bending and torsion. The torsion and shear in the transverse beams introduced certain amount of additional shear in the joint. The transverse beams, at the same time, also provided increased area to resist the shear. Besides the shear and torsion, bi-axial bending of the transverse beams also occurred about the vertical axis and about the axis along the length of the transverse beams. The lower portion of the beam was not significantly deformed by the lateral shear applied along

the top of the beam and acted as a stiffer element, loaded primarily in flexure about the vertical axis.

Strains observed in the bottom bars of the transverse beams appear to support the observed flexural action in the lower portion of the beams. Figure 3.36 shows the strain history of the bottom bar at the gage location TB8. The bar had increased tensile strain due to the additive effect of flexure and torsion during the negative loading cycle and a reduced compressive strain during the positive loading direction. The behavior of transverse beam bars at locations close to the joint was determined by the relative magnitude of flexure, torsion and shear. The strain history of the transverse beam bars at these locations depended on the load resisted and the resulting diagonal cracking of beams due to the shear. A typical strain history is shown in Fig. 3.37. The hoop stirrups in the transverse beams were gaged on both the horizontal and vertical legs. Strain variation in both the horizontal and the vertical leg of a hoop close to the joint at locations indicated, is shown in Figs. 3.38 and 3.39, respectively. The strain level in both legs of the hoop indicate the effectiveness of transverse beams in resisting shear and torsion applied by the slab.

Specimen S2 (α=15.3, ρ_t=1.15%, λ=4.65, f'_c=4460 psi)

With three layers of joint hoop reinforcement and with transverse beams and slab, the joint in this specimen had the most confinement of all the specimens. The flexural-shear cracks in the main beams and slab extended

through almost the entire length of beams. Most of these cracks were, however, located within a distance equal to the depth of the beams from the joint.

Columns of this specimen experienced hair line flexural cracks, some of which extended across the full depth. The cracks across the width of the slab, as shown in Fig. 3.40(a), seem to follow the spacing of transverse reinforcement in the slab. Figure 3.40(b) shows the cracking pattern at the end of seventh cycle. This specimen did not suffer a splitting crack at the interface of transverse beam web and slab as was observed in specimen S1. The slab, therefore, could effectively transfer the load to the transverse beams.

Three types of cracks were observed in the transverse beams. The diagonal cracks on the end face of transverse beams (Fig. 3.40(b)) resulted from the horizontal shear applied by the slab to the beam web. The torsional cracks were located close to the joint where torsion was maximum. A few shallow cracks ran parallel to the axis of transverse beams on either side of it. These cracks, as explained for the specimen S1, are due to the bending of the upper portion of the beam as a cantilever about its longitudinal axis with the lower uncracked portion providing a stiffer support.

The general shape of the hysteresis loops for this specimen, as shown in Fig. 3.3(c), was similar to that of specimen S1. The specimen was loaded below the yield level during the first two cycles. During the last cycle, the

intended displacement ductility could not be achieved because of the limited stroke of actuator. With each additional cycle, the subassembly resisted higher load because a larger number of bars in the slab became effective. The pinching of the hysteresis loops was similar to that for specimen S1, but the stiffness of the reloading branches was relatively higher. The energy dissipation for each cycle is given in Table 3.1 and the normalized energy dissipation with ductility level is plotted in Fig. 3.6. For displacement ductilities greater than 1.75, this specimen displayed higher energy dissipation capacity than the rest of S-series and X-series specimens.

Data from strain gages attached to the reinforcement of the main beams did not indicate any slippage of bars through the joint. Strain history of reinforcing bars at gage locations EB1 and WB1 is shown in Figs. 3.41 and 3.42 respectively. Designating the yield cycle of the hysteresis loops as the first cycle, the main beam bars at gage location close to the joint of EB1, yielded during the first cycle. By the third cycle, the bars had also yielded at the gage location WB1 at a distance of half the effective depth of beam away from the face of column. High strains of 0.025 in the bars close to the joint, as indicated in Fig. 3.41, resulted in a one-half inch wide crack at the bottom of beam to column junction on either side of the joint.

Slab bars closest to the main beams, yielded during

the first cycle. Strain in the slab bars decreased with the distance from the main beam. The crack across the full width of slab at the column face indicated yielding in all the slab bars by the end of the test. Figures 3.43 and 3.44 illustrate the behavior described above. The increased load resistance of the subassembly for each additional cycle, is attributed to this progressively increased participation of slab bars.

Column bars of this specimen were gaged identical to those of specimen S1. Strain in these gages generally remained well below yield, indicating an elastic behavior of the column. The gage at a location just below the joint, however, strained close to the yield level during the last two loading cycles. This explains the hair line cracks in the bottom column as seen in Fig. 3.40(b).

Transverse beams of this specimen were subjected to full yield load applied by the slab. The cracking pattern shown in Fig. 3.40(b), clearly indicates the modes of resistance provided by the beams, and as explained in the beginning of this sub-section. The strain gage data substantiates the existence of shear, torsion and bending in the beams. Figures 3.45 and 3.46 illustrate the flexural and torsional behavior. Gages TB7 and TB8 indicate a predominant flexural behavior in the lower portion of the transverse beam. The different magnitudes of strain in the main bars of the transverse beams for positive and negative loading are due to the bending and torsion of the beams at

the same time. The tensile strain in the bar due to torsion is additive to the tensile strain due to bending for loading in one direction and is partly neutralized due to the compressive strain due to bending for loading in the opposite direction.

Hoop stirrups of the transverse beams resisted a combination of shear and torsion. Their continued straining under load reversals without yielding is typically demonstrated by the load vs. strain plot of gage TH1, shown in Fig. 3.47.

The normalized joint shear stress coefficient (α=15.3) for this specimen was the largest among all the specimens. However, the level of actual joint shear stress was the same as for the specimen S1. The joint shear stress coefficients, joint shear stresses and the strength of concrete for all the specimens are given in Table 3.3. The Three layers of hoop reinforcement (ρ_t=1.15%) in the joint provided better confinement of the joint core, as is shown by their delayed yielding until the third cycle (Fig. 3.48). The strain history for the diamond hoop in the top layer of joint confining reinforcement is shown in Fig. 3.49.

Specimen S3 (α=12.5, ρ_t=0.76%, λ=4.39, f'_c=4100 psi)

Specimen S3 had significantly lower joint shear stress (798 psi) than specimens S2 and S3. The transverse hoop reinforcement for this specimen consisted of two layers of hoops, as in specimen S1. The lower joint shear stress and a lower joint hoop reinforcement in the specimen,

TABLE 3.3 ACTUAL AND NORMALIZED SHEAR STRESSES

Specimen	Concrete Strength (psi) f'_c	Joint Shear Stress (psi) v_j	Normalized Shear Stress Coeff. α
X1	4980	930	13.2
X2	4880	945	13.5
X3	4500	696	10.4
S1	6030	1023	13.2
S2	4460	1024	15.3
S3	4100	798	12.5

resulted in a combined effect similar to that of specimen S2, which had a higher shear stress as well as a larger amount of transverse hoop reinforcement. The transverse beams of this specimen also had a lower amount of longitudinal reinforcement than the specimens S1 and S2, as is shown in Fig. A.2.

The specimen was loaded through two elastic cycles before the yield cycle. The beams and slab cracked considerably even during the elastic cycles. The flexural-shear cracks in the beams became more prominent during the yield cycle and spread through a length equal to twice the effective depth of beam on either side of the joint. The cracking pattern in the slab and the beams is shown in Figs. 3.50(a) and 3.50(b), respectively.

The shear and torsional cracks in the transverse

beams first appeared during the third cycle (considering the yield cycle as the first cycle) at a displacement ductility of approximately 2.0. The columns, just like in the specimen S2, suffered a few hair line flexural cracks across the full depth. By the fourth cycle, a 1/8th in. crack had formed at the intersection of slab and transverse beam, extending across the full slab width. During the fifth cycle, the cracks in the main beams became wider and a major crack of 1/4 in. width appeared at the main beam and column junction, extending through half the depth of the beam web. By the end of the test , the crack at the main beam and column junction had increased to a width of 1/2 inch.

As in the case of specimen S1, the transverse beam suffered a splitting crack at the junction of its web and the slab. With successive cycles, this crack extended through the full width of the transverse beam. Crushing of concrete along the crack was observed during the latter loading cycles.

The hysteresis loops for this specimen are shown in Fig. 3.3(f). Unlike specimen S1 and S2, this specimen did not show a higher load carrying capacity with increased displacement ductilities. The load carrying capacity, however, remained stable through all the loading cycles. As illustrated in Fig. 3.8, this specimen dissipated more energy than specimen S2, up to a displacement ductility of 1.6. For higher ductilities, the increase in energy dissipation for each additional displacement was smaller

than for the specimen S2.

The main beam reinforcement yielded at the face of the column in the first post-yield cycle. Strain-history of gage EB3 at this location is shown in Fig. 3.51. The reduction in compressive strain at point A during the positive half of the loading cycle indicates the beginning of slippage. At a distance of half the effective depth of beam away from the face of column, the main beam bars yielded in the fourth cycle with no evidence of slippage. The top bars of the main beam behaved similar to the lower beam bars except that no slippage occurred in the top bars. This is attributed to the large compression area available at the top due to the presence of the slab. Load vs. strain plot of gage EB1 attached to the top bar is shown in Fig. 3.52.

The bars in the slab appear to have yielded simultaneously with the top bars of the main beam. The load vs. strain plot of gage S2, attached to the slab bar at location shown in Fig. 3.53, indicates yielding in the third cycle. As shown in Fig. 3.53, the slab bar began to slip soon after yielding and the slippage continuously increased during during the last three cycles.

Although the bottom column suffered some hair line cracks, the strain gage data of the middle bar did not indicate any yielding. The strain-history of the middle bar of the column at the top of the joint , center of the joint, and bottom of the joint, was identical to that observed in

the specimens S1 and S2.

The transverse hoop reinforcement in the joint remained elastic, except for the diamond shape hoop in the upper layer which indicated a gradual increase in strain past the yield level. This is the only specimen in both the X-series and S-series specimens in which the joint reinforcement remained elastic. The strain-histories of the square hoop and the diamond shaped transverse reinforcement in the lower layer are given in Figs. 3.54 and 3.55 respectively.

The transverse beam behavior for this specimen was in general identical to that of specimen S1. The splitting crack at the slab and transverse beam junction and the slippage of slab bars, prevented a complete load transfer by the slab to the transverse beams. This resulted in a considerable drop in the strain of longitudinal transverse beam bars, particularly away from the joint. Figure 3.56 illustrates the dominant flexural behavior at the gage location TB7. During the positive half of loading cycles the tensile strains due to flexure and torsion add up to give a higher strain in the bar. For negative loading the compressive strain due to flexure and tensile strain due to torsion cancel each other and result in a lower strain value. During the last three loading cycles the sliding shear crack at the junction of slab and transverse beam prevented any further transfer of shear to the beams. As a result, there is very little increase in the cyclic strain

during these cycles.

In this specimen, close to the face of joint the torsional effect was dominant over the flexural behavior. The strains in the longitudinal bars were, therefore, tensile, irrespective of the direction of loading. Such a behavior at the gage location TB2 is shown in Fig. 3.57.

All the hoop stirrups in the transverse beams of this specimen remained elastic, indicating lower shear and torsion in the beams. A typical strain plot for a hoop close to the joint is shown in Fig. 3.58. Again, the reduction in strain during the last three cycles, when the slab bars had severe slippage, is readily noticeable.

CHAPTER IV

DISCUSSION OF TEST RESULTS

4.1 General

The discussion of test results requires a thorough understanding of the parameters varied during the study before a reasonable comparison can be made between the behavior of various specimens. Some of the variables are predefined while others are unintentionally introduced for a variety of reasons depending upon the nature of an experimental program. At the same time, it is also equally important to be aware of the variables kept constant during the study.

In this study, the primary variables included the joint shear stress, joint hoop reinforcement, and the presence or absence of transverse beams and slab. The forces acting on a joint are shown in Fig. 2.3. The joint shear stresses given in Table 4.1, were calculated by

$$v_j = (1.1\ f_{ya}(A_s+A_s')-V_{col})/bh \qquad (4.1)$$

where

v_j = joint shear stress,

f_{ya} = actual yield strength of beam reinforcement,

A_s = area of bottom reinforcement in beams,

A'_s = area of top reinforcement in beams,

V_{col} = shear in the column,

= $\sum M_{beam}/height_{col}$,

and b,h = the width and depth of the column respectively.

TABLE 4.1 JOINT SHEAR STRESSES

Specimen	Column Shear (Kip)	Joint Shear (kip)	Joint Shear Stress (psi)	Concrete Strength (psi)	Normalized Shear Stress Coeff. α
X1	40.04	188.8	930	4980	13.2
X2	37.04	191.8	945	4880	13.5
X3	30.25	141.4	696	4500	10.4
S1	41.88	207.7	1023	6030	13.2
S2	41.68	207.9	1024	4460	15.3
S3	37.19	162.0	798	4100	12.5

The beams and columns of the subassemblages were designed based on the Appendix A provisions of the ACI Code (14). Because the objective of this study was to evaluate joints with reinforcement less than that recommended by the ACI-ASCE Committee 352 Recommendations (11), the joint hoop reinforcement was kept at a minimum for practicality and adequacy of confinement (ρ_t=0.75% - 1.15%). The percentage of joint hoop reinforcement was calculated by

$$\rho_t = A_{sj}/b(d-d') \qquad (4.2)$$

where

A_{sj} = area of all the hoop legs,

ρ_t = percent transverse reinforcement in the joint,

b = width of column,

and d-d'= distance between top and bottom beam reinforcement.

In the S-series specimens, the transverse beams were loaded along their top due to tension and compression forces in the slab. Such indirect loading induced shear, torsion and bending in the transverse beams. This in turn caused an additional shear to be applied to the joint. The amount of shear transferred from the transverse beams to the joint depends upon: (1) the deformation compatibility between transverse beams and the joint, and (2) the slab to transverse beam load transfer mechanism. The transverse beams also act as an extension of column width in resisting the joint shear but again, the contributory area can not be defined exactly. When using Eq. 4.1 to calculate the shear stress in the slab specimens only a portion of the slab equal to one-half of the effective depth of the main beam on either side of the beam width was considered effective in applying shear to the joint. The resulting shear force was then assumed to be resisted entirely by the joint.

A certain amount of variation in the ultimate strength of concrete, even with the same mix proportions, is

always expected. Although the strength of concrete was not a variable in this study some degree of disparity was introduced among the specimens due to the use of ready mixed concrete in some specimens and hand mixed concrete in others, and the different ages of concrete on the test date for different specimens.

The column to beam flexural strength ratios based on the nominal yield strength of reinforcement and the specified strength of concrete was 1.5. However, the flexural strength ratios calculated using the actual compressive strength of concrete and taking into account the strain hardening effect of steel varied between 1.21 and 1.37. The member sizes and the overall subassemblage dimensions were kept constant during this study. Except for the column reinforcement, which was of grade 60 steel, all the other reinforcements were of grade 40 steel. Because each specimen was cast in three stages, the concrete in the lower column, the joint and beams, and the top column did not have exactly the same strength. The flexural strength computations for each of the components of the subassembly, were done with their respective concrete strengths.

The beam-column subassemblages were subjected to a quasi-static predetermined displacement routine. The specimens were loaded until the load vs. column load-point displacement curves indicated yielding of the specimen. Based on this yield displacement , the subsequent imposed

displacement ductilities were incremented by a displacement ductility of one-half. The X-series specimen had a very distinct yielding point on the load vs. displacement curve and the loading routines closely followed the prescribed loading history. However, in the S-series specimens, due to the progressive yielding of the slab reinforcement , some difficulty was experienced in locating the yield point. The loading routines, therefore, deviated slightly from the intended loading history. Also specimen S2 was subjected to two repeat cycles at ductilities of 1.95 and 2.4 and this had a very distinct effect on its performance.

4.2 Effect of Joint Reinforcement

Specimens X1, X3, S1 and S3 had the same percentage of transverse joint hoop reinforcement (ρ_t = 0.76%) which was placed in the joint in two layers. Each layer of reinforcement in the joint in all the specimens consisted of a square and a diamond shaped hoop. Specimens X2 and S2 had a higher percentage of transverse hoop reinforcement (ρ_t = 1.15%) placed in three layers within the joint. The effect of joint reinforcement on the behavior of a joint is examined separately for X-series and S-series specimens.

Specimens X1 and X2 had the same level of joint shear stress and concrete strength as given in Table 4.1. Any difference in their behavior was then due to the different amount of confinement and shear resistance provided by the transverse hoops. Comparing Figs. 3.8 and 3.16, it can be seen that the higher percentage of joint reinforcement in

specimen X2, kept the joint core well intact. At the center of a joint, where the diagonal cracks cross each other, concrete tends to disintegrate very rapidly and a hollow core develops if there is no confining hoop to keep the concrete from spalling out. Also, the flexural damage in the main beams of specimen X2 was more spread out than for specimen X1, where the damage was mostly in the joint or in a region of beams very close to the joint.

Specimen X2, with relatively better core confinement than specimen X1, suffered less shear deformation in the joint than the specimen X1. Figures 3.5(a) and 3.5(b) clearly illustrate the higher stiffness and lower shear deformation in the joint of specimen X2. The loss of stiffness in the joint for specimen X1 appears to have also influenced its load carrying capacity. Specimen X1 experienced a loss of strength after the first three loading cycles while the specimen X2 maintained its load carrying capacity through five cycles. A relatively larger pinching of the force vs. deformation hysteresis loops and a higher stiffness degradation for the specimen X1 can be seen from the Figs. 3.3(a) and 3.3(b).

The overall effect of a variable on the behavior of a particular specimen can be best judged by comparing the energy dissipation for equivalent ductilities. Normalized energy dissipation for the specimens X1 and X2 is given in Table 3.2 and a plot of energy dissipation vs. displacement ductility is given in Fig. 3.6. It can be seen that the

energy dissipated by specimen X2 was consistently higher than the energy dissipated by specimen X1 for all the ductility levels considered. This comparison seems to indicate a superior behavior of specimen X2 due to the higher percentage of transverse reinforcement (ρ_t = 1.15%).

The effect of a higher percentage of transverse hoop reinforcement in specimens with transverse beams and slab can be illustrated by comparing the behavior of specimens S1 and S2. The S-series specimens generally had a larger displacement of the column load point at yield and hence a lower maximum displacement ductility than the X-series specimens for the same displacement limit of the test set up. Specimen S1 had the highest yield displacement (2.2 in.) of all the specimens which limited the displacement ductility to 2.4. Specimen S2 achieved a relatively higher displacement ductility of 2.7. Both these specimens had a comparable level of joint shear stress, as given in Table 4.1. However, specimen S1 had a thirty five percent higher concrete strength than the specimen S2. The loading history for both the specimens followed the prescribed routine except that in the case of specimen S1, the third and fourth cycles were repeated to study the effect of repeat cycles.

As observed by Meinheit and Jirsa (12), the shear strength of the joint was dependent upon the concrete strength and once the joint concrete cracked, its shear strength degraded irrespective of concrete compressive strength. The effect of concrete strength on the behavior

of specimen S1 and S2 in the post-cracking range, will therefore be minimal.

The effect of transverse hoop reinforcement on the behavior of specimens S1 and S2, can be readily observed by comparing the cracking patterns of the two specimens shown in Figs. 3.30 and 3.40(b). Specimen S2 had more damage in the main beams and which spread over a larger area than the specimen S1. This indicated that a higher percentage of joint reinforcement (ρ_t=1.15%) in specimen S2 provided a better confinement in limiting the shear deformation of the joint core and imposed more flexural action in the main beams. This fact is further substantiated by comparing the influence of joint core confinement on the response of the transverse beams. Apparently, a larger shear deformation of the joint core than the transverse beams in specimen S1 caused a horizontal shear crack (Fig. 3.30) at the junction of the slab and the transverse beam. This substantially reduced the participation of transverse beams in resisting the lateral load on the subassembly. The main beams also experienced damage in a limited area close to the joint as most of the energy was probably dissipated by the shear mechanism in the joint of specimen S1. On the other hand, the well confined core of specimen S2, with its higher shear stiffness, forced a larger contribution of load resistance by the transverse beams. This is clearly seen (Fig. 3.40) from the shear cracks extending all the way to the end of the transverse beams in the specimen S2.

The hysteresis curves of specimens S1 and S2, shown in Figs. 3.3(d) and 3.3(e), did not indicate a significant difference in the load carrying capacity and the stiffness characteristics of the two specimens. Specimen S2 showed a higher load resistance than specimen S1 for all the loading cycles. This however may not be a conclusive evidence of better performance by specimen S2. The repeated load cycles in specimen S1 obviously must have contributed to some reduction in its strength and stiffness.

A final observation can be made by considering the energy dissipated by each specimen. Figure 3.6 shows the energy dissipated vs. ductility plot. Due to the higher strength concrete, specimen S1 dissipated more energy than the specimen S2 up to a displacement ductility of 2.0. Once the joint cracked and became dependent almost entirely on confinement for its strength, specimen S2, with a higher joint reinforcement distributed over three layers, dissipated more energy. With its well confined joint core, the higher energy dissipation in specimen S2 resulted from well spread shear and flexural cracking in the main and transverse beams.

With the shear stress level and other parameters as given in Table 4.1, it may be concluded that the transverse hoop reinforcement in the joint of 1.15% provided sufficient confinement to the joint core to force cracking away from the joint and into the beams. An equal increase in joint reinforcement of X-series and S-series specimens, improved

the behavior of S-series specimens more than the X-series specimens.

4.3 Effect of Joint Shear Stress

The effect of joint shear stress on the behavior of beam-column subassemblages was determined by comparing specimens X1 and X3 of X-series and specimens S1 and S3 of S-series specimens. The values of variables for these specimens are given in Table 4.1. The joint shear stresses were calculated using Eq. (4.1) of Section 4.1. For the specimens with a slab, the negative reinforcement in the slab was considered effective over a slab width extending one-half the effective depth of main beam from each side of the beam.

The effect of joint shear stress level on the behavior of X-series specimens is examined first. Specimens X1 and X3 have the same percentage of joint reinforcement with the same number of layers of hoops within the joint. Although specimen X1 had ten percent higher concrete strength than specimen X3, it did not significantly affect the behavior of joint in the post-cracking range.

Specimen X1 had a joint shear stress thirty three percent higher than specimen X3. A comparison of crack propagation and shear stiffnesses of joints in the two specimens, indicated a marked influence of joint shear stress level on the subassemblage behavior. Figures 3.7 and 3.24 show the damage at the end of seventh load cycle in the joints of specimens X1 and X3 respectively. The joint of

specimen X1, with the higher shear stress, experienced relatively more damage and deterioration of shear stiffness than the specimen X3. The early damage in the joint of specimen X1, due to the higher shear stress, caused significant shear deformation of joint. This resulted in a larger displacement of the column load-point during the first yield cycle. A rapid deterioration of the joint stiffness for specimen X1 can be readily seen by comparing Figs. 3.5(a) and 3.5(c). With a lower shear stress, the joint in specimen X3 maintained its stiffness over a larger number of load reversals and forced extensive flexural cracking in the beams away from the column face. Failure in specimen X1 was clearly a joint shear failure while the specimen X3 showed hinging in beams with an ultimate joint degradation due to a lack of adequate confinement.

A further comparison of behavior of these two specimens can be made by considering the hysteretic behavior. Figures 3.3(a) and 3.3(c) show the hysteresis loops of specimens X1 and X3, respectively. Specimen X1 showed a reduction in strength after three loading cycles compared to the specimen X3 which exhibited no significant loss of strength.

The lower joint shear stress had the most noticeable effect on the energy dissipation characteristics of the two specimens. As shown in Fig. 3.6, specimen X3 showed hysteretic behavior far superior to that of specimen X1 and dissipated sixty six percent more energy during the last

cycle.

For the specimens without transverse beams and slab, it may be concluded that the level of joint shear stress had a very significant effect on the behavior of the joint and the subassemblage. Specimen X3, with a joint shear stress of $10.4\sqrt{f'_c}$ (v_j=696 psi), had a significantly better behavior than the specimen X1 which had a joint shear stress of $13.2\sqrt{f'_c}$ (v_j=930 psi).

The effect of joint shear stress was not as obvious for the specimens with transverse beams and slab. For the S-series, specimens S1 and S3 are compared to evaluate the effect of joint shear stress on their behavior. Specimens S1 and S3 had the same percentage of joint hoop reinforcement and the same member sizes. However, specimen S1 had a concrete strength forty seven percent higher than the concrete strength for specimen S3. As explained in Section 4.2, the higher concrete strength increased the initial shear strength of joint, but did not affect its behavior after the concrete had cracked. In view of the effect of concrete strength on the behavior of a joint, a comparison of behavior based entirely on the shear stress in the joint normalized with respect to the concrete strength, may not be very realistic. The normalized joint shear stresses along with the actual joint shear stresses are given in Table 4.1. Specimen S1 had a joint shear stress of $13.2\sqrt{f'_c}$ (v_j=1023 psi) compared to $12.5\sqrt{f'_c}$ (v_j=798 psi) for the specimen S3.

Due to the presence of transverse beams which provide additional shear area, the conspicuous effect of joint shear stress observed in X-series specimens was not as clearly visible in the S-series specimens. The transverse beams in both the S1 and S3 specimens, did not show any significant shear cracks. Both the specimens suffered a horizontal sliding shear crack at the junction of slab and transverse beam (Figs. 3.30 and 3.50(b)). Flexural cracks in the main beams of specimen S1 were closely spaced near the joint and their spacing increased rapidly with the distance away from the joint. In specimen S3, the flexural cracks were spread evenly through the entire length of main beams. This particular cracking pattern, also noted in the specimens X1 and X3, did indicate relatively more degradation of the joint core in specimen S1.

A comparison of hysteresis loops provides an additional insight into the behavior of these two specimens. It should, however, be kept in mind that specimen S1 had two repeat cycles in its loading history as explained earlier. Neither of these two specimens showed any strength decay, as observed from the hysteresis loops shown in Figs. 3.3(d) and 3.3(f). Specimen S1 did, however, indicate some degradation of stiffness which could have been caused by the higher shear stress in the joint and also partly due to the repeat cycles.

The amount of energy dissipated by each specimen for equivalent displacement ductilities did not provide any

conclusive evidence of an improved behavior of specimen S3 over specimen S1. However, the energy dissipation vs. ductility plot shown in Fig. 3.6, showed some tendency of better energy dissipation by the specimen S3.

From the above discussion of the behavior of specimen S1 and S3, it may be concluded that the joint shear stress level did not have as prominent of an effect on the behavior of specimens with transverse beams and slab, as it had on the behavior of specimens without transverse beams and slab. The additional shear area provided by the transverse beams appeared to have reduced the effect of large disparity in shear stress level in the joint.

4.4 Effect of Transverse Beams and Slab

Transverse beams in the S-series specimens were loaded indirectly by the tensile and compressive forces applied by the slab along their length. These forces caused shear, bending and torsion in the transverse beams. As such, the joint shear force calculated by Eq.(4.1) is not resisted entirely by the joint itself and the computation of joint shear stress based on the joint shear area only may not be exact. The transverse beams provide an additional shear area and resist some unknown portion of the total joint shear. Although, the transverse beams provide some degree of confinement to the joint core, their effectiveness is dependent upon the shear stiffness of the joint relative to the shear stiffness of transverse beams. Particularly, when the transverse beams are loaded in torsion, the

interface between the transverse beam and the joint is subjected to a maximum torque. If the joint core is not well confined, the incompatibility in shear stiffness of the joint and transverse beams will result in deformation incompatibility at the joint to transverse beam interface. A joint with adequate confinement and sufficient stiffness will be able to resist the shear and torsion applied to it by the transverse beams. A weaker and less stiff joint, on the other hand, is not able to absorb the shear and torsion forces from the transverse beams without excessive deformation. The excessive deformation of the joint and the associated torsional rotation of the transverse beam resulted in high strains and stresses at the slab to transverse beam interface. If the transverse beam-slab interface could not resist the high stresses, a sliding shear crack developed at the interface which rendered the transverse beams ineffective. The behavior of the joint then becomes similar to that of specimens without any transverse beams and the level of joint shear stress becomes increasingly important. Specimens S1 and S3 are typical examples of such a behavior. The horizontal sliding shear crack at the slab-transverse beam junction of these two specimens is shown in Figs. 3.30 and 3.50(b).

For a joint with a sufficient amount of confining reinforcement, the joint shear deformation and the associated torsional rotation of the transverse beam are small. In such a case, the transverse beams are effective

and provide resistance to loads from the slab in direct shear, flexure and torsion. The cracks in the transverse beams of specimen S2 shown in Fig. 3.40(b) are typical of such a combination of load resisting mechanism. The specimen then dissipates a much larger amount of energy and the overall behavior of the subassemblage is superior to the specimens with the same level of joint shear stress and confining reinforcement, but without transverse beams.

In view of the above discussion, the behavior of S-series specimens is now compared to the X-series specimens. As shown in Table 4.1, the S-series specimens had eight to fifteen percent higher joint shear stress than their corresponding X-series specimens. The column to beam flexural strength ratio for both the X-series and S-series specimens was generally the same and is given in Table 2.3.

With two layers of transverse hoop reinforcement (ρ_t=0.76%) in the joint of S1 and S3 specimens, similar to that in specimens X1 and X3, the behavior of S-series specimens was not an improvement over the corresponding X-series specimens. The inadequate confinement of the joint by the transverse hoop reinforcement, resulted in the shear crack at the slab to transverse beam junction of both the S1 and S3 specimens as shown in Figs. 3.30 and 3.50(b). The mechanism of this crack growth has been explained earlier in this section. The higher joint shear stress in the specimens S1 and S3 relative to the specimens X1 and X3, in fact, proved more detrimental to the joint after the

transverse beams became partly ineffective due to the reasons given earlier. A comparison of energy dissipation capacity of the specimen X1 and S1, and the specimen X3 and S3, shown in Fig. 3.6, substantiates this explanation.

A reasonable improvement in the behavior due to the presence of transverse beams can be seen from a comparison of specimen X2 and S2. Both these specimens had three layers of joint hoop reinforcement (ρ_t=1.15%). The joint shear stress in the S2 specimen was eight percent higher than the joint shear stress in the X2 specimen. The most important change in the behavior of specimen S2 with its increased joint shear stiffness, was the increased participation of transverse beams in resisting the joint shear. Their effectiveness could be readily seen by the shear, flexural and torsional cracks shown in Fig. 3.40 (b). The superior behavior of the specimen S2 over the specimen X2, is also obvious from the comparison of energy dissipation by the two specimens (Fig. 3.6). The specimen S2 continuously dissipated an increasing amount of energy through all the loading cycles.

To summarize, it may be concluded that a certain minimum amount of transverse joint hoop reinforcement must be provided to effectively improve the joint behavior due to the presence of transverse beams. The amount of joint reinforcement will, of course, depend upon the torsional stiffness of the transverse beams. The mere presence of the transverse beams will be somewhat beneficial only if they

are not loaded and act just as an extension of the column width in the joint area. An increase in the area of the slab to transverse beam junction may preclude the possibility of a sliding shear crack at the junction, as was observed in this series of tests, and make the transverse beams more effective. It may however be pointed out that with an increased width of the slab, the conclusion regarding the effectiveness of the transverse beams may be different.

4.5 Overall Response of Joint

The behavior of a beam-column subassembly depends on the performance of the beam to column joint. Given the satisfactory behavior of the beam-column joint, flexural hinging in the columns should be avoided to assure the lateral stability of a building frame under seismic loading. Accordingly, a column to beam flexural strength ratio of greater than 1.0 is well accepted and implied by all codes. Based on the experimental study, column to beam flexural strength ratios of 1.21 to 1.37 gave the desired subassemblage behavior. However, a minimum column to beam flexural strength ratio of 1.5 is recommended.

The ACI-ASCE Committee 352 (11) recommends adequate confinement of the joint by specifying a maximum joint hoop spacing and also limits the level of normalized joint shear stress to $20\sqrt{f'_c}$ for an interior joint. While the importance of joint confinement and the influence of joint shear stress on the behavior of subassembly was well

recognized separately, a single index representing the confinement as well as the joint shear stress will be more convenient and appropriate.

The effect of joint hoop reinforcement, joint shear stress level and the effect of transverse beams has been discussed individually in the previous sections. A number of researchers have recommended the use of joint hoop reinforcement distributed over a larger number of layers. Confinement of the joint improves with the number of layers of hoops, but beyond a certain number of hoops, these become a handicap in construction. The joint hoops closer to the center of the joint are understood to be more effective than the hoops closer to the beam main reinforcement. The improvement in joint behavior is also observed to be not linearly related with the total amount of transverse reinforcement in the joint. Based on the results of this experimental study, an odd number of layers of transverse reinforcement with one layer at the mid-depth of a joint seems essential to prevent the formation of a hollow joint core.

The influence of concrete strength is noticeable only during the early cycles of load reversals. Once the concrete has cracked, the joint behavior becomes dependent mostly on the confinement provided by the transverse hoop reinforcement and the effect of concrete strength becomes less significant.

Transverse beams at a beam to column connection are

generally loaded indirectly by the slab. If the transverse beams are not loaded, these provide an additional shear area and help reduce the effect of joint shear stress. However, if the transverse beams are loaded, as in this experimental study, improvement in the joint behavior depends entirely on the relative shear stiffness of the joint to the transverse beams. For an improvement in the joint behavior, a certain amount of joint confinement must be present for the transverse beams to be effective.

The joint shear stress is perhaps the most important single factor that determines the behavior of a joint. In the current design recommendations (46), the normalized joint shear stress is to be within a certain specified limit and could have any smaller value depending upon the design of beams and columns. The joint confinement is specified independent of the joint shear stress level. For specimens with very low joint shear stress, no reduction in the joint hoop reinforcement is provided.

A unified approach that compensates for any variation in parameters influencing the joint behavior and gives a single performance index representing the overall behavior, is proposed. This factor, referred to as the joint index, Ω, is calculated by

$$\Omega = v_j/(\eta\sqrt{(nA_{sj}f'_c)}) \qquad (4.2)$$

where

v_j = joint shear stress,

n = number of layers of hoops in the joint,

A_{sj} = total area of joint hoops,

f'_c = ultimate compressive strength of concrete,

and

η = 1.1 for specimens with transverse beams

= 1.0 for specimens without transverse beams.

The joint shear stress is calculated by

$$v_j=(1.25\ f_y(A_s+A'_s) - V_{col})/bh \qquad (4.3)$$

where

A_s, A'_s = bottom and top areas of reinforcement in beams,

f_y = nominal yield stress of steel,

b = width of column,

h = depth of column,

V_{col} = shear in the column

and the factor 1.25 represents the effect of strain hardening in the reinforcement.

Shear in the column is on average about twenty percent of the shear induced by the bending of beams for a critical combination of moments. Therefore, substituting 0.20 V_j instead of V_{col} and combining equations (4.2) and (4.3), we have

$$\Omega = (A_s+A'_s)f_y/(\eta bh\sqrt{(nA_{sj}f'_c)}) \qquad (4.4)$$

The joint performance index (PI), Ω, can be readily

calculated using Eq. (4.4) and represents the total effect of all the significant variables. It should, however, be remembered that this formulation presumes a strong column-weak beam design with a minimum flexural strength ratio of 1.5.

The joint index calculated as above for all the specimens in X-series and S-series is given in Table 4.2. The validity of the proposed performance index can be best demonstrated by considering the hysteretic energy dissipation of each specimen as a measure of its performance. The energy dissipated for various displacement ductilities are given in Table 3.2 and plotted in Fig. 3.6. The rank of these specimens with respect to their performance based on energy dissipation , as given by Fig. 3.6, is shown in parenthesis in the last column of Table 4.2. Comparing their ranking based on the energy dissipation and the joint performance index, a complete agreement between the actual performance and the proposed joint index is readily recognized.

The performance index can also be used for design subject to the following conditions:

(1) the joint index should be equal to or less than 10.0 for a satisfactory performance of the joint,

(2) an odd number of hoops should be used at equal spacing in the joint to ensure one hoop at mid-depth of the joint,

(3) the column to beam flexural strength ratio should

TABLE 4.2 JOINT PERFORMANCE INDEX

Specimen	Joint Shear Stress (psi)	Joint Shear Stress Coeff. α	Joint Performance Index Ω†	Rank Based on PI
X1	930	13.2	12.89	(6)
X2	945	13.5	10.64	(4)
X3	696	10.4	10.17	(2)
S1	1023	13.2	10.65	(5)
S2	1024	15.3	10.11	(1)
S3	798	12.5	10.31	(3)

† calculated by Eq. (4.4)

be equal to or greater than 1.5.

This empirical formulation is based on the effectiveness of each variable that influences the behavior of a joint. With the given column size and main beam reinforcement, the number of hoops required in the joint for a specified reinforcement bar size can be easily calculated. One particular advantage of this unified approach is the comparative evaluation of joints which is essential for an optimum design.

CHAPTER V

ANALYTICAL MODEL

5.1 General

With the increased use of non-linear analysis for reinforced concrete buildings subjected to an earthquake type loading, it has become essential to understand the hysteretic behavior of members. Because a closed form hysteretic model based on the material properties of an element was extremely complex, attention has been focussed on using the hysteretic behavior of members observed during experimental tests. With a strong-column and weak-beam design philosophy, most of the non-linear behavior is confined to the beams close to the beam to column connection. Several hysteretic models that approximate the test results of beam to column connections have been proposed. The degree of complexity and performance varied from one model to another. These hysteretic models essentially duplicated the hysteretic behavior of test specimens. How realistically these test specimens represented the behavior of components of an actual building is open to questions.

In the nonlinear dynamic analysis, a building frame is represented by a suitable analytical model. Inelastic

deformations in the frame members are considered by inserting nonlinear rotational springs at locations where hinging is expected. The nonlinear character of the rotational spring is represented by a hysteretic model suitable for the member involved. Complexity of the analytical model used depends upon the purpose of nonlinear analysis and the type of building. Multi-degree of freedom models with a one-to-one correspondence between the elements of an actual and the idealized building frame, are considered complex models. The cost of a time-history analysis based on such complex models is usually excessive and prohibits more than a few runs. While such complex models provide a relatively accurate and complete response of a building frame, the simpler models aim at the overall response of the system. The shear beam idealization and the equivalent single degree of freedom system are examples of simpler models. They are reasonably accurate and require much less computation.

5.2 Existing Hysteresis Models

Elasto-plastic and simple bilinear hysteresis models have been commonly used both for steel and reinforced concrete. Reinforced concrete members, when subjected to a cyclic loading, suffer stiffness degradation. Such a reduction in stiffness is not accounted for by these models. As a result, an unrealistically high energy dissipation is assumed which grossly underestimates the response.

Based on the observed hysteretic behavior of

reinforced concrete members, the Clough model (22), shown in Fig. 5.1(a), provides for the reduction in stiffness during the reloading stages. During each loading cycle, the reloading slope is defined by the maximum displacement attained during the previous cycle. By virtue of its simplicity and yet realistic representation, the Clough model has been widely used.

Models based on a tri-linear primary curve dissipate energy prior to the yielding stage. Although this is realistic and desirable, it makes the model more complicated without much gain in accuracy at large displacement levels.

Experimental results also indicate some degree of softening in the unloading branches. The Takeda model (23), shown in Fig. 5.1(b), was developed from tests on components which represented only the flexural behavior. It attempts to duplicate the stiffness characteristics observed at different stages of cracking, yielding, unloading and reloading in successive cycles. With sixteen rules operating on a tri-linear primary curve, the Takeda model is one of the most complicated models. Its accuracy has, however, been verified by various researchers. Because it provides for energy dissipation, even at pre-yielding stage, and seeks to define load reversals within the bounds of large amplitude cycles, it is realistic and accurate. The softening of stiffness in the unloading branch is considered by defining the slope of unloading segment for post-yielding region (K_3) as

$$K_3=K_1(D_y/D_{max})^{\beta} \qquad (5.1)$$

where

K_1 = slope of a line connecting yield point to cracking point in the opposite direction,

D_y = yield displacement,

D_{max} = maximum displacement in loading direction, and

β = constant less than 1.0

The Takeda model does not include pinching of the hysteresis loops which is commonly observed in the tests of beam to column connections. This pinching is attributed primarily to shear deformations in the joint and slippage of main beam bars.

A simplified version of the original tri-linear Takeda hysteresis system called the Otani model (25) has been used to represent the bond slip in tensile reinforcement at the ends of frame members. The Otani hysteresis model, with its bi-linear primary curve, has rules similar to to those of Clough model with the exception that this model accounts for load reversals at small amplitudes.

The Sina model (Fig. 5.1(c)) is another derivation of Takeda model and includes the pinching effect not considered by Takeda hysteresis rules. The primary curve is similar to that of Takeda, but it has nine rules compared to the sixteen rules proposed by Takeda. Pinching is accounted for by defining a crack-closing point which marks the beginning

of increased stiffness after the low incremental stiffness near the origin. The crack closing moment is assumed constant and is determined by the moment resisted either by the beam main reinforcement or by the bond stress if any slippage of the main bar is anticipated. The rotation at crack-closing is assumed to occur at seventy five percent of the maximum residual deformation achieved previously. The Sina model rules are described in detail in Reference (37).

The bilinear model has been modified to accomplish the effect of stiffness degradation without losing its simplicity. This hysteresis model, called Q-Hyst model (Fig. 5.1(d)) has only four rules and is found to reasonably approximate the response measured during the shaking table tests on small scale frames. Details of this model and its comparison with other models are given in Reference (37) also.

5.3 Proposed Hysteresis Model

The proposed hysteresis model has been based on the hysteretic behavior observed during the tests on interior beam to column connections. Although, the primary purpose of the experimental study was to establish the influence of various parameters on joint behavior, it also provided a valuable insight into the hysteretic behavior of interior beam-column subassemblages. Some of the important observations from the hysteretic behavior as shown in Figs. 3.5(a) to 3.5(f) are:

(1) pinching of the hysteresis loops was observed in

all the specimens and the crack-closing point (marking the beginning of the stiffening branch during reloading) was essentially the same for the hysteresis loops of all specimens,

(2) all the specimens showed a lower stiffness during each successive reloading cycle,

(3) degradation of the unloading stiffness was observed and appeared to be a function of the maximum displacement attained during the cycle,

(4) for specimens with proper joint confining reinforcement and with joint performance index as prescribed in Section 4.5, the load carrying capacity increased in successive cycles,

(5) the hysteresis loops were essentially symmetric.

The proposed hysteresis model, shown in Fig. 5.2, consists of a symmetrical bilinear primary curve with a break point determined by the yielding of reinforcement in the main beams and the portion of the slab considered effective.

The hysteresis loops of beam to column connections which performed satisfactorily, as indicated by their joint performance index, showed a post yield stiffness of approximately five percent of the elastic stiffness. Specimen S2, with hysteresis loops shown in Fig. 3.5(e), is a typical example. This value is in agreement with that used by Clough (22) in his degrading stiffness model.

The slope of the unloading branch in the post-

yielding region was observed to decrease with increase in the maximum displacement. Based on the experimental results, the slope was defined as

$$K_3=K_1(\theta_y/\theta_{max})^{\beta} \qquad (5.2)$$

where

K_1 = slope of the elastic branch,

θ_y = rotation of joint at the yielding of beams

θ_{max} = maximum rotation during loading, and

β = constant, assumed 0.20.

In the Takeda model, the unloading stiffness was considered to deteriorate more rapidly with increased displacement and hence, he used a β value of 0.50.

The model consists of six primary rules , which define the envelope loop, and another five secondary rules to consider small amplitude load reversals within the main loop.

Pinching of the hysteresis loops has a significant effect on the energy dissipation capacity of a system. The location of the crack-closing point, which defines the end of the low incremental stiffness at mid-cycle, determines the degree of pinching introduced in the model. The hysteretic behavior of the full scale beam-column subassemblages observed during this study indicated a rather stationary crack-closing point at the cracking moment level on the elastic curve for all the test specimens. The crack-closing point for this model was, therefore, set at

that point. Such a location simplifies the computation involved and also evenly compensates for the energy loss due to the linearization of observed hysteresis loops.

The details of the hysteresis rules for the proposed model are given in Appendix F.

The bilinear primary curve of this model was used to simplify and reduce the number of hysteresis rules. Such a representation is not exact for the reinforced concrete components as it ignores any energy dissipated prior to the yield point. The purpose of this model, however, was to study structures loaded well beyond the yield point.

5.4 Proposed Analytical Model

A simple analytical model was developed to analyze multistory reinforced concrete moment resisting building frames subjected to earthquake forces. The concept of the analytical model was based on the current design philosophy of strong columns and weak beams.

In this model, the columns were assumed to remain elastic with all of the inelastic action occurring in the beams. The beams are considered to provide rotational restraints at the beam to column connections and are idealized in the model as nonlinear rotational springs external to the joint. The stiffness variation of such springs with the rotation of the joint, is defined by the hysteresis rules developed from the tests on the beam to column connections. The model, therefore, takes into account the stiffness degradation, softening of unloading

stiffness with successive cycles, pinching of hysteresis loops and the slippage of main bars through the joint.

Because the main purpose of this part of the study was to develop a simplified analytical model, attention was focussed mainly on the overall behavior of the frame rather than the individual member response. Figures 5.3(a) and 5.3(b) show an original frame and the equivalent analytical model, respectively.

The proposed model is in conformity with the seismic design procedures and has a strong intuitive value to it. It takes into account most of the sources of inelastic deformations as observed in the tests on beam-column subassemblages. Yet it is simple, inexpensive and reasonably realistic.

Some disadvantages of currently available analytical models are discussed in the following paragraphs.

In the finite element models, in which each member of the frame is represented by an equivalent element, the beam to column connections are usually assumed infinitely rigid and the inelastic deformations in the beams and columns are considered concentrated at the ends. Both of these assumptions are contrary to the observed behavior. Also, the cost of using such a model for dynamic analyses restricts its application to the final analysis only.

The equivalent single degree of freedom model for a multistory frame, is an oversimplification and much of the intuitive feeling for a real behavior is lost.

The shear building model has been based on the assumption of infinitely rigid floors, thus allowing hinging in the columns. This is in direct contradiction with the accepted design philosophy of building frames and thus does not model the desired building response.

In the proposed analytical model, solution techniques generally accepted for the nonlinear dynamic analysis of multi-degree of freedom system, were used. The nonlinear problem was approximated as a sequence of successively changing linear systems. The response was then calculated over a short time step for each linear system.

5.4.1 Assumptions

In order to simplify the solution, several assumptions were made in formulating the mathematical model. Such assumptions were necessary to avoid an expensive and complex solution. Some of these assumptions related to frame idealization while others were made for material behavior and solution technique. All the assumptions are realistic and do not significantly affect the accuracy of the solution. The assumptions are as follows:

(1) The frame is idealized as an elastic column. The beams at each floor level are replaced by an equivalent inelastic rotational spring external to the joint.

(2) The columns are considered massless line elements.

(3) Axial deformations in beams and columns are neglected. Because of this assumption, all the

joints displace horizontally through the same distance. Therefore, the deformed shape of one column is assumed to represent the deformed shape of the building frame.

(4) Masses are assumed lumped at the story levels of the elastic column.

(5) Stiffness of the system remains constant over the time increment.

(6) The column axial loads are assumed to remain unchanged during the analysis.

(7) The first floor columns are assumed rigidly connected to the foundation and no rotation of the foundation is permitted.

(8) The earthquake input is assumed horizontal and in the plane of the frame.

(9) The P-Δ effect is included in the stiffness formulation

5.4.2 Element Stiffness Matrix

The analytical model essentially consists of a stack of beam-column assemblages, with the beams idealized as rotational springs at the joints and the columns represented by the elastic elements. Each element shown in Fig. 5.4, is assumed to have a rotational and translational degree of freedom at each node.

The element stiffness matrix is formulated in the form

$$\{P\}=[k]\{\delta\} \tag{5.3}$$

in which $\{P\}$ and $\{\delta\}$ are ,respectively, the force and the displacement vectors at the nodal coordinates of the element and [k] is the element stiffness matrix.

The stiffness matrix for a uniform column element is given by

$$[k] = 2\,EI/L^3 \begin{bmatrix} 6 & & & \text{sym.} \\ 3L & 2L^2 & & \\ -6 & -3L & 6 & \\ 3L & L^2 & -3L & 2L^2 \end{bmatrix} \tag{5.4}$$

The P-Δ effect is included by considering the geometric stiffness of the element. If the axial force is assumed constant along the length of the element, the geometric stiffness of a beam element is given by

$$[k_g] = N/(30L) \begin{bmatrix} 36 & & & \text{sym.} \\ 3L & 4L^2 & & \\ -36 & -3L & 36 & \\ 3L & -L^2 & -3L & 4L^2 \end{bmatrix} \tag{5.5}$$

in which N is the axial force. The geometric stiffness matrix when subtracted from the elastic stiffness matrix, has the same softening effect as the gravity forces. The combined stiffness matrix is then given by

$$[k_e] = [k] - [k_g] \tag{5.6}$$

5.4.3 System Stiffness Matrix

The system stiffness matrix was assembled from the element stiffness matrices and the stiffness of the rotational springs. The global degrees of freedom were numbered as shown in Fig. 5.5. The rotational degrees of freedom were numbered consecutively beginning at the first floor followed by the horizontal degrees of freedom at the floor levels, and the constrained degree of freedom of freedom at the base is labelled last of all.

The structural stiffness matrix is constructed by adding the element stiffness coefficients to the system stiffness matrix at the appropriate locations.

The nonlinear rotational stiffness of the springs is then superimposed on the elastic system stiffness matrix. The total system stiffness matrix is then given by

$$\{\Delta F\} = [[K_s] + [K_{sp}]] \quad \{\Delta R\} \tag{5.7}$$

where

$\{\Delta F\}$ = incremental force,

$[K_s]$ = elastic system stiffness matrix,

$[K_{sp}]$ = diagonal rotational spring stiffness,and

$\{\Delta R\}$ = incremental deformation.

The total structural stiffness matrix is then condensed to retain the horizontal degrees of freedom only

by using the static condensation process. The same method is assumed applicable in reducing the mass and damping matrices.

Using the Gauss-Jordan elimination procedure, the structural stiffness matrix is partitioned as follows

$$\begin{bmatrix} \{0\} \\ \{F_\delta\} \end{bmatrix} = \begin{bmatrix} [I] & -[\bar{T}] \\ 0 & [\bar{K}] \end{bmatrix} \begin{bmatrix} \{\theta\} \\ \{\delta\} \end{bmatrix} \tag{5.8}$$

where

$\{\theta\}$ = rotational degrees of freedoms to be condensed,

$\{\delta\}$ = vector corresponding to horizontal degrees of freedom,

$[\bar{K}]$ = the reduced stiffness matrix,

and $[\bar{T}]$ statically relates the coordinates $\{\theta\}$ and $\{\delta\}$.

5.5 Mass and Damping Matrices

The masses for each story were assumed lumped at the beam to column connection. These masses were associated with horizontal degrees of freedom only and their rotational inertia was neglected. The mass matrix of the system was, therefore, a diagonal matrix.

$$[M] = \begin{bmatrix} m_1 & & & & 0 \\ & m_2 & & & \\ & & m_3 & & \\ & & & \ddots & \\ 0 & & & & m_n \end{bmatrix} \tag{5.9}$$

Based on the type of structure and the material

involved the modal damping ratios for a structure can be estimated. The damping matrix needed explicitly for the numerical solution of a nonlinear system is determined by (42)

$$[C]=[M][\sum^{N}_{n=1}(2\zeta_n\omega_n/M_n)\{\phi\}_n\{\phi\}_n^T][M] \qquad (5.10)$$

where

$[C]$= damping matrix,

$[M]$= mass matrix,

$\{\phi\}_n$= nth mode shape

ζ_n= modal damping ratio for the nth mode,

ω_n= natural frequency for the nth mode.

In this equation, the contribution to the damping matrix of each mode is proportional to the modal damping ratio. Any undamped modes will, therefore, contribute nothing to the damping matrix.

5.6 Unbalanced Forces

In the numerical solution of a nonlinear system, the finite size of the time step results in overshooting at the break points of the force-deformation curve. If the residual forces due to the overshooting are not eliminated, the solution will not converge to the true response.

One solution to this problem is to reduce the size of time step sufficiently to minimize the error due to overshooting. This is an expensive solution because all the computations must be performed at the smaller time

step. A reduction of time step only in the vicinity of break-points will be more economical, but difficult to achieve for a multiple degree of freedom system under earthquake loading.

In this study, the moment resisted by the rotational spring is corrected at the end of the time step whenever a change in stiffness is encountered (Fig. 5.6). In the next time step, this unbalanced moment is then applied as an external load to the joint.

Before the moments can be applied to the joint as external loads, these are converted to equivalent lateral forces by the condensation process used for the of stiffness matrix. These correction forces are then subtracted from the story forces in the next time step (33).

5.6 Solution Technique

For dynamic analysis, the nonlinear equations of motion are solved by the step-by-step numerical integration method. The nonlinear behavior of the system is approximated by a sequence of successively changing linear systems. The stiffness and the damping characteristics of the system are assumed to remain constant during the short time step.

For a multi-degree of freedom system, the incremental equation of motion for a small time step, is expressed as

$$M\,\Delta\ddot{X} + C\,\Delta\dot{X} + K\,\Delta X = -M\,\Delta\ddot{X}_g \qquad (5.11)$$

where

M = mass matrix,

C = constant damping matrix,

K = stiffness matrix at the beginning of time step,

ΔX = incremental relative displacement vector,

$\Delta \dot{X}$ = incremental relative velocity vector,

$\Delta \ddot{X}$ = incremental relative acceleration vector,and

$\Delta \ddot{X}_g$ = incremental base acceleration vector.

The above condition of dynamic equilibrium is established at the beginning of each time step. With the assumption that the structural characteristics do not change during the time increment, the response is calculated at the end of each time step. The structural stiffness is then revised based on the response at the end of last time step and the process is repeated for each increment of time. The response at a time step is then the sum of all the increments to that time.

The integration of the nonlinear equations of motion (Eq. 5.11) is performed by the Wilson-θ method (29). This method provides an efficient solution technique and is unconditionally stable, regardless of the magnitude of the time step. For $\Delta t/T$ smaller than about 0.01 the numerical error is small, where T is the natural period.

In this method, the acceleration is assumed to vary linearly over the extended time interval $\tau=\theta\Delta t$, where $\theta \geq 1.0$. It has been shown by Wilson et al. (29) that for $\theta \geq 1.37$, the method becomes unconditionally stable.

Using the linear acceleration assumption over the

extended time step, it follows from Fig. 5.7 that

$$\dot{X}_{t+\tau} = \dot{X}_t + (\tau/2)(\ddot{X}_{t+\tau} + \ddot{X}_t) \tag{5.12}$$

$$X_{t+\tau} = X_t + \tau\dot{X}_t + (\tau^2/6)(\ddot{X}_{t+\tau} + 2\ddot{X}_t) \tag{5.13}$$

Equation (5.13) gives

$$\ddot{X}_{t+\tau} = (6/\tau^2)(X_{t+\tau} - X_t) - (6/\tau)\dot{X}_t - 2\ddot{x}_t \tag{5.14}$$

and from Eqs. (5.12) and(5.14), we have

$$\dot{X}_{t+\tau} = (3/\tau)(x_{t+\tau} - x_t) - 2\dot{x}_t - (\tau/2)\ddot{X}_t \tag{5.15}$$

Rewriting Eqs. (5.14) and (5.15) in the incremental form over an extended time interval τ, we have

$$\hat{\Delta}\ddot{X}_t = (6/\tau^2)\hat{\Delta}X_t - (6/\tau)\dot{X}_t - 3\ddot{X}_t \tag{5.16}$$

and

$$\hat{\Delta}\dot{X}_t = (3/\tau)\hat{\Delta}X_t - 3\dot{X}_t - (\tau/2)\ddot{X}_t \tag{5.17}$$

in which the symbol ($\hat{}$) identifies the increment associated with the extended time step τ.

The incremental Eq. (5.11) for the time increment $\tau=\theta\Delta t$, becomes

$$M\,\hat{\Delta}\ddot{X}_t + C\,\hat{\Delta}\dot{X}_t + K_t\,\hat{\Delta}X_t = \hat{\Delta}F_t \qquad (5.18)$$

where $\hat{\Delta}F_t$ is the incremental external force.

Substituting Eqs. (5.16) and (5.17) in the incremental equation of motion (5.18), we get the incremental displacement $\hat{\Delta}X_t$ in the form

$$\bar{K}_t\hat{\Delta}X_t = \hat{\Delta}F_t \qquad (5.19)$$

where

$$\bar{K}_t = K_t+(6/\tau^2)M+(3/\tau)C \qquad (5.20)$$

and

$$\hat{\Delta}F_t = \hat{\Delta}F_t+M(6\dot{X}_t/\tau+3\ddot{X}_t)+C(3\dot{X}_t+\tau\ddot{X}_t/2) \qquad (5.21)$$

The incremental displacement $\hat{\Delta}X_t$ is then obtained by solving Eq. (5.19) using any of the standard method for solving a set of linear equations.

Knowing $\hat{\Delta}X_t$, the incremental acceleration $\hat{\Delta}\ddot{X}_t$ for the extended time interval τ is obtained from Eq. (5.16) and for the normal time interval Δt, the incremental acceleration is given by

$$\Delta\ddot{X}_t = \hat{\Delta}\ddot{X}_t/\theta \qquad (5.22)$$

For the regular time interval Δt instead of τ, the Eq. (5.12) and (5.13) can be rewritten in the incremental form as

$$\Delta\dot{X}_t = \ddot{X}_t\,\Delta t + \Delta\ddot{X}_t\,\Delta t/2 \tag{5.23}$$

and

$$\Delta X_t = \dot{X}_t\,\Delta t + \ddot{X}_t\,\Delta t^2/2 + \Delta\dot{X}_t\,\Delta t^2/6 \tag{5.24}$$

With $\Delta\ddot{X}_t$ known, the incremental velocity and the incremental displacement for the time interval Δt, is easily obtained from Eqs. (5.23) and (5.24). At the end of time interval Δt, the displacement is then,

$$X_{t+\Delta t} = X_t + \Delta X_t \tag{5.25}$$

and the velocity becomes

$$\dot{X}_{t+\Delta t} = \dot{X}_t + \Delta\dot{X}_{t+\Delta t} \tag{5.26}$$

Finally, the initial acceleration for the next time step is calculated from the equation of dynamic equilibrium at the time $t+\Delta t$ by

$$M\,\ddot{X}_{t+\Delta t} + C\,\dot{X}_{t+\Delta t} + K_{t+\Delta t}\,X_{t+\Delta t} = F_{t+\Delta t} \tag{5.27}$$

and the process is repeated for the next time step.

CHAPTER VI

ANALYTICAL STUDY

6.1 General

Three typical reinforced concrete moment resisting frames were analyzed using the proposed analytical model and the Takeda model with the 'LARZ' program (37). The buildings were subjected to a specified ground motion and their responses calculated using the two different analytical models were compared. A brief description of the frames and the study parameters is given first, followed by the comparison of results and the merits of the proposed model.

6.2 Study Frames

Three moment resisting building frames MRF1, MRF2 and MRF3 with five, seven and ten stories respectively, were designed according to the current seismic provisions of the Uniform Building Code (44). Each frame had two bays with the columns assumed fixed at the foundation level. Figure 6.1 shows the three frames with their overall dimensions.

In conformity with the design of subassemblages for the experimental study, the frame members were proportioned to achieve a column to beam flexural strength ratio of 1.5.

For a practical design, it is only possible to maintain the column to beam flexural strength ratio within certain range of the target values. For the external columns, which are subjected to significant changes in the axial load due to the overturning effect, such a ratio could only be defined as an average value.

The material properties used in the design of frames are given in Table 6.1. The ultimate moment capacities of the beams and the interaction diagrams for the columns were determined by a computer program for section analysis. The column axial loads were assumed constant over a few stories to reduce the number of different sections used for beams and columns of the frames. Tables 6.2(a) through 6.2(c) give the actual and assumed axial loads for the columns of frames MRF1,MRF2 and MRF3, respectively.

It was not possible to maintain the same flexural strength ratio of columns to beams at the roof level without unnecessarily increasing the column size. The column to beam flexural strength ratios at the external and internal connections of all the stories of frames MRF1,MRF2 and MRF3 along with the beam and column section types used in each frame are given in Tables 6.3(a) through 6.3(c), respectively. Figure 6.2 shows the cross sectional and the longitudinal reinforcement details of all types of beam and column sections used in the frames.

6.3 Analysis Procedure

The reinforced concrete moment resisting frames MRF1,

TABLE 6.1 ASSUMED MATERIAL PROPERTIES FOR FRAMES

Concrete	f'_c = Compressive strength	4,000 psi
	f_t = Tensile strength	470
	ε_0 = Strain at maximum stress	0.003
	ε_u = Ultimate strain	0.004
	E_c = Modulus of Elasticity	3,600 ksi
Steel	f_{sy} = yield stress	60,000 psi
	E_s = Modulus of elasticity	29,000 ksi
	ε_{sh} = Strain hardening strain	0.0018
	f_{su} = Ultimate strength	98,000 psi
	ε_{su} = Strain at ultimate strength	0.03

MRF2 and MRF3 described above, were analyzed using a computer program named 'SIMPLE' (47) which was developed specifically for this study. The program was based on the analytical model proposed in Chapter V for the nonlinear dynamic analysis of reinforced concrete frames. The primary purpose of the analytical model and the associated computer program was to develop a simple analysis tool suited particularly for the design of frames without stiffness interruptions. Because the control of lateral displacements caused by an earthquake are of fundamental importance in the design of a building, this procedure is aimed at determining story level displacements with as little data preparation as possible and at a very low cost. Additional information

TABLE 6.2(a) COLUMN AXIAL FORCES DUE TO DEAD LOAD IN MRF1

Level	External Column			Internal Column		
	Section* Type	Nominal Force (kip)	Assumed Force (kip)	Section† Type	Nominal Force (kip)	Assumed Force (kip)
Roof	E11	41	60	I11	81	120
5	E11	81	60	I11	162	120
4	E12	122	160	I12	243	320
3	E12	162	160	I12	324	320
2	E12	203	160	I12	405	320
1	-	-	-	-	-	-

* E12 = exterior column section #2 of frame #1

† I23 = interior column section #3 of frame #2

TABLE 6.2(b) COLUMN AXIAL FORCES DUE TO DEAD LOAD IN MRF2

Level	External Column			Internal Column		
	Section Type	Nominal Force (kip)	Assumed Force (kip)	Section Type	Nominal Force (kip)	Assumed Force (kip)
Roof	E21	41	80	I21	81	160
7	E21	81	80	I21	162	160
6	E21	122	80	I21	243	160
5	E22	162	220	I22	324	440
4	E22	203	220	I22	405	440
3	E22	243	220	I22	486	440
2	E22	284	220	I22	567	440
1	-	-	-	-	-	-

TABLE 6.2(c) COLUMN AXIAL FORCES DUE TO DEAD LOAD IN MRF3

Level	External Column			Internal Column		
	Section Type	Nominal Force (kip)	Assumed Force (kip)	Section Type	Nominal Force (kip)	Assumed Force (kip)
Roof	E31	41	80	I31	81	160
10	E31	81	80	I31	162	160
9	E31	122	80	I31	243	160
8	E32	162	220	I32	324	440
7	E32	203	220	I32	405	440
6	E32	243	220	I32	486	440
5	E32	284	220	I32	567	440
4	E33	324	360	I33	648	720
3	E33	365	360	I33	729	720
2	E33	405	360	I33	810	720
1	-	-	-	-	-	-

TABLE 6.3(a) BEAM AND COLUMN SIZES FOR FRAME MRF1

Level	Beam		External Column			Internal Column		
	X-section	Reinforcement	X-section	Reinforcement	Moment Ratio	X-section	Reinforcement	Moment Ratio
Roof	12x22	Top=6-#7 Bot.=4-#7	16x16	A_s=8-#11	0.81	20x20	A_s=8-#11	0.72
5	12x22	Top=6-#7 Bot.=4-#7	16x16	A_s=8-#11	1.56	20x20	A_s=8-#11	1.42
4	12x22	Top=6-#7 Bot.=4-#7	18x18	A_s=12-#10	1.85	22x22	A_s=12-#11	1.80
3	14x24	Top=6-#8 Bot.=4-#8	18x18	A_s=12-#10	1.52	22x22	A_s=12-#11	1.50
2	14x24	Top=6-#8 Bot.=4-#8	18x18	A_s=12-#10	1.54	22x22	A_s=12-#11	1.55

TABLE 6.3(b) BEAM AND COLUMN SIZES FOR FRAME MRF2

Level	Beam		External Column			Internal Column		
	X-section	Reinforcement	X-section	Reinforcement	Moment Ratio	X-section	Reinforcement	Moment Ratio
Roof	14x24	Top=4-#8 2-#7 Bot.=4-#7	18x18	A_s=8-#11	0.77	22x22	A_s=12-#10	0.80
7	14x24	Top=4-#8 2-#7 Bot.=4-#7	18x18	A_s=8-#11	1.51	22x22	A_s=12-#10	1.56
6	14x24	Top=4-#8 2-#7 Bot.=4-#7	18x18	A_s=8-#11	1.44	22x22	A_s=12-#10	1.54
5	14x24	Top=4-#8 2-#7 Bot.=4-#7	20x20	A_s=12-#10	1.70	24x24	A_s=12-#11	1.83
4	16x26	Top=4-#8 4-#7 Bot.=4-#8	20x20	A_s=12-#10	1.51	24x24	A_s=12-#11	1.55
3	16x26	Top=4-#8 4-#7 Bot.=4-#8	20x20	A_s=12-#10	1.53	24x24	A_s=12-#11	1.57

TABLE 6.3(b) (continued)

Level	Beam		External Column			Internal Column		
	X-section	Reinforce-ment	X-section	Reinforce-ment	Moment Ratio	X-section	Reinforce-ment	Moment Ratio
2	16x26	Top=4-#8 4-#7 Bot.=4-#8	20x20	A_s=12-#10	1.55	24x24	A_s=12-#11	1.60

TABLE 6.3(c) BEAM AND COLUMN SIZES FOR FRAME MRF3

Level	Beam		External Column			Internal Column		
	X-section	Reinforce-ment	X-section	Reinforce-ment	Moment Ratio	X-section	Reinforce-ment	Moment Ratio
Roof	14x24	Top=4-#8 2-#7 Bot.=4-#7	20x20	A_s=8-#10	0.79	22x22	A_s=12-#10	0.80
10	14x24	Top=4-#8 2-#7 Bot.=4-#7	20x20	A_s=8-#10	1.58	22x22	A_s=12-#10	1.56
9	14x24	Top=4-#8 2-#7 Bot.=4-#7	20x20	A_s=8-#10	1.57	22x22	A_s=12-#10	1.55
8	14x24	Top=4-#8 2-#7 Bot.=4-#7	24x24	A_s=12-#10	2.24	24x24	A_s=12-#11	1.83
7	16x26	Top=4-#8 4-#7 Bot.=4-#8	24x24	A_s=12-#10	2.15	24x24	A_s=12-#11	1.56
6	16x26	Top=4-#8 4-#7 Bot.=4-#8	24x24	A_s=12-#10	2.12	24x24	A_s=12-#11	1.57

TABLE 6.3(c) (continued)

Level	Beam		External Column			Internal Column		
	X-section	Reinforcement	X-section	Reinforcement	Moment Ratio	X-section	Reinforcement	Moment Ratio
5	16x26	Top=4-#8 4-#7 Bot.=4-#8	24x24	A_s=12-#10	2.14	24x24	A_s=12-#11	1.59
4	16x26	Top=4-#8 4-#7 Bot.=4-#8	28x28	A_s=16-#10	2.89	28x28	A_s=16-#10	1.94
3	18x28	Top=8-#8 Bot.=4-#8	28x28	A_s=16-#10	2.73	28x28	A_s=16-#10	1.93
2	18x28	Top=8-#8 Bot.=4-#8	28x28	A_s=16-#10	2.80	28x28	A_s=16-#10	1.94

about the program is given in Appendix G.

All frames were analyzed using a base acceleration from the first ten seconds of the N-S component of the El Centro, 1940 earthquake. The base acceleration was normalized to a maximum value of 0.5g and was kept constant for all analyses (Fig. 6.3).

The Wilson-θ method which was used in this study for the numerical solution of differential equations ensures stability and convergence for a θ value of 1.37 and more. Although this solution technique is unconditionally stable for any size of time step, for accuracy an increment of 0.01 second with a θ value of 1.4 was used in this study.

One method of constructing a damping matrix is by considering a linear combination of the mass and stiffness matrices. An alternate approach described in Section 5.5 was used in this study. In this procedure, the contribution to the damping matrix by each mode is explicitly specified by assigning modal damping ratios for each mode. For the purpose of comparison with the LARZ program (37), a modal damping ratio of 10% was used for all modes.

6.4 Comparison of Results

To evaluate the proposed model, the results of analyses were compared with that of LARZ program (37) developed at The University of Illinois. The performance of the LARZ program has already been tested by comparing its calculated results with those measured during the shaking table tests of small scale multi-story frames. Because the

Takeda hysteresis model has been found to give reasonable results, this option in the LARZ program was used for analyses.

The scope of this analytical study was limited to the analyses of three building frames subjected to a common base acceleration input. As mentioned earlier, the objective of this study was to develop a tool that provided reasonably accurate story level displacements; an item checked repetitively during the design stage of a building. In this study, no attempt was made to duplicate the story level displacement time-histories provided by the more complicated and costly LARZ program. For a ten story two-bay frame, the proposed model requires input data for for only ten elements as compared to the input data for fifty elements needed by the LARZ program. The computational time and the storage space required by the SIMPLE program is correspondingly smaller.

The absolute maximum story level displacements for frames MRF1, MRF2 and MRF3 calculated by the SIMPLE program and the LARZ program are given in Table 6.4. It can be seen that the maximum top story displacements calculated by the proposed model for all three frames are in good agreement with correspondent displacements obtained by the LARZ program. The deformed shapes of frames MRF1, MRF2 and MRF3 for maximum story displacements are presented in Figs. 6.4(a), (b) and (c) respectively.

For the frame MRF1, a very close correlation is

TABLE 6.4 MAXIMUM ABSOLUTE STORY DISPLACEMENTS (in.)

Level	MRF1		MRF2		MRF3	
	LARZ	SIMPLE	LARZ	SIMPLE	LARZ	SIMPLE
Roof	-	-	-	-	8.61	8.52
10	-	-	-	-	8.15	7.89
9	-	-	-	-	7.35	7.03
8	-	-	8.29	8.38	6.48	6.37
7	-	-	7.93	7.76	5.63	5.53
6	7.64	7.69	6.71	6.60	4.71	4.89
5	6.53	6.30	5.29	5.09	3.64	4.05
4	4.71	4.33	3.92	4.56	2.48	2.82
3	3.07	2.89	2.55	3.36	1.49	1.98
2	1.38	1.28	1.12	1.43	0.60	0.74

observed between the two models with a maximum difference of 7% at the first story level. Comparing the response of all frames, it appears that the proposed model calculated larger displacements at the lower story levels than the LARZ program. The largest difference in maximum story displacements occurred at the second and third story levels. Displacements calculated by the proposed model for the upper stories were generally within 5% of the values calculated by the LARZ program.

Relative story displacements for these frames are also plotted in Figs. 6.4(a), (b) and (c). The story drifts for these frames were calculated by both models to be less than 1.5% of the story height. For frame MRF1, the relative story displacements in the top two stories were larger than those calculated by the LARZ program and smaller in the lower stories. For the seven and ten story frames, the relative story displacements did not appear to have a definite correlation with those calculated by the LARZ program. These interstory displacements tended to fluctuate more dramatically with the SIMPLE program than with the LARZ program. This is attributed to the presence of higher modes in the response calculated by the proposed model. The larger contribution of higher modes is partly due to the assumption of a uniform damping of 10% for all modes and partly due to the idealization of the frame by a single elastic column, which obviously did not have system damping comparable to that for the LARZ model. The absence of

higher frequencies in the LARZ output is due to the near elimination of any contribution from the higher modes in the formulation of the damping matrix.

The displacement response of MRF1 at the first, third, fourth and fifth story levels is given in Fig. 6.5(a). The higher frequency content noticed at the first story level is progressively damped out in the upper stories. Figure 6.5(b) presents the displacement history of frame MRF2 at the first, third, fifth and roof levels. The calculated response of the frame MRF3 is plotted in Fig. 6.5(c). The wave form for the story displacements had the same shape for all the stories, but the amplitude progressively increased for higher story levels. This displacement pattern over the height of the frames indicated that the frames responded approximately in the fundamental mode. The LARZ program also showed a similar behavior. The higher frequency content at small amplitude is observed in the response of all frames. For large amplitudes at the roof level, most of the higher frequencies are damped out.

A typical hysteretic response of the inelastic rotational spring at the fifth story level of the frame MRF2 is shown in Fig. 6.6. The significant number of small amplitude reversals within the larger loop underline the importance of rules which define the inner loops for the hysteresis model.

In conclusion, it may be said that the SIMPLE model achieved the desired objective of this analytical study. It

calculated maximum story displacements comparable with the more complex model. With its simpler idealization, use of fewer elements, ease of data preparation and lower computational cost, it provides an ideal tool for the design of building frames. It may, however, be pointed out that if the intention of the analysis were to calculate the individual member behavior and an accurate time-history of various responses, then a complex model will be more appropriate.

CHAPTER VII

SUMMARY AND CONCLUSIONS

7.1 Summary

The primary objective of this research was to study the behavior of interior beam to column connections of reinforced concrete moment resisting frames. The investigation was divided into two parts: (1) the experimental investigation of beam to column connections and (2) the analytical study of beam-column subassemblies.

7.1.1 Experimental Investigation

The main purpose of the experimental investigation was:

(1) to study the effect of joint shear stress level on the behavior of beam to column connections subjected to quasi-static load reversals,

(2) to examine the effect of joint core confinement provided by joint hoop reinforcement and by transverse beams and slab on the behavior of beam to column connection,

(3) to develop a simple and economical joint design procedure.

To accomplish these objectives, six full scale

interior beam-column subassemblages were constructed. Three of the subassemblages consisted of beams and columns only (referred to as X-series) and the other three had in addition transverse beams and slab (referred to as S-series). The ratio of flexural strengths of columns to that of beams was kept constant close at 1.5 in all the specimens. In the S-series specimens only a part of the slab was considered effective in flexural strength computations. Variables for the test specimens included the joint transverse hoop reinforcement ratio (ρ_t = 0.75% to 1.15%) and the magnitude of joint shear stress ($10\sqrt{f_c'}$ to $15\sqrt{f_c'}$, psi units). The presence or absence of transverse beams and slab was an additional variable. The transverse joint hoop reinforcement was provided either in two or three layers. Each layer consisted of a square and a diamond shape hoop.

During testing the specimens were held vertically in the testing frame with pin supports near the ends of beams and columns. Slabs in the S-series specimens were stiffened externally with steel channels at the beam support to prevent any premature failure of slab slab. An average of thirty electrical resistance strain gages were placed on the reinforcement in and around the joint to continuously record the strain variations during the loading cycles. The X-series specimens also had two LVDTs placed diagonally at the joint to measure its shear deformation. All specimens were subjected to six or seven loading cycles. During the test

strain gages and the LVDTs were read by a scanner unit at discrete points in each loading cycle. The crack development at each loading stage was carefully recorded and marked on the specimen.

Based on the effects of various parameters observed during the experimental investigation, a simple formulation for design and evaluation of joints was proposed. Current design recommendations for beam to column joints require two independent conditions to be satisfied for a desirable performance of the joint. It places an upper limit on the magnitude of shear stress in the joint and specifies a certain minimum amount of joint hoop reinforcement to ensure proper confinement. However, there is no provision for the interaction of variables involved and it makes the comparison of different designs of a joint difficult. The suggested procedure introduces a new index referred to as the joint performance index or simply the joint index. This index integrates the effect of joint shear stress level, joint hoop reinforcement, number of layers of joint hoops and the effect of presence of transverse beams and slab. Such an index provides a convenient tool for an economical design of a joint and makes comparison of different joints possible. The validity of this approach was tested against the performance of joints tested during the experimental investigation. An excellent agreement was found between the proposed index and the observed behavior of the joints. A limiting value of the joint index was then recommended for a

safe design.

7.1.2 Analytical Investigation

The analytical part of this research dealt with the nonlinear dynamic analysis of reinforced concrete moment resisting building frames. The main objective of this study was to develop a simple analytical model of building frames that could be employed as a design tool for the seismic design of buildings. For such a purpose, this study was further subdivided into two parts. In the first part, a hysteresis model for beam-column subassemblage was developed from the hysteretic behavior of test specimens observed during the experimental investigation. The proposed model for the hysteretic behavior of beam-column subassemblages takes into account the stiffness degradation, pinching effect, reduction of stiffness at unloading and the effect of bar slippage through the joint.

The second part dealt with the development of a simple analytical idealization of a building frame that provided a cheap and convenient tool for checking the drift limits of frames during the design process. The proposed model is based on the accepted design philosophy of strong columns and weak beams. It is therefore, assumed that the building frame to be analyzed has been designed according to such a philisophy. In this model, columns are assumed to remain elastic with all the inelastic action taking place in the beams. The beams are further assumed to provide rotational restraints at the story levels and are,

therefore, replaced by equivalent rotational springs. These rotational springs are assumed to follow the rules of the hysteretic model described earlier. An interior column with rotational restraints at the story levels is assumed to have the same displacement pattern as the entire frame. The floor mass of the column tributary area is considered concentrated at each story level. Such a representation required a minimum amount of data preparation and needed comparatively less storage and computational effort. A computer program named SIMPLE for the nonlinear dynamic analysis of frames was specifically written for the proposed model. The maximum story displacements of three test frames showed good agreement with those calculated by the LARZ program using the Takeda hysteresis model

7.2 Conclusions

The following conclusions were reached from the results of the experimental and analytical investigations:

(1) The joint shear stress level significantly affected the behavior of beam to column connections without transverse beams and slab. However, the magnitude of joint shear stress did not have a noticeable effect on specimens with transverse beams and slab. The additional shear area provided by the transverse beams muted the deteriorating influence of higher shear stress on the joint.

(2) Equal increases in the joint reinforcement of specimens with and without transverse beams and

slab, improved the behavior of former specimens more than the ones without transverse beams and slab.

(3) A well confined core in specimens with transverse beams and slab is a pre-requisite for the effective participation of confining members.

(4) The joint performance index proposed in Section 4.5, accurately reproduced the performance of all the test specimens. This procedure provides a simple tool for an economical design of beam to column joints. It also allows the comparison of joints with different values of parameters. A joint performance index of ten or less is recommended for a satisfactory performance of the joint.

(5) A minimum column to beam flexural strength ratio of 1.5 was found suitable for design.

(6) Column bars in all specimens showed more slippage than the beam bars.

(7) Confinement of the joint core by transverse hoop reinforcement improved the behavior and was observed to be equally important for specimens with transverse beams and slab. Proper distribution of the joint reinforcement over a number of layers is essential for the hoops to be fully effective. For a maximum effectiveness of the confining reinforcement, a joint must have an odd number of layers of hoops with a minimum of three layers.

(8) Specimens with a lower joint shear stress dissipated

relatively more energy than the specimens which had a higher joint shear stress along with more confining reinforcement in the joint.

(9) Higher strength of concrete affected the joint behavior only prior to cracking. Specimens with a higher concrete strength dissipated more energy before cracking. In the post-cracking stage, the behavior was mostly dependent upon the joint shear stress level and the confinement of joint core.

(10) The proposed hysteretic model realistically represented the hysteretic behavior of the beam-column subassemblages observed during the tests. It provided for large as well as small amplitude load reversals.

(11) The simplified representation of the building frame by an elastic column with nonlinear rotational restraints at story levels was found to have good agreement of maximum story displacements with the more complex LARZ program. It required a minimum amount of data preparation and was economical for repetitive runs. For frames without abrupt stiffness changes, such a model provided a convenient design tool for frequent checks of story drifts during the design stage.

7.4 Recommendations for Future Research

The experimental and analytical study reported here satisfactorily met the intended objectives within the scope

of this research. However, it also served to identify the areas which needed further investigation. Some of these areas recommended for future research are given below.

Experimental Study

1) The interaction of slab, transverse beams and the joint needs more investigation. Further tests of beam-column subassemblages instrumented specifically for this purpose could lead to a better understanding of the shear resistance mechanism.
2) The slippage of column bars was observed in all test specimens. Various researches have been directed towards preventing the slippage of bars through the joint. A research solely directed towards understanding the slip mechanism and its propagation through the joint as affected by other joint variables is desirable.
3) The effect of the length of transverse beams with slab could be significant in determining the permissible shear stress level in the joint. A study aimed at determining the effective width of slab and the effective length of transverse beams could provide new insight into the joint behavior in a real building.
4) A statistical study using the proposed joint performance index to evaluate the joints tested during previous investigations is recommended.
5) The behavior of beam to column connections under

dynamic loading could be different. The common procedure of simulating the earthquake loading with a quasi-static loading routine may not provide the true response. Further tests under dynamic loading are recommended.

Analytical Study

1) The proposed hysteresis model should be adapted to one of the more complex programs. This will help evaluate its performance compared to other hysteresis models without the prejudice of the associated analytical model.
2) A further improvement of the analytical model to include all the frame columns and a shear wall will be very usefull. The model could then provide time-histories for story displacements, overturning moments and the base shear.
3) Damping has a significant effect on the building response calculated by various programs. A further study on the effect of damping seems appropriate.

BIBLIOGRAPHY

BIBLIOGRAPHY

EXPERIMENTAL STUDY

1. Hanson, N.W., and Conner,H.W., "Seismic Resistence of Reinforced Concrete Beam-Column Joints," Journal of the Structural Division, ASCE, No. ST5, October, 1967, pp 533-560.

2. Higashi, Y., and Ohwada, Y., "Failing Behavior of Reinforced Concrete Connections Subjected to Lateral Loads," Memoirs of Faculty of Technology, Tokyo Metropolitan University # 19, 1969.

3. Megget, L.M., "Anchorage of Beam Reinforcement in Seismic Resistant Reinforced Concrete Frames," Master of Engineering Report, Department of Civil Engineering, University of Canterbury, New Zealand, February, 1971.

4. Townsend, W.H., and Hanson, R.D., "The Inelastic Behavior of Beam-Column Connections," Doctoral Dissertation, University of Michigan, March, 1972.

5. Renton, G.W., "The Behavior of Beam-Column Joints Under Cyclic Loading," Master of Engineering Report, Department of Civil Engineering, University of Canterbury, New Zealand, 1972.

6. Patton, R.N., "Behavior Under Seismic Loading of Reinforced Concrete Beam-Column Joints With Anchor Blocks," Master of Engineering Report, Department of Civil Engineering, University of Canterbury, New Zealand, 1972.

7. Smith, B.J., "Exterior Reinforced Concrete Joints WithLow Axial Load Under Seismic Loading," Master of Engineering Report, Department of Civil Engineering, University of Canterbury, New Zealand, 1972.

8. Uzumeri, S.M. and Seckin, M., "Behavior of Reinforced Concrete Beam-Column Joints Subjected to Slow Load Reversals," Report No. 74-05, Department of Civil Engineering, University of Toronto, March, 1974.

9. Jirsa, J.O., Meinheit, D.F. and Woolen, J.W., "Factors Influencing the Shear Strength of Beam-Column Joints," Proceedings U.S. National Conference on Earthquake Engineering, EERI, Ann Arbor, Michigan, June, 1975, pp. 297-305

10. Lee, D., Wight, J.K. and Hanson, R.D., "Original and Repaired Beam-Column Subassemblages Subjected to Earthquake Type Loading," Report No. UMEE 76S4, Department of Civil Engineering, University of Michigan, April, 1976.

11. Recommendations for Design of Beam-Column Joints in Monolithic Concrete Structures, ACI-ASCE Committee 352, ACI Journal Proceedings, Vol. 73, No. 7, July, 1976, pp. 375-393.

12. Meinheit, D.F. and Jirsa, J.O., "The Shear Strength of Beam-Column Joints," CESRL Report No. 77-1, Departmen of Civil Engineering, University of Texas at Austin, January, 1977.

13. Fenwick, R.C. and Irvine, H.M., "Reinforced Concrete Beam-Column Joints for Seismic Loading," Report No. 142, Department of Civil Engineering, University of Auckland, New Zealand, March, 1977.

14. Building Code Requirements for Reinforced Concrete, American Concrete Institute, ACI 318-77.

15. Birss, G.R., "The Elastic Behavior of Earthquake Resistant Reinforced Concrete Interior Beam-Column Joints," Masters Thesis, University of Canterbury, New Zealand, February, 1978.

16. Paulay, T., Park, R. and Priestley, M.J.N., "Reinforced Concrete Beam-Column Joints Under Seismic Actions," ACI Journal, November, 1978, pp. 588-593

17. Scribner, C.F. and Wight, J.K., "Delaying Shear Strength Decay in Reinforced Concrete Flexural Members Under Large Load Reversals," Report No. UMEE 78R2, Department of Civil Engineering, University of Michigan, May, 1978.

18. Soleimani, D., Popov, E. and Bertero, V.V., "Hysteretic Behavior of Reinforced Concrete Beam-Column Subassemblages," ACI Journal, November, 1979. pp. 1179-1195.

19. Buckingsale, C.W., Park, R. and Paulay, T., "Post-elastic behavior of Reinforced Concrete Beam-column Joints, Research Report No: 80-20, Department of Civil Engineering, University of Canterbury, New Zealand.

20. Zhang, L. and Jirsa, J.O., "Shear Strength of Reinforced Concrete Beam-Column Joints," presented at ACI Convention at Dallas, Febrary, 1981.

21. Housner, G.W., "Behavior of Structures During Earthquakes," Proceedings of Engineering Mechanics Division, ASCE, October, 1959. pp. 109-129.

22. Clough, R.W., "Effect of Stiffness Degradation on Earthquake Ductility Requirement," Str. and Mat. Research Report NO. 66-16, University of California, Berkeley, October, 1966.

23. Takeda, T., Sozen, M. et al., "Reinforced Concrete Response to Simulated Earthquakes," Journal of Structural Division, ST 12, ASCE, December, 1970. pp. 2557-2573.

24. Gates, W.E., "Design Lessons Learned from the Performance of Instrumented High-Rise Buildings in the San Fernando Earthquake," Proceedings, Fifth World Conference in Earthquake Engineering, Vol. I, Rome, June, 1973. pp. 900-909

25. Otani, S. and Sozen, M., "Behavior od Multi-story Frames during Earthquakes," SRS Report No: 392, Department of Civil Engineering, University of Illinois, Urbana-Champagne, November, 1972.

26. Mckevitt, Anderson, Nathan and Cheng., "Towards a Simple Energy Method for Seismic Design of Structures," Proceedings of the 2nd. US National Conference on Earthquake Engineering, Stanford, August, 1979. pp. 383-392

27.Celebi, M. and Penzien, J., "Experimental Investigation into the Seismic Behavior of Critical Regions of Reinforced Concrete Components as Influenced by Moment and Shear," Report No. UCB/EERC 73-4, Earthquake Engineering Research Center, University of California, Berkeley, California, January 1973.

28. Chopra A.K. and Kan, C., "Effects of Stiffness Degradation on Ductility Requirements for Multi-story Buildings," Journal of Earthquake Engineering and Structural Dynamics, Vol. 2., 1973. pp. 35-45.

29. Wilson, E.L., Farhoomand, I. and Bathe, K.J., "Nonlinear Dynamics of Complex Structures," Journal of Earthquake Engineering and Structural Dynamics, Vol. 1, 1973. pp. 241-252.

30. Hart, G.C. and Vasudaven, R., "Earthquake Design of Buildings: Damping," Journal of Structural Division, ASCE, January, 1975. pp. 11-30.

31. Gulkan, P. and Sozen, M.A., "Inelastic Response of Reinforced Concrete Structures to Earthquake Motions," ACI Journal, Vol. 71, December, 74. pp. 604-610.

32. Shibata, A. and Sozen, M., "Substitute Structure Method for Seismic Design in Reinforced Concrete," Journal of Structural Division, ASCE, January, 1976. pp. 1-18.

33. Luyties III, W.H., Anagnostopoulos, S.A. and Biggs, J.M., "Studies on the Inelastic Dynamic Analysis and Design of Multi-story Frames," Report No. R76-29, Department of Civil Engineering, MIT, July, 1976.

34. Anderson, J.C. and Townsend, W.H., "Models for Reinforced Concrete Frames With Degrading Stiffness," Journal of Structural Division, ASCE, December, 1977. pp. 2361-2376.

35. Viwathanatepa, S., Popov, E., and Bertero, V., "Seismic Behavior of Interior Beam-Column Subassemblages," Report No. UCB/EERC-79/14, University of California, Berkeley, June, 1979.

36. Iwan, W.D. and Gates, N.C., "Estimating Earthquake Response of Simple Hysteretic Structures," Journal of Engineering Mechanics Division, ASCE, June, 1979. pp. 391-405.

37. Saiidi, M. and Sozen, M., "Simple and Complex Models for Nonlinear Seismic Response of Reinforced Concrete Structures," Structural Research Report No. 465, Department of Civil Engineering, University of Illinois, Urban-Champaign, 1979.

38. Moehle, J.P. and Sozen, M.A., "Experiments to Study Eartquake Response of Reinforced Concrete Structures wih Stiffness Interuptions," Structural Research Series Report No. 482, Department of Civil Engineering, University of Illinois, Urban-Champagne, August, 1980.

39. Banon, H., Biggs, J. et al., "Seismic Damage in Reinforced Concrete Frames," Journal of Structural Division, ASCE, September, 1981. pp. 1713-1729.

RELATED REFERENCES

40. Hawkins, N.M., Kobayashi, A.S. and Fourney, M.E., "Reversed Cyclic Loading Bond Deterioration Tests," Structures and Mechanics Report No: SM 75-5, Department of Cicil Engineering, University of Washington, Seattle, November, 1975.

41. Kaar, P.H., Fiorato, A.E., Carpenter, J.E. and Corley, W.G., "Limiting Strains of Concrete Confined by Rectangular Hoops," PCA Report No. RD 053.01D, 1978.

42. Clough, R.W. and Penzien, J., Dynamics of Structures McGraw Hill, Inc., 1975.

43. Paz, Mario, Structural Dynamics, Van Nostrand Reinhold Environmental Engineering Series, 1980.

44. Uniform Building Code, 1979 edition, International Conference of Building Code Officials, Whittier, California 1979.

45. Clough, R.W. and Bertero, V.V., "Laboratory Model Testing for Earthquake Loading," Journal of Mechanics Division, ASCE, December 1977.

46. Draft Recommendations #6, ACI-ASCE Committee 352, Presented at Committee Meeting at ACI Convention, Atlanta, February 1982.

47. Durrani, A.J., "Experimental and Analytical Study of Beam to Column Connections Subjected to Reversed Cyclic Loading," PhD Dissertation, Department of Civil Engineering, University of Michigan, Ann Arbor, July, 1982.

FIGURES

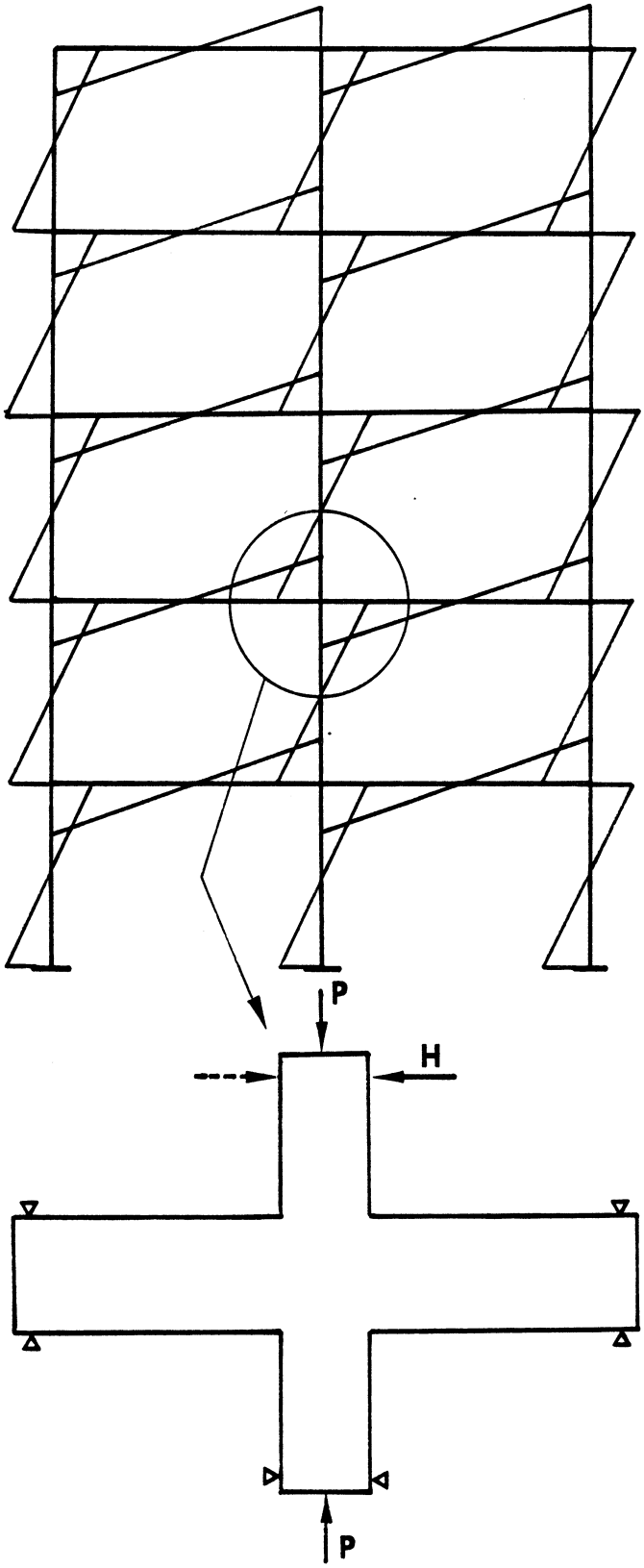

Fig. 2.1 Test Subassembly of Beam to Column Connection

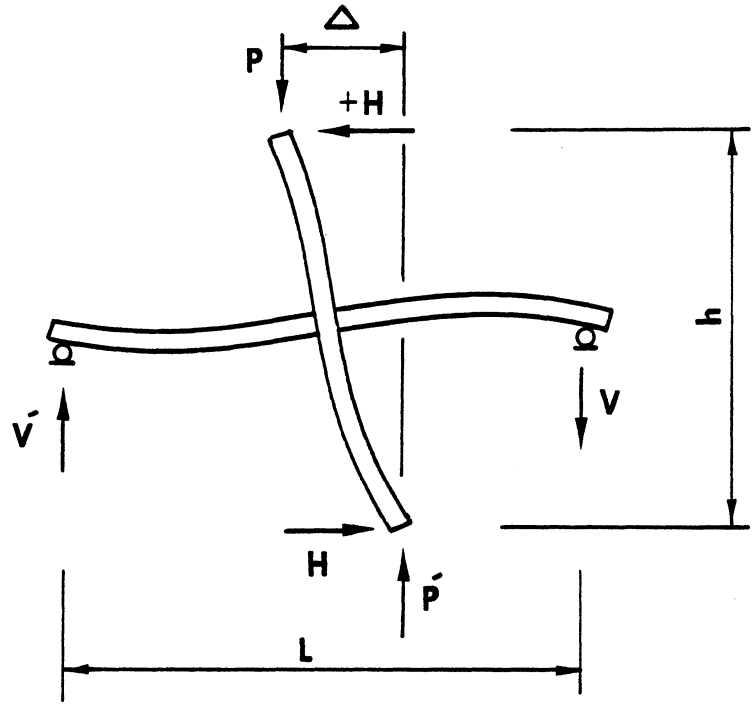

Fig. 2.2 Deformed Shape of Beam-Column Subassemblage

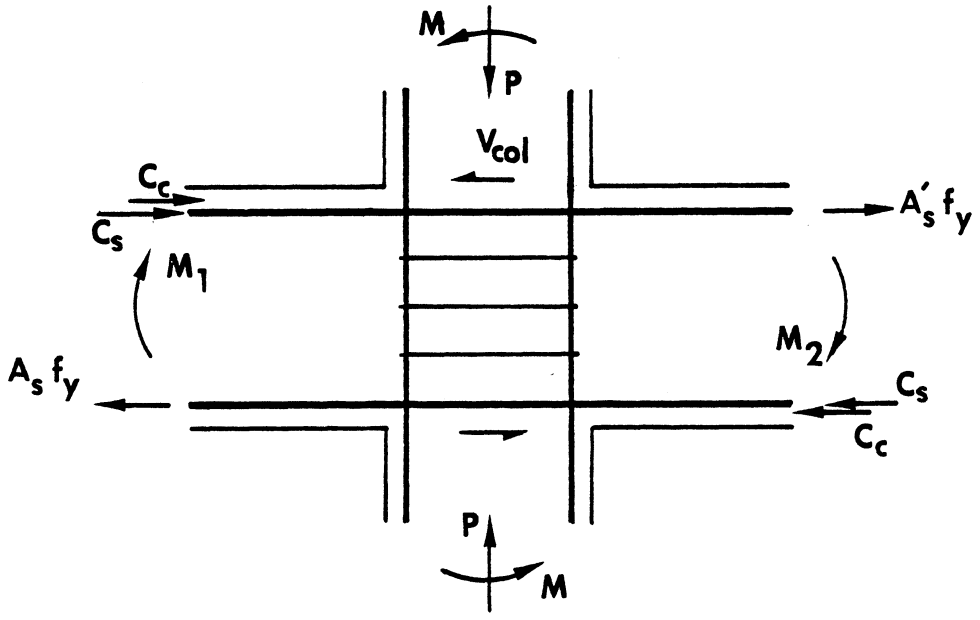

Fig. 2.3 Critical Combination of Forces Acting on a Joint

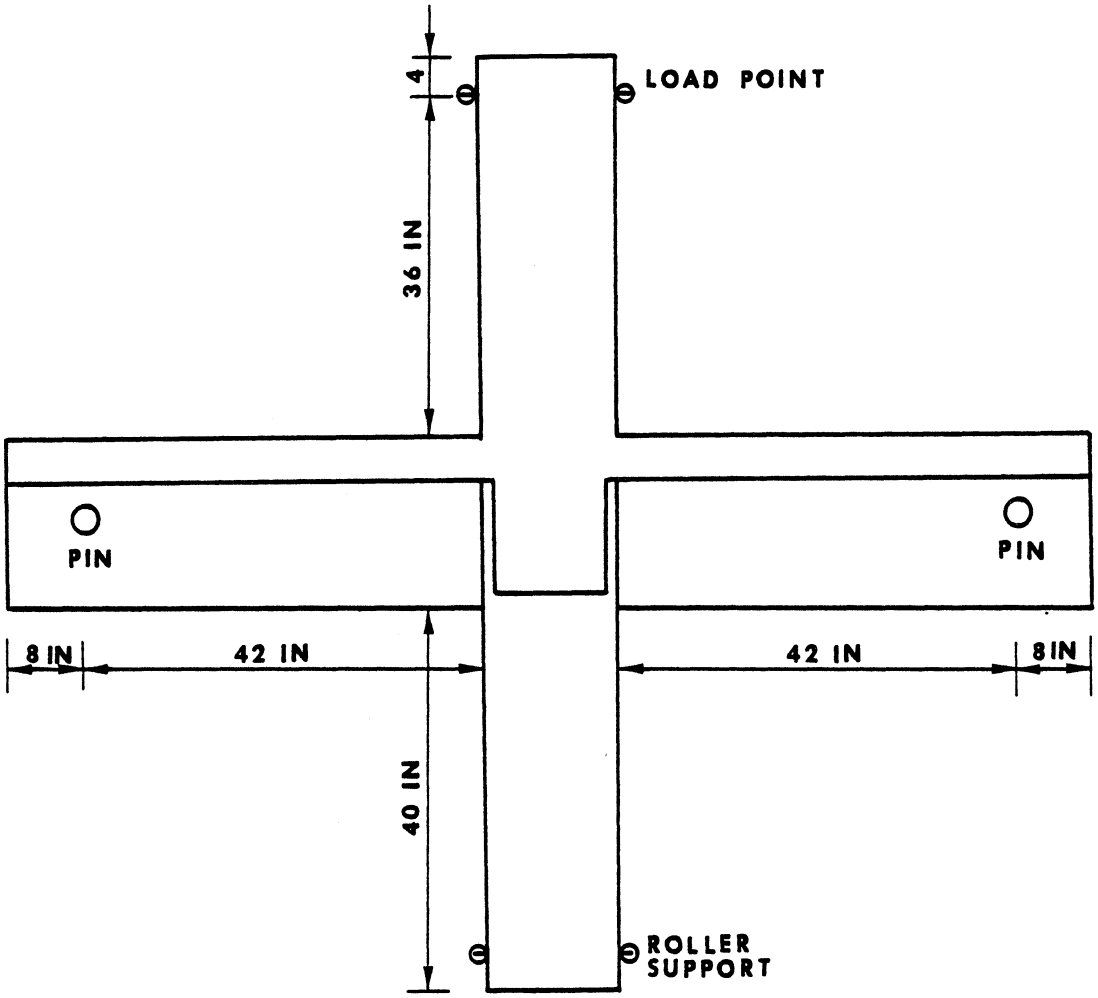

Fig. 2.4 Overall Dimensions of a Specimen

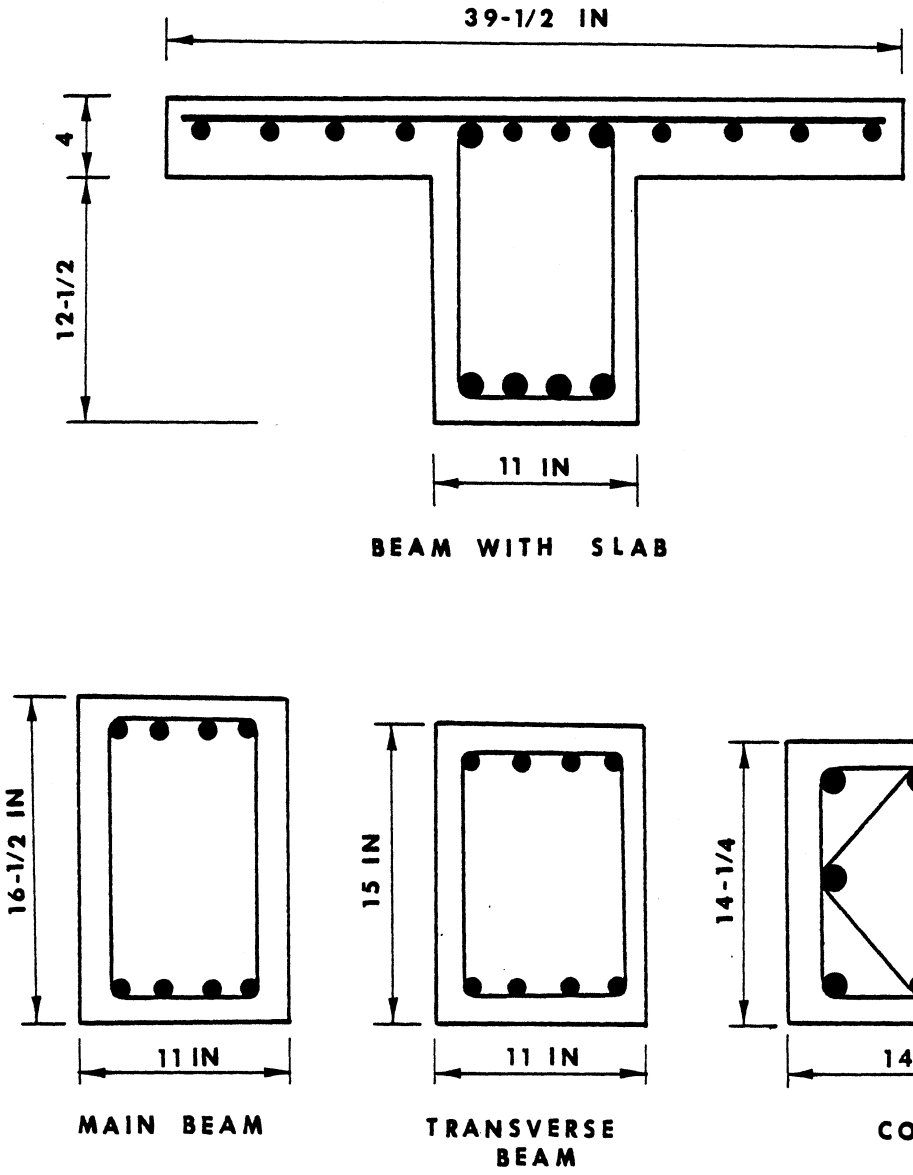

Fig. 2.5 Beam, Slab and Column Cross Sections

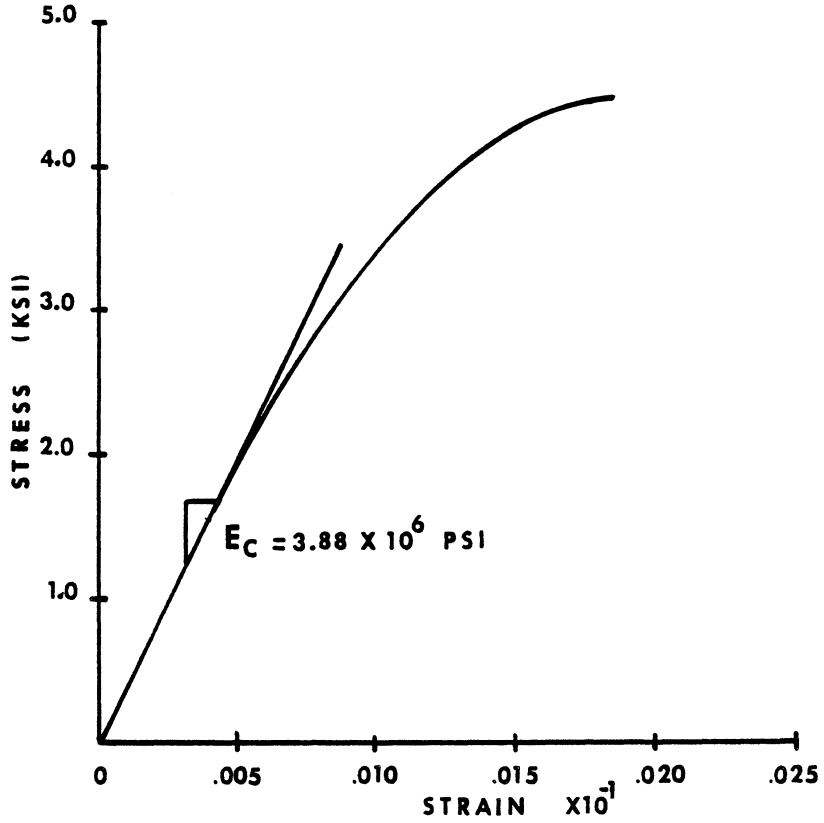

Fig. 2.6 Typical Stress vs. Strain Curve for Concrete

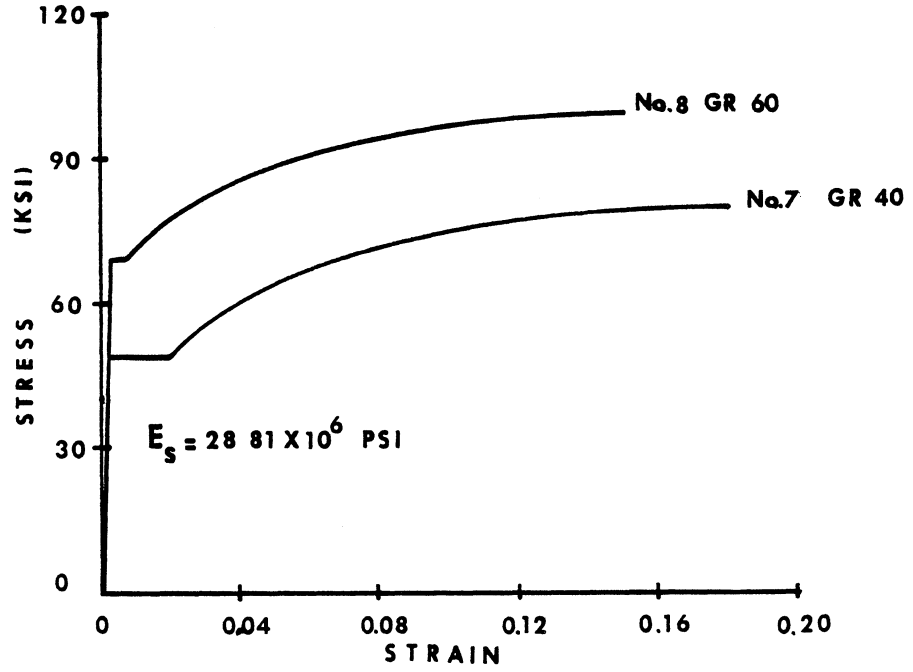

Fig. 2.7 Typical Stress vs. Strain Curve for Steel

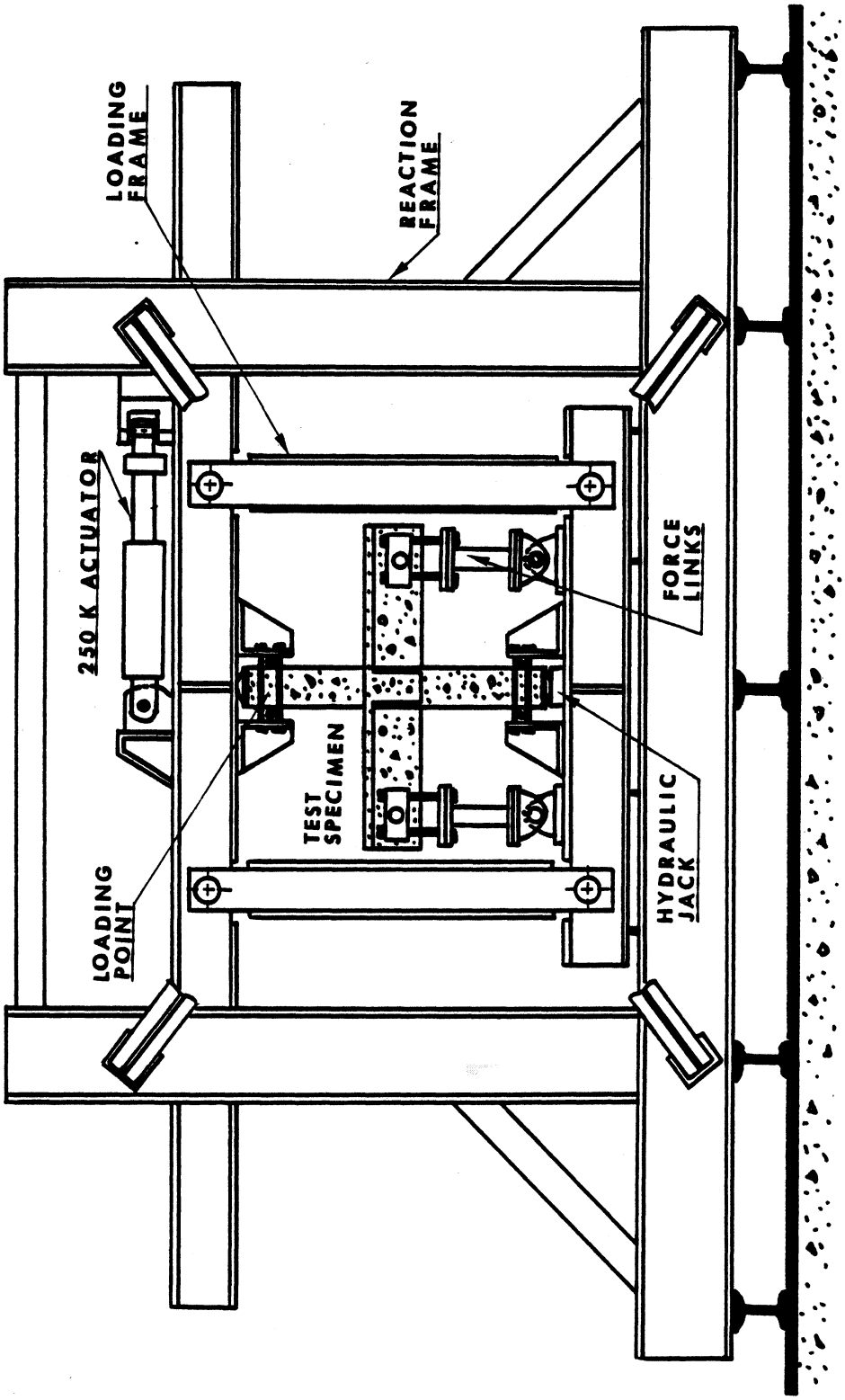

Fig. 2.8 Testing Frame

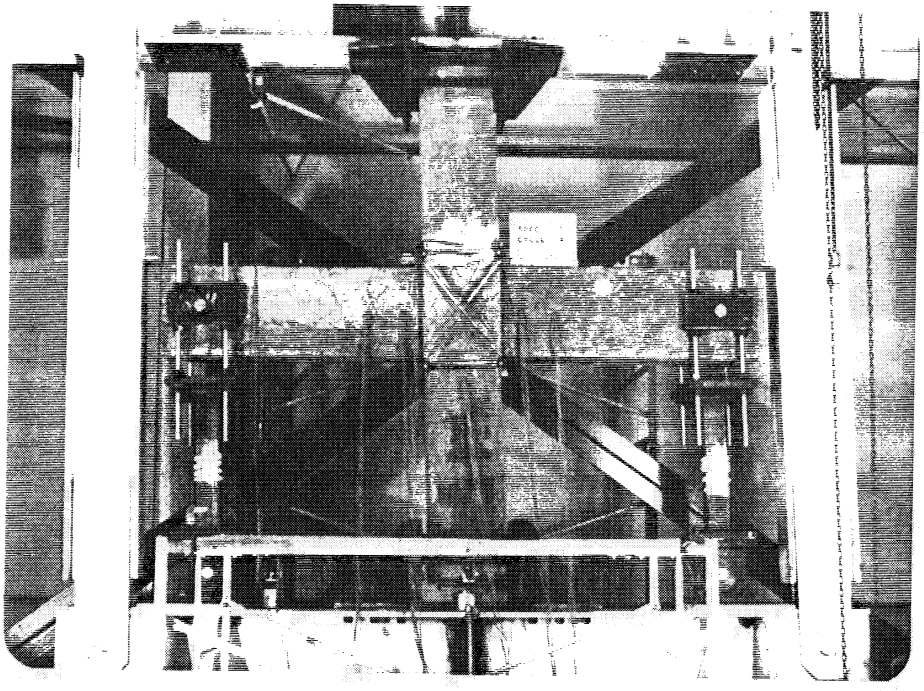

Fig. 2.9 An X-Series Specimen in the Testing Frame

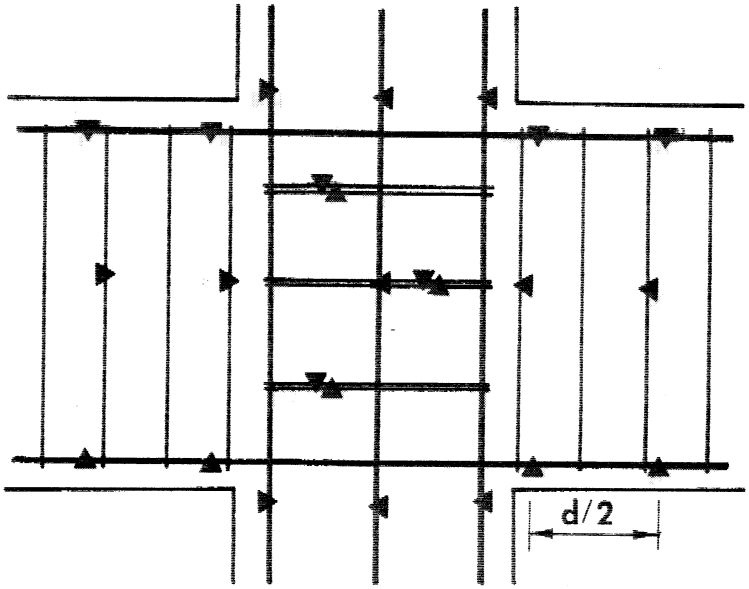

Fig. 2.10 Typical Strain Gage Location in an X-Series Specimen

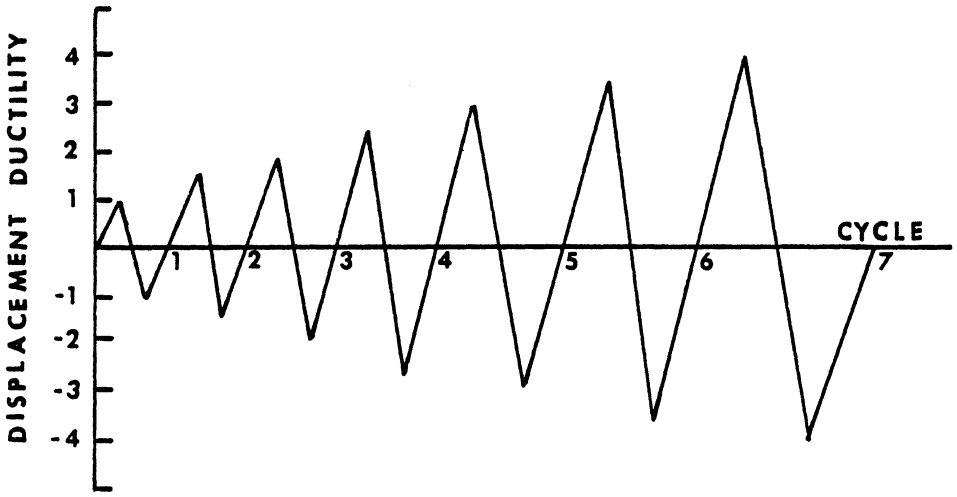

Fig. 2.11 Typical Loading Routine

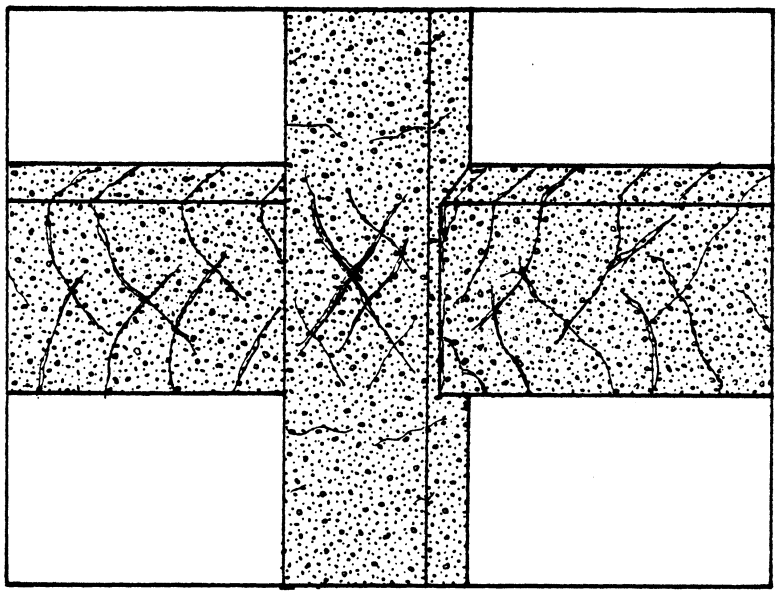

Fig. 3.1 Typical Cracking Pattern in an X-Series Specimen

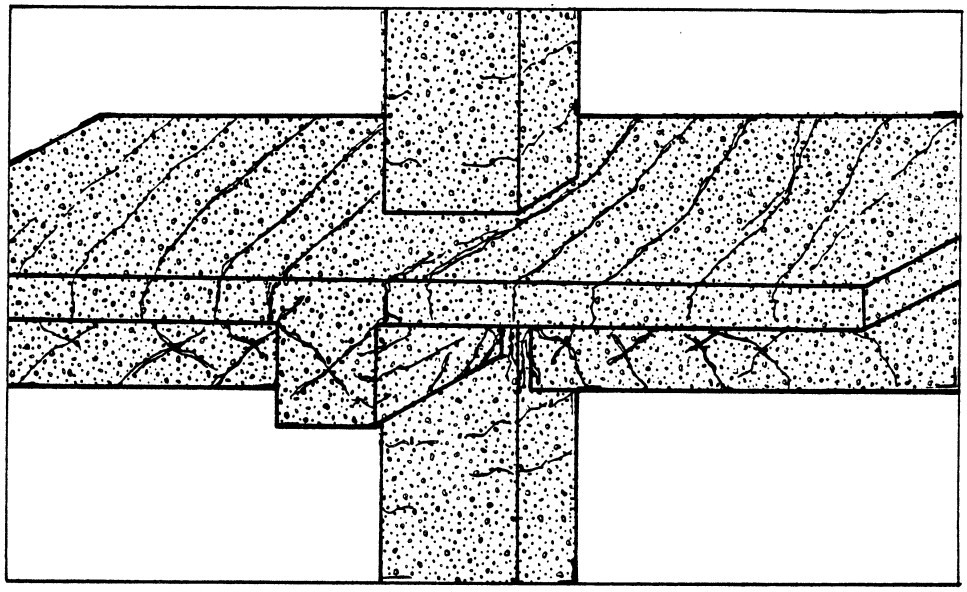

Fig. 3.2 Typical Cracking Pattern in a S-Series Specimen

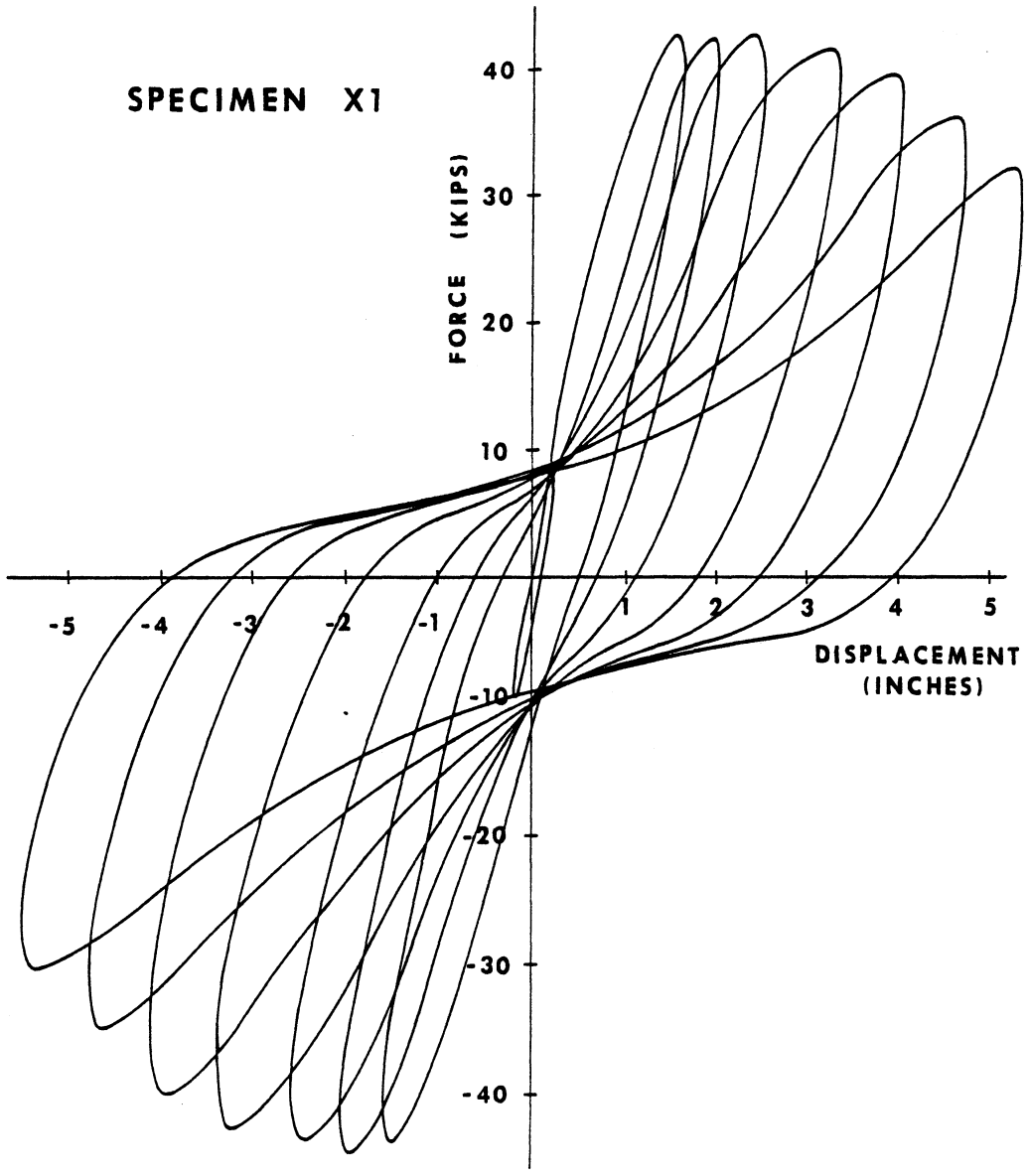

Fig. 3.3(a) Column Load vs. Column Load Point Displacement Hysteresis Curves for Specimen X1

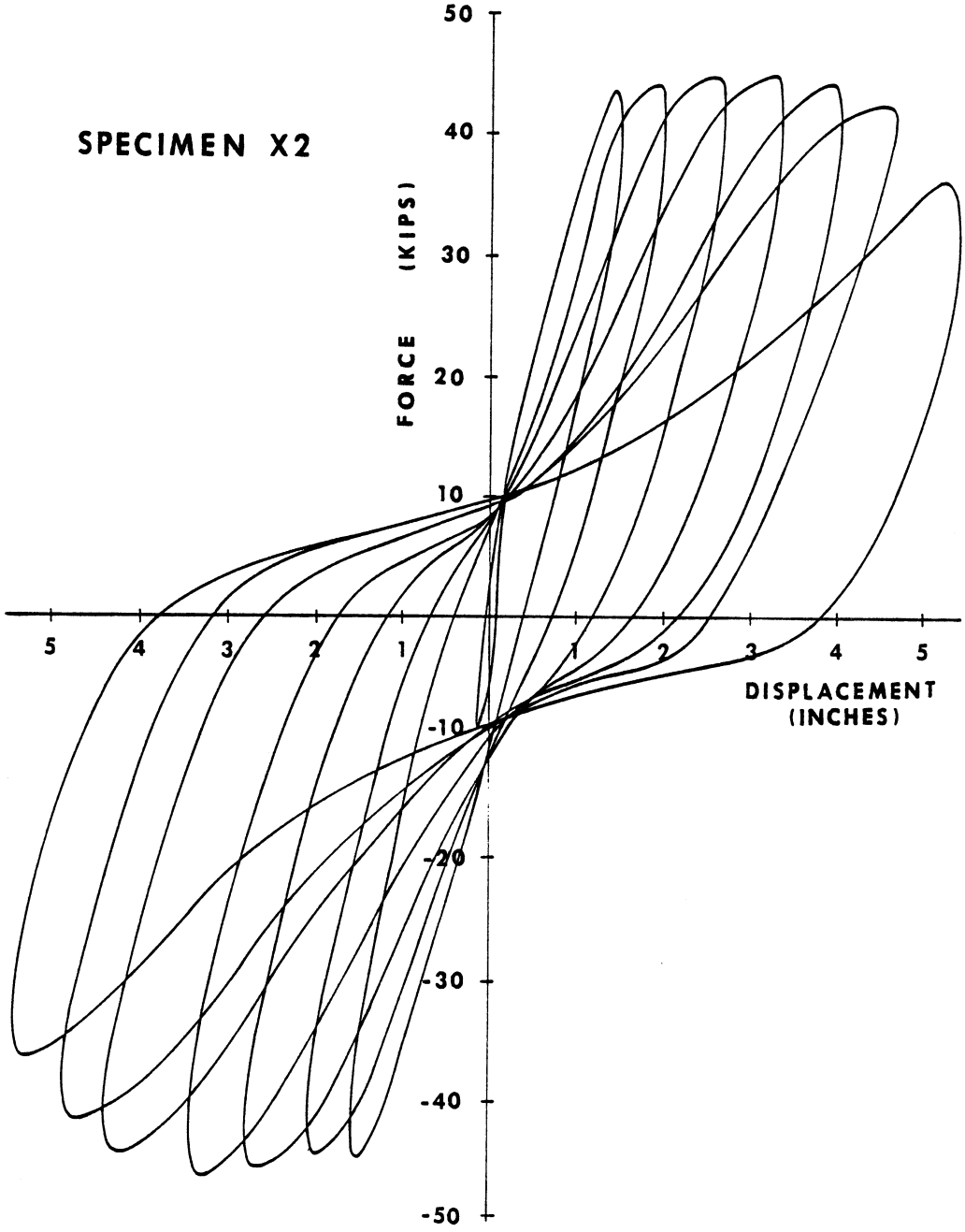

Fig. 3.3(b) Column Load vs. Column Load Point Displacement Hysteresis Curves for Specimen X2

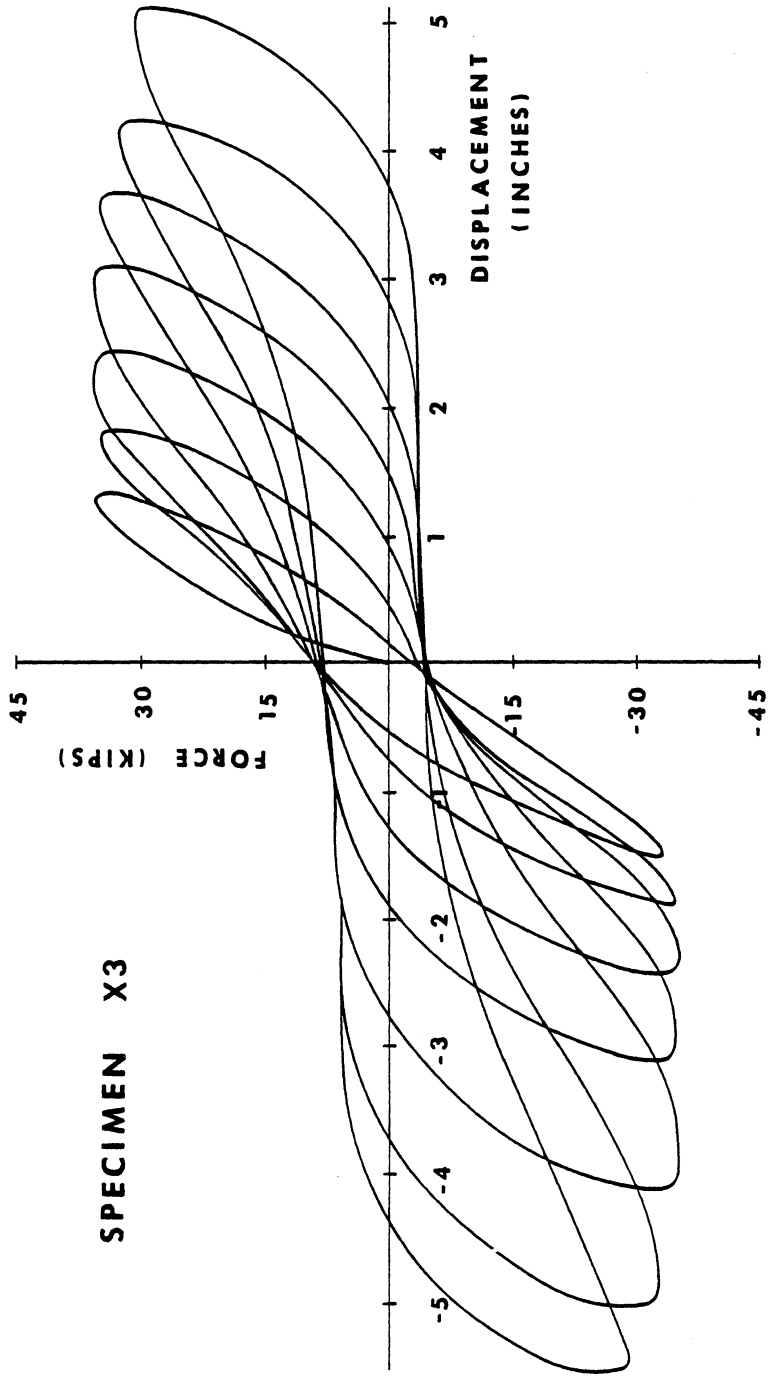

Fig. 3.3(c) Column Load vs. Column Load Point Displacement Hysteresis Curves for Specimen X3

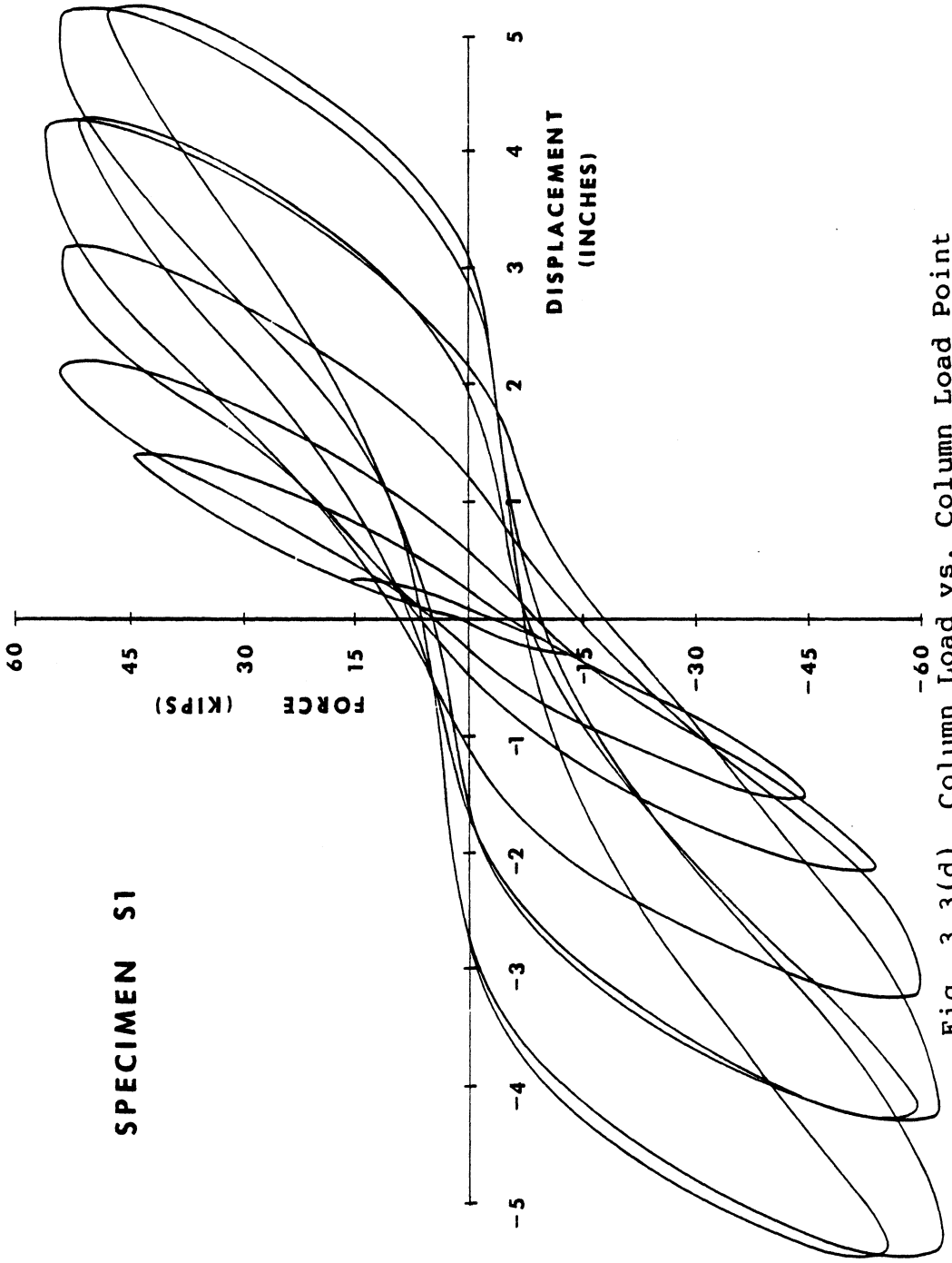

Fig. 3.3(d) Column Load vs. Column Load Point Displacement Hysteresis Curves for Specimen S1

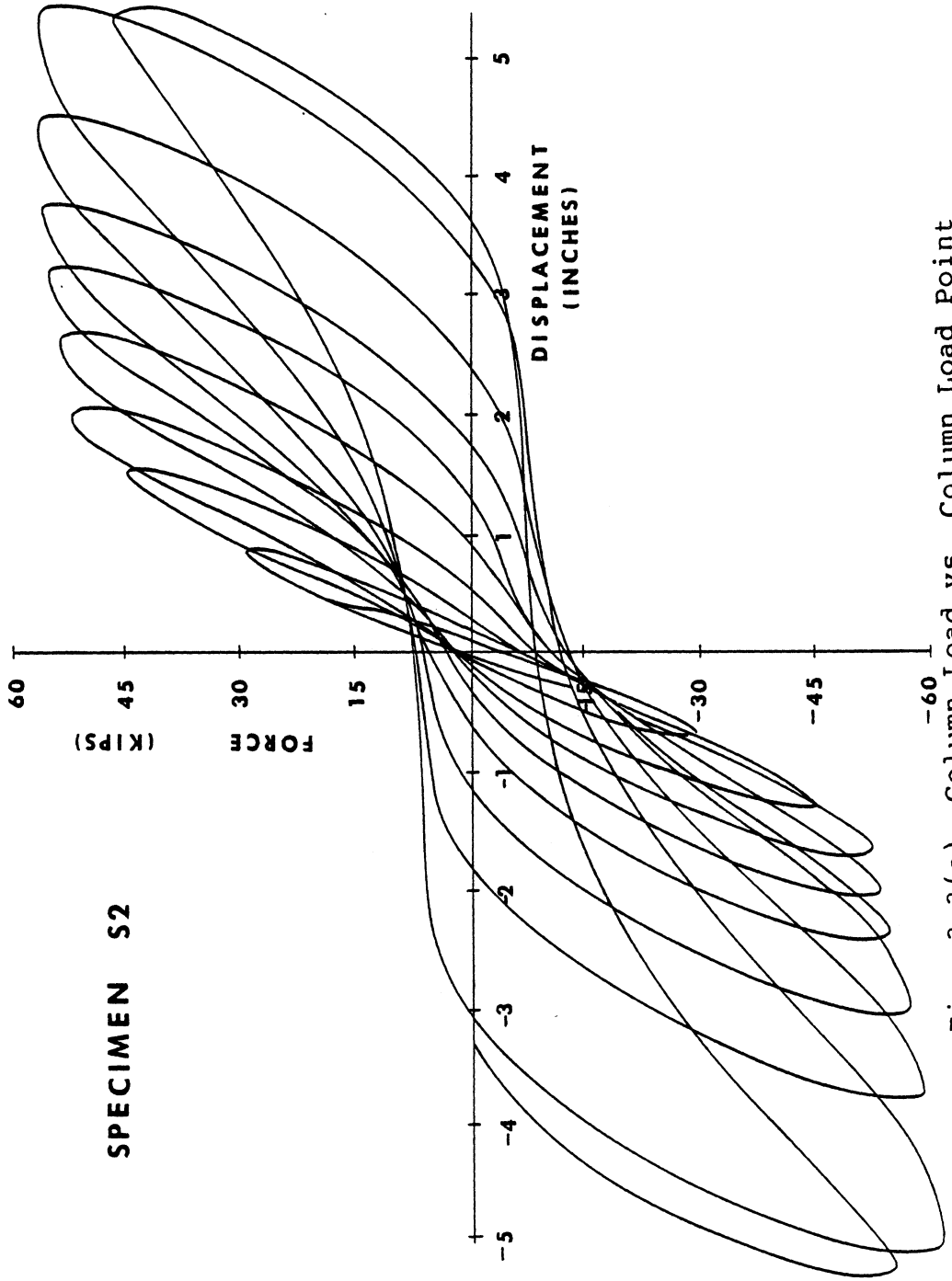

Fig. 3.3(e) Column Load vs. Column Load Point Displacement Hysteresis Curves for Specimen S2

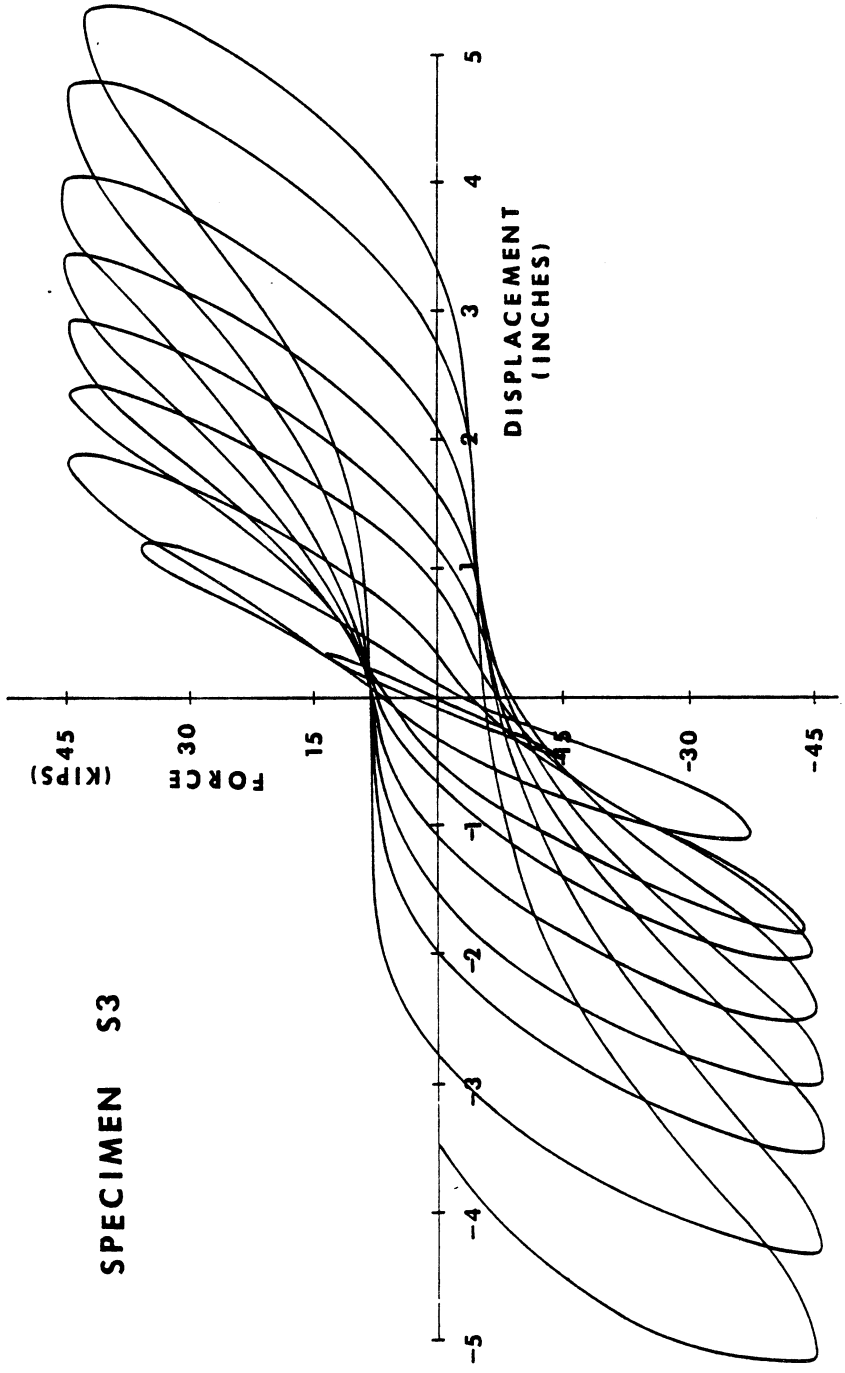

Fig. 3.3(f) Column Load vs. Column Load Point Displacement Hysteresis Curves for Specimen S3

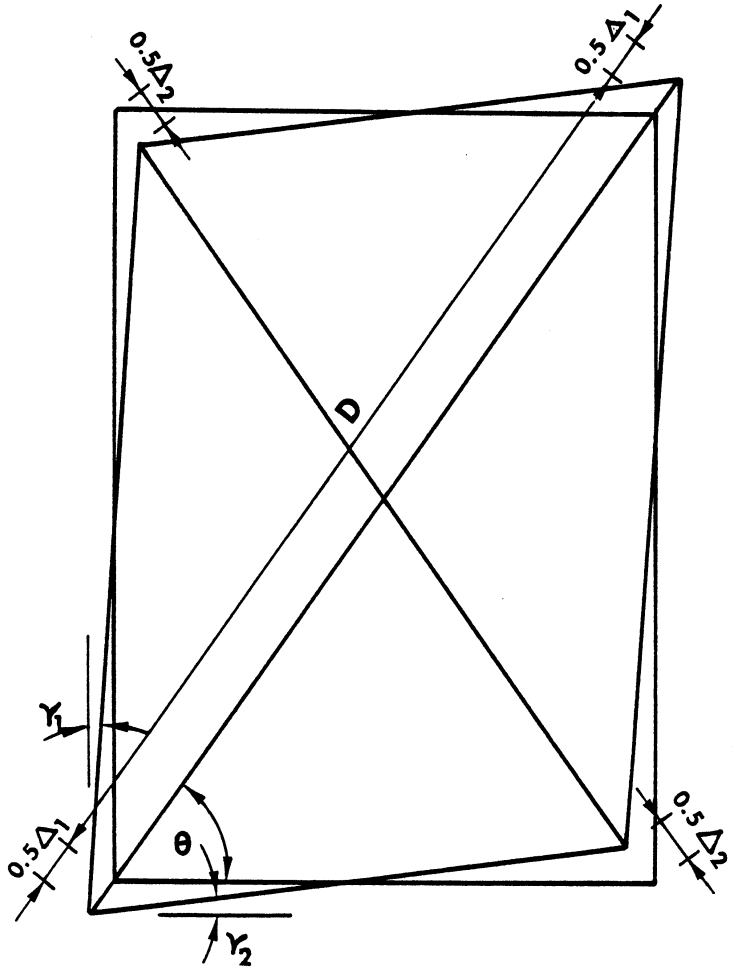

Fig. 3.4 Joint Shear Deformation Model

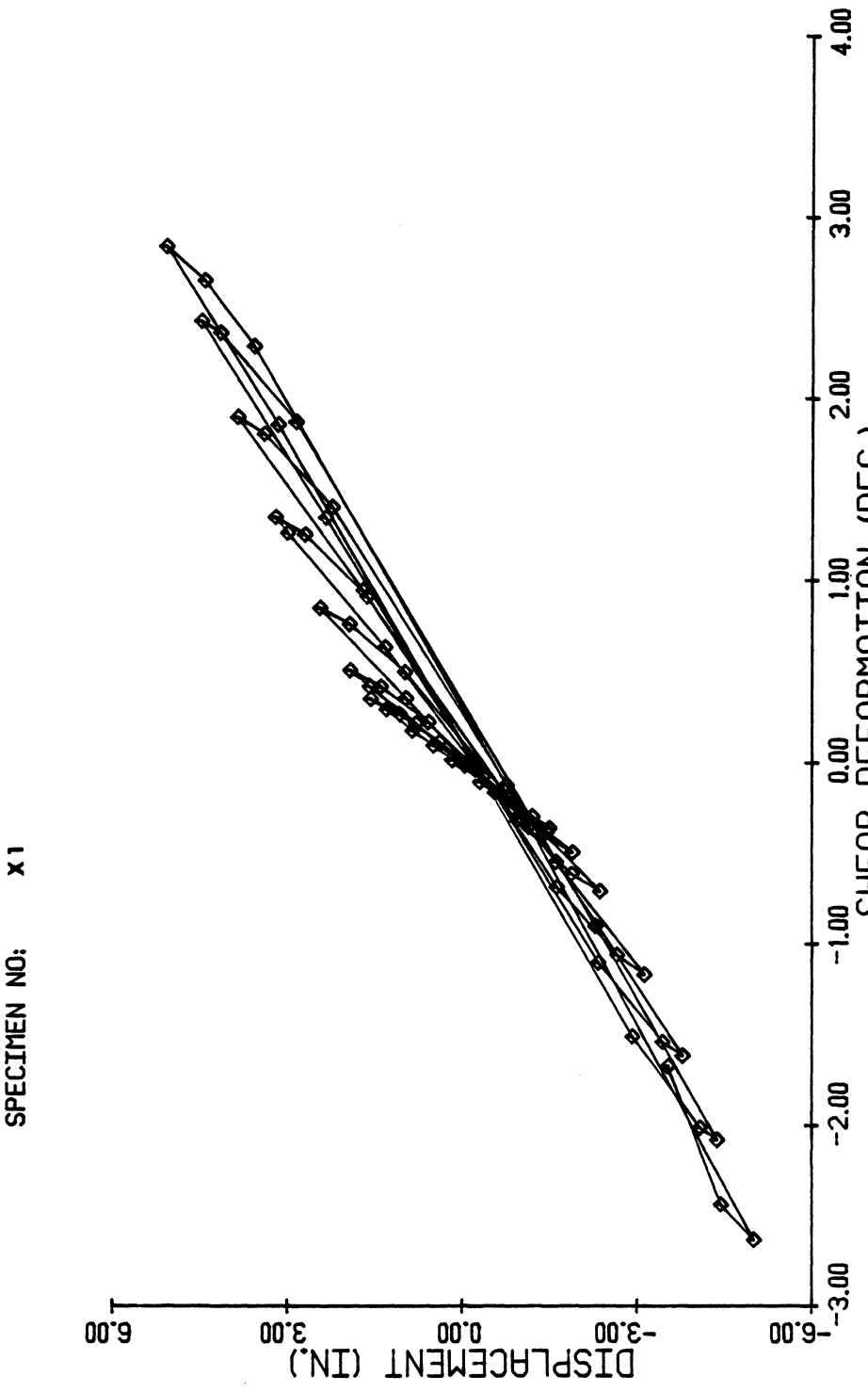

Fig. 3.5(a) Column Load Point Displacemnet vs. Joint Shear Deformation for Specimen X1

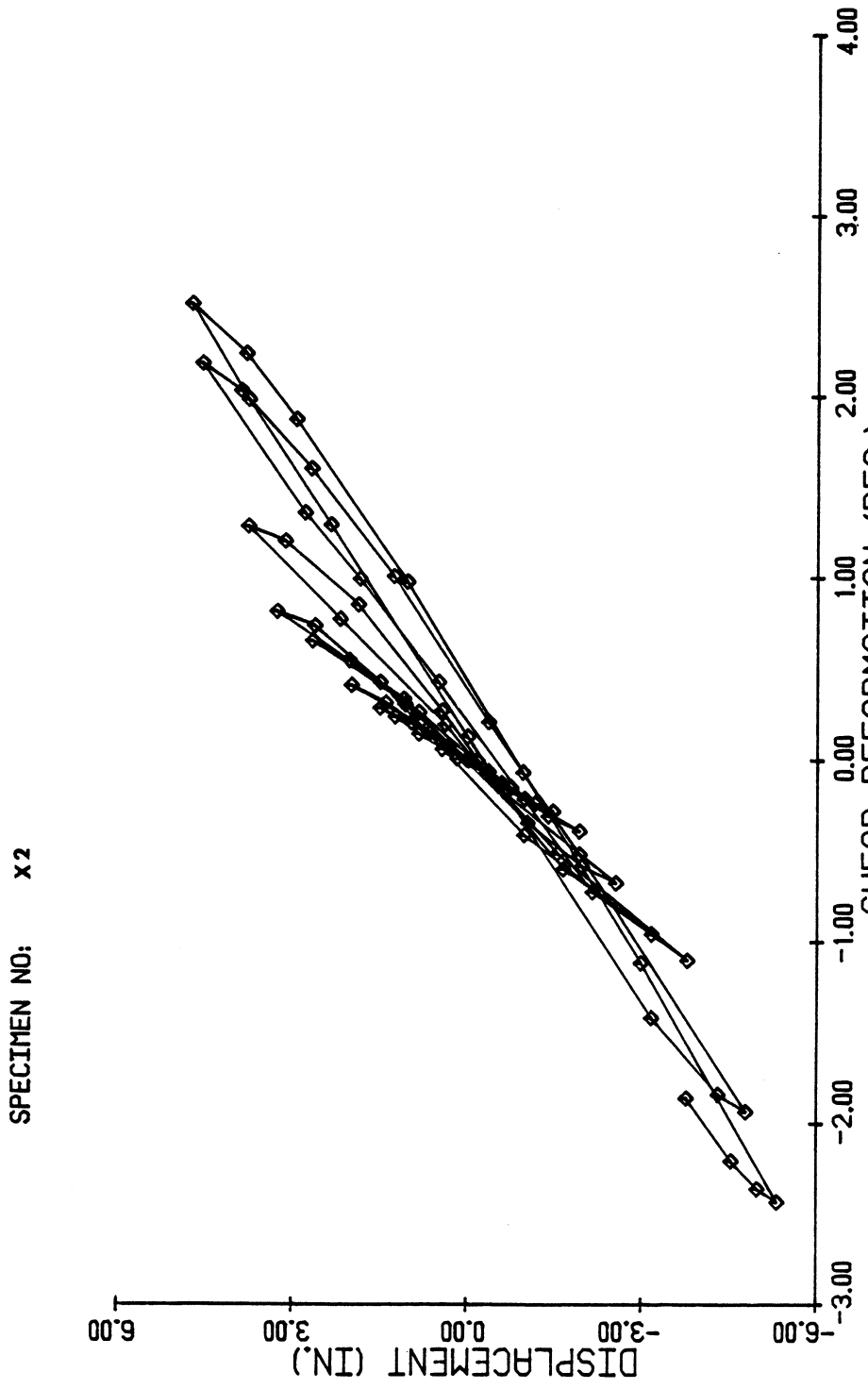

Fig. 3.5(b) Column Load Point Displacement vs. Joint Shear Deformation for Specimen X2

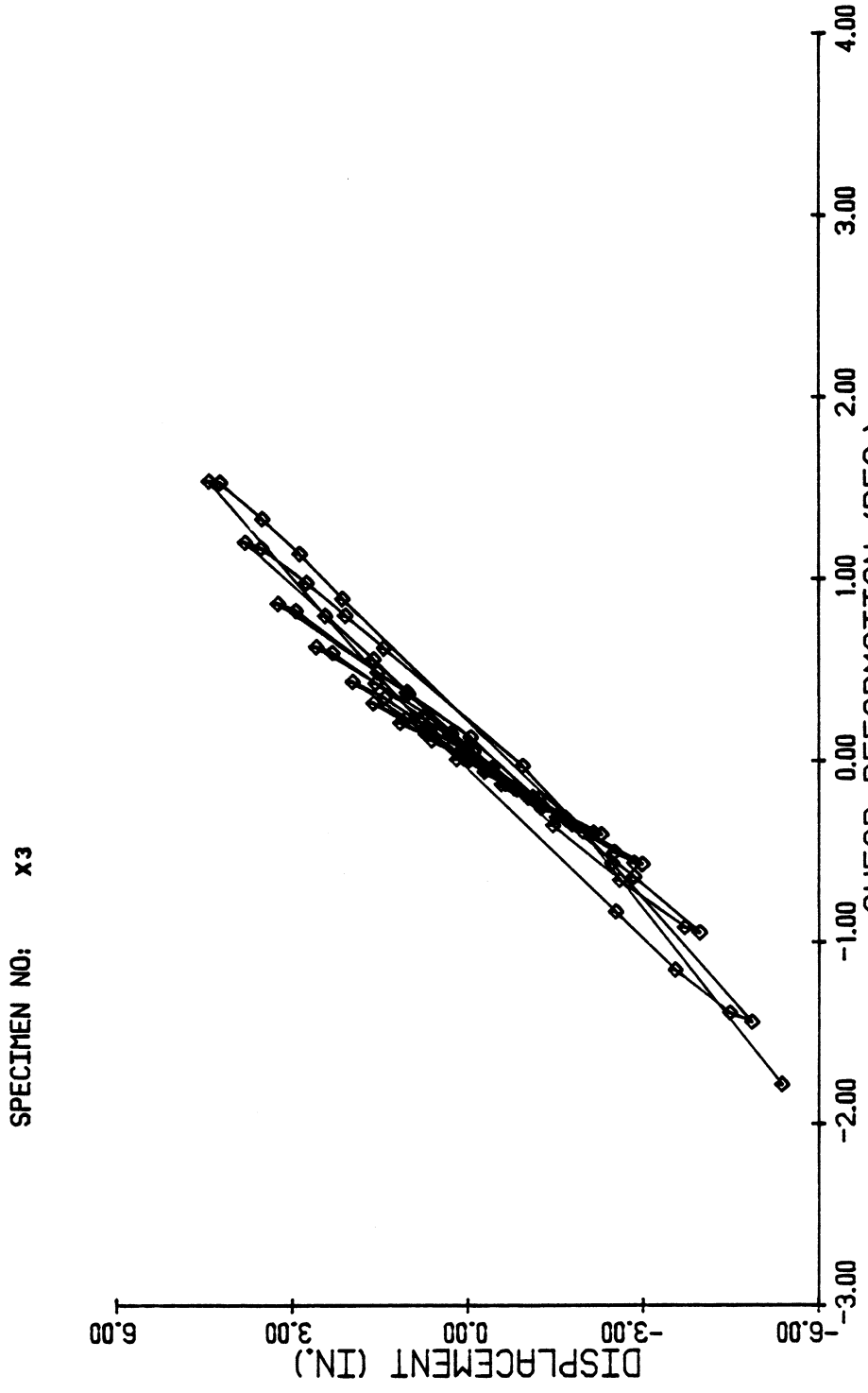

Fig. 3.5(c) Column Load Point Displacement vs. Joint Shear Deformation for Specimen X3

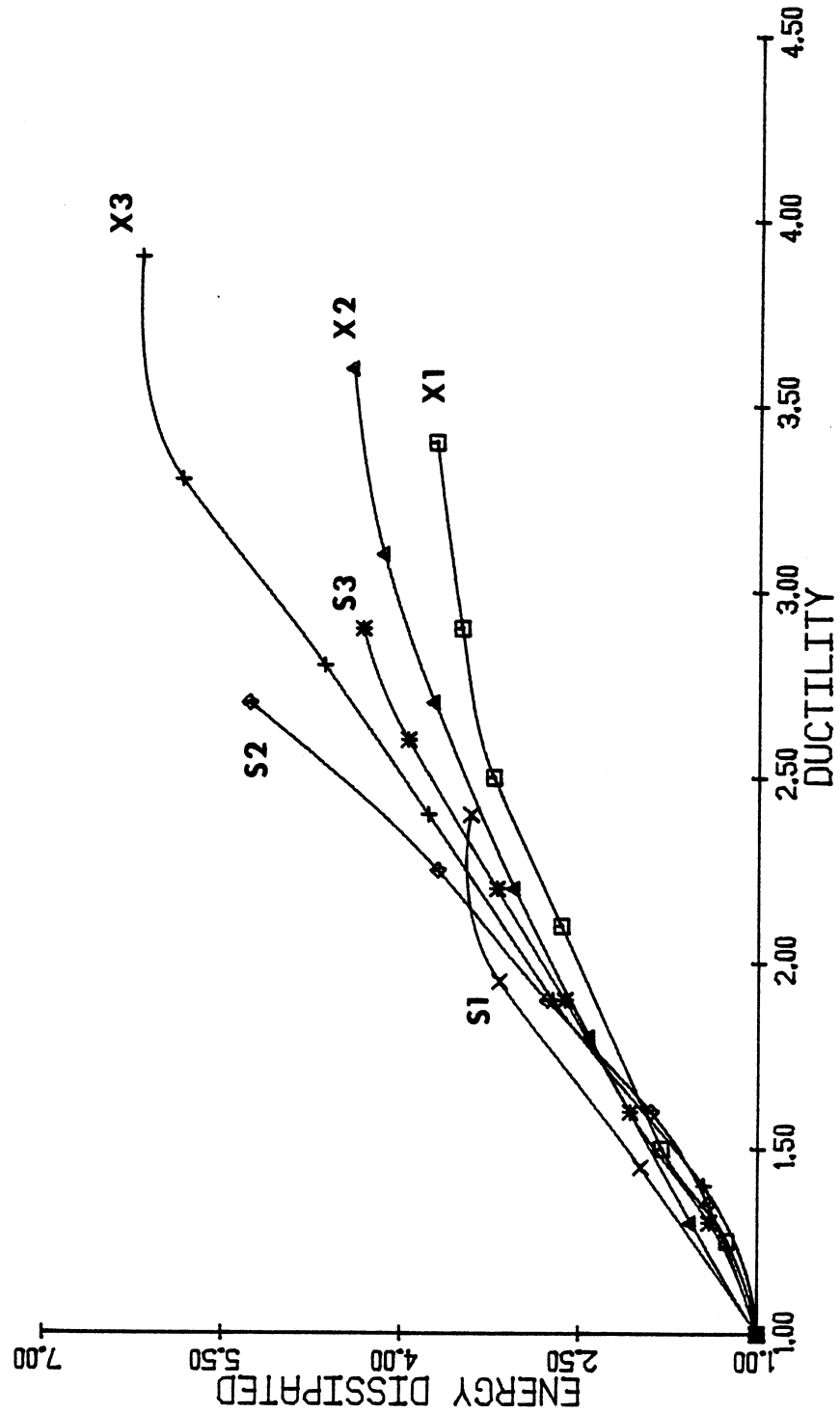

Fig. 3.6 Normalized Energy Dissipation vs. Displacement Ductilities for all Specimens

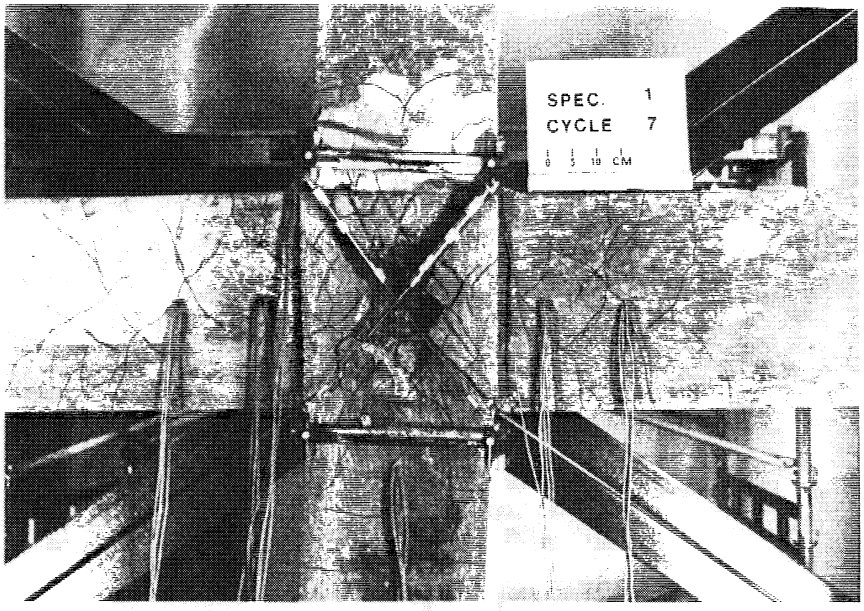

Fig. 3.7 Cracks in Specimen X1 at the End of Seventh Loading Cycle

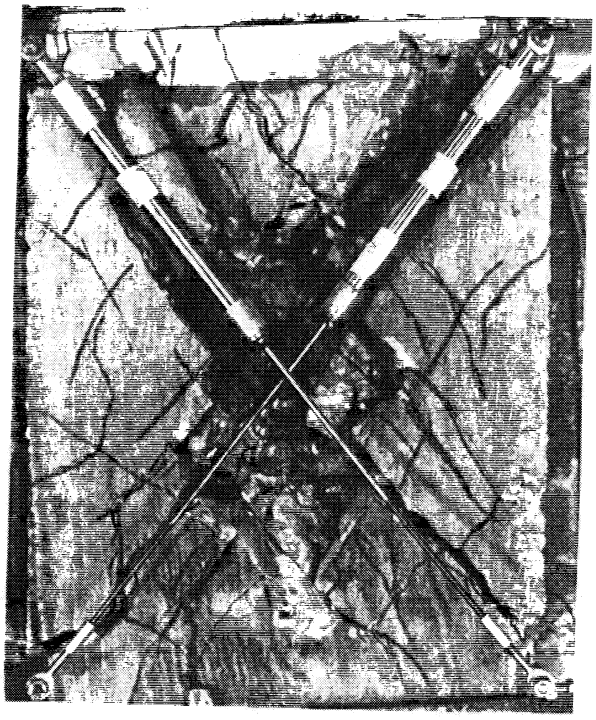

Fig. 3.8 Formation of Hollow Joint Core at the Intersection of Diagonal Cracks

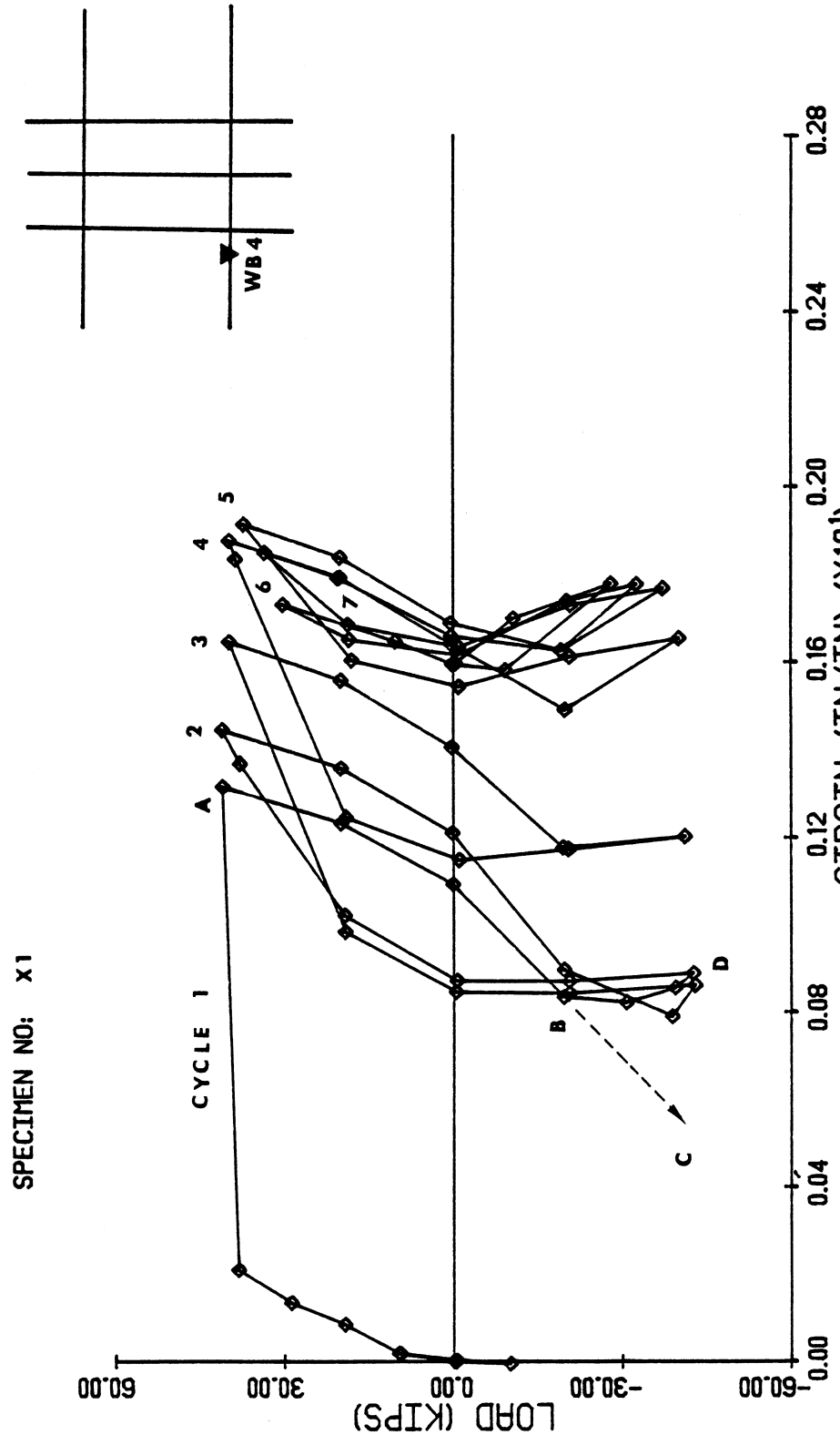

Fig. 3.9 Column Load vs. Strain in Main Beam Reinforcement at WB4 for Specimen X1

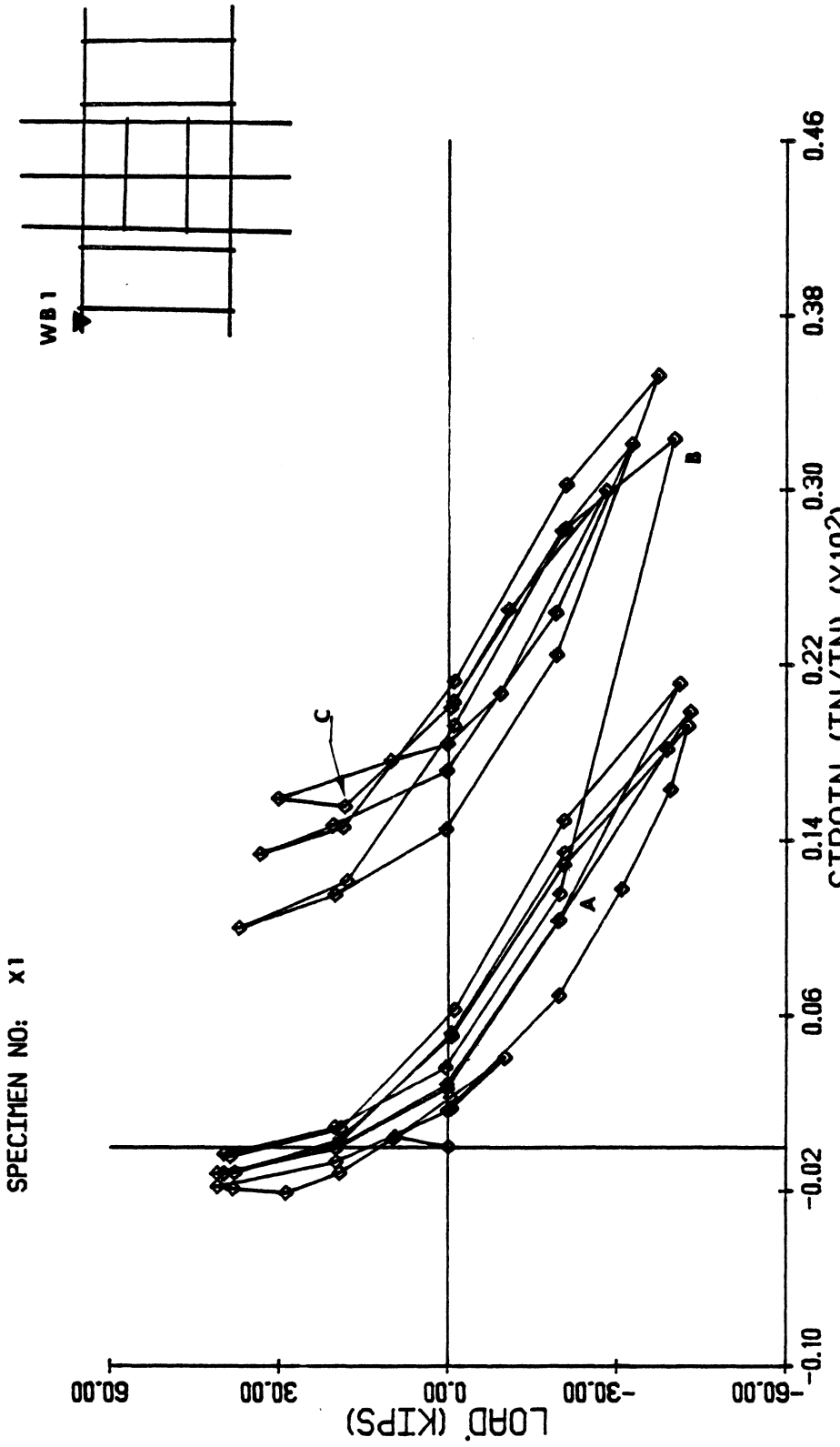

Fig. 3.10 Column Load vs. Strain in Main Beam Reinforcement at WB1 for Specimen X1

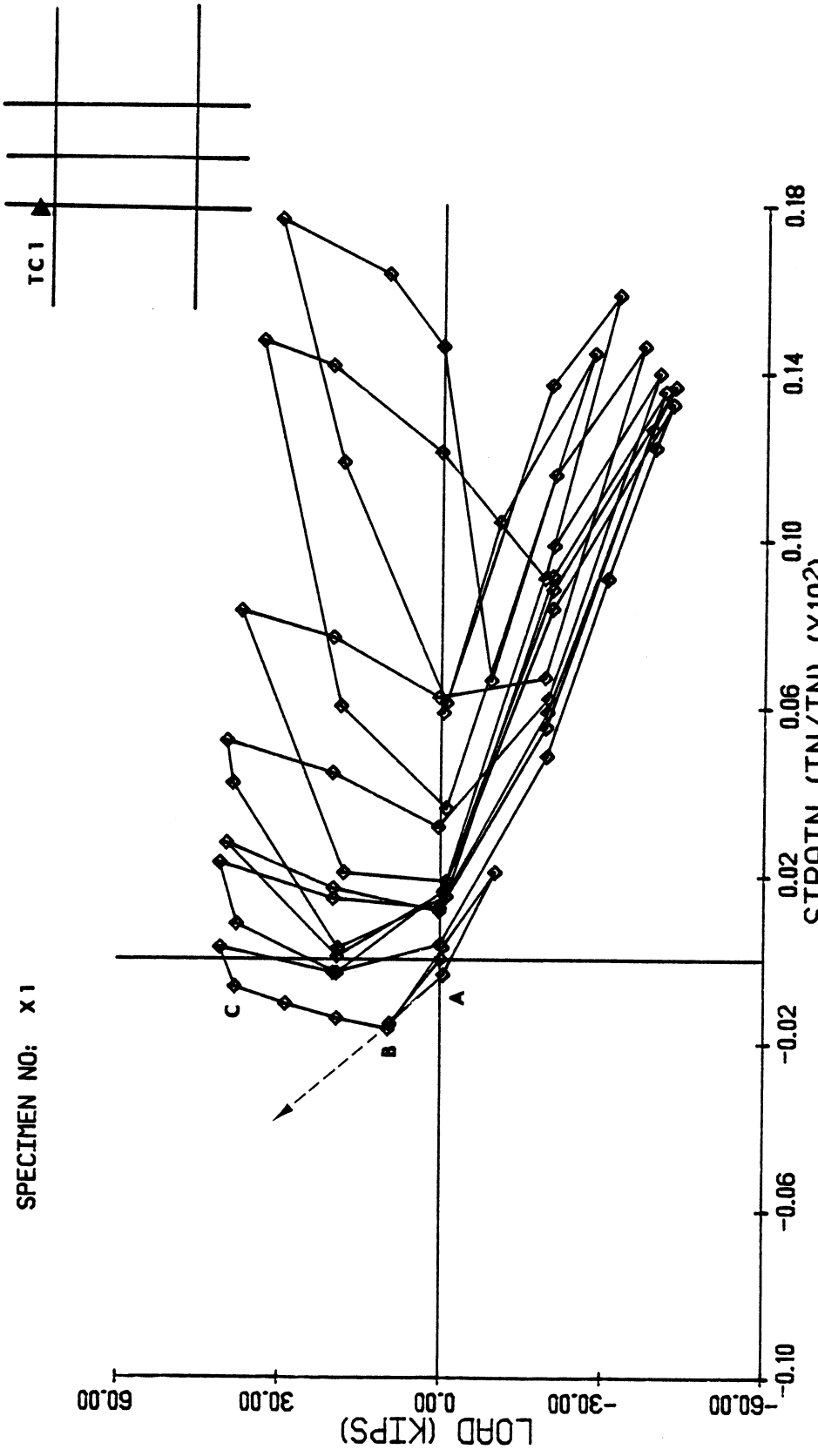

Fig. 3.11 Column Load vs. Strain in Column Reinforcement at TC1 for Specimen X1

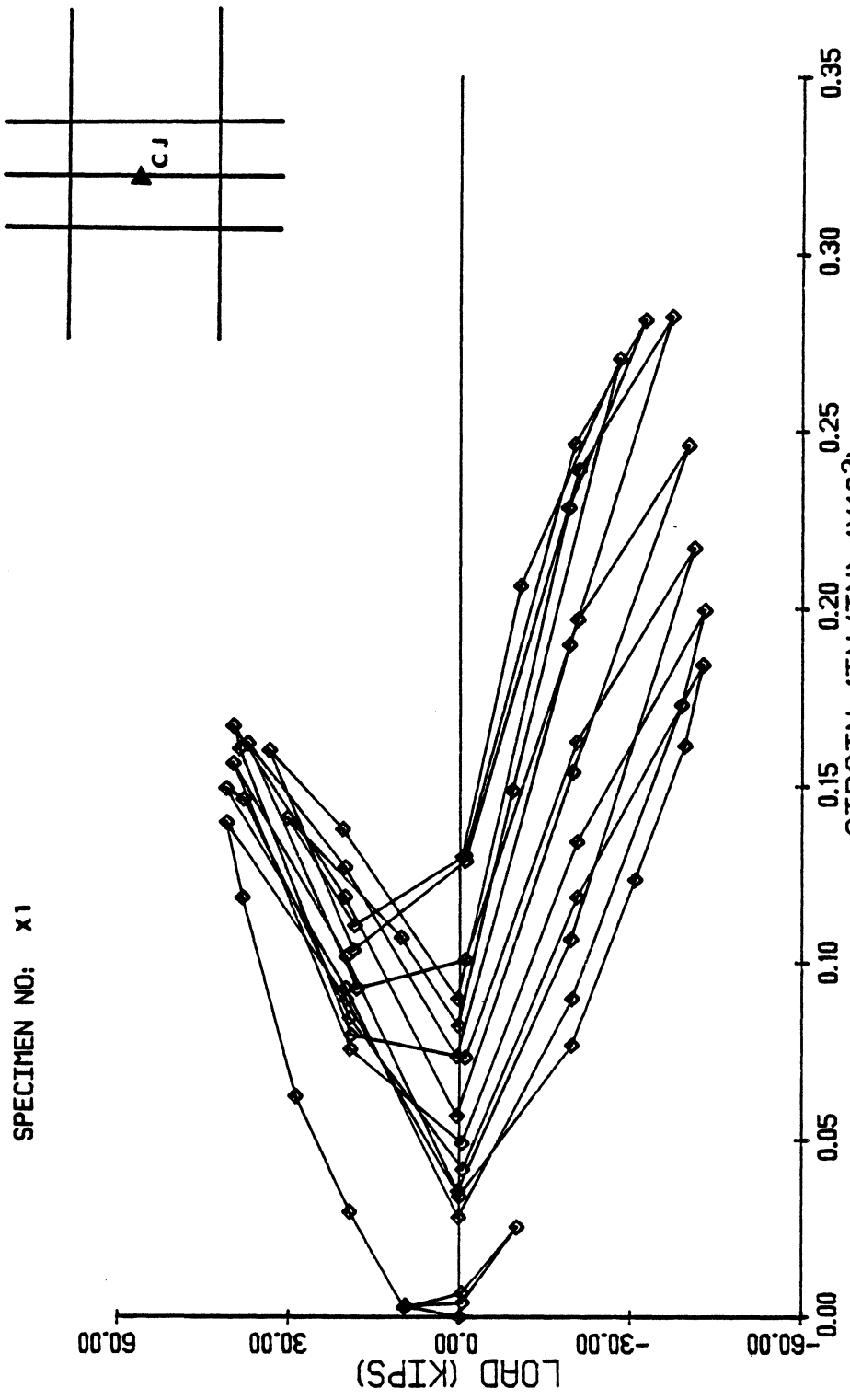

Fig. 3.12 Column Load vs. Strain in Column Reinforcement at CJ for Specimen X1

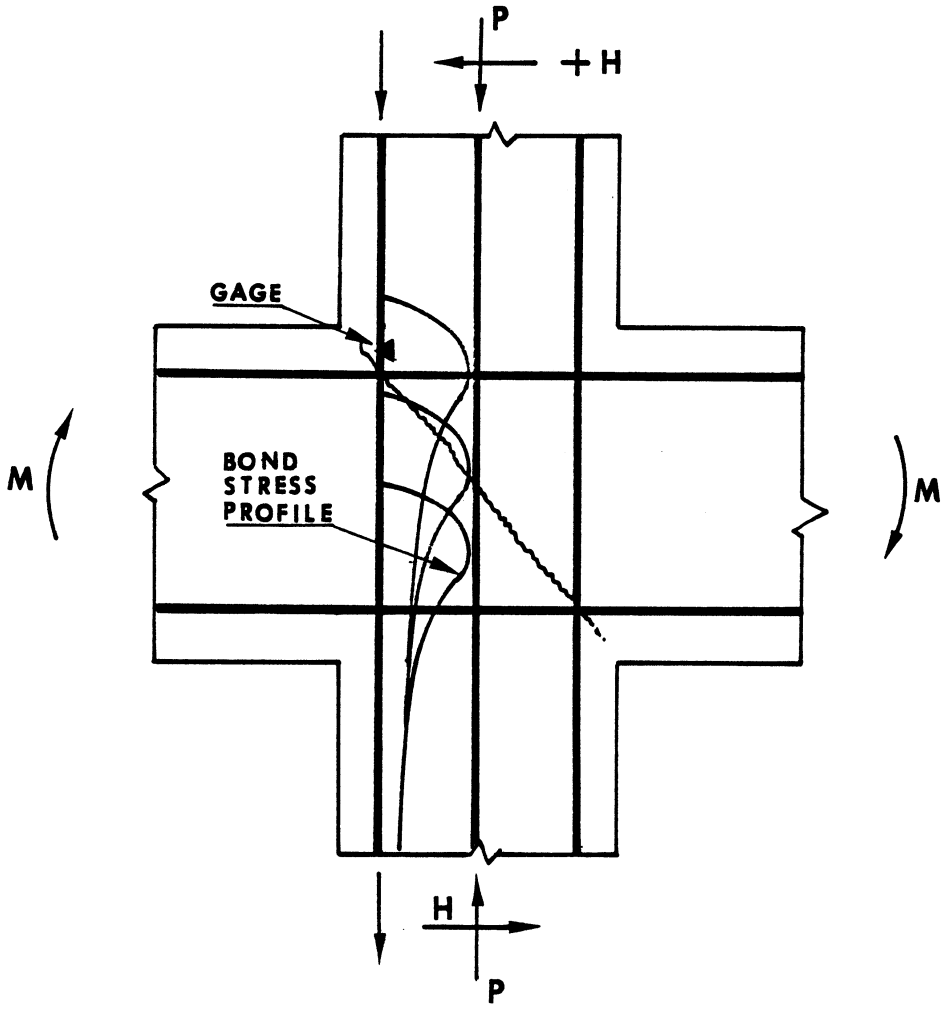

Fig. 3.13 Propagation of Bond Stress with Slippage in the Column Bars

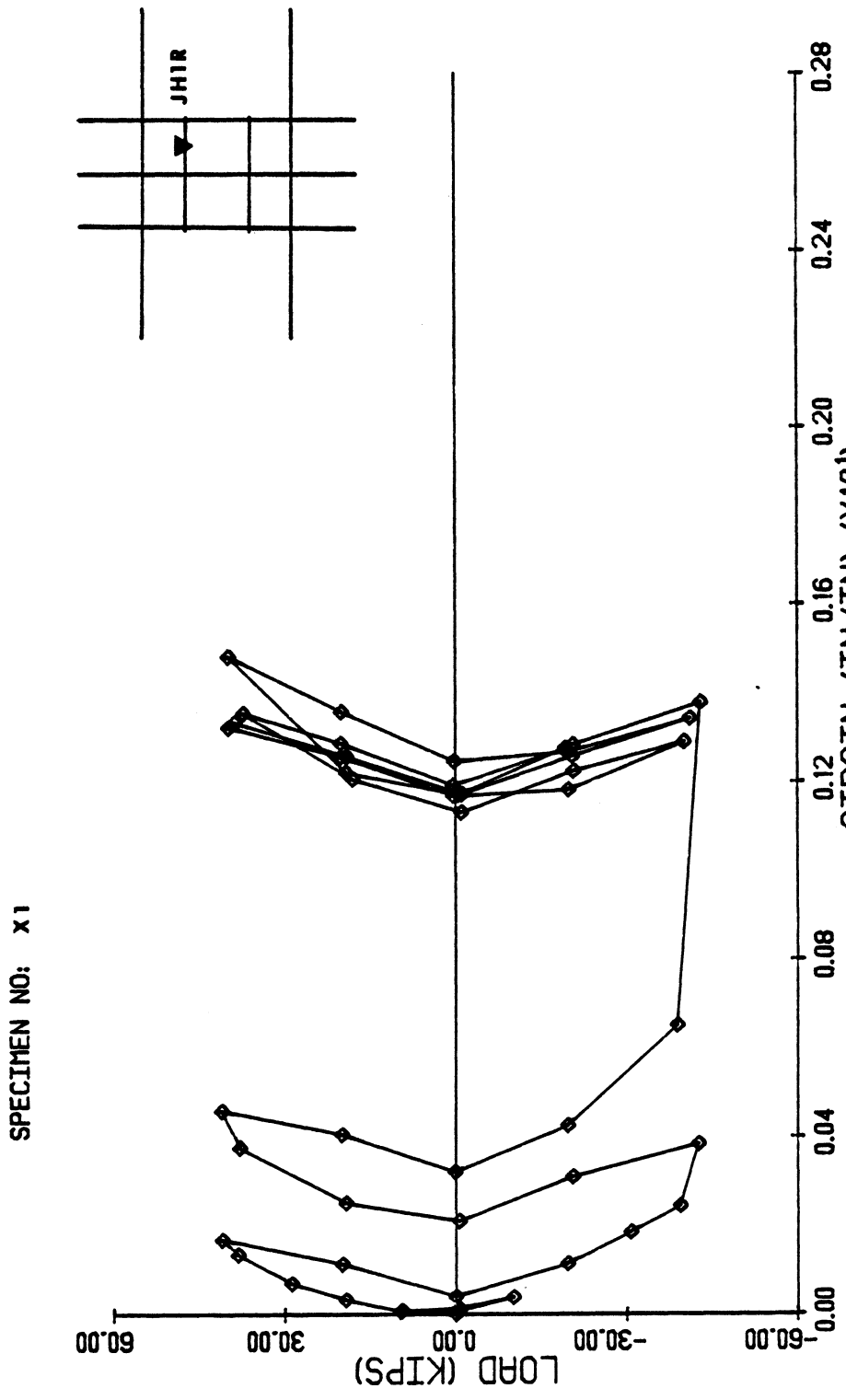

Fig. 3.14 Column Load vs. Strain in Square Joint Hoop at JH1R for Specimen X1

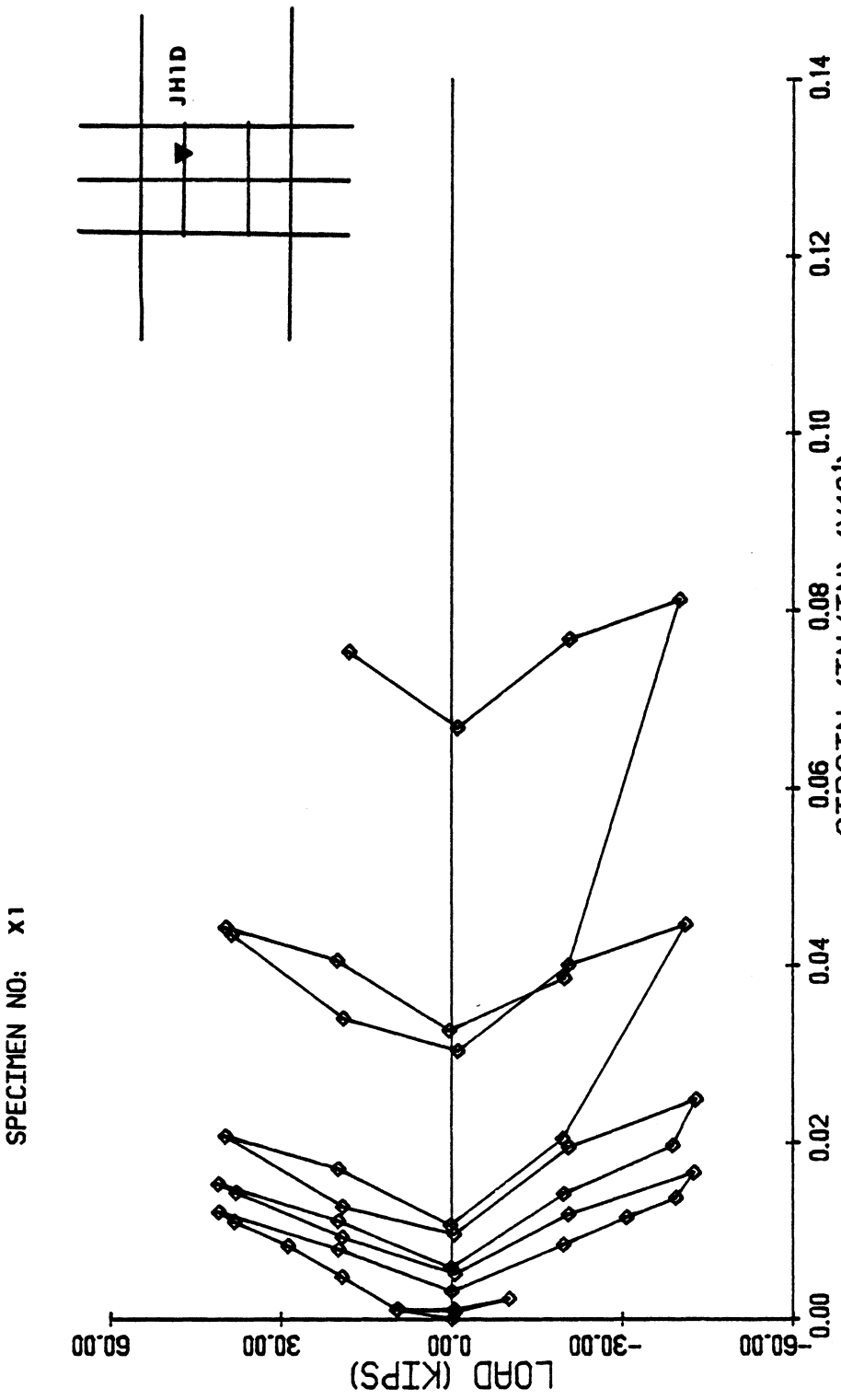

Fig. 3.15 Column Load vs. Strain in Diamond Shape Joint Hoop at JH1D for Specimen X1

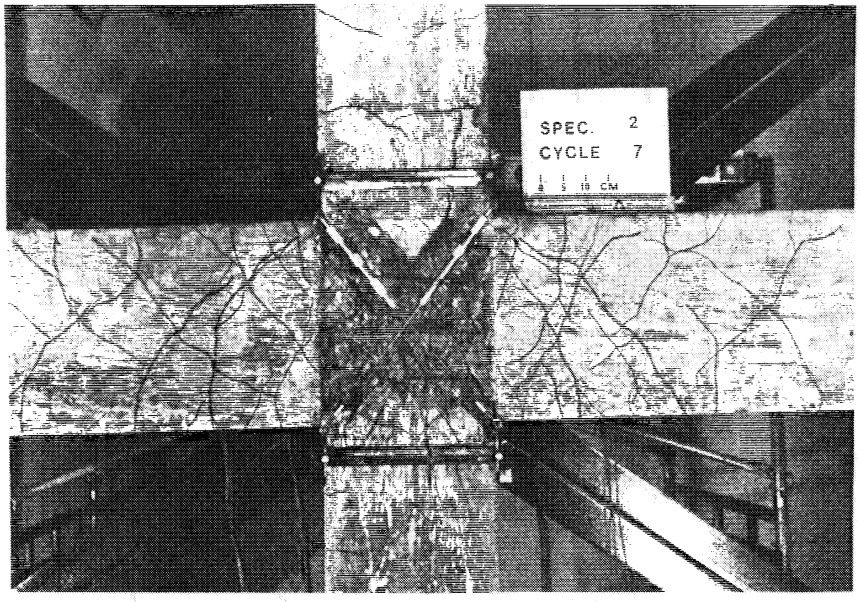

Fig. 3.16 Specimen X2 at the End of Seventh Loading Cycle

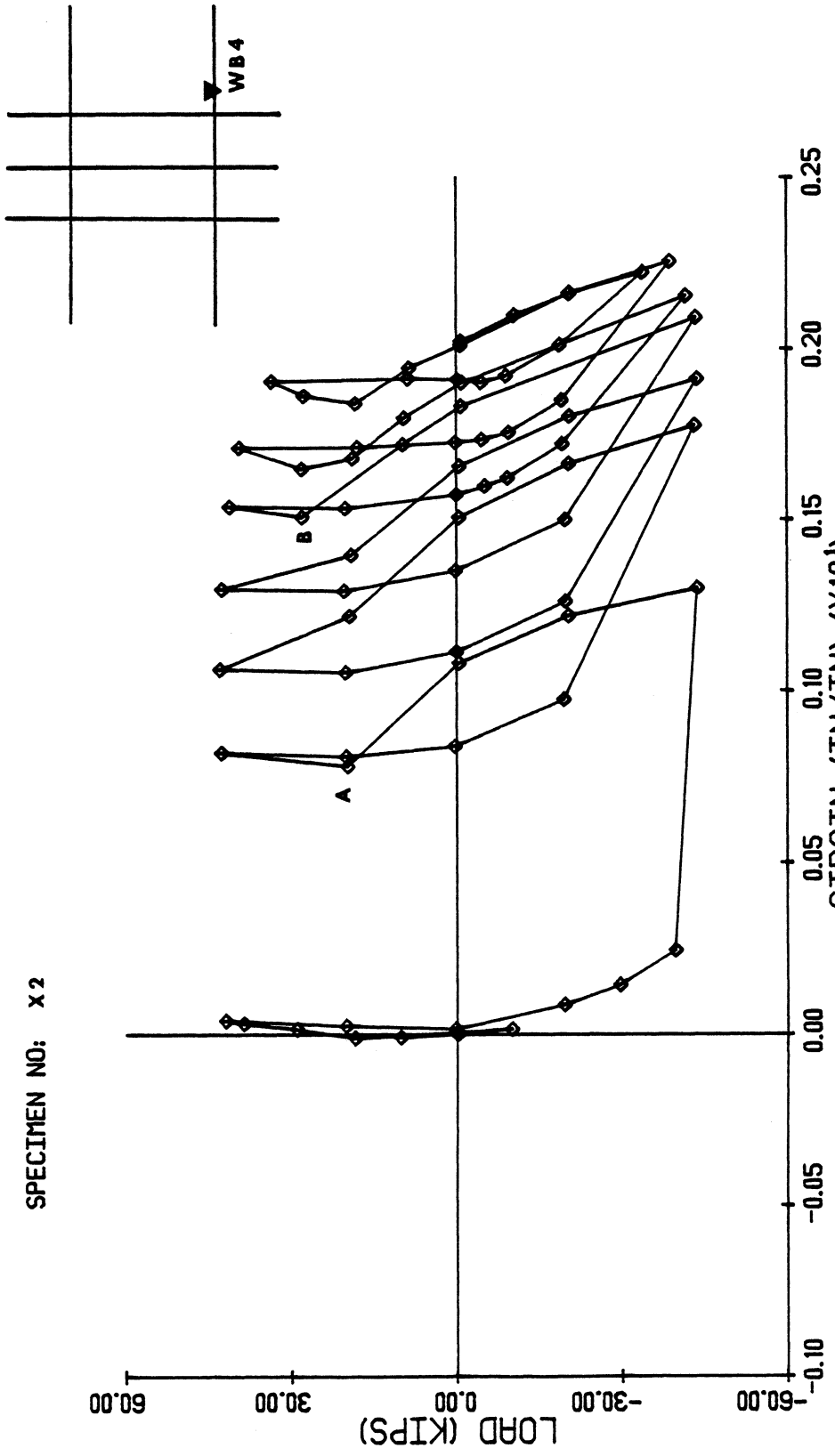

Fig. 3.17 Column Load vs. Strain in Main Beam Reinforcement at WB4 for Specimen X2

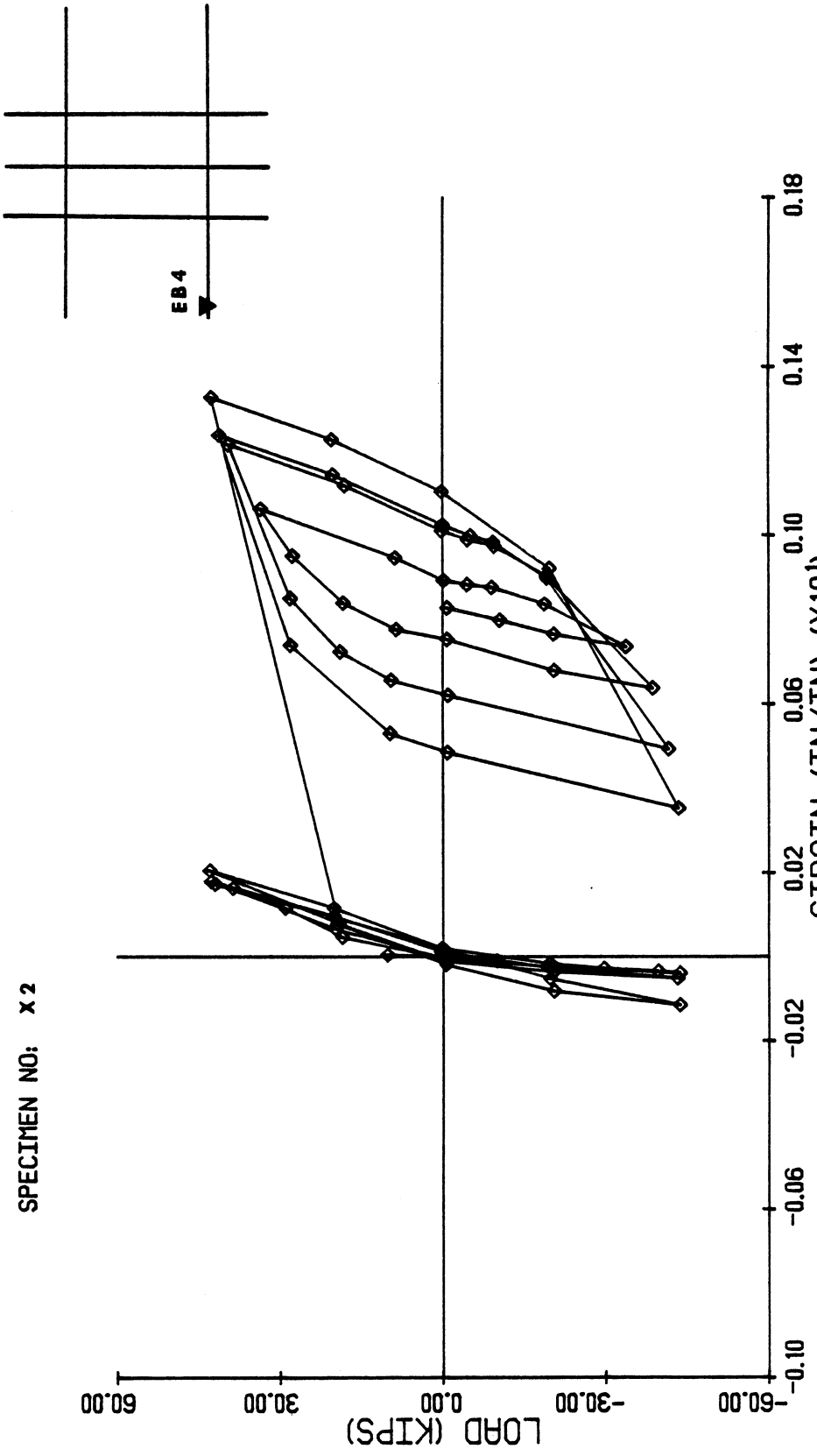

Fig. 3.18 Column Load vs. Strain in Main Beam Reinforcement at EB4 for Specimen X2

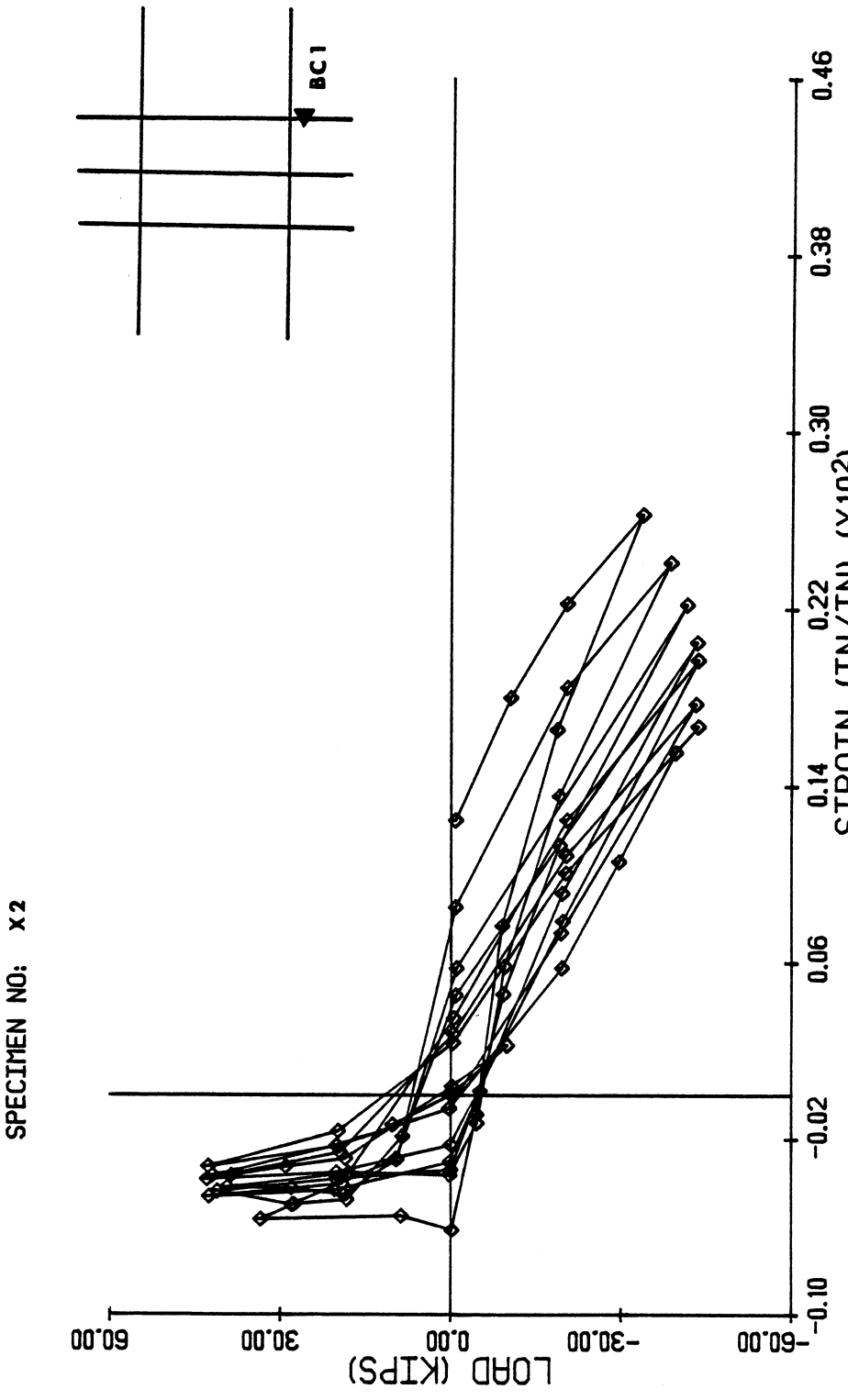

Fig. 3.19 Column Load vs. Strain in Column Reinforcement at BC1 for Specimen X2

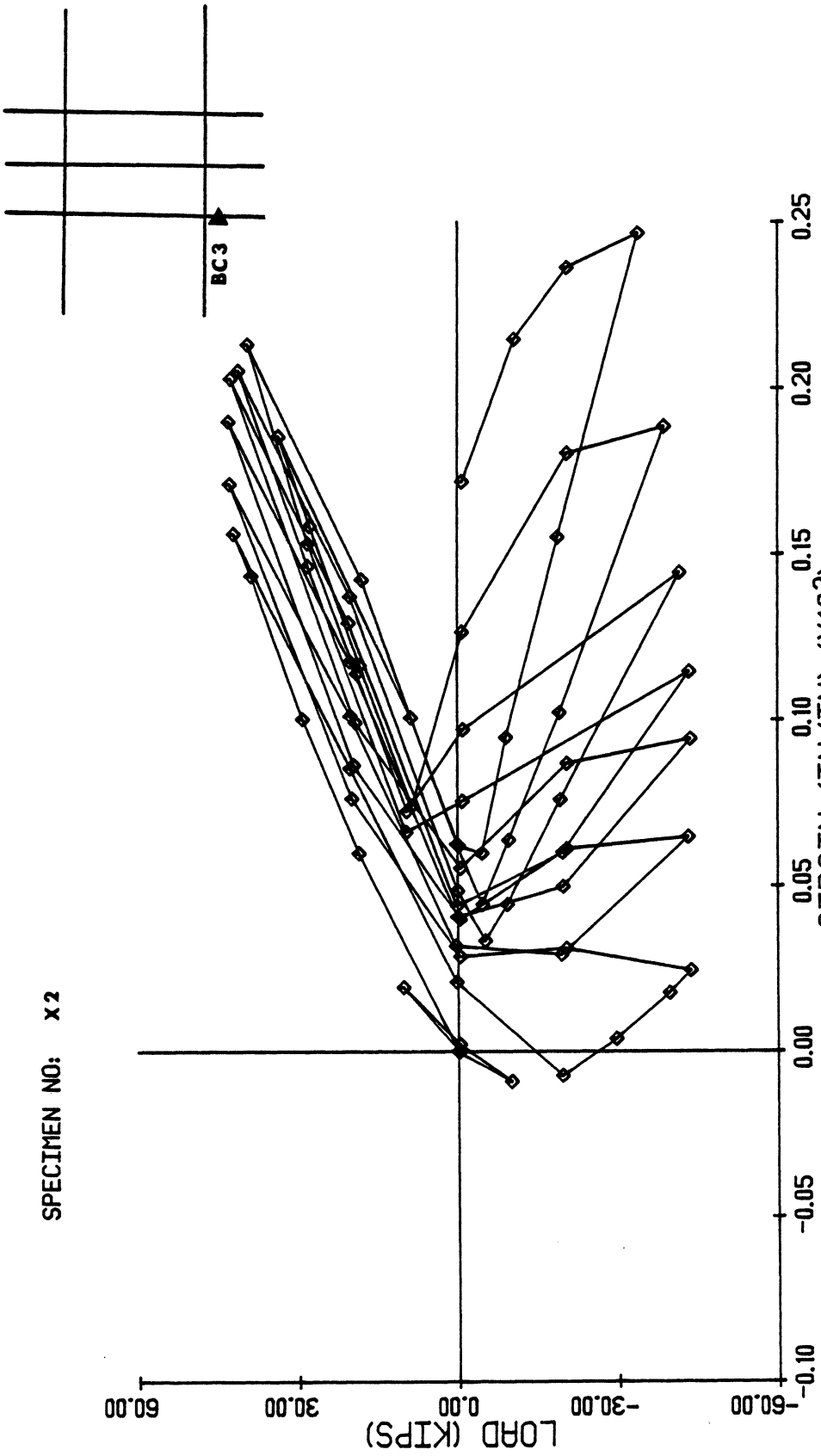

Fig. 3.20 Column Load vs. Strain in Column Reinforcement at BC3 for Specimen X2

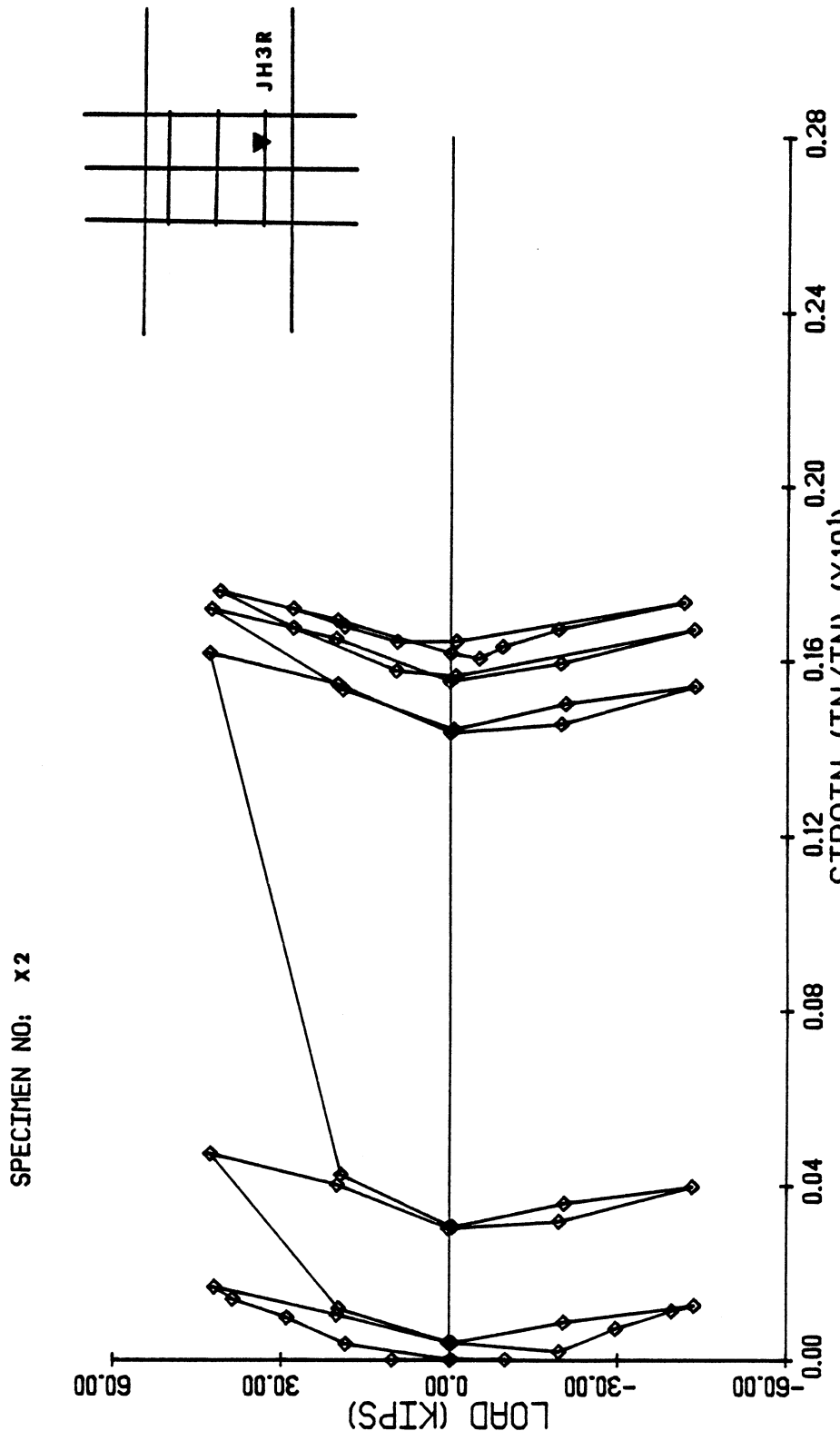

Fig. 3.21 Column Load vs. Strain in Square Joint Hoop at JH3R for Specimen X2

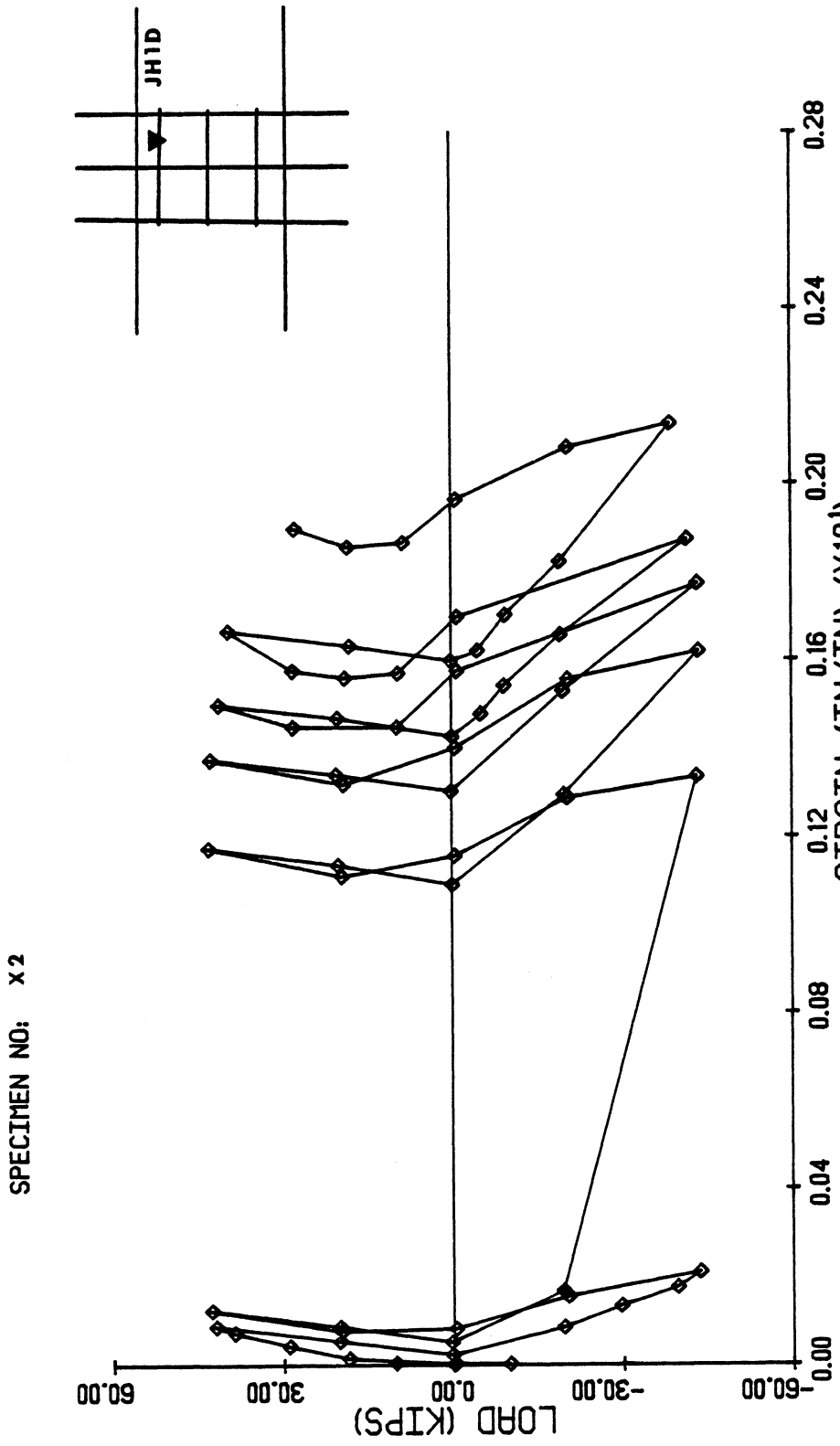

Fig. 3.22 Column Load vs. Strain in Diamond Shape Joint Hoop at JH1D for Specimen X2

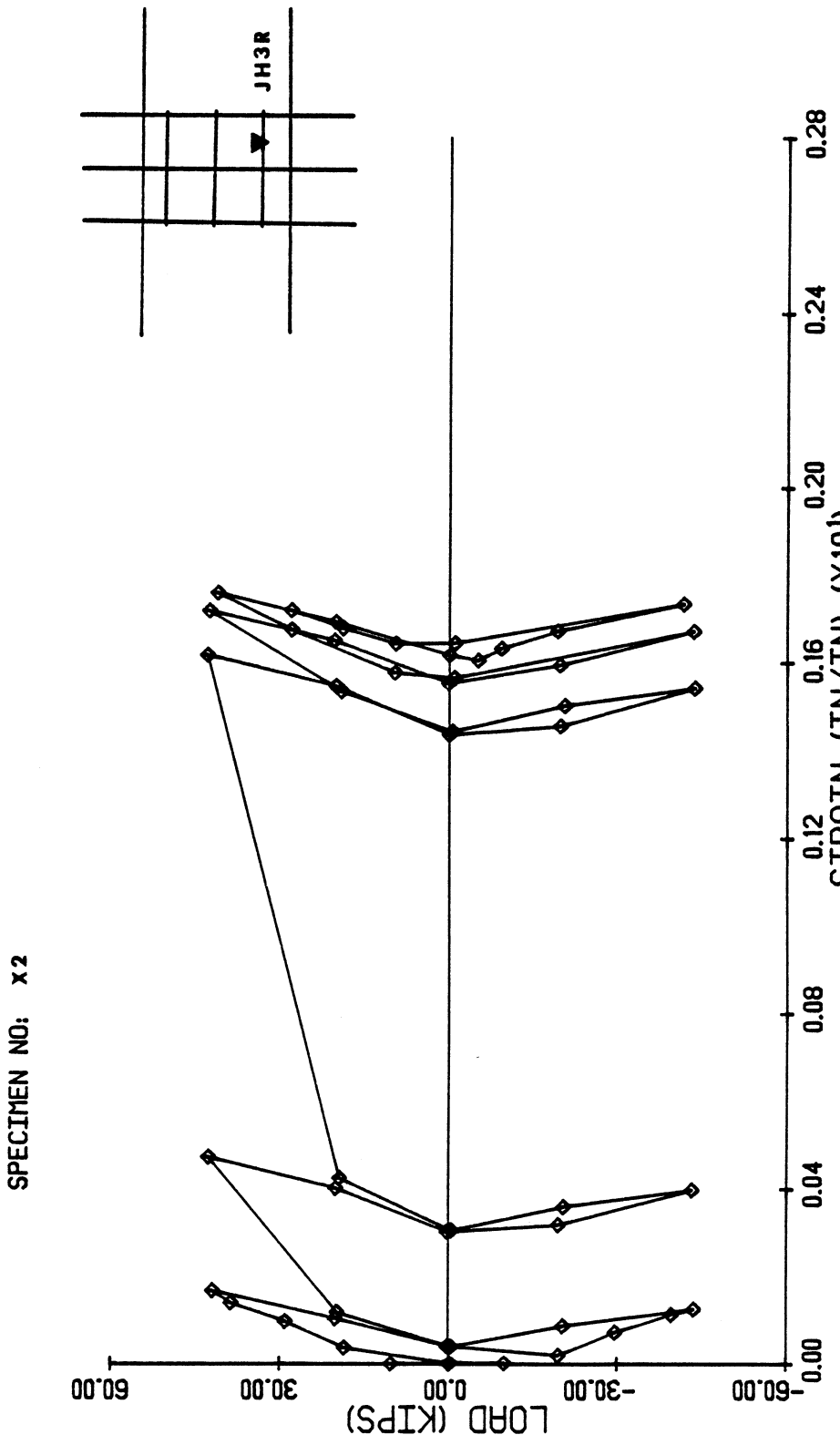

Fig. 3.21 Column Load vs. Strain in Square Joint Hoop at JH3R for Specimen X2

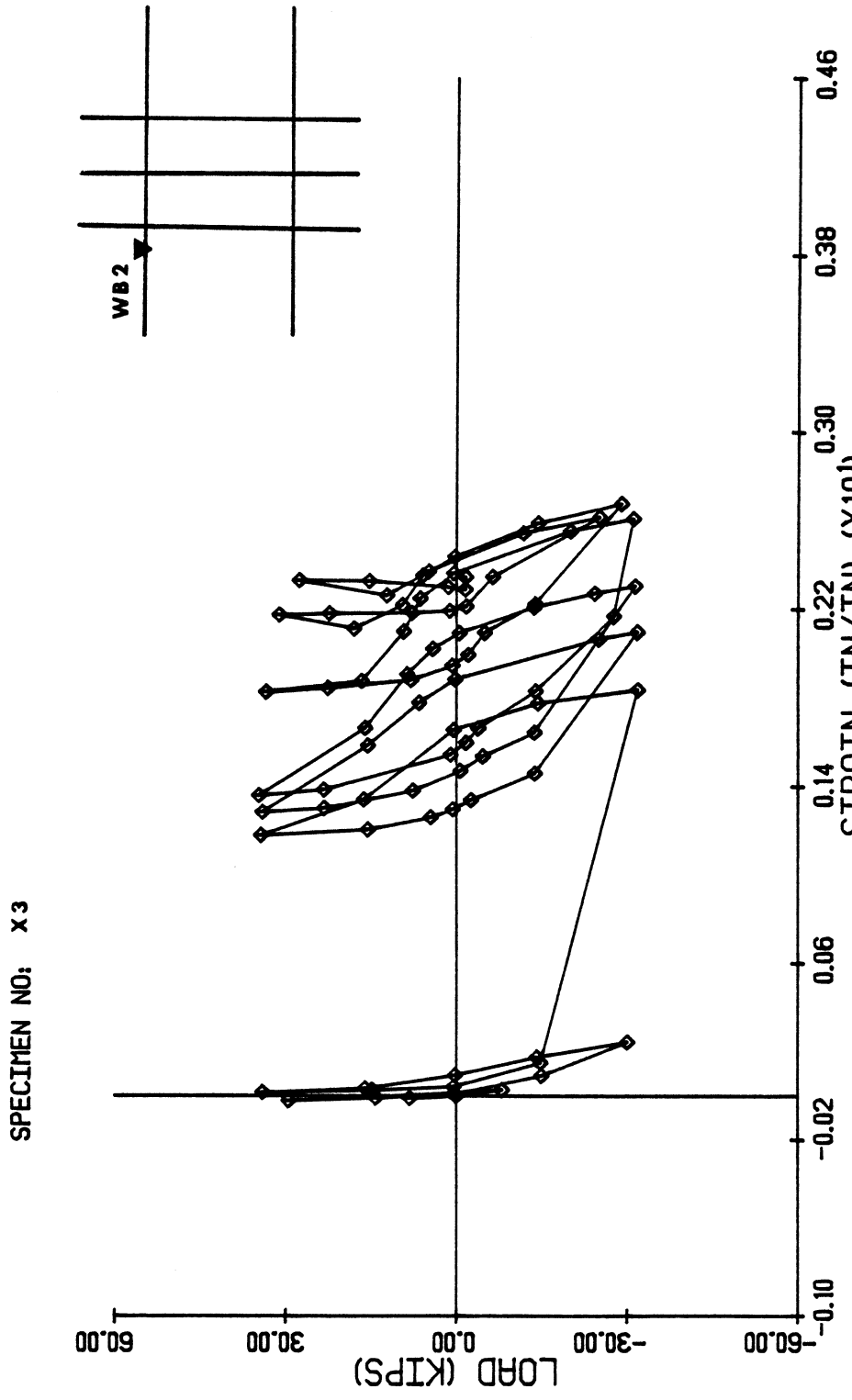

Fig. 3.25 Column Load vs. Strain in Main Beam Reinforcement at WB3 for Specimen X3

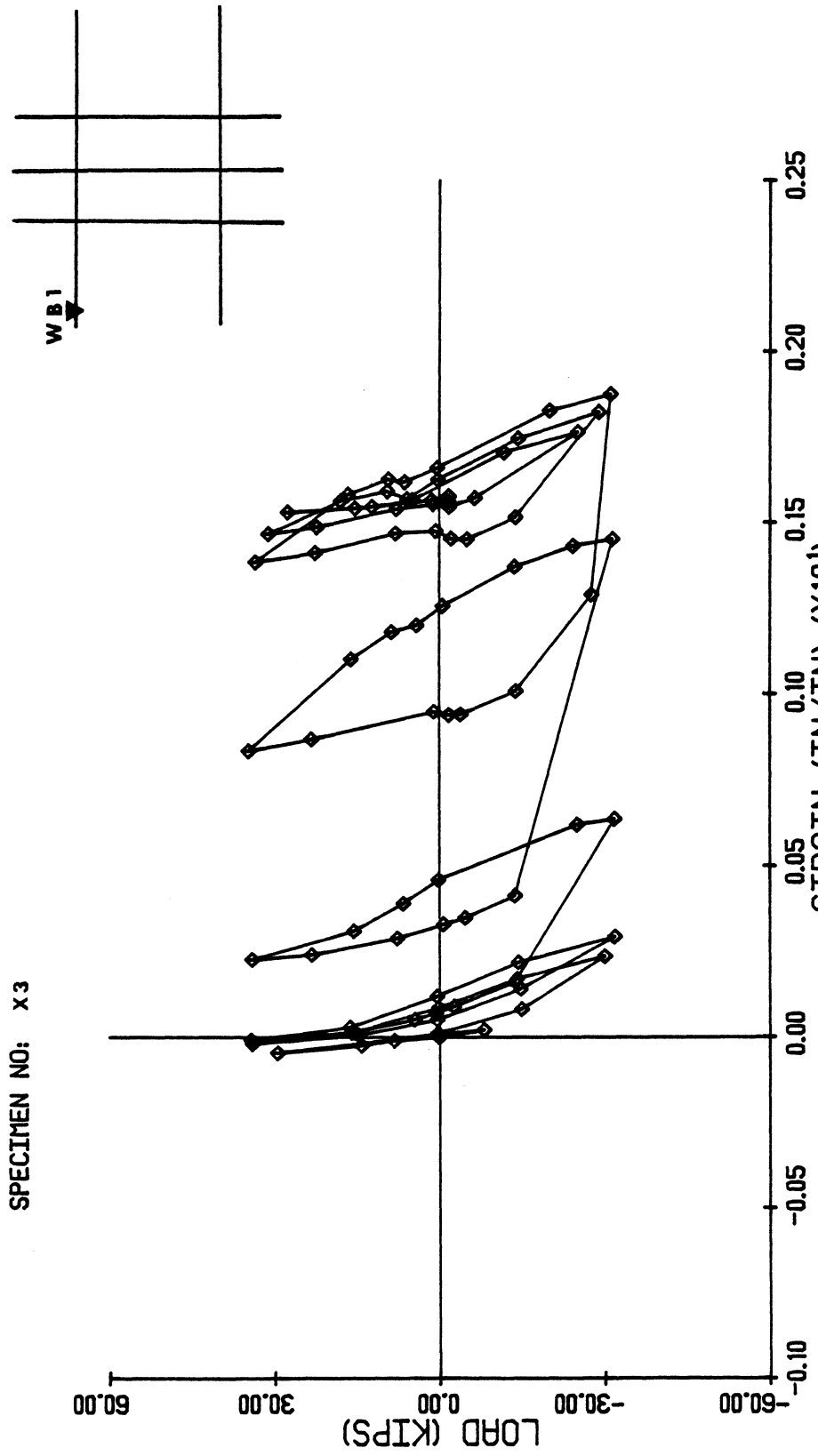

Fig. 3.26 Column Load vs. Strain in Main Beam Reinforcement at WB1 for Specimen X3

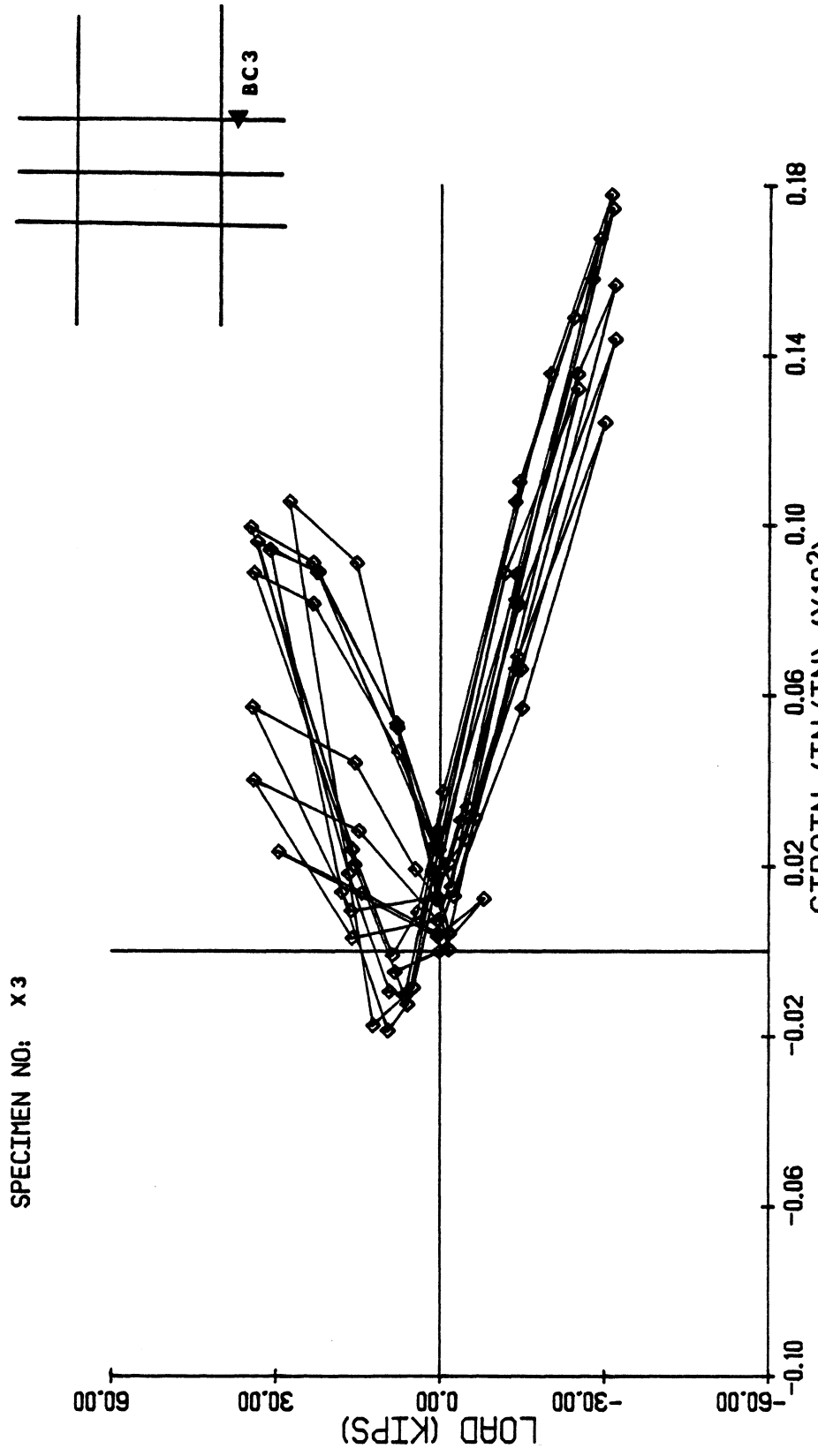

Fig. 3.27(a) Column Load vs. Strain in Column Reinforcement at BC3 for Specimen X3

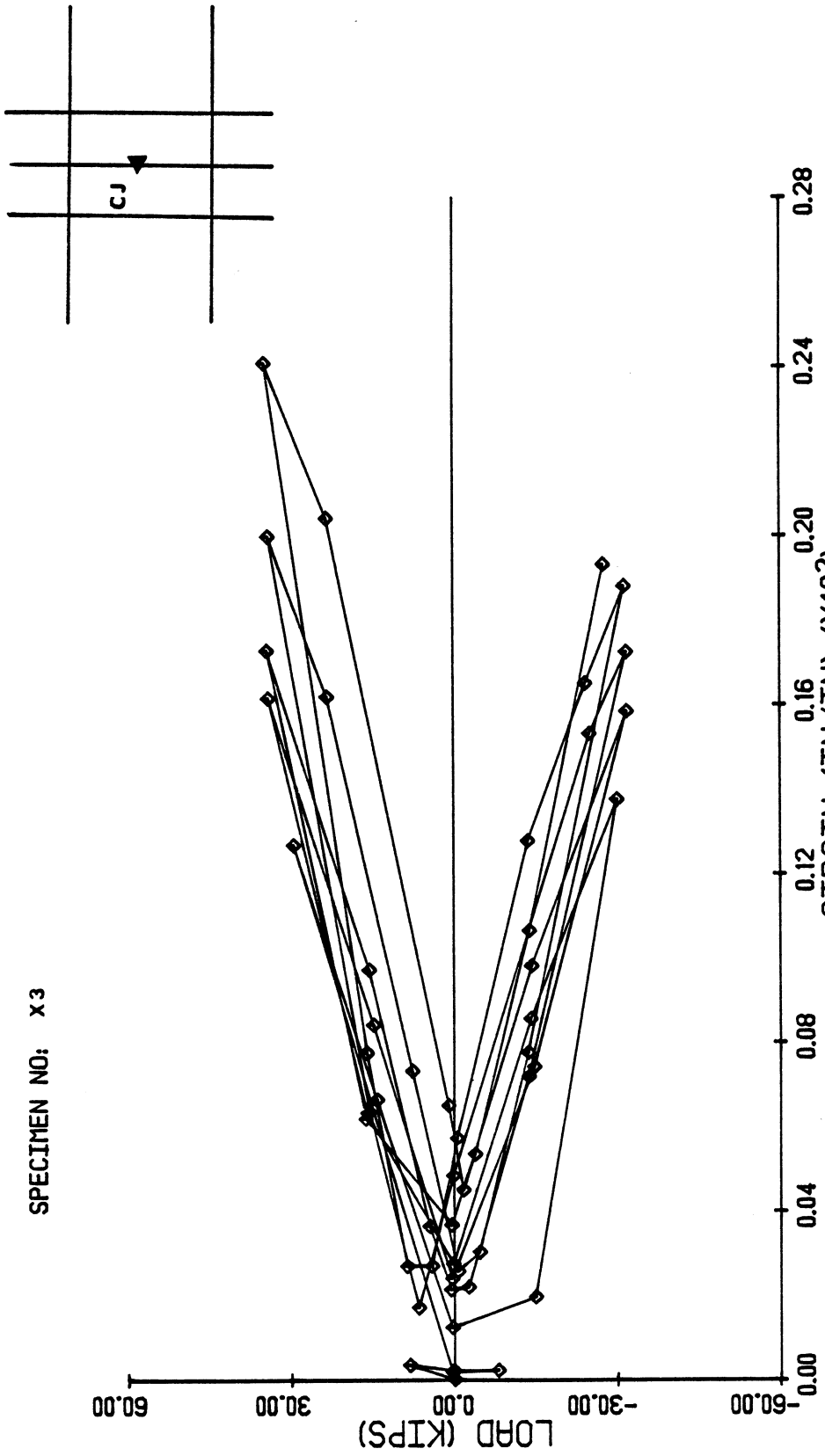

Fig. 3.27(b) Column Load vs. Strain in Column Reinforcement at CJ for Specimen X3

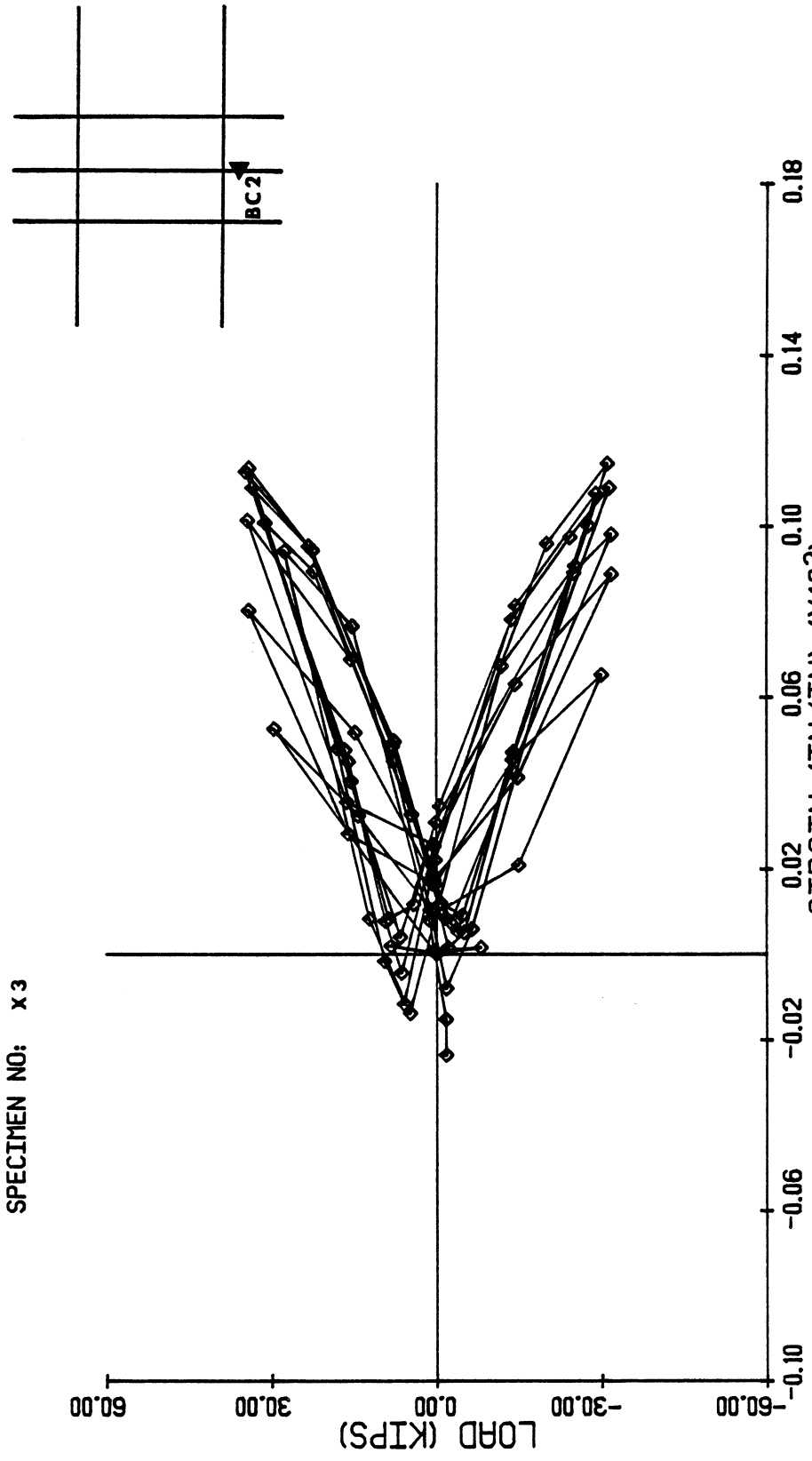

Fig. 3.27(c) Column Load vs. Strain in Column Reinforcement at BC2 for Specimen X3

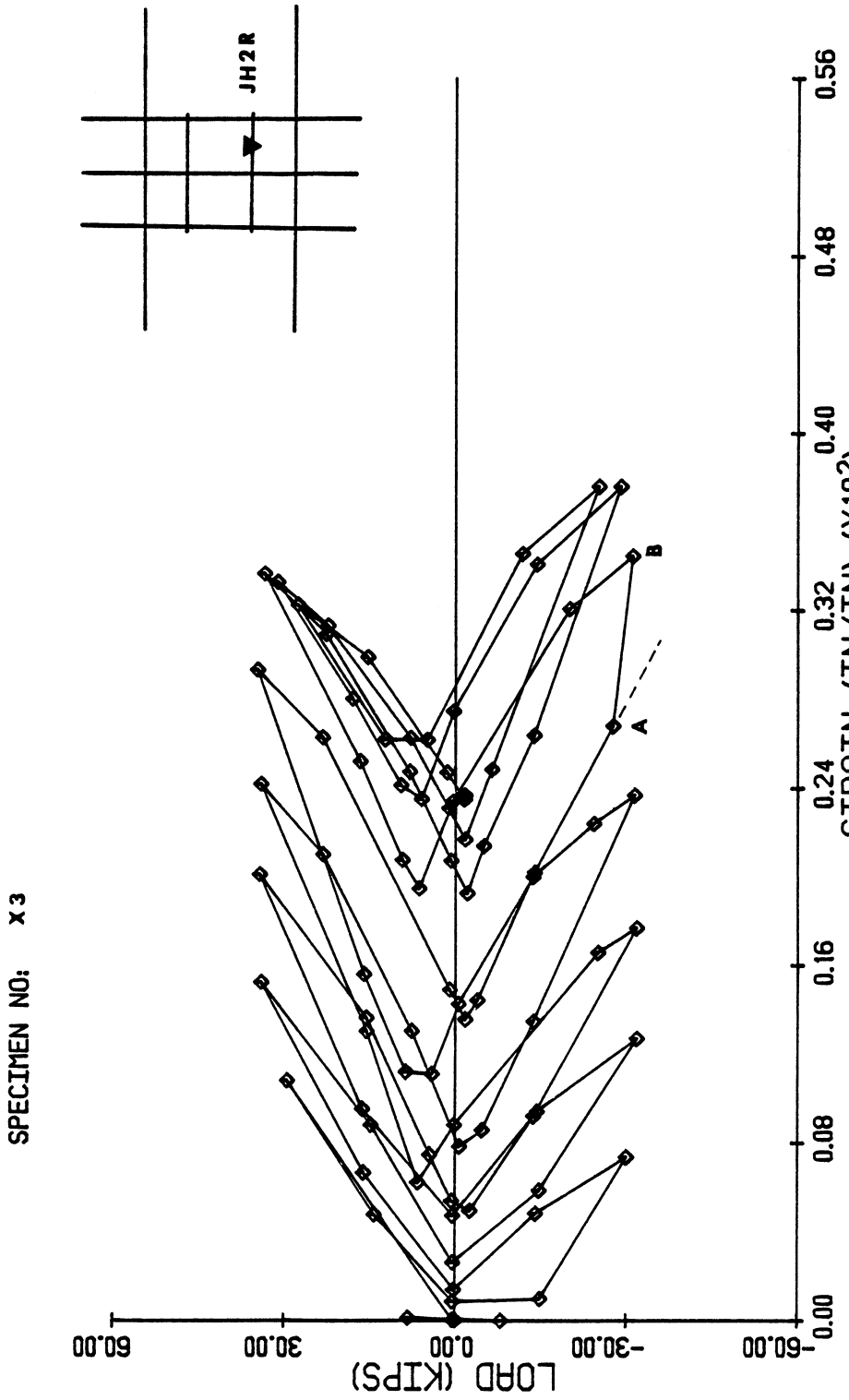

Fig. 3.28(a) Column Load vs. Strain in Square Joint Hoop at JH2R for Specimen X3

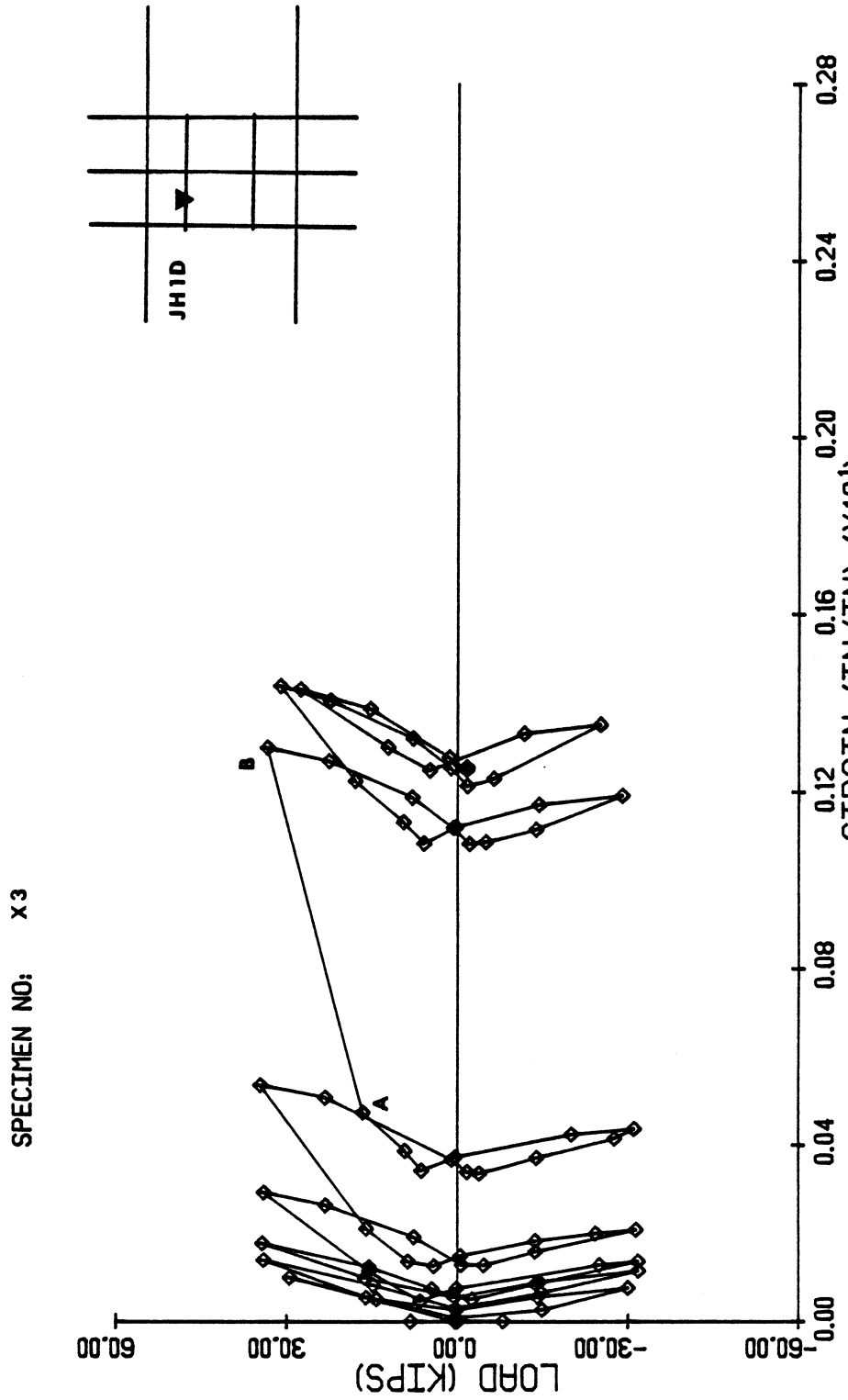

Fig. 3.28(b) Column Load vs. Strain in Diamond Shape Joint Hoop at JH1D for Specimen X3

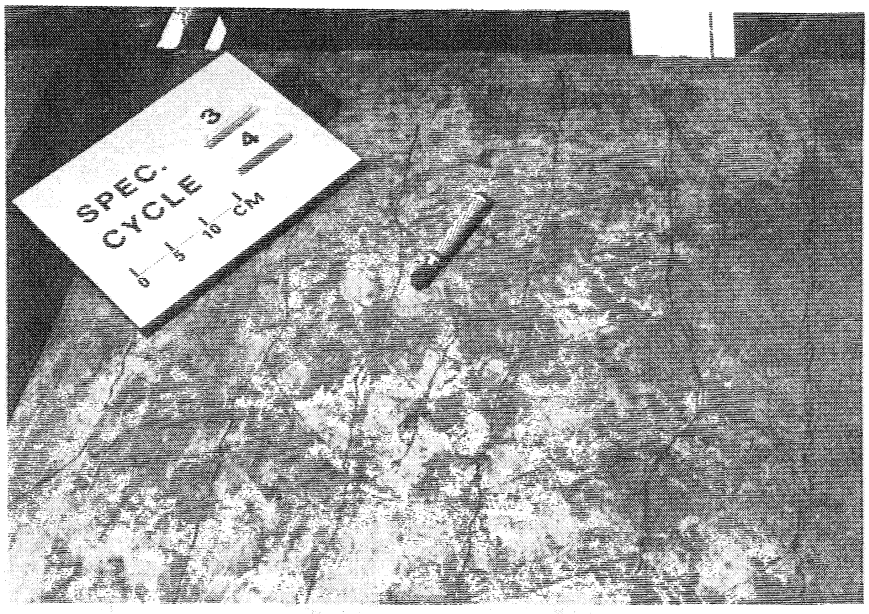

Fig. 3.29 Cracks in the Slab of Specimen S1 at the End of Fourth Loading Cycle

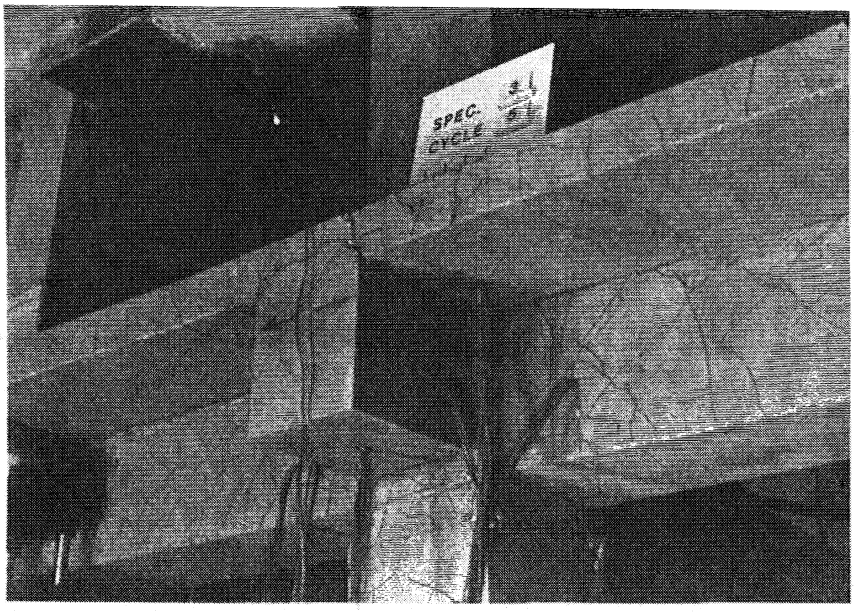

Fig. 3.30 Cracking Pattern in Specimen S1 at the End of Fifth Loading Cycle

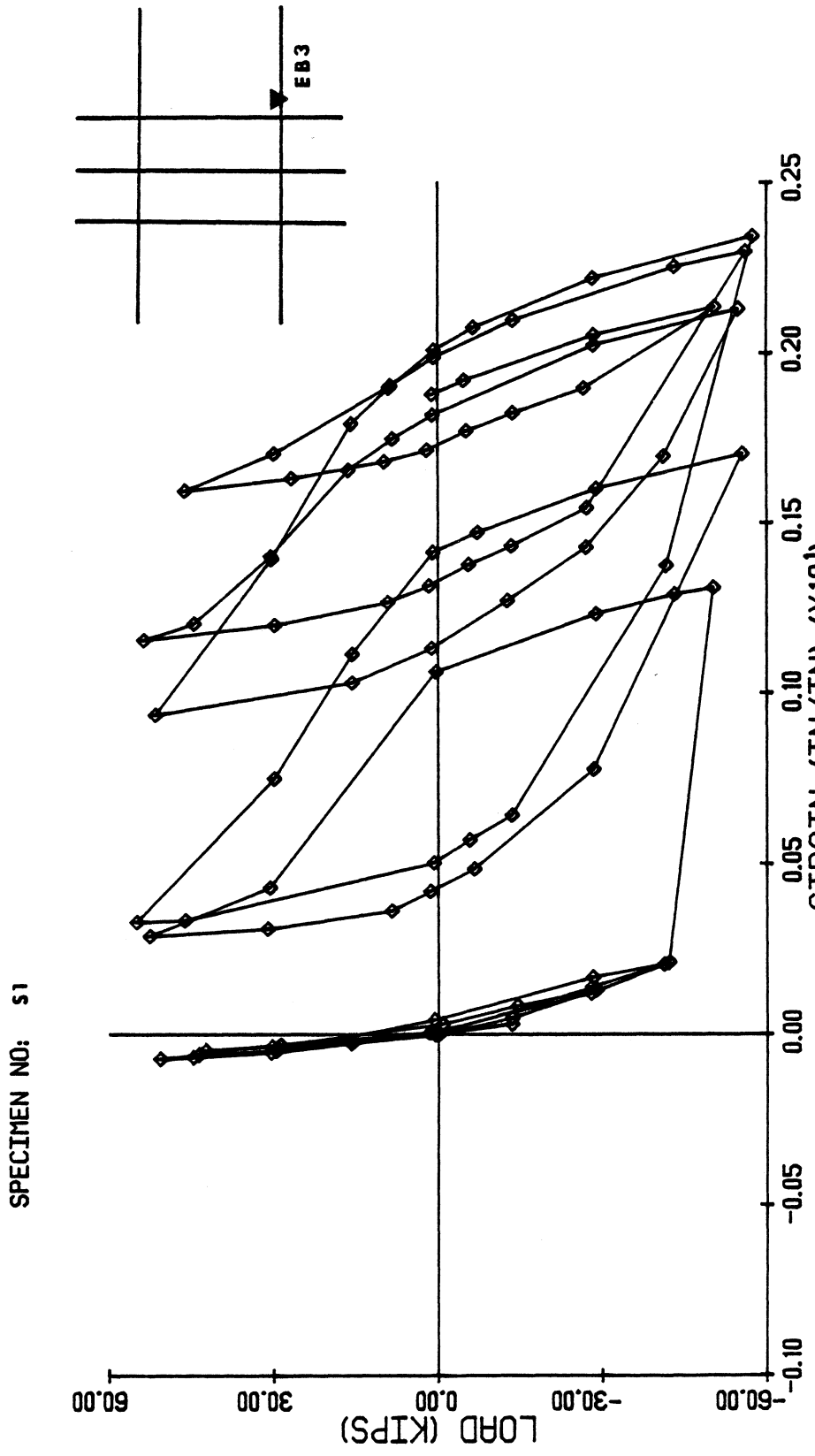

Fig. 3.31 Column Load vs. Strain in Main Beam Reinforcement at EB3 for Specimen S1

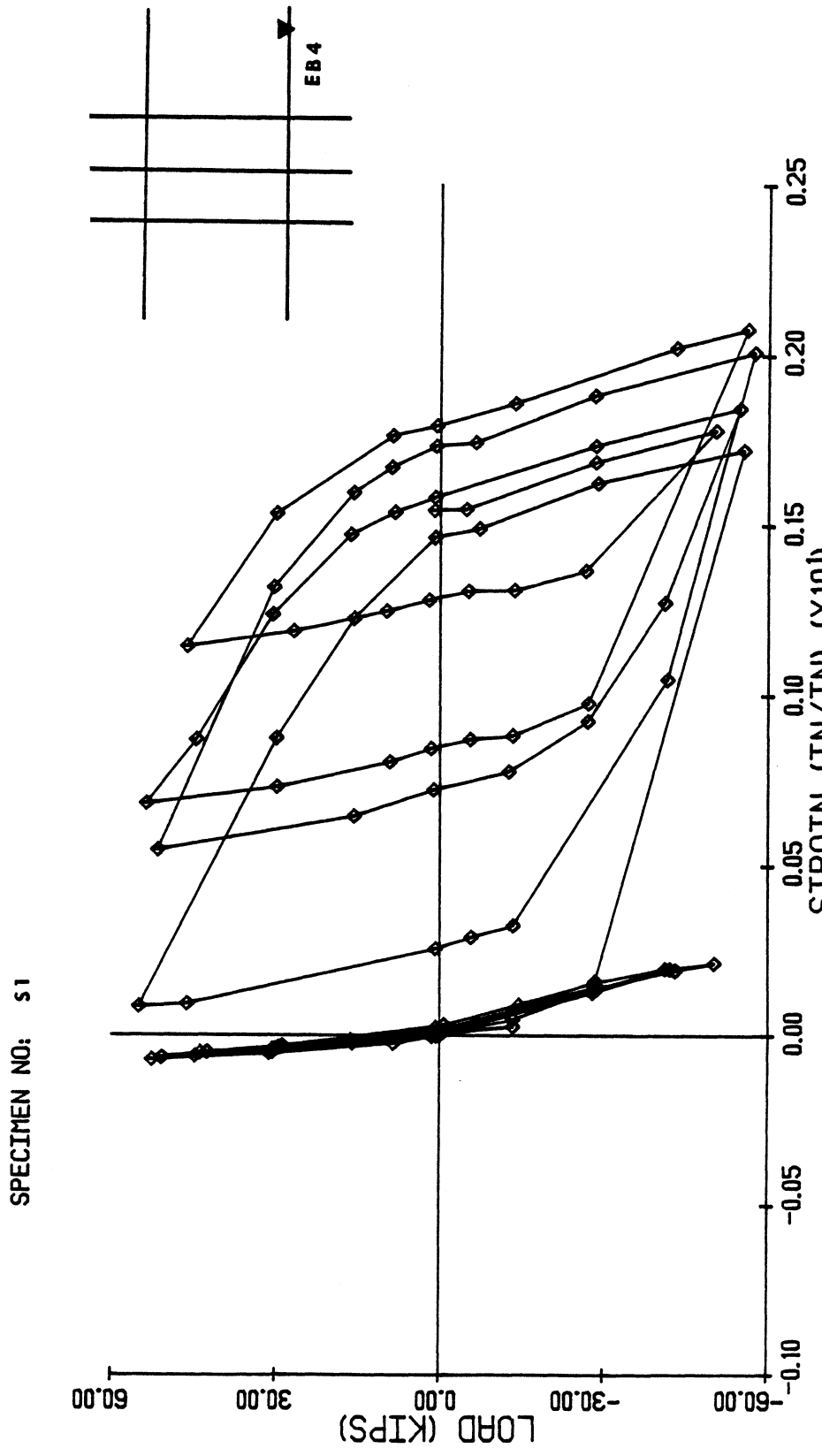

Fig. 3.32 Column Load vs. Strain in Main Beam Reinforcement at EB4 for Specimen S1

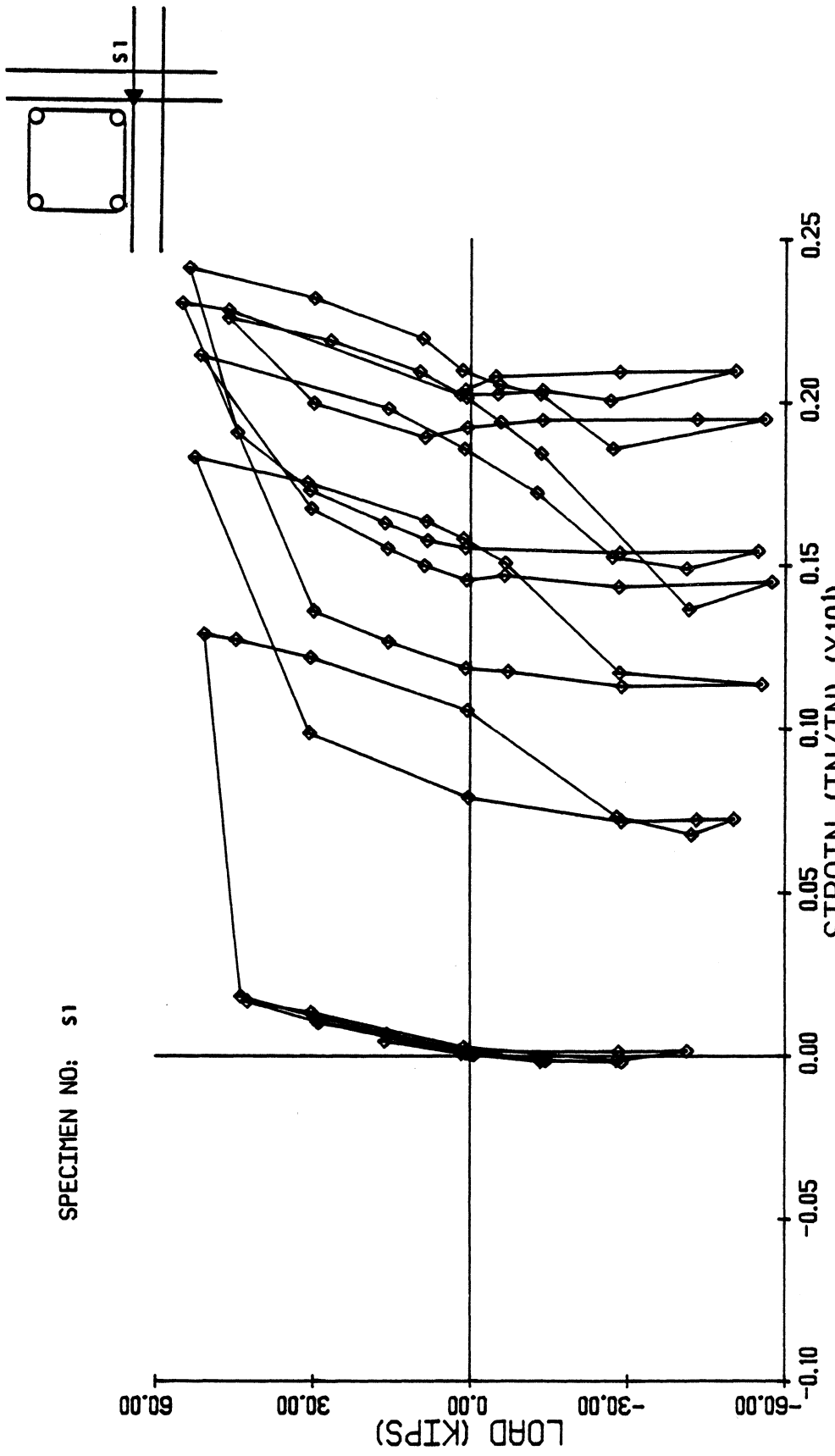

Fig. 3.33 Column Load vs. Strain in Main Slab Bar at S1 for Specimen S1

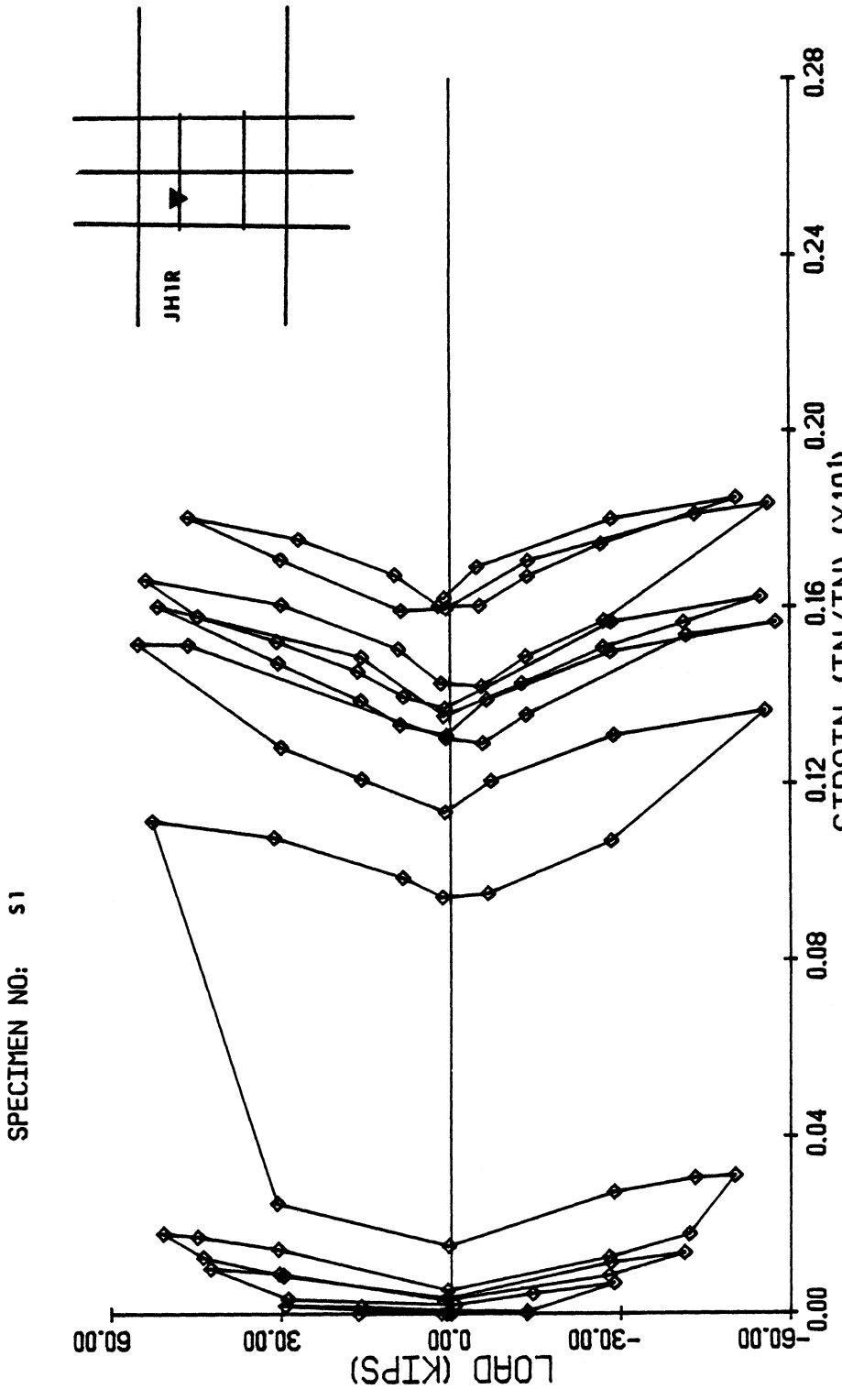

Fig. 3.34 Column Load vs. Strain in Square Joint Hoop at JH1R for Specimen S1

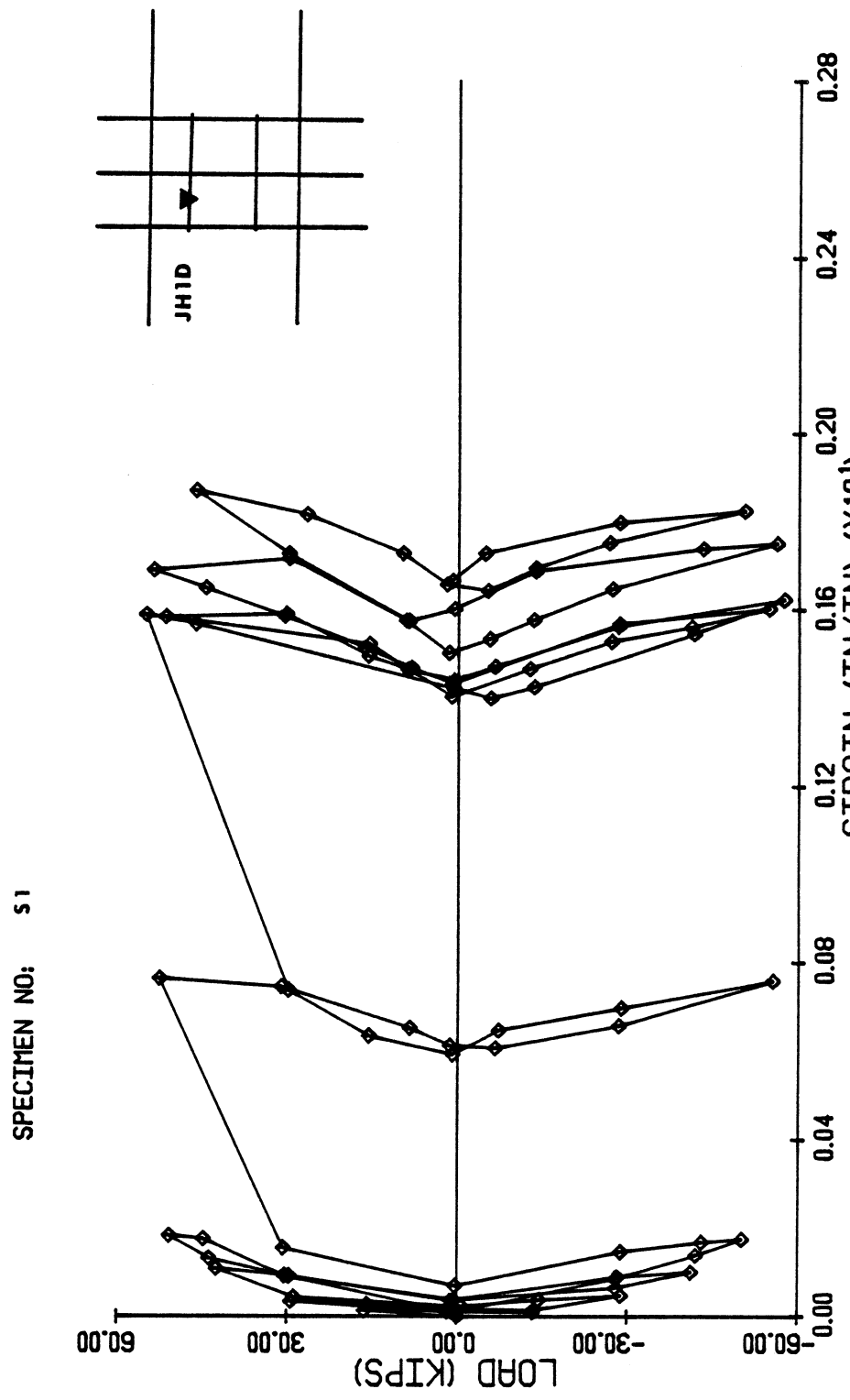

Fig. 3.35 Column Load vs. Strain in Diamond Shape Joint Hoop at JH1D for Specimen S1

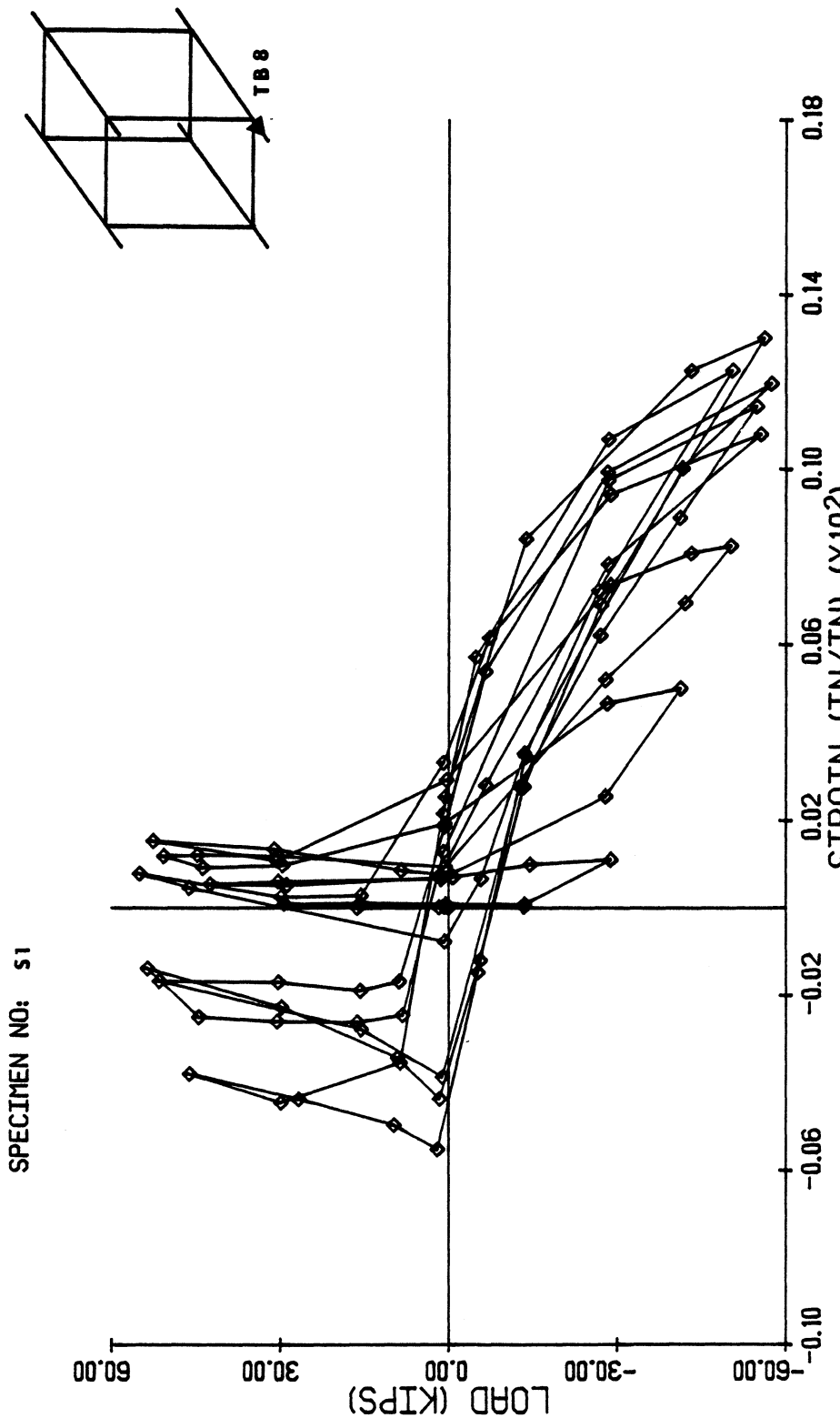

Fig. 3.36 Column Load vs. Strain in Trans. Beam Main Reinforcement at TB8 for Specimen S1.

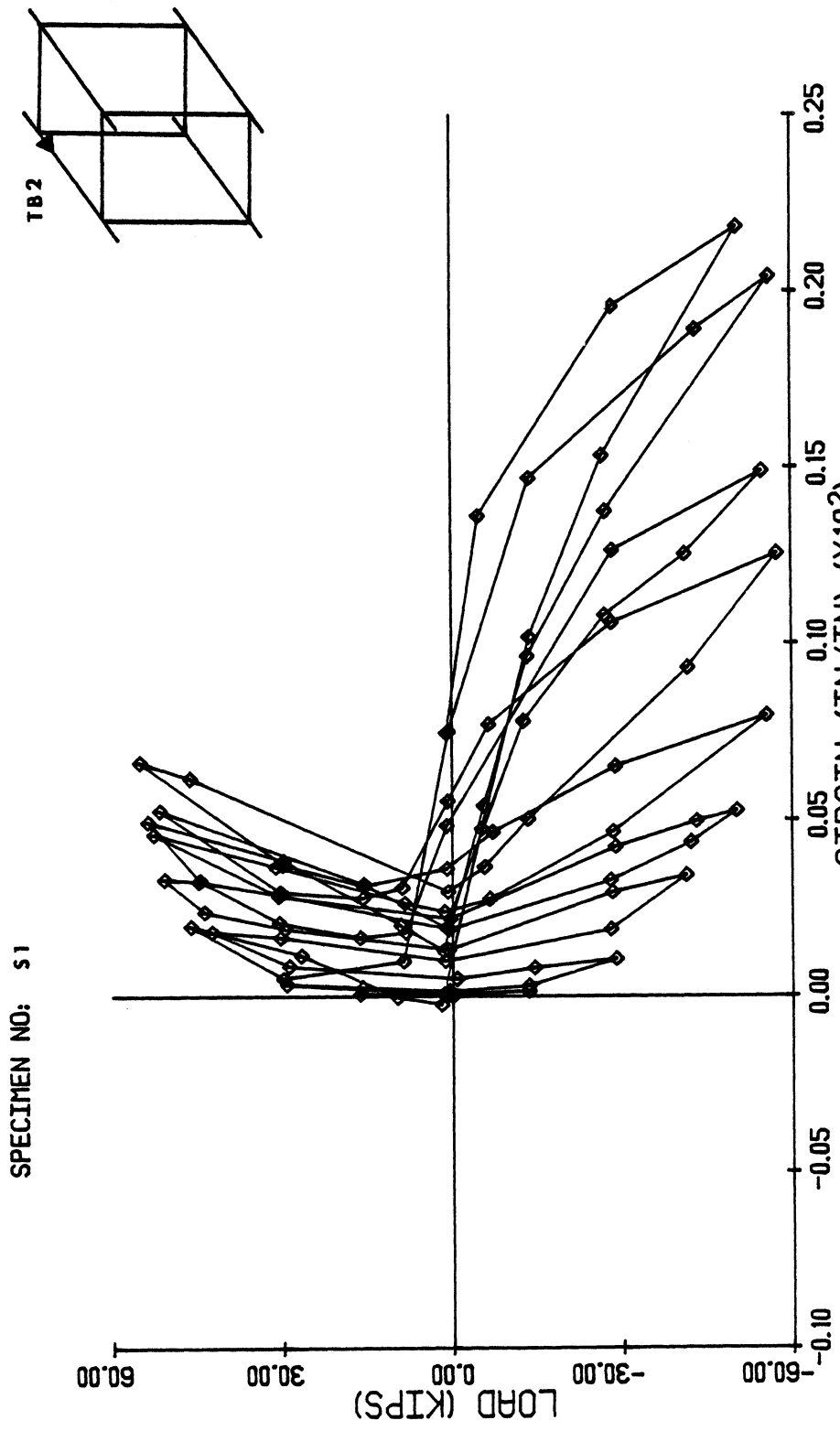

Fig. 3.37 Column Load vs. Strain in Trans. Beam Main Reinforcement at TB2 for Specimen S1

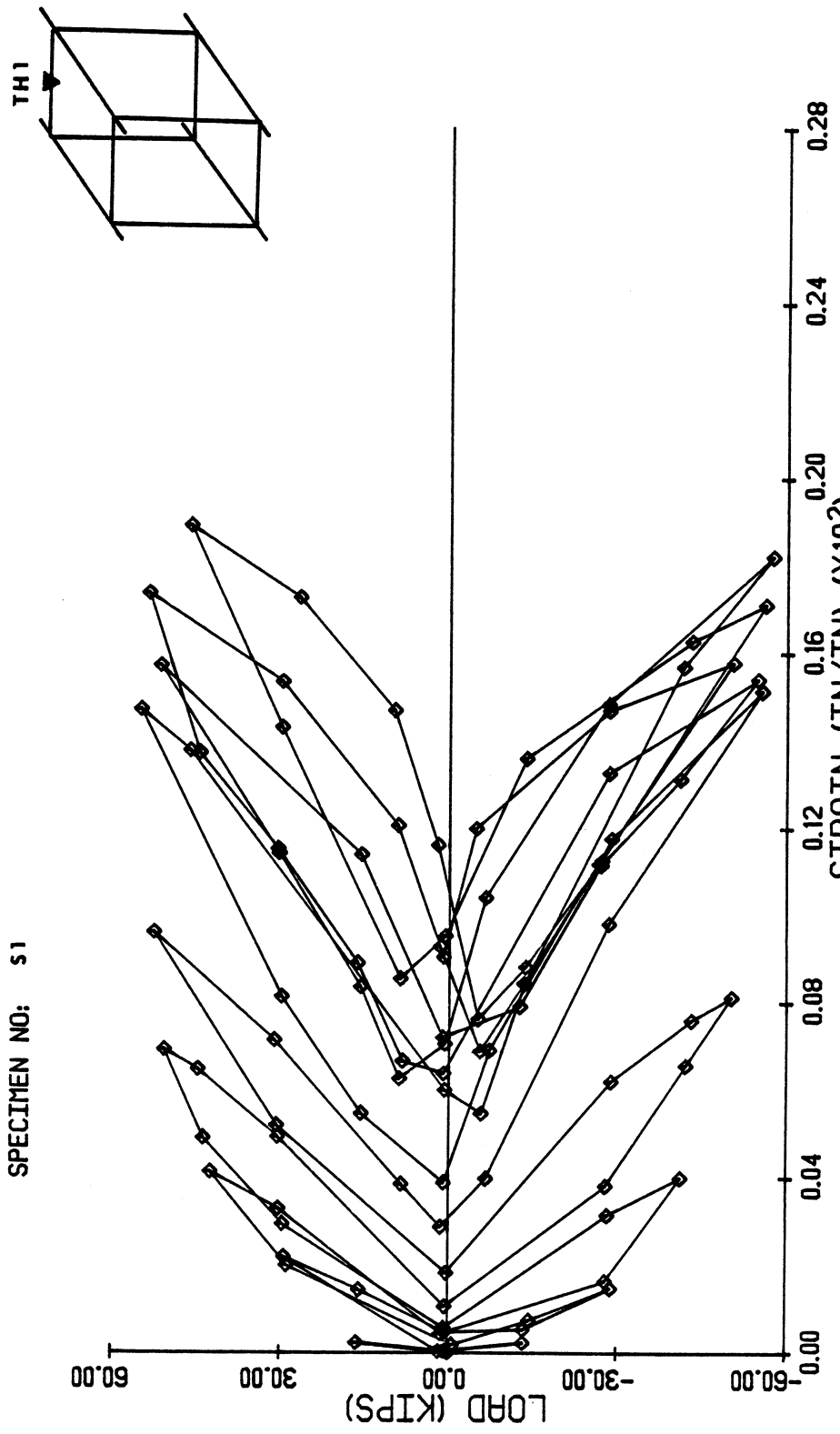

Fig. 3.38 Column Load vs. Strain in Trans. Beam Hoop Reinforcement at TH1 for Specimen S1

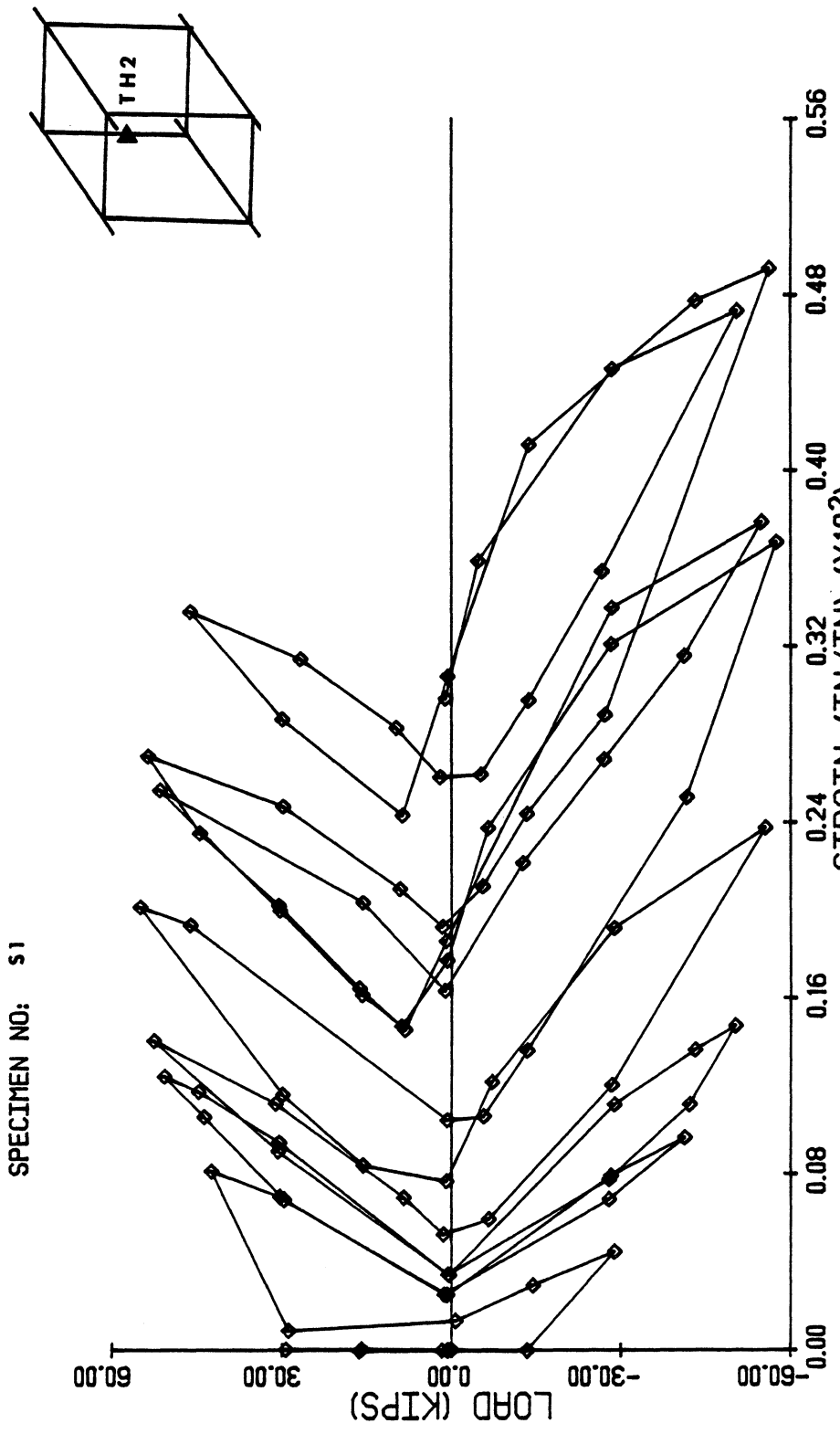

Fig. 3.39 Column Load vs. Strain in Trans. Beam Hoop Reinforcement at TH2 for Specimen S1

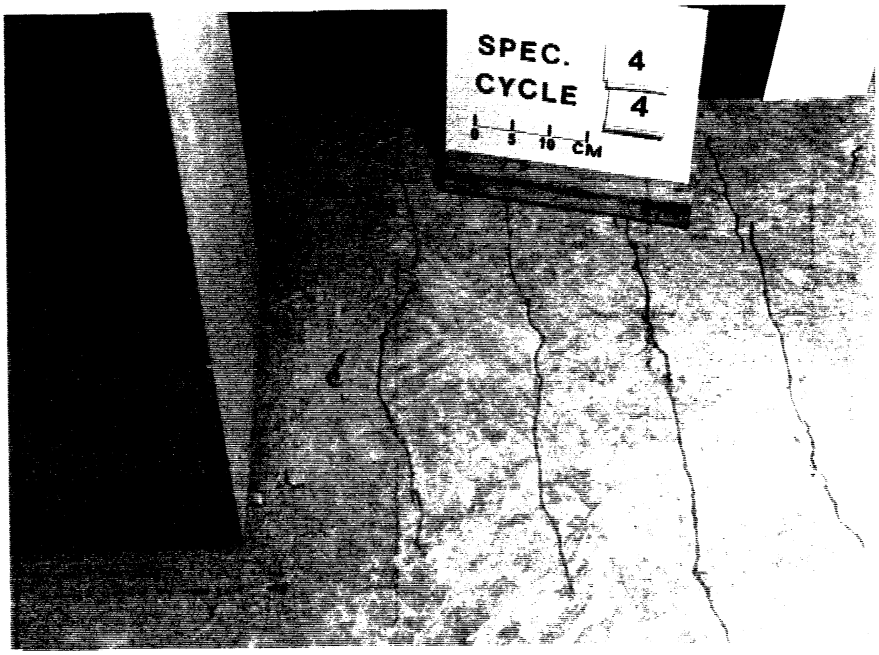

Fig. 3.40(a) Cracks in the Slab of Specimen S2 at the End of Fourth Loading Cycle

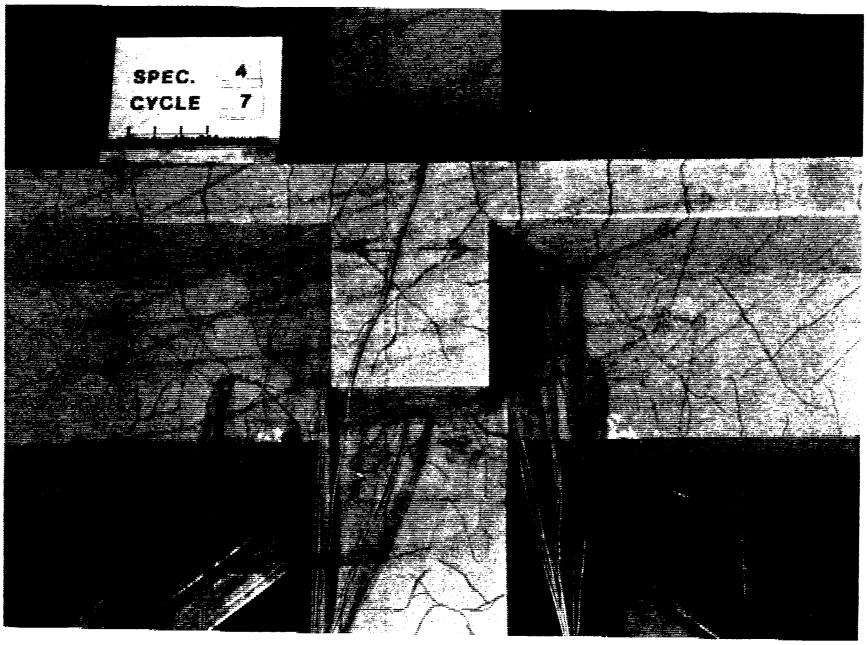

Fig. 3.40(b) Cracking Pattern in Specimen S2 at the End of Seventh Loading Cycle

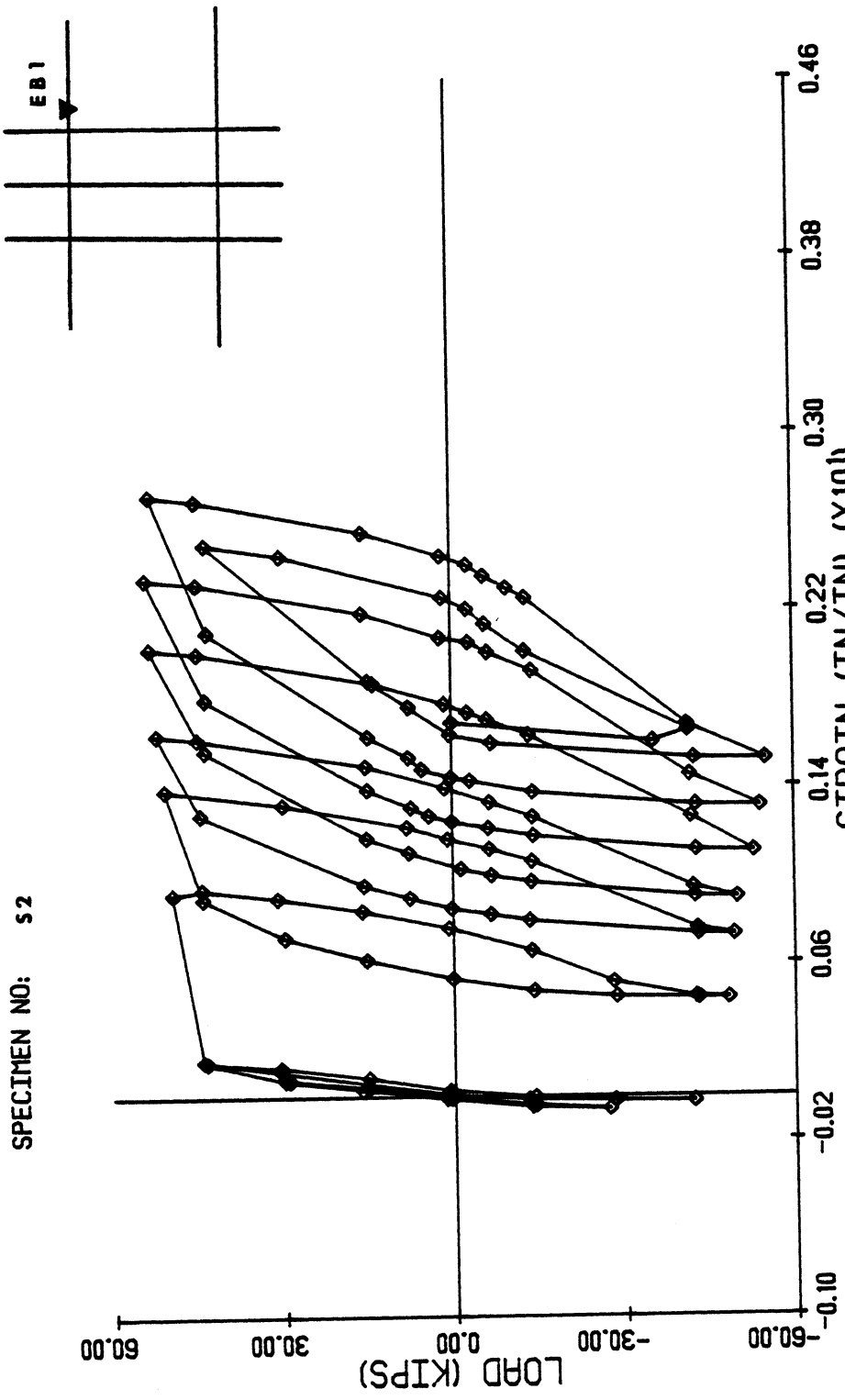

Fig. 3.41 Column Load vs. Strain in Main Beam Reinforcement at EB1 for Specimen S2

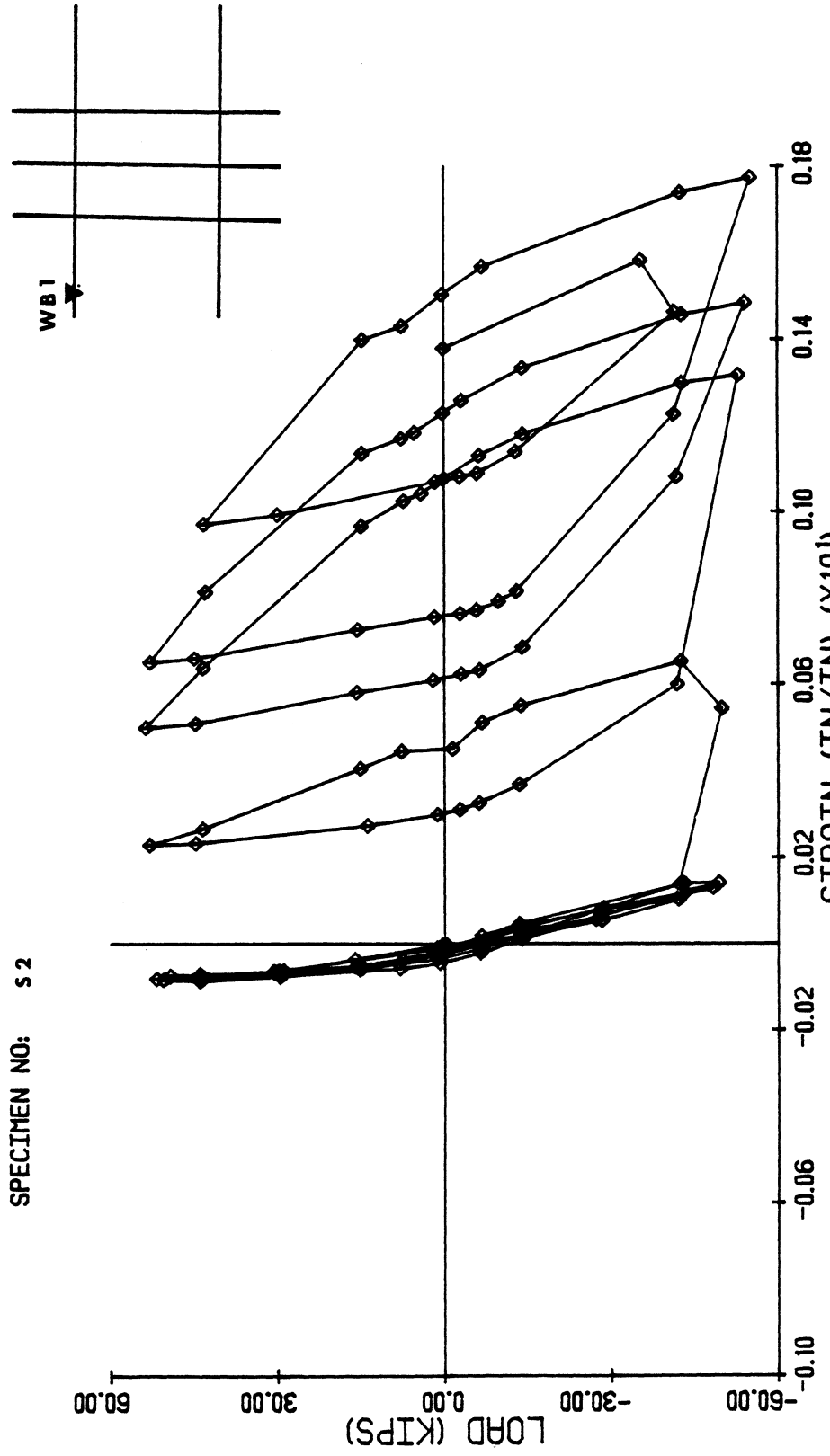

Fig. 3.42 Column Load vs. Strain in Main Beam Reinforcement at WB1 for Specimen S2

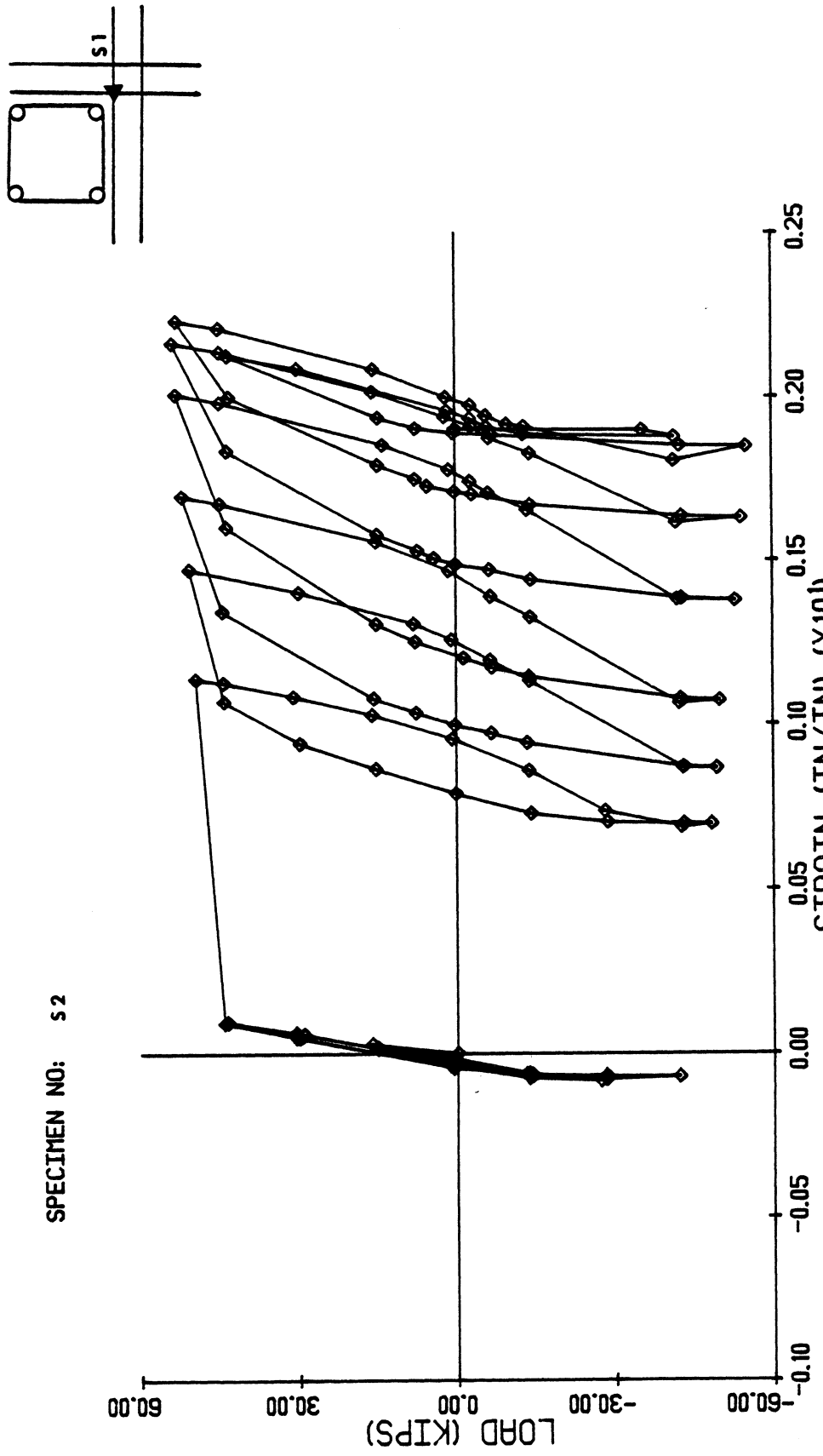

Fig. 3.43 Column Load vs. Strain in Main Slab Bar at S1 for Specimen S2

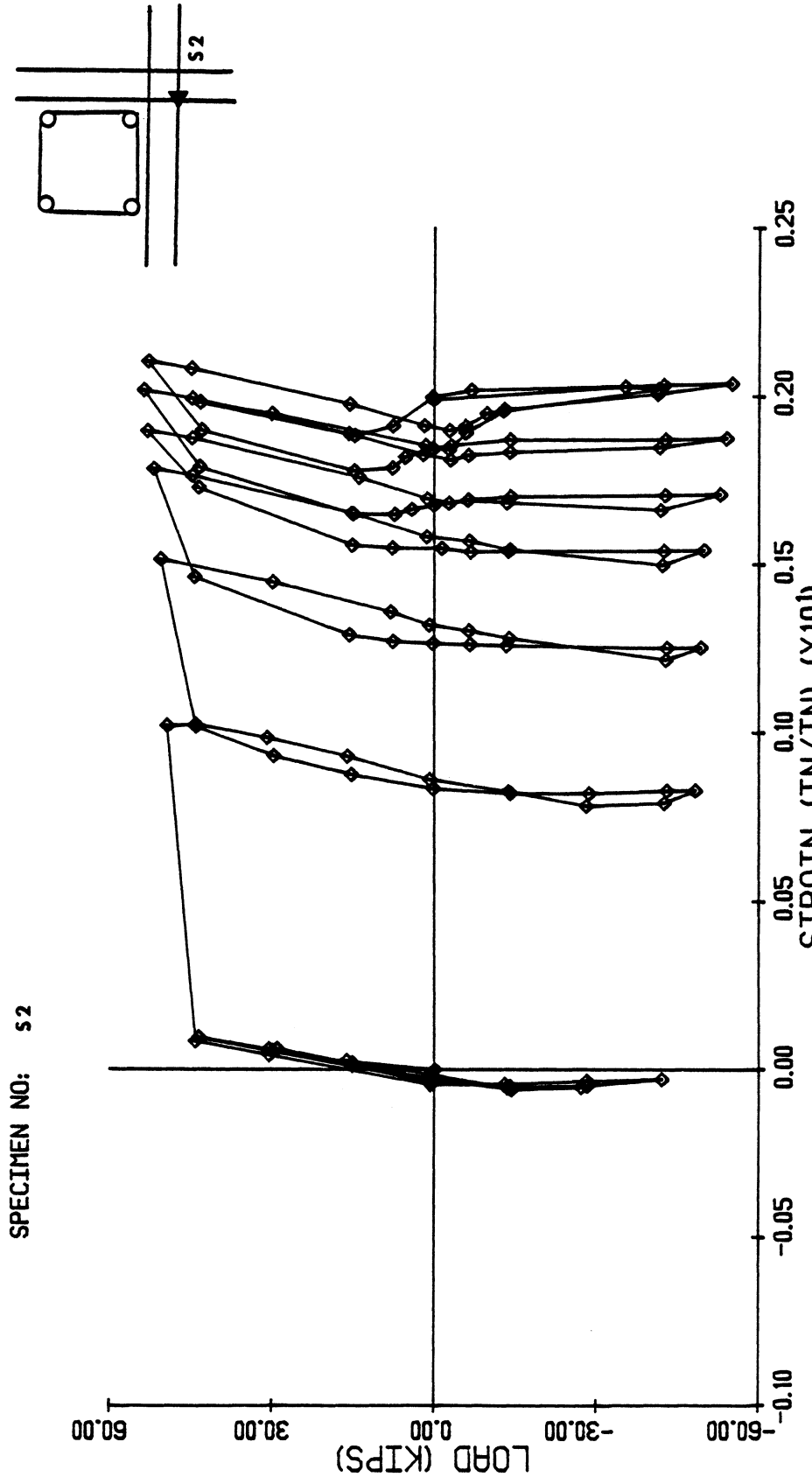

Fig. 3.44 Column Load vs. Strain in Main Slab Bar at S2 for Specimen S2

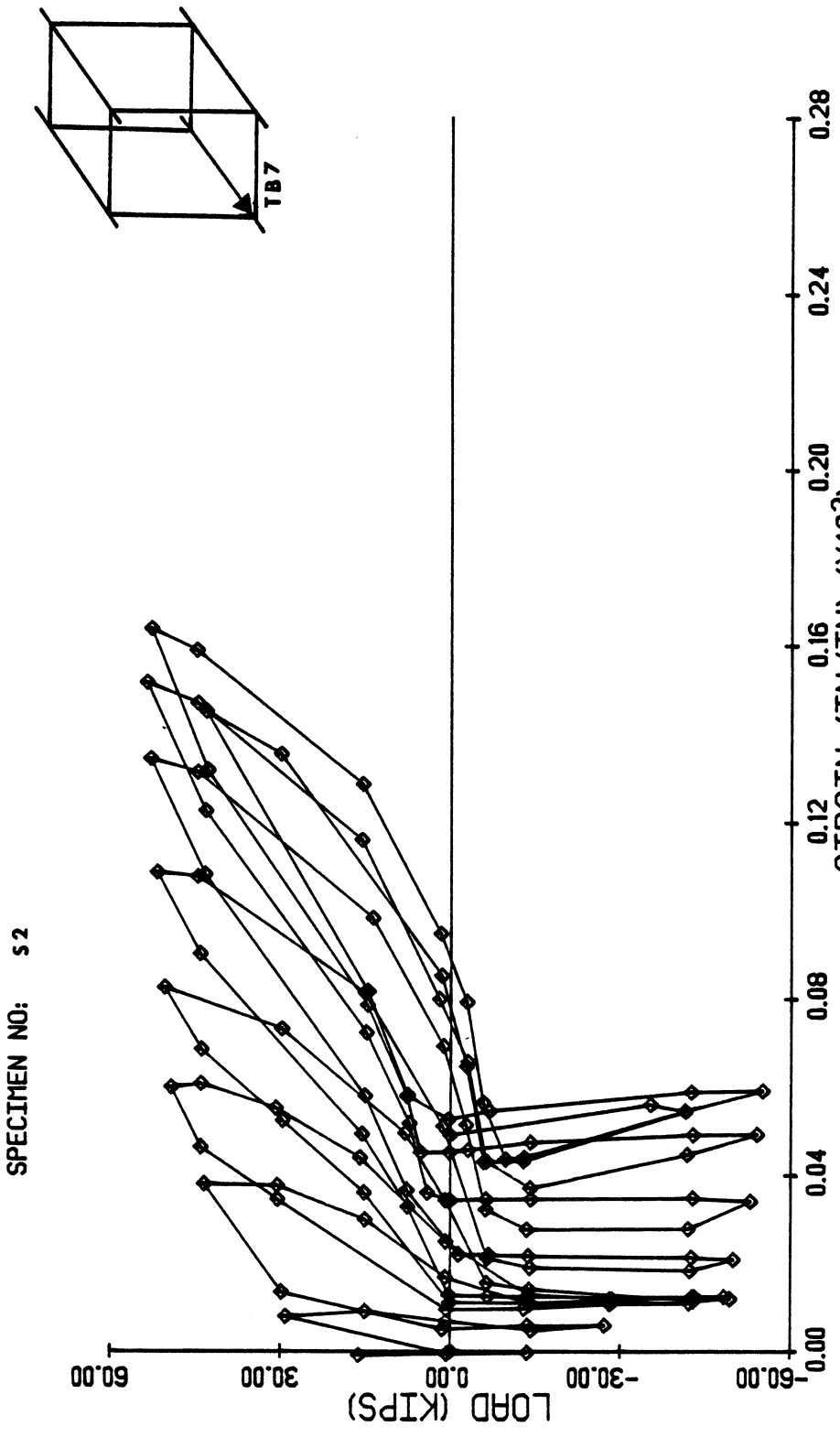

Fig. 3.45 Column Load vs. Strain in Trans. Beam Main Reinforcement at TB7 for Specimen S2

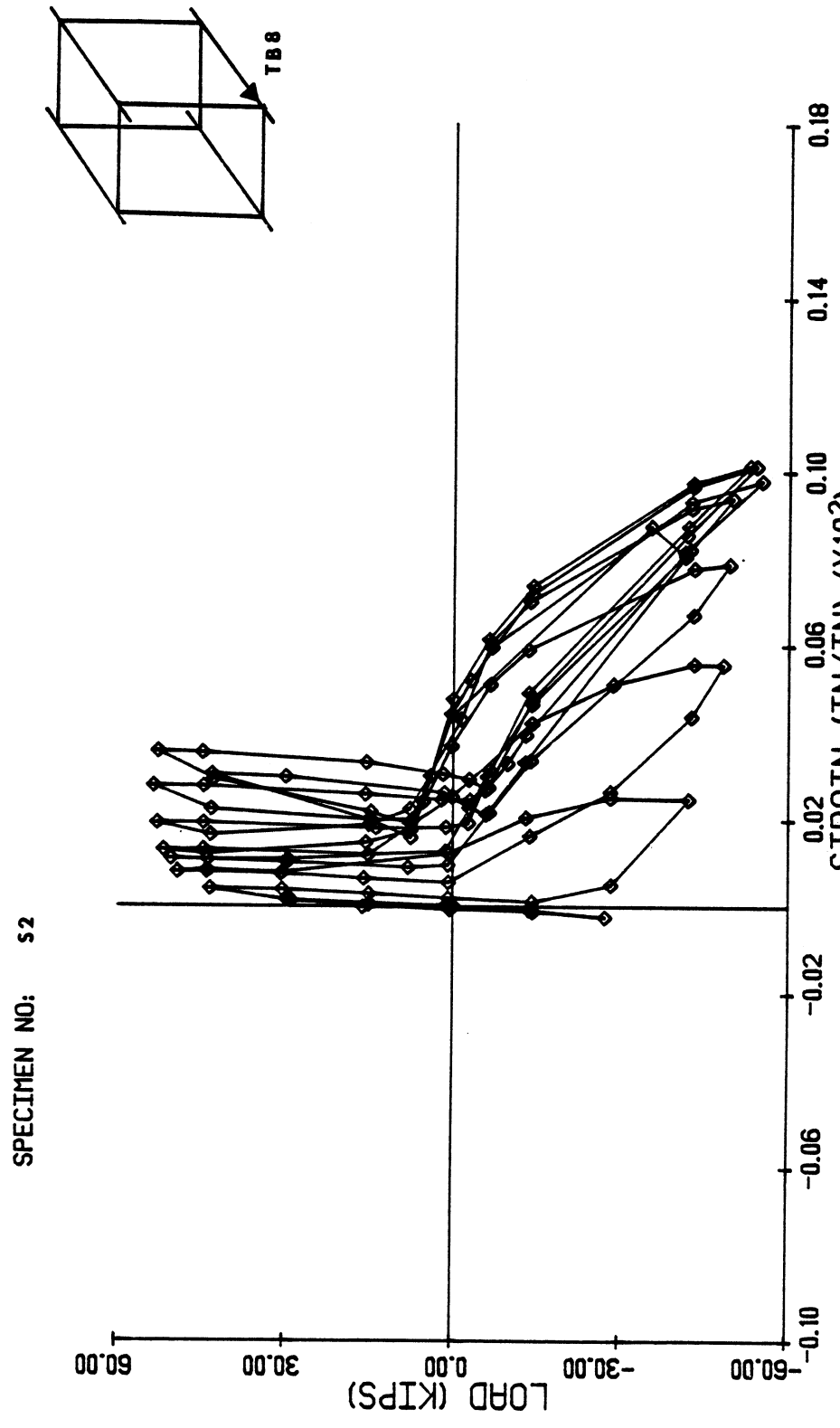

Fig. 3.46 Column Load vs. Strain in Trans. Beam Main Reinforcement at TB8 for Specimen S2

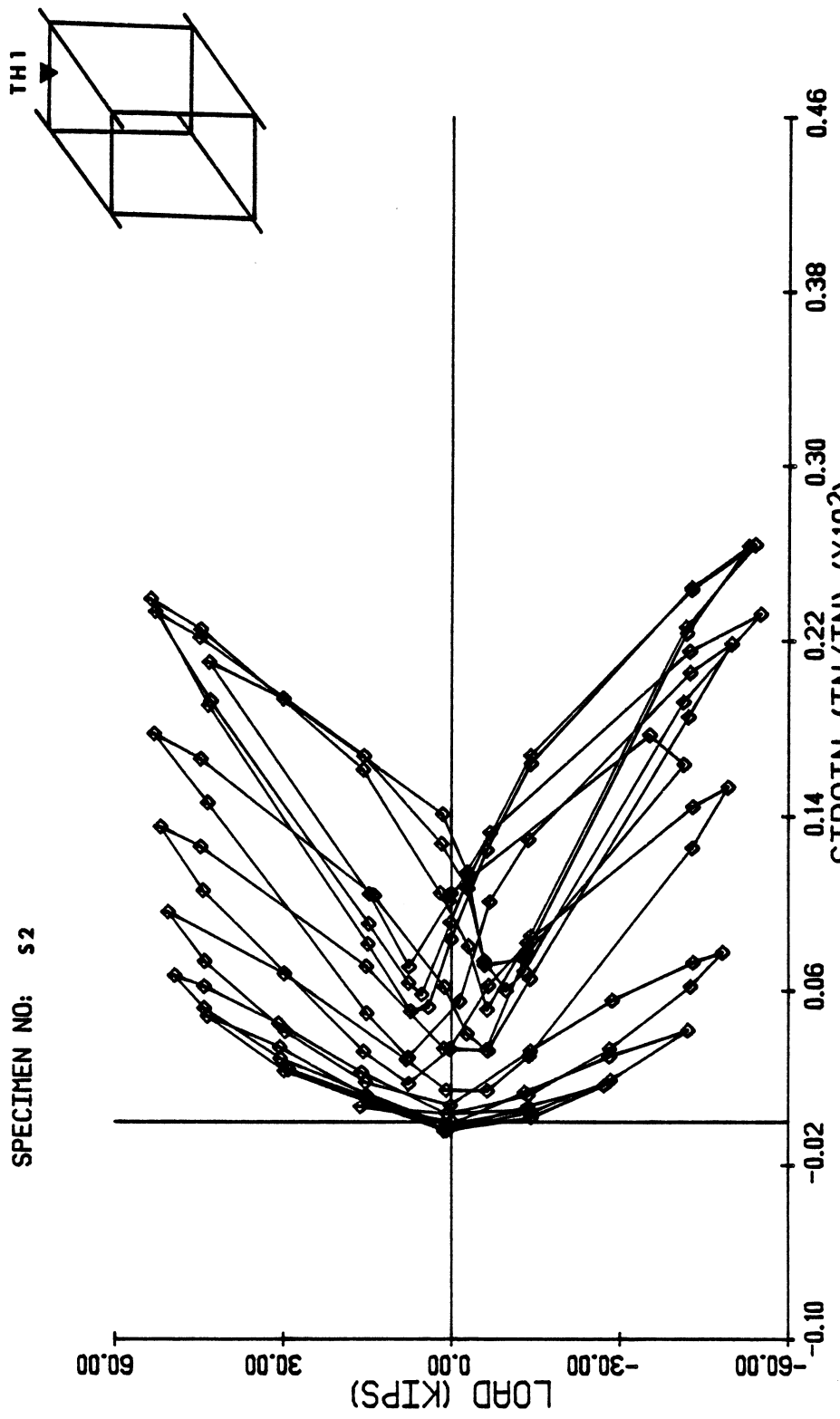

Fig. 3.47 Column Load vs. Strain in Trans. Beam Hoop Reinforcement at TH1 for Specimen S2

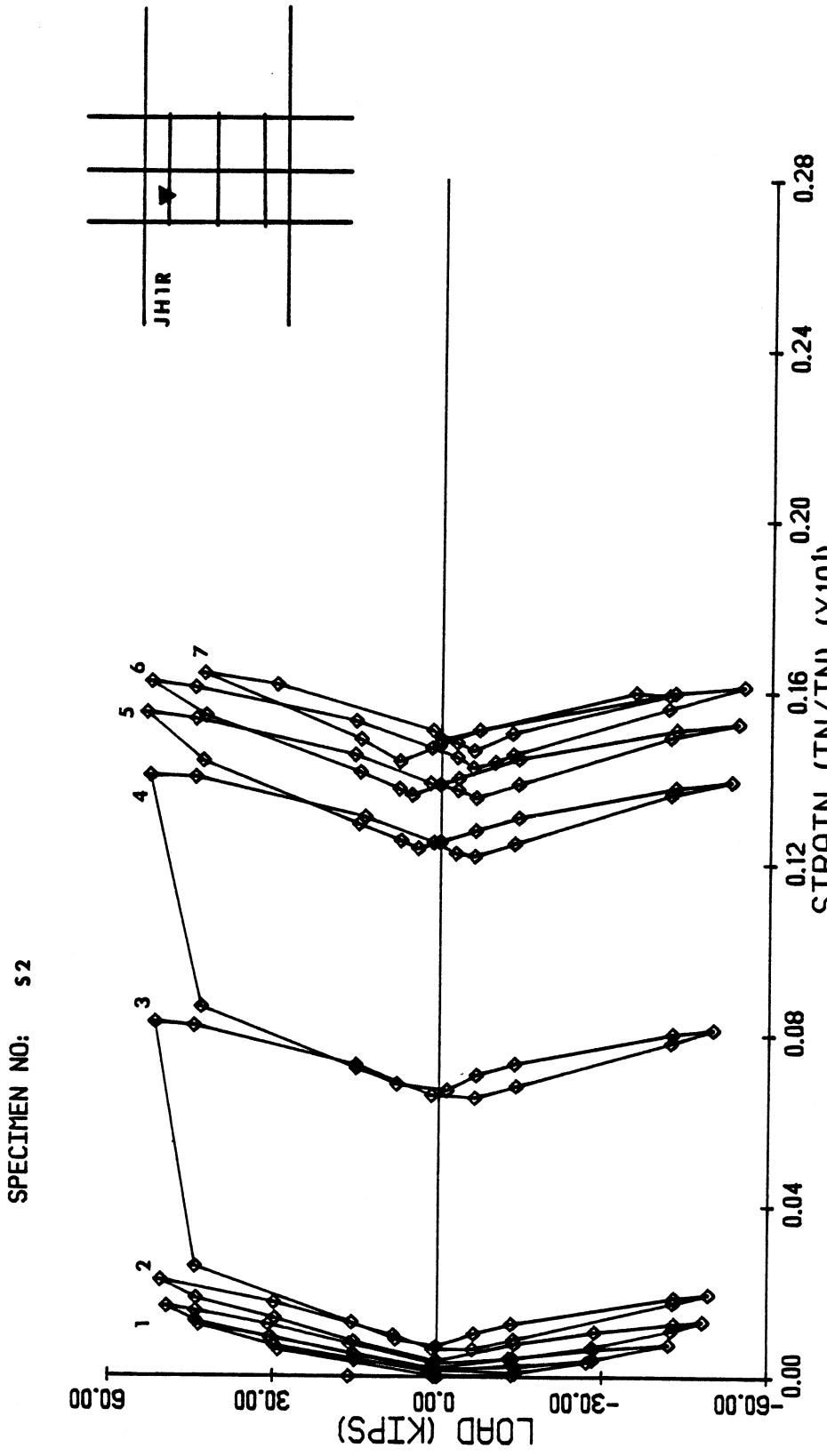

Fig. 3.48 Column Load vs. Strain in Square Joint Hoop at JH1R for Specimen S2

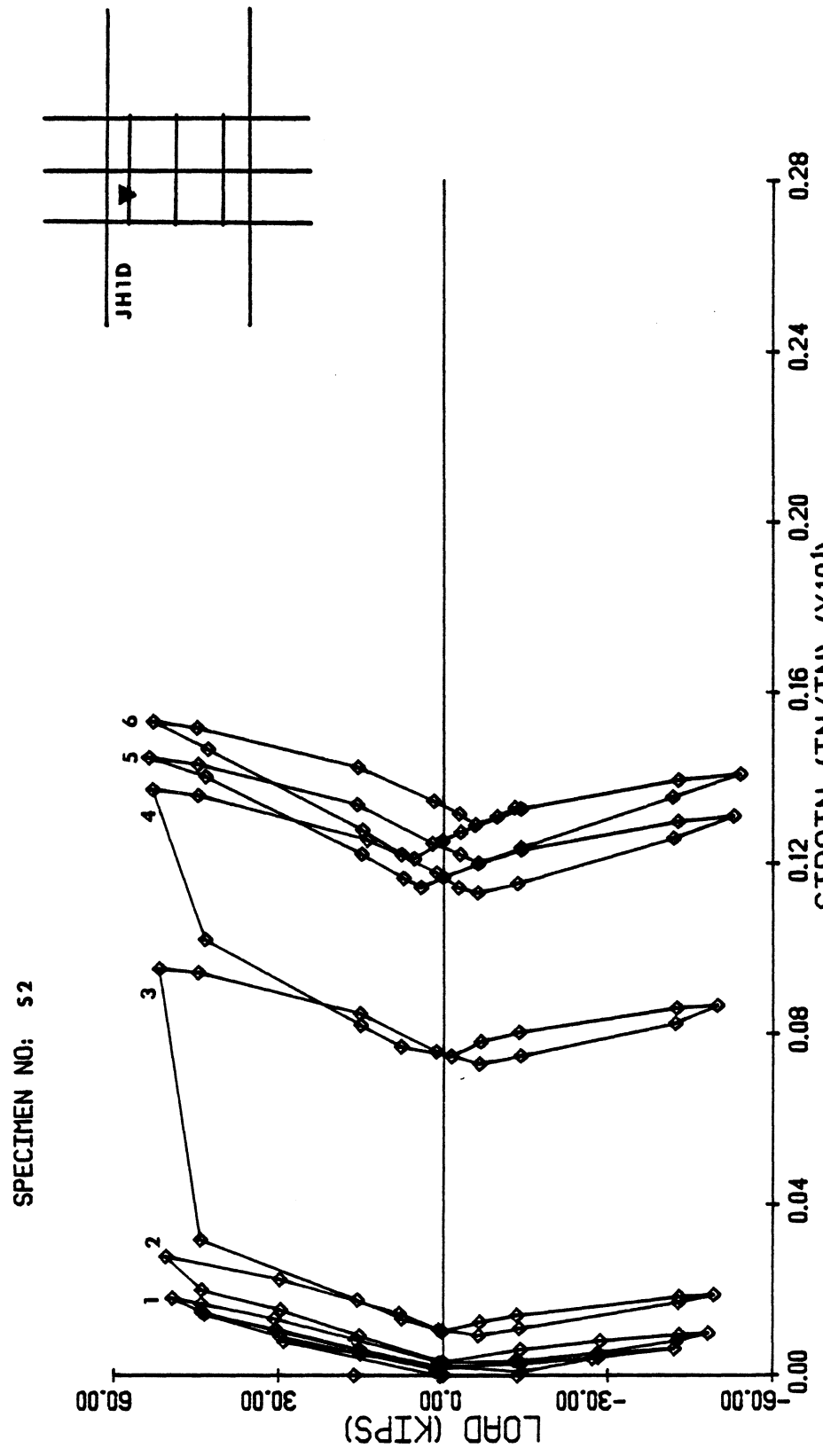

Fig. 3.49 Column Load vs. Strain in Diamond Shape Joint Hoop at JH1D for Specimen S2

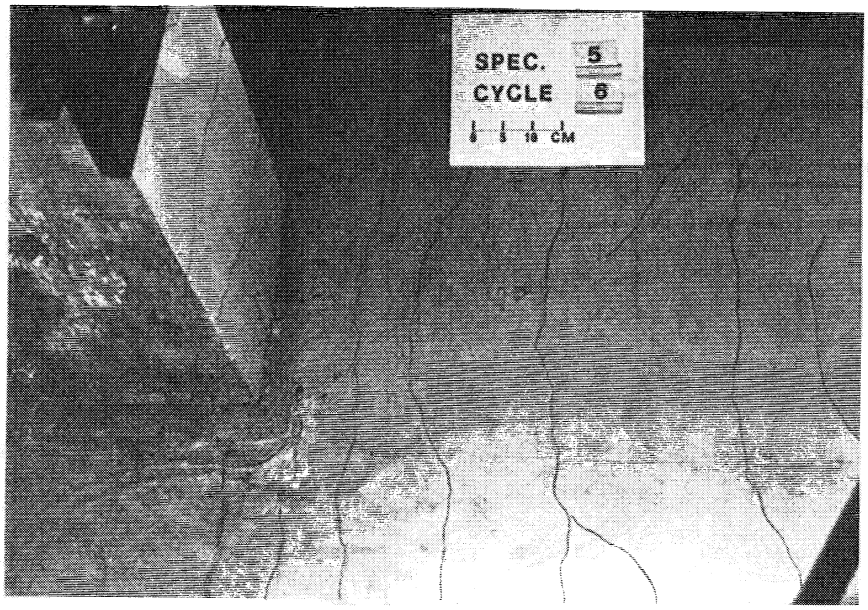

Fig. 3.50(a) Cracks in the Slab of Specimen S3 at the End of Sixth Loading Cycle

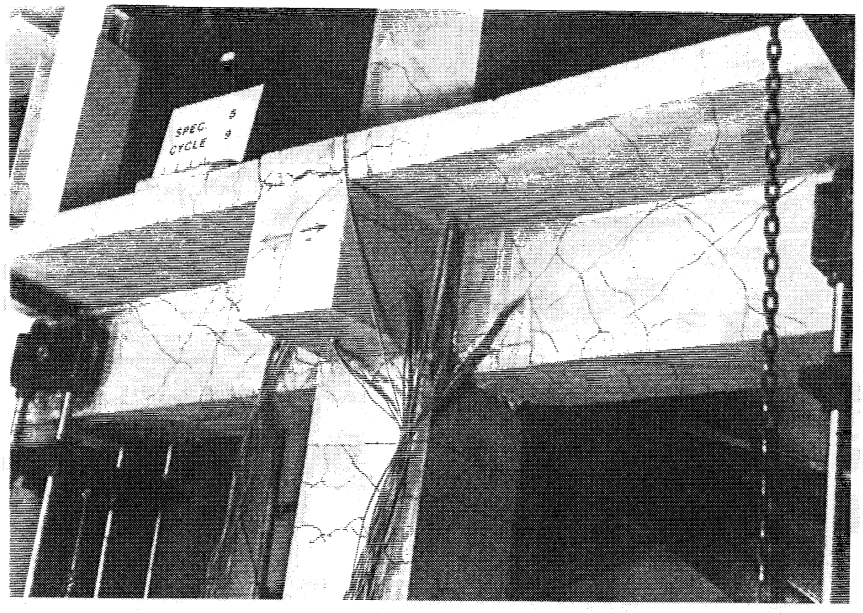

Fig. 3.50(b) Cracking Pattern in Specimen S3 at the End of Seventh Post-yield Loading Cycle

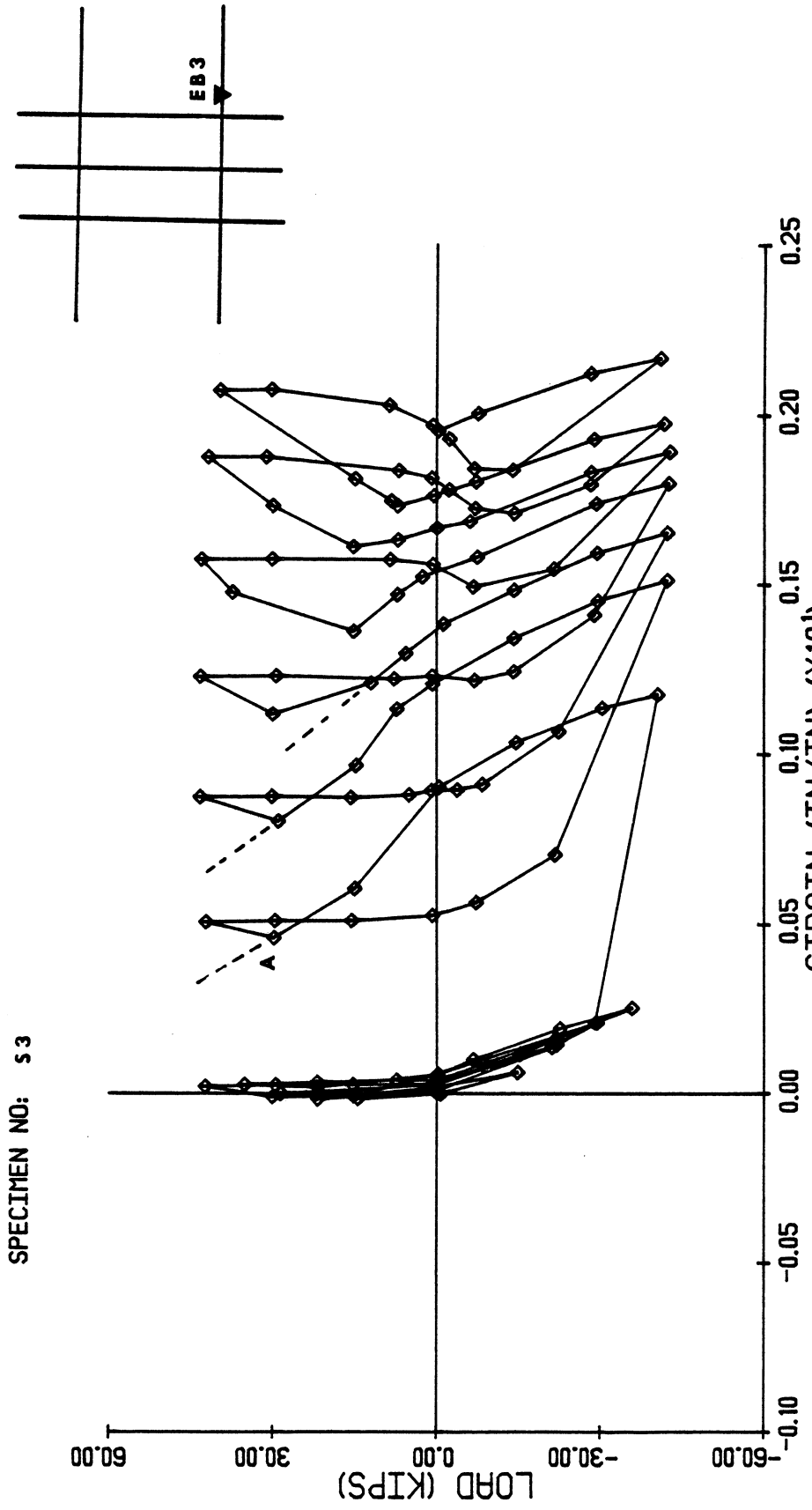

Fig. 3.51 Column Load vs. Strain in Main Beam Reinforcement at EB3 for Specimen S3

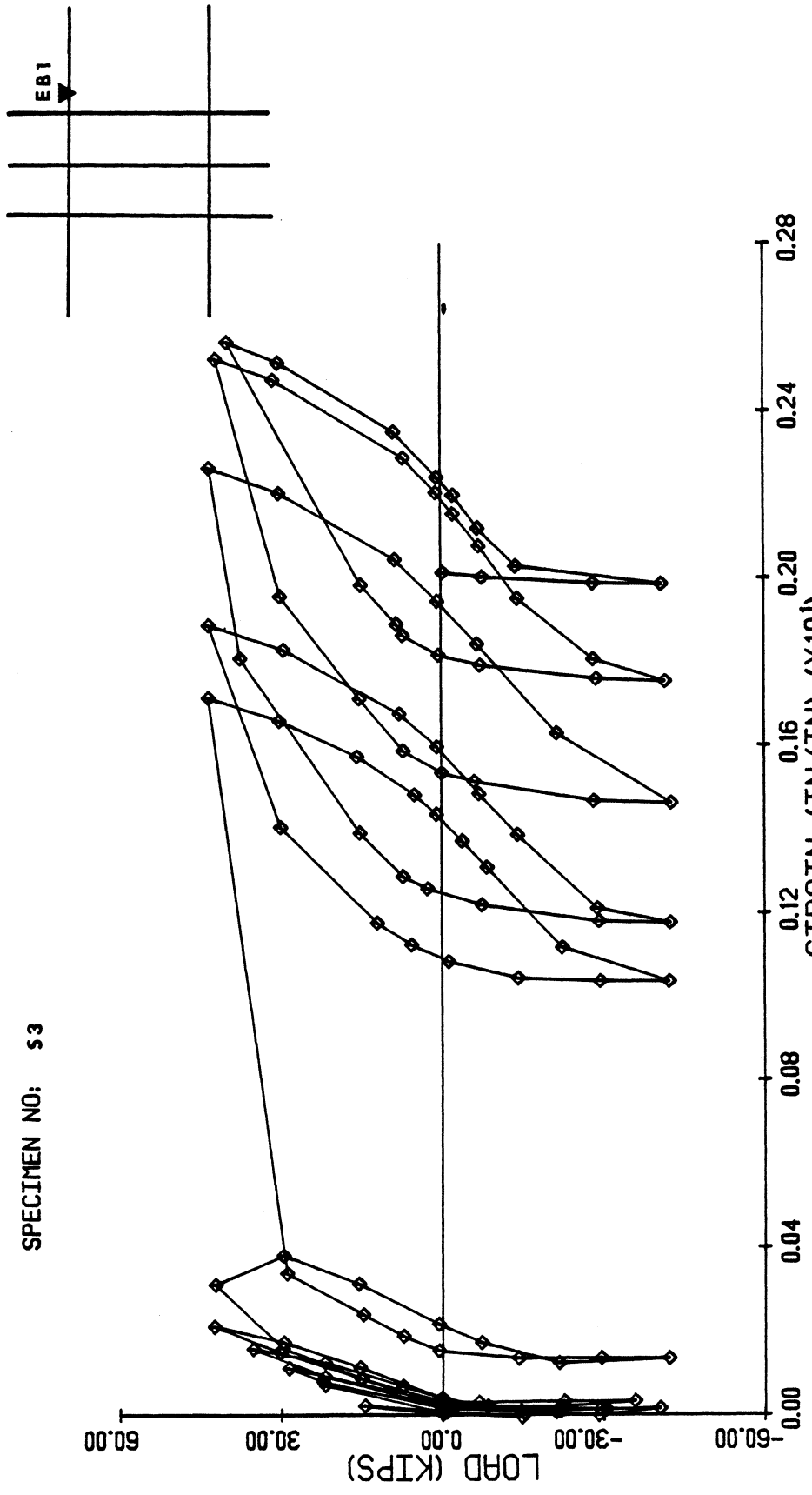

Fig. 3.52 Column Load vs. Strain in Main Beam Reinforcement at EB1 for Specimen S3

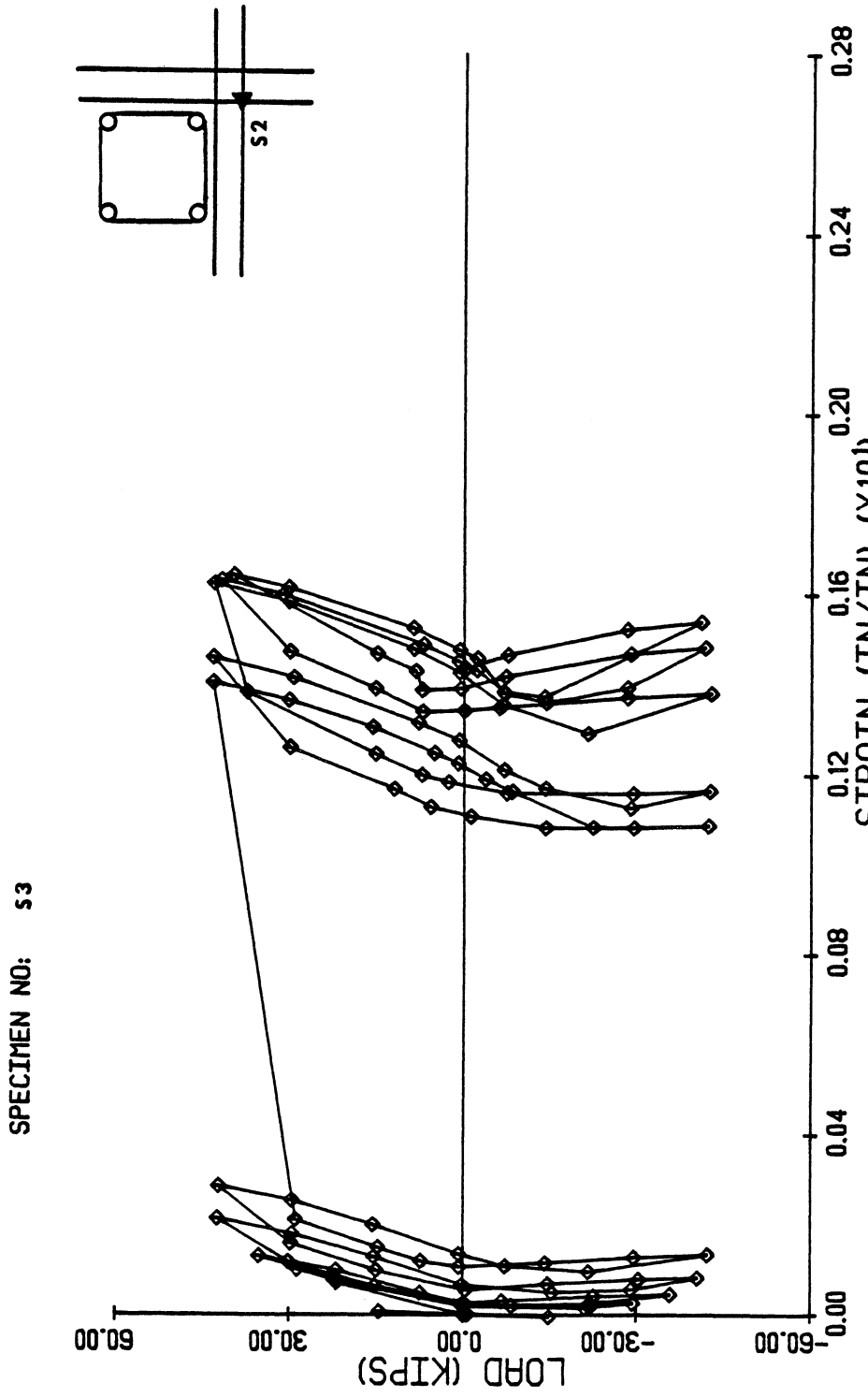

Fig. 3.53 Column Load vs. Strain in Main Slab Bar at S2 for Specimen S3

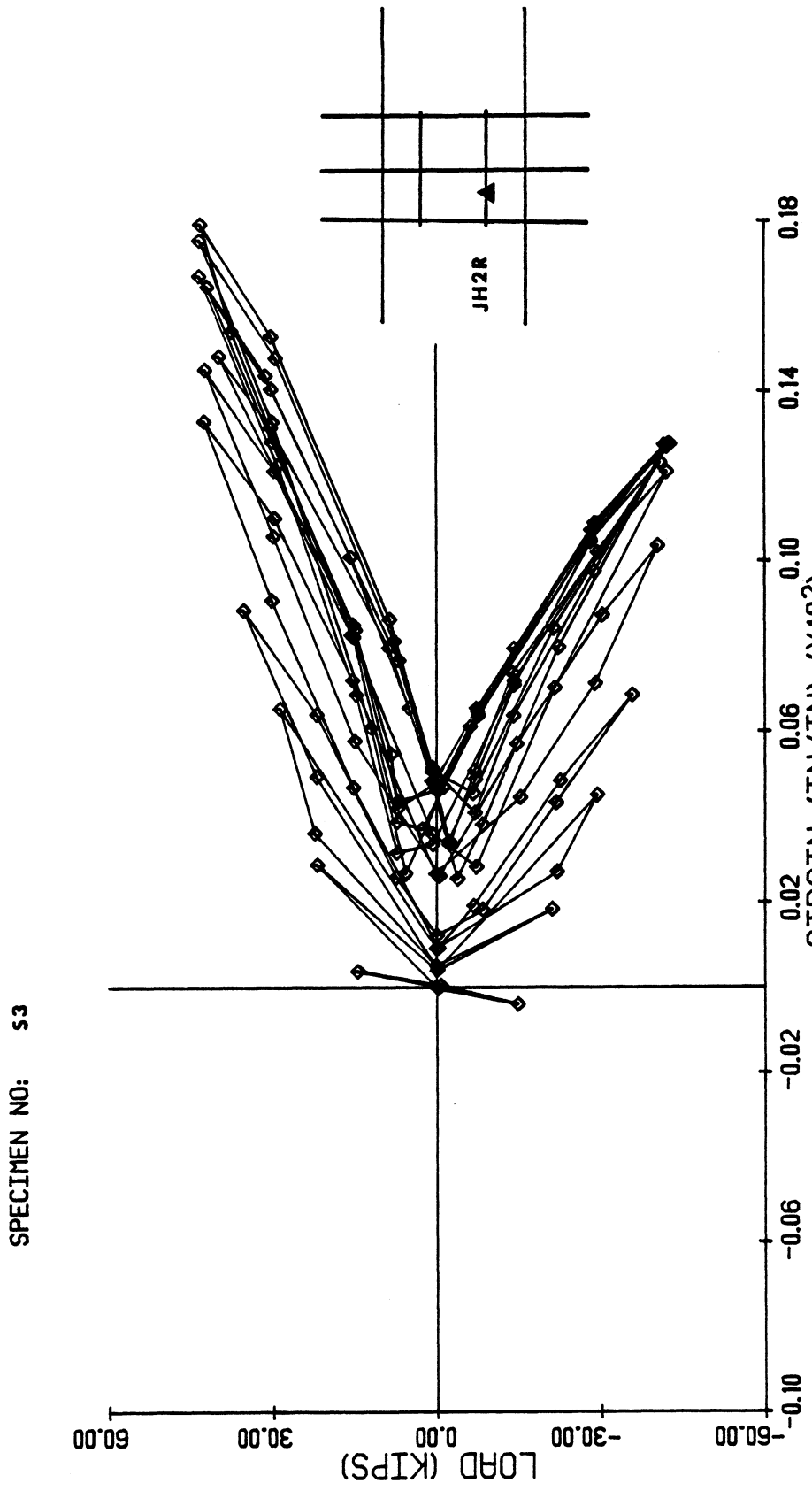

Fig. 3.54 Column Load vs. Strain in Square Joint Hoop at JH2R for Specimen S3

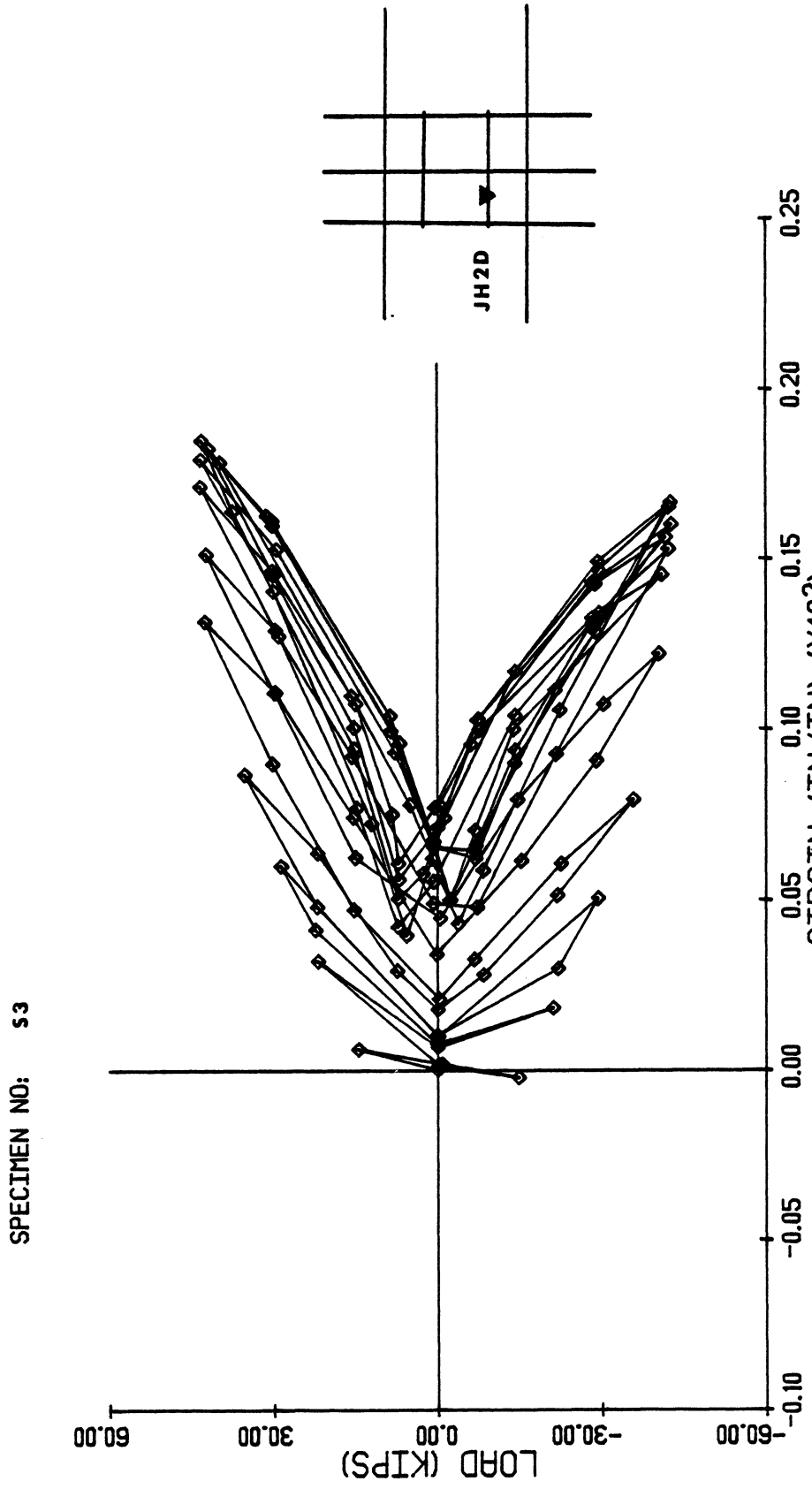

Fig. 3.55 Column Load vs. Strain in Diamond Shape Joint Hoop at JH2D for Specimen S3

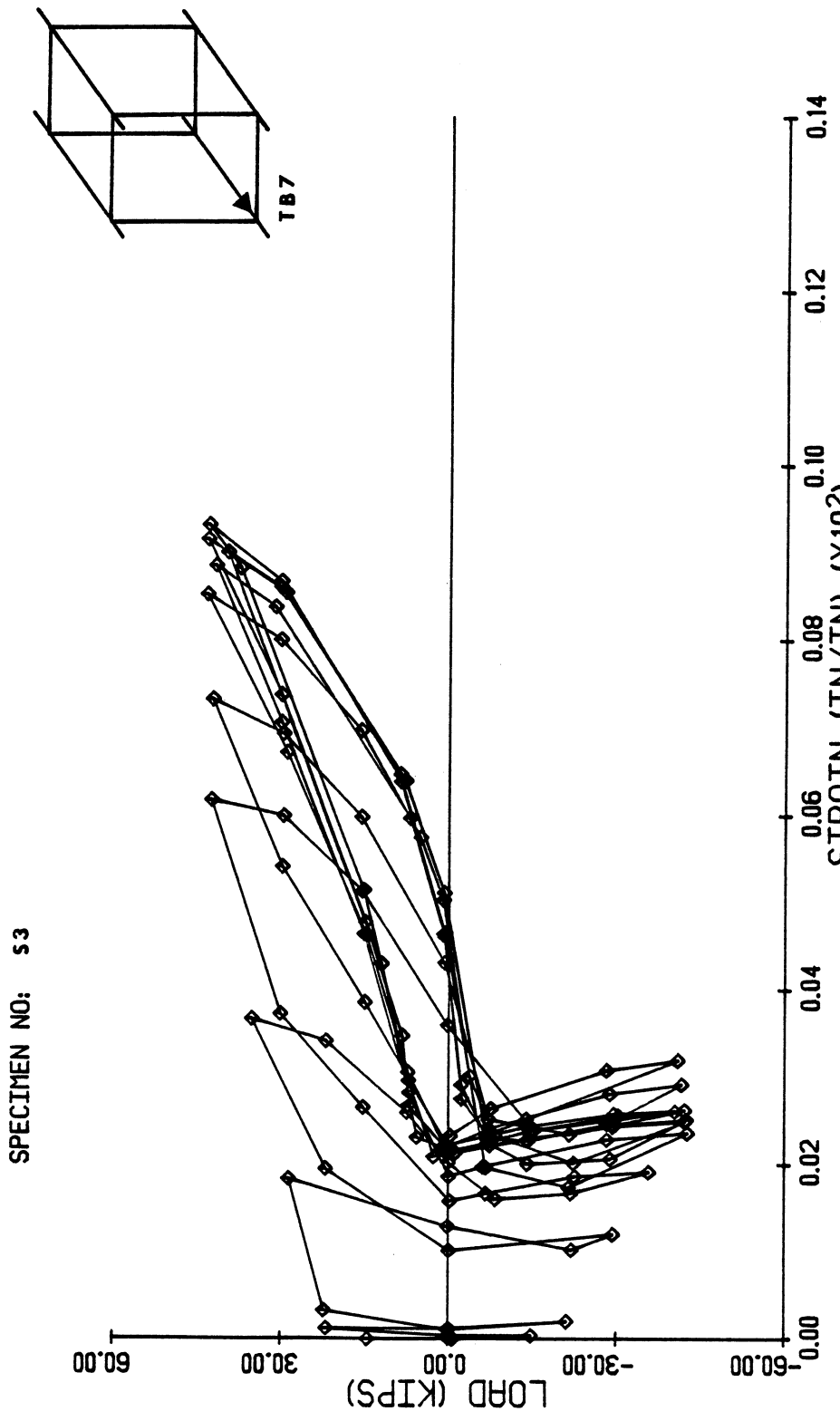

Fig. 3.56 Column Load vs. Strain in Trans. Beam Main Reinforcement at TB7 for Specimen S3

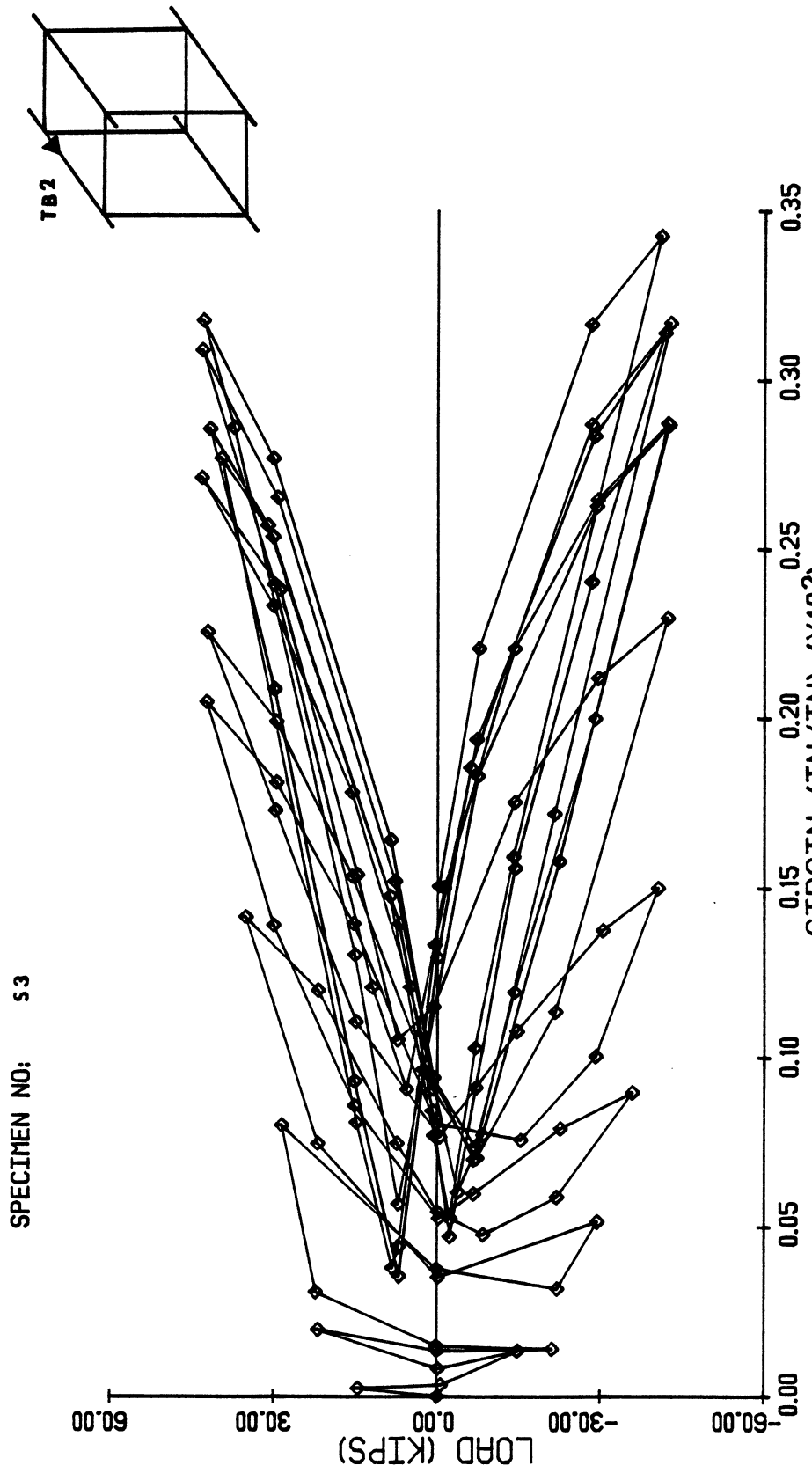

Fig. 3.57 Column Load vs. Strain in Trans. Beam Main Reinforcement at TB2 for Specimen S3

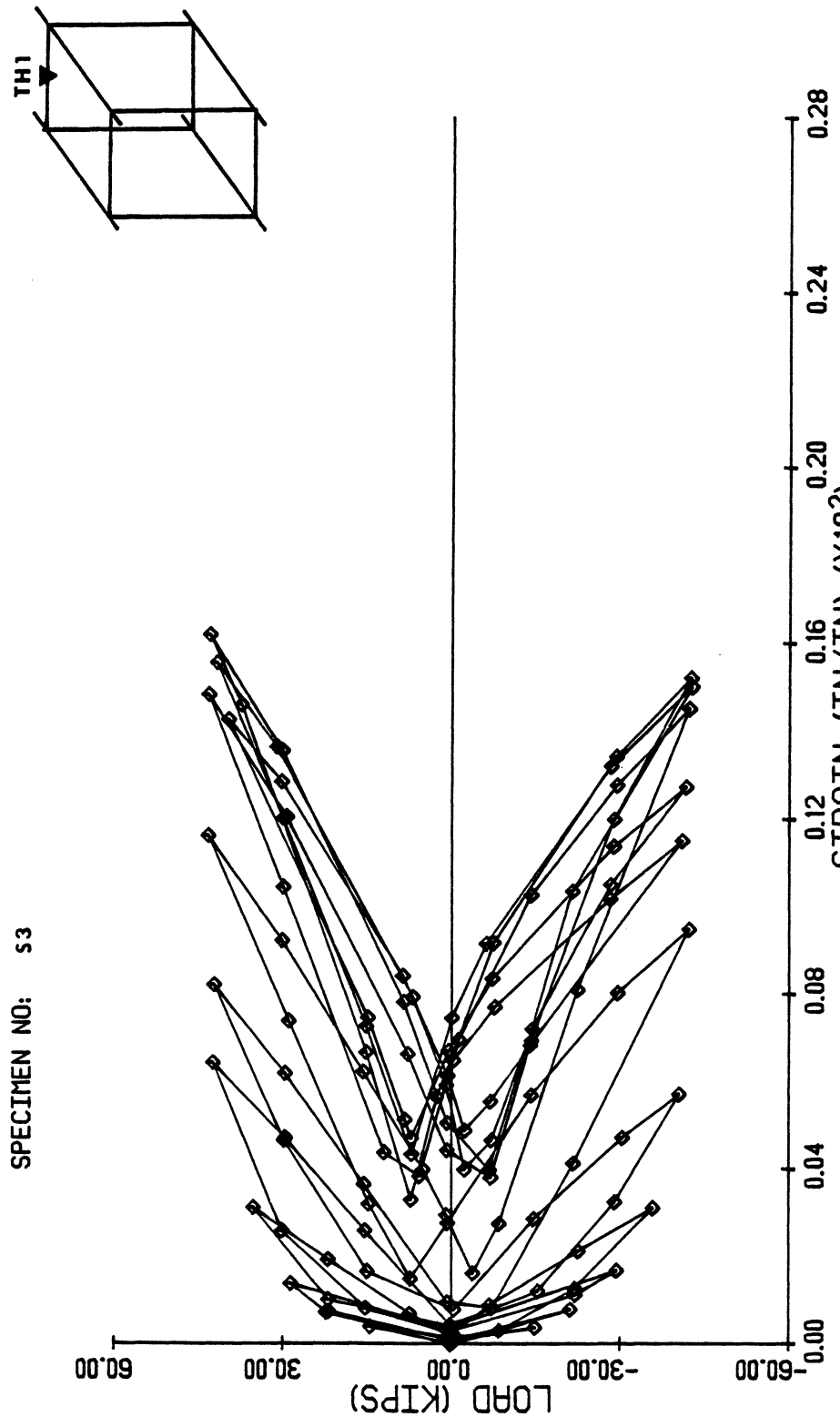

Fig. 3.58 Column Load vs. Strain in Trans. Beam Hoop Reinforcement at TH1 for Specimen S3

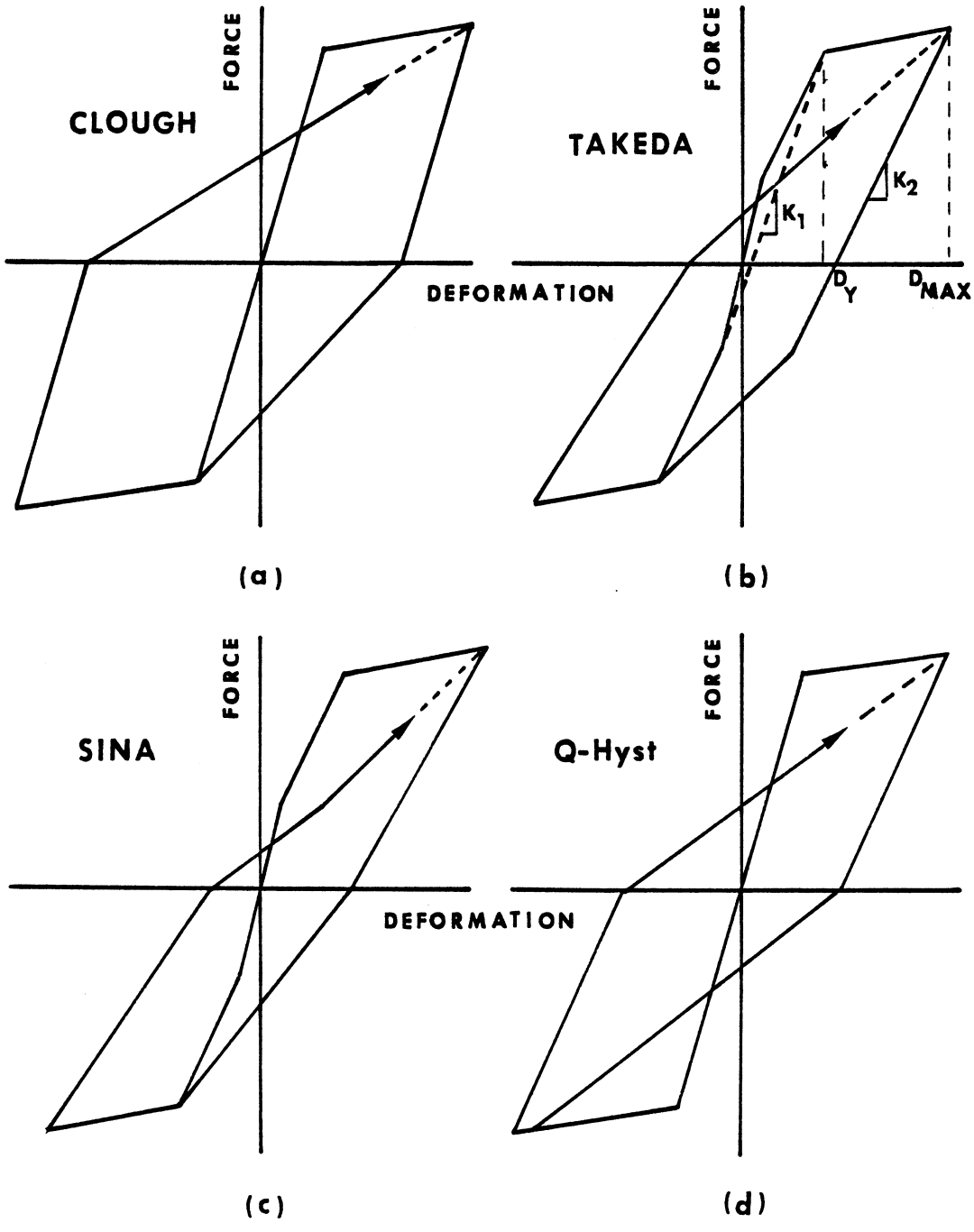

Fig. 5.1 Hysteresis Models

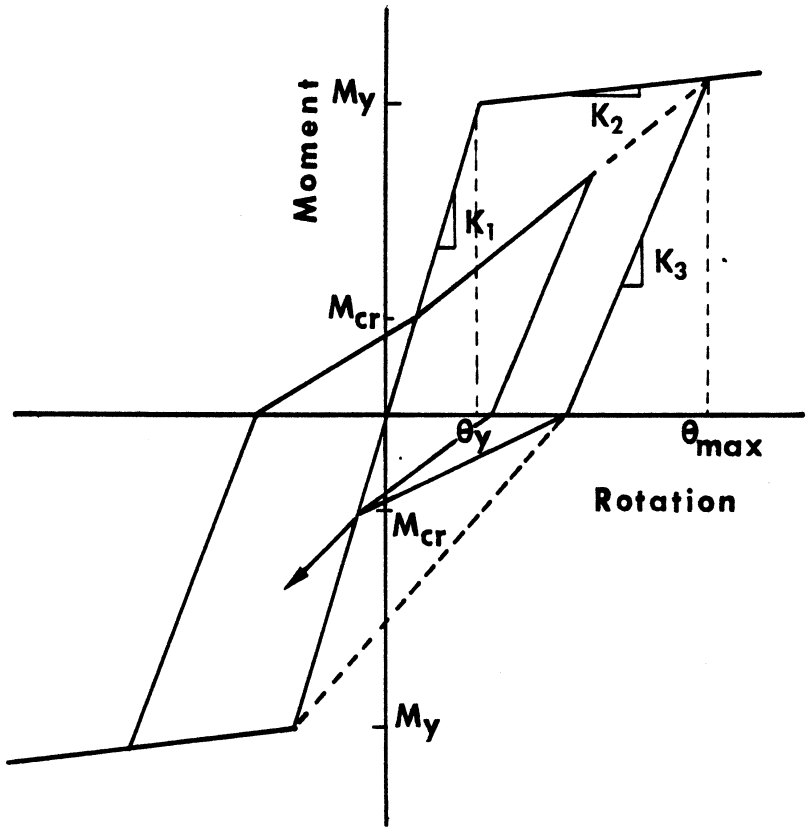

Fig. 5.2 Proposed Hysteresis Model

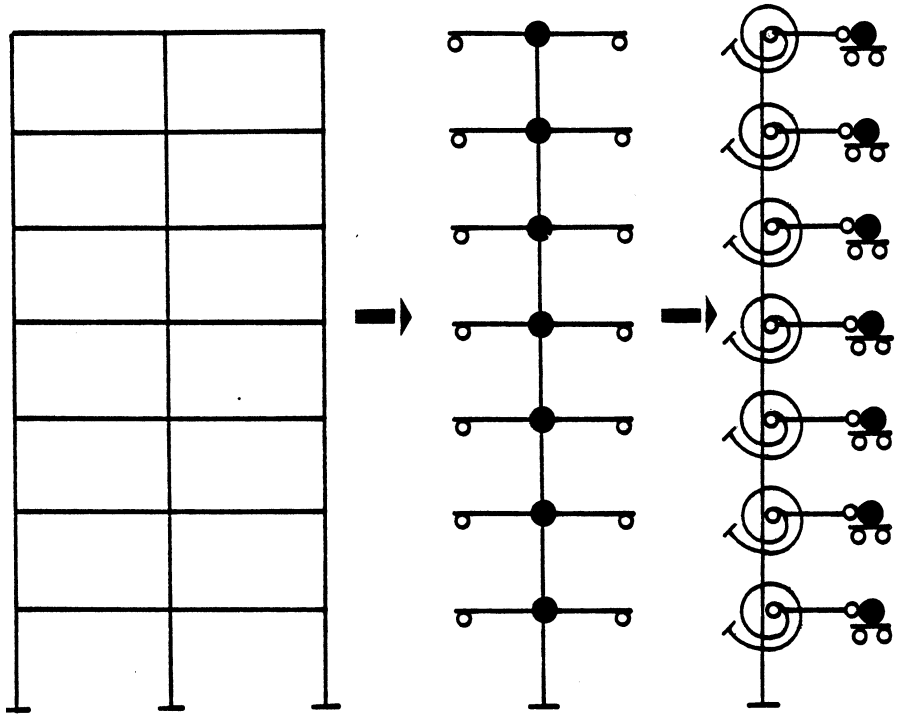

Fig. 5.3 Proposed Analytical Model

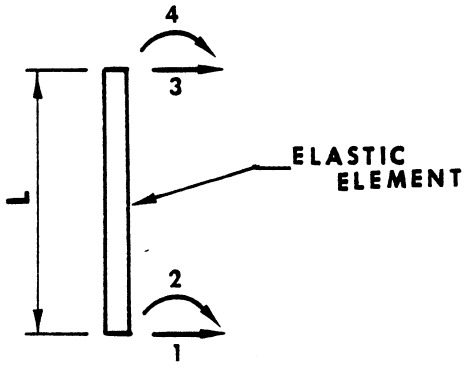

Fig. 5.4 Nodal Degrees of Freedom of an Element

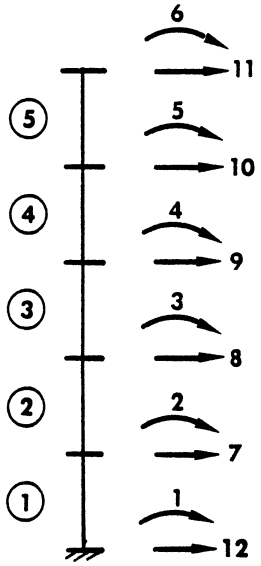

Fig. 5.5 Numbering Scheme for Global Degrees of Freedom

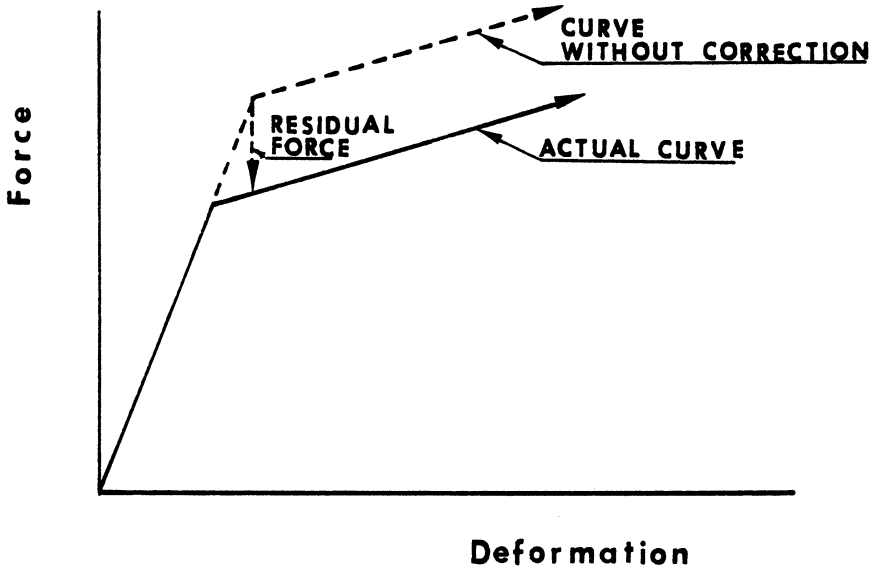

Fig. 5.6 Correction of Residual Forces at Change of Stiffness

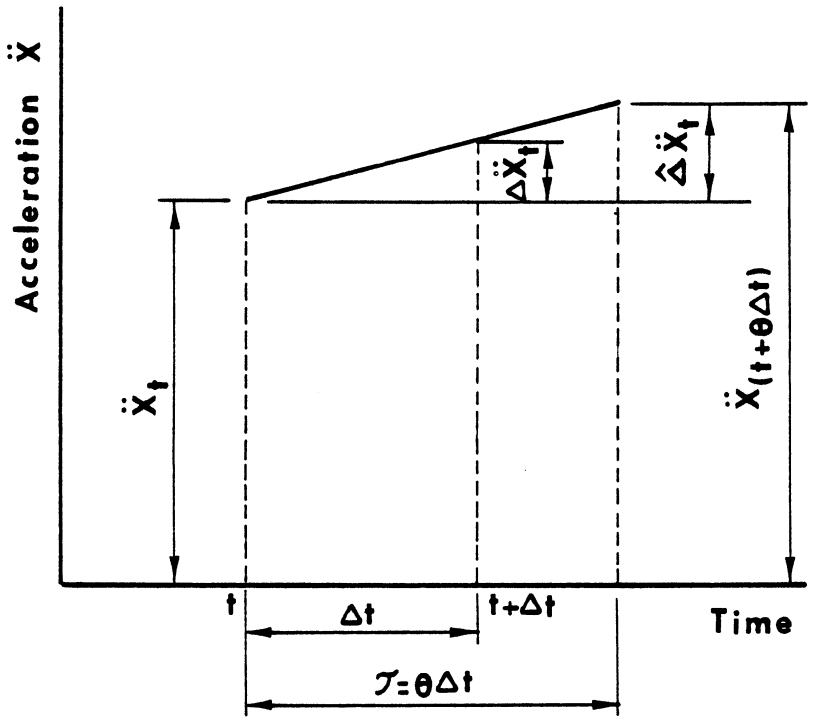

Fig. 5.7 Linear Acceleraion over Extended Time Period

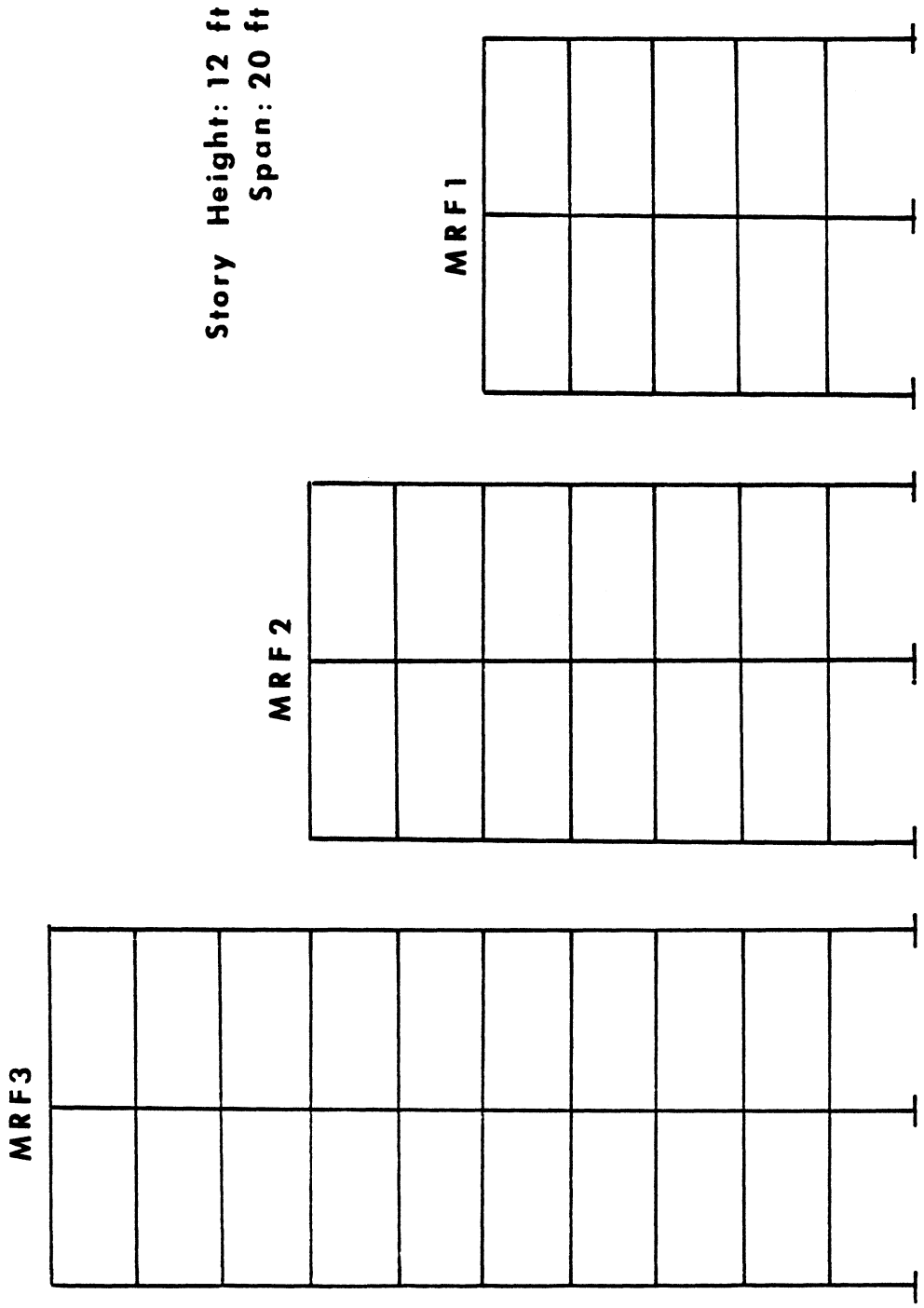

Fig. 6.1 Frames MRF1, MRF2 and MRF3 Used for Analyses

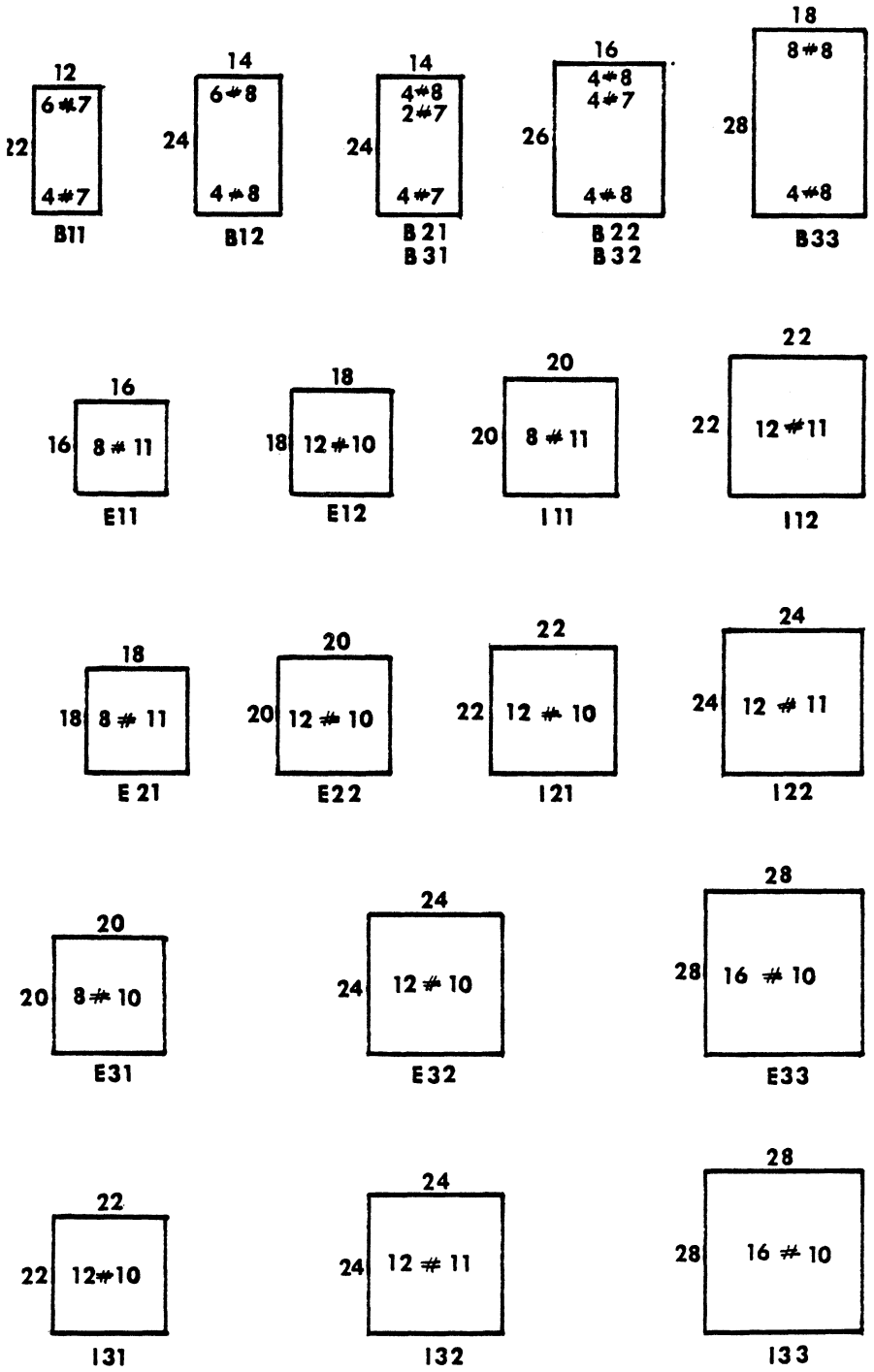

Fig. 6.2 Cross Sectional Details of Frame Members

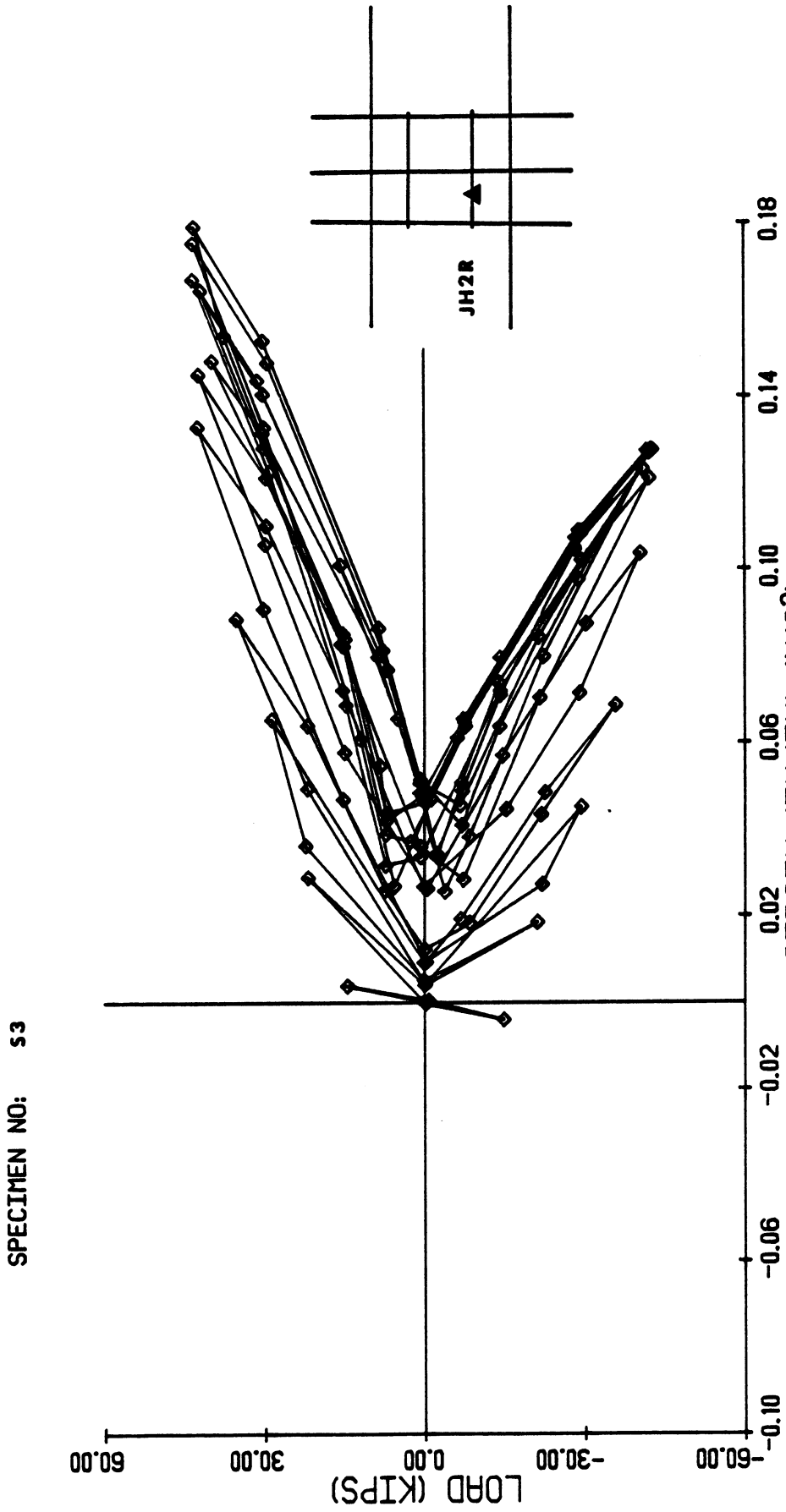

Fig. 3.54 Column Load vs. Strain in Square Joint Hoop at JH2R for Specimen S3

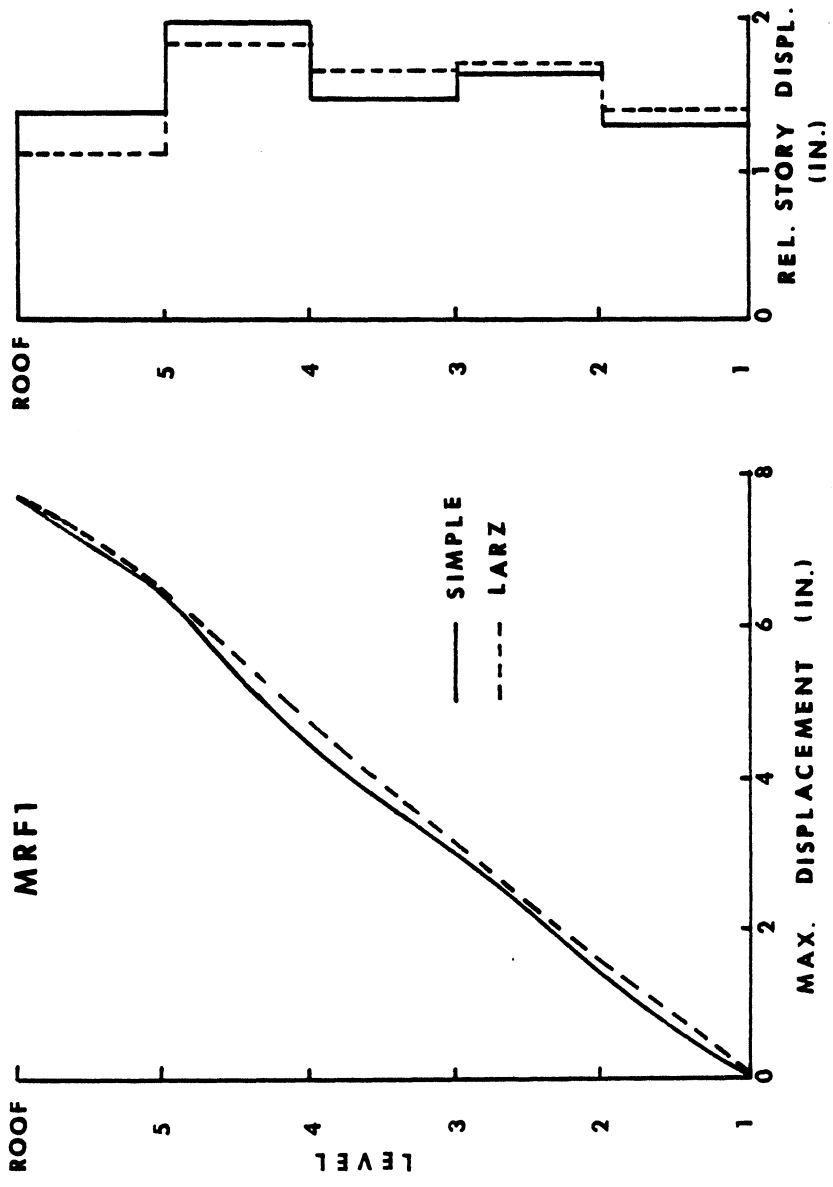

Fig. 6.4(a) Absolute Maximum and Relative Story Displacements of Frame MRF1

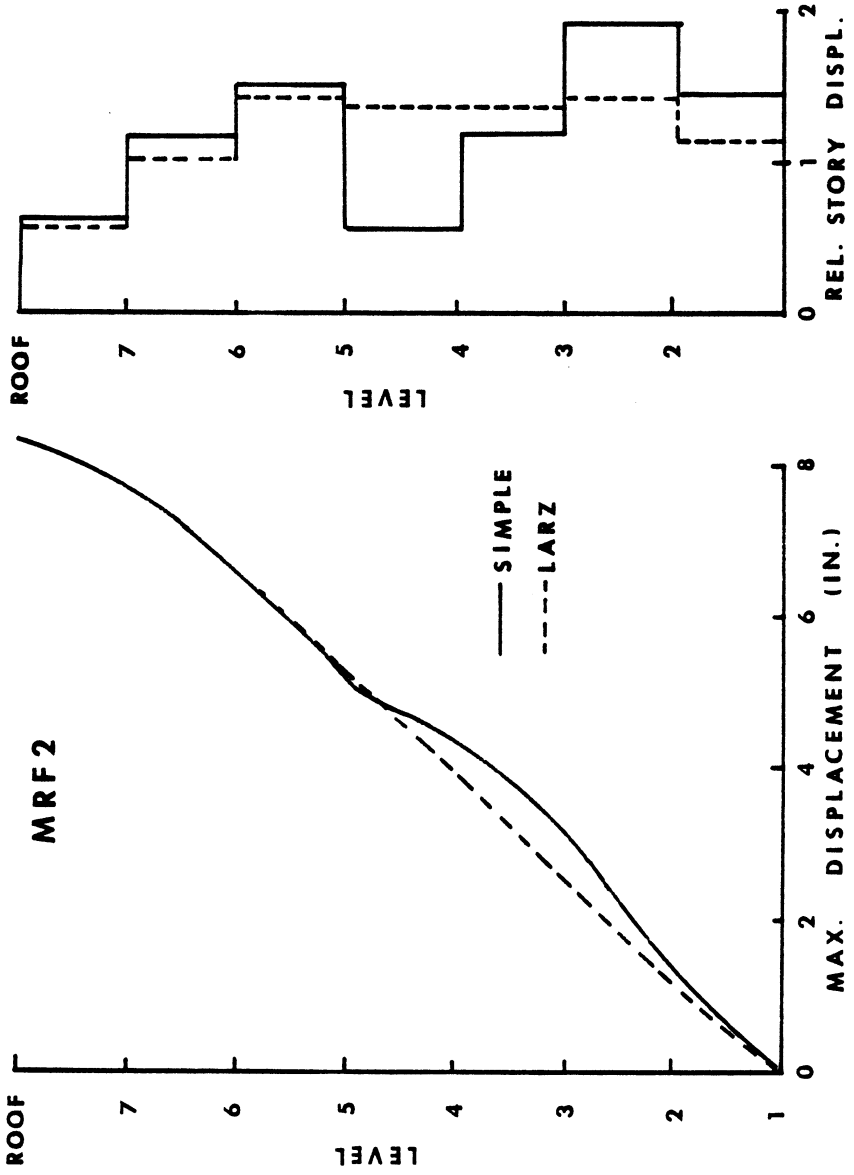

Fig. 6.4(b) Absolute Maximum and Relative Story Displacements of Frame MRF2

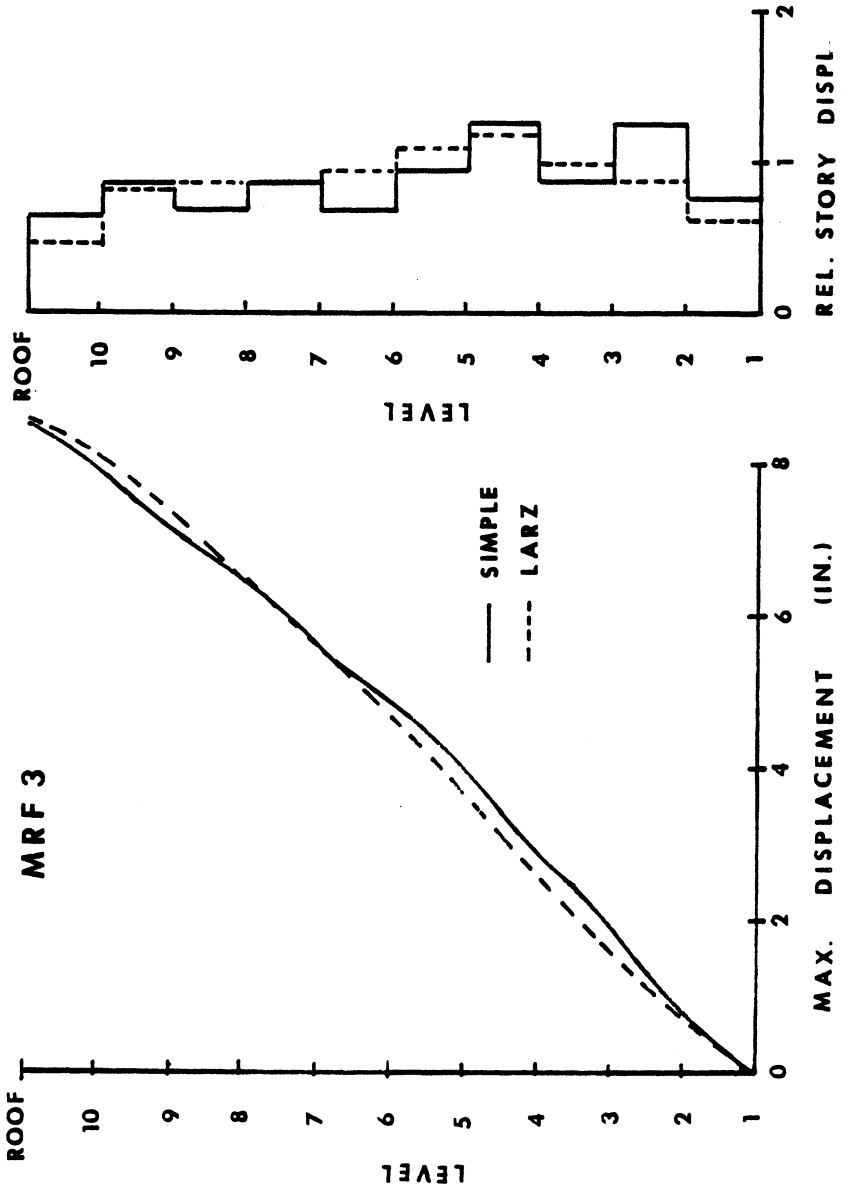

Fig. 6.4(c) Absolute Maximum and Relative Story Displacements of Frame MRF3

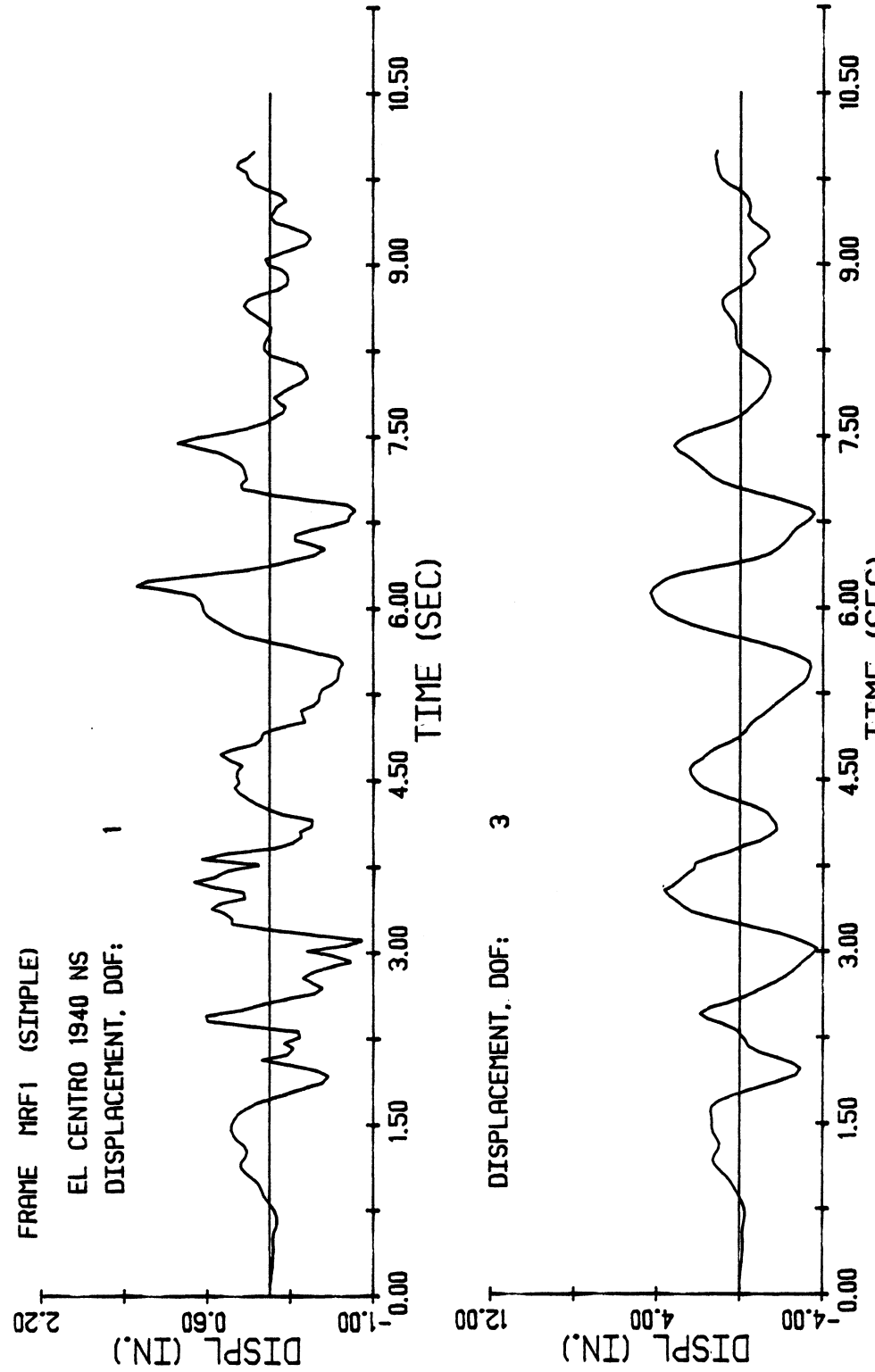

Fig. 6.5(a) Displacement Response at Story Level One and Three of Frame MRF1

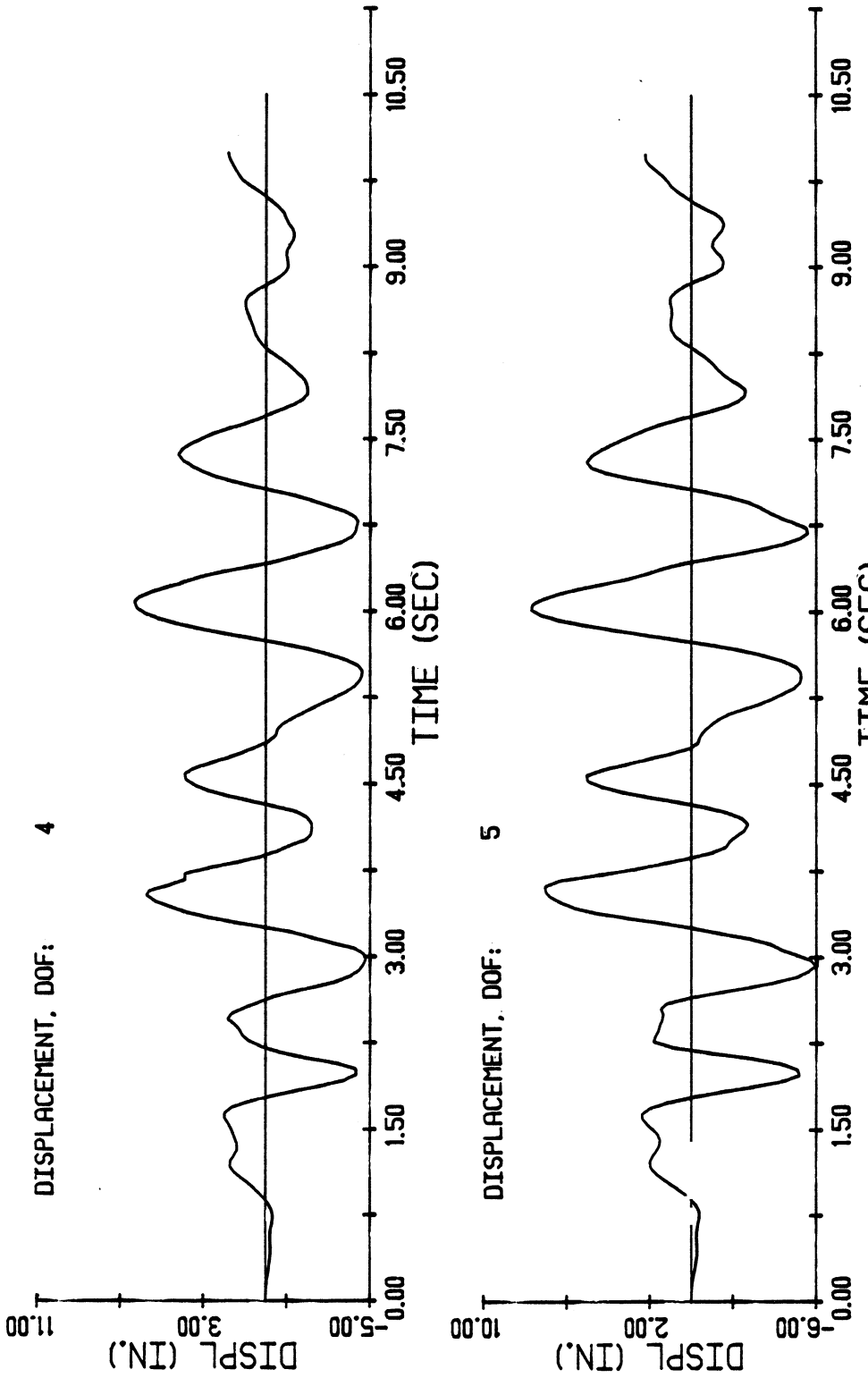

Fig. 6.5(a) Contd. Displacement Response at Story Level Four and Five of Frame MRF1

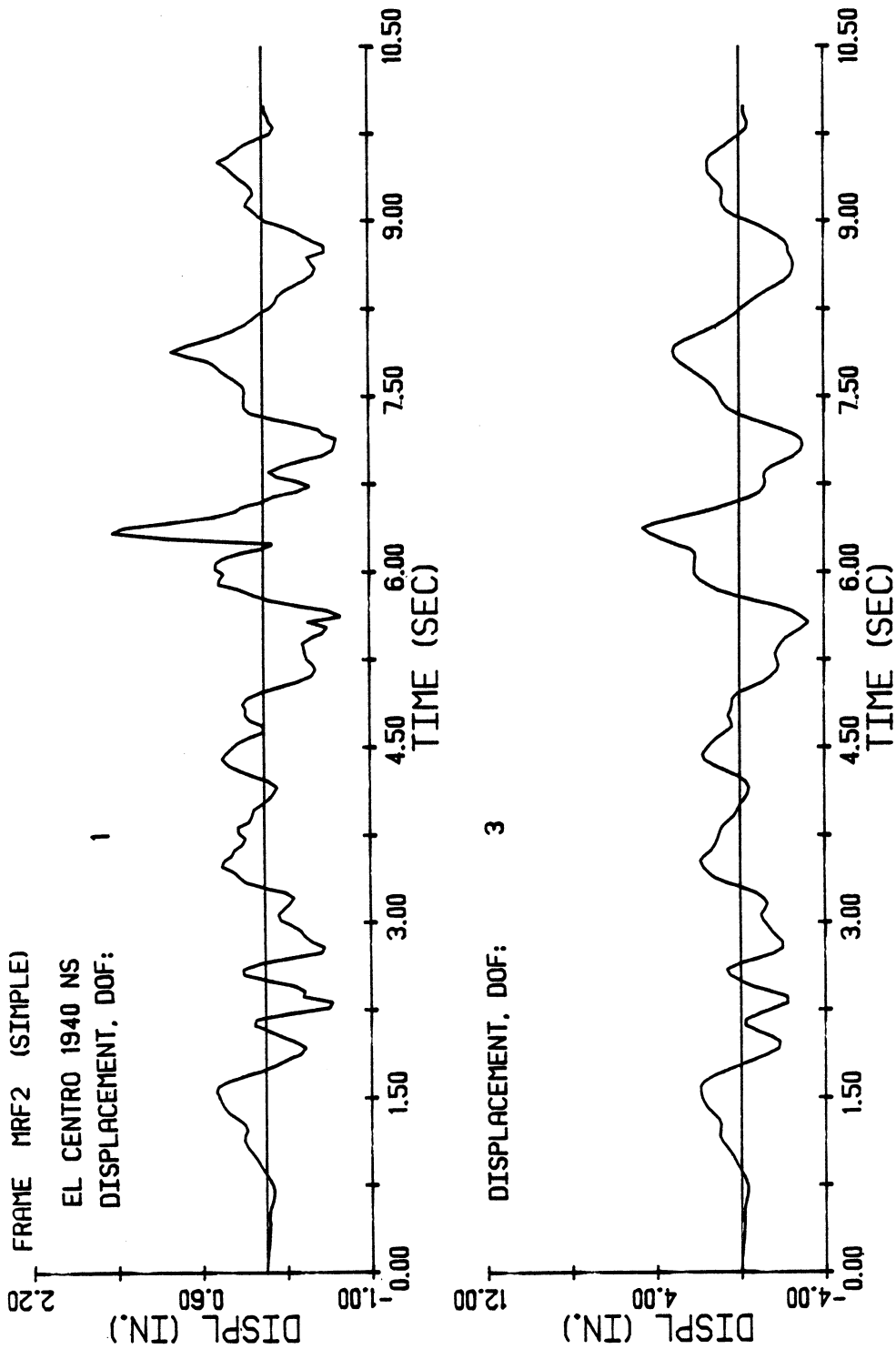

Fig. 6.5(b) Displacement Response at Story Level one and Three of Frame MRF2

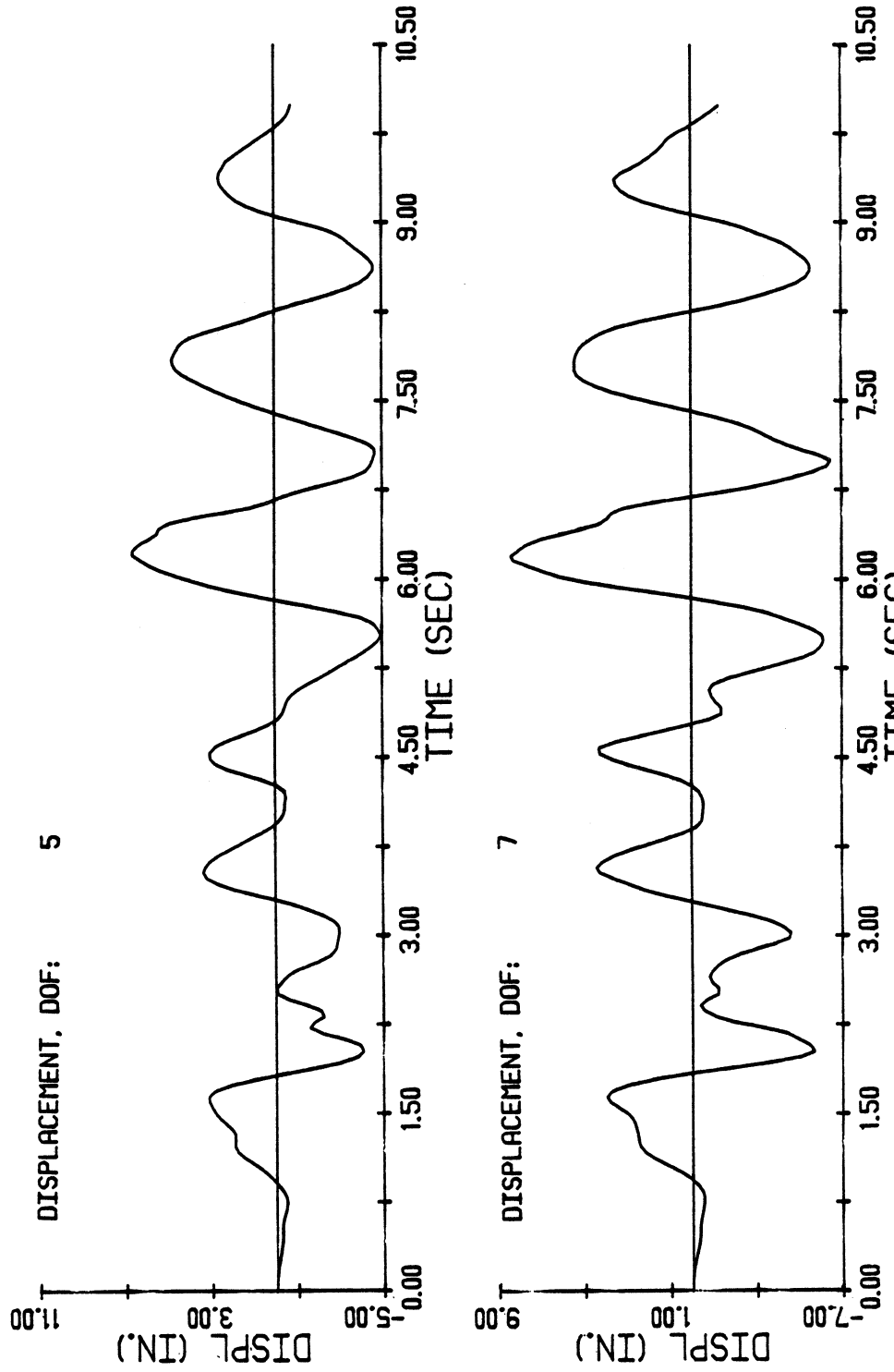

Fig. 6.5(b) Contd. Displacement Response at Story Level Five and Seven of Frame MRF2

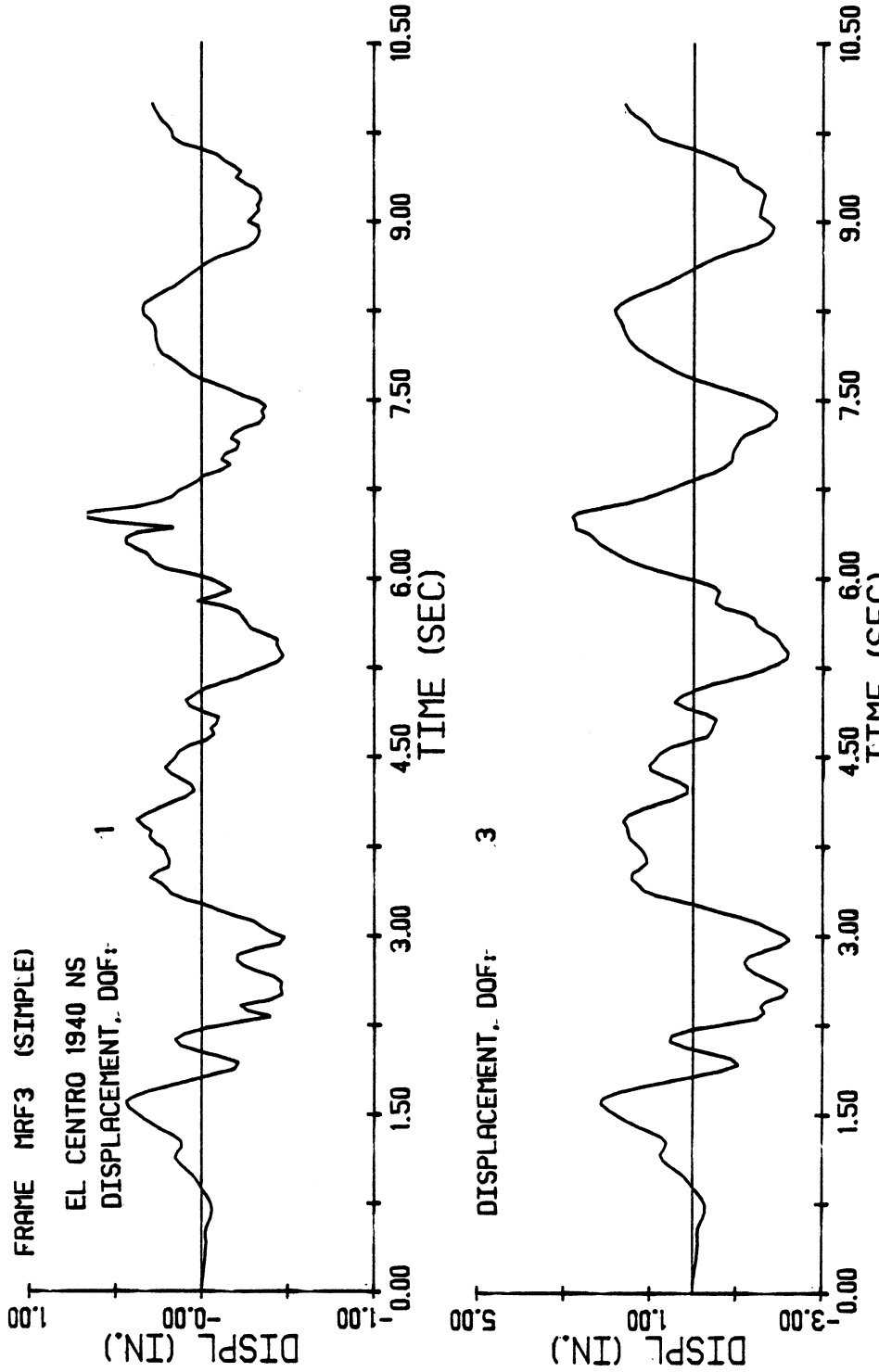

Fig. 6.5(c) Displacement Response at Story Level one and Three of Frame MRF3

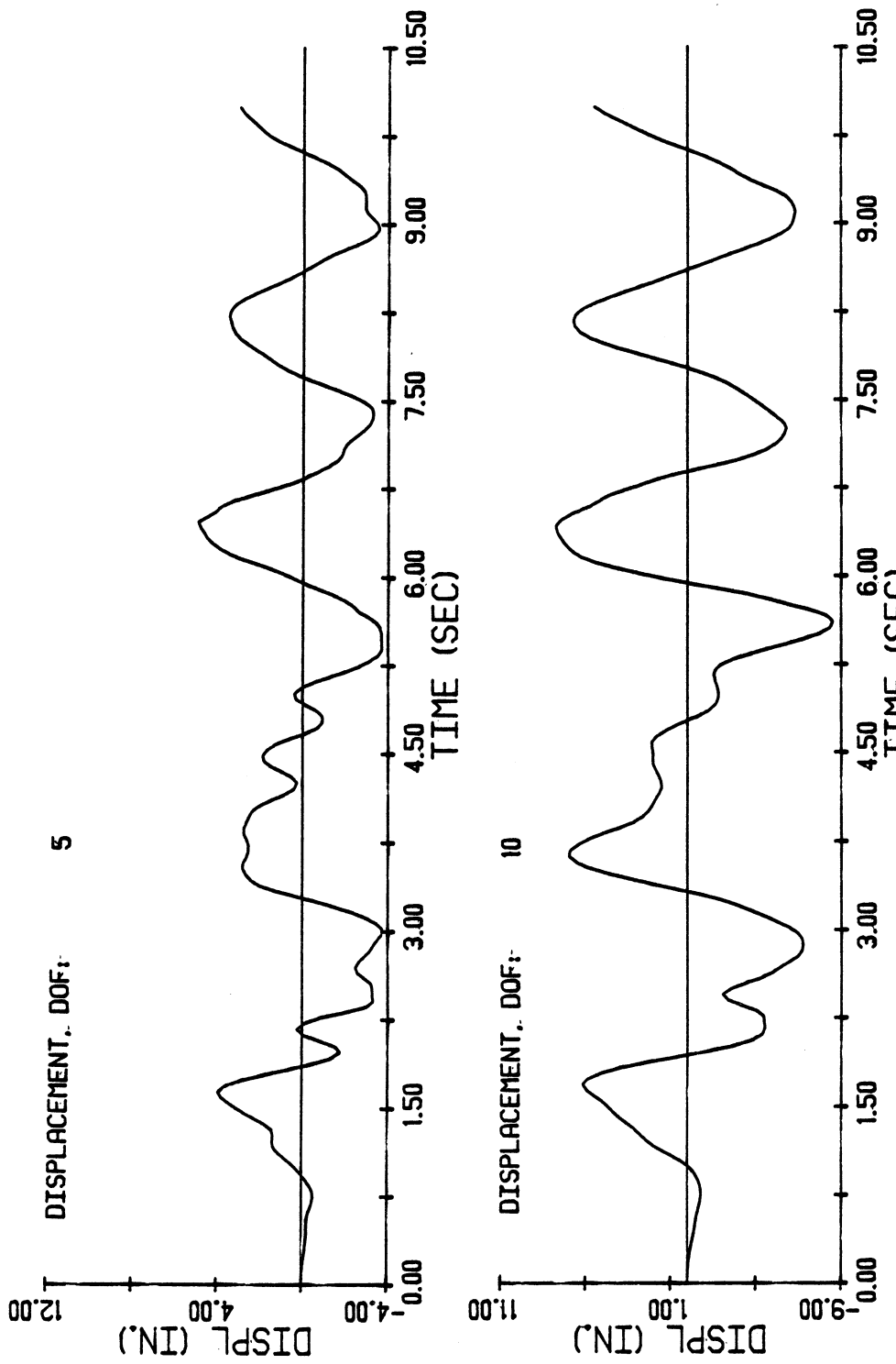

Fig. 6.5(c) Contd. Displacement Response at Story Level Five and Ten of Frame MRF3

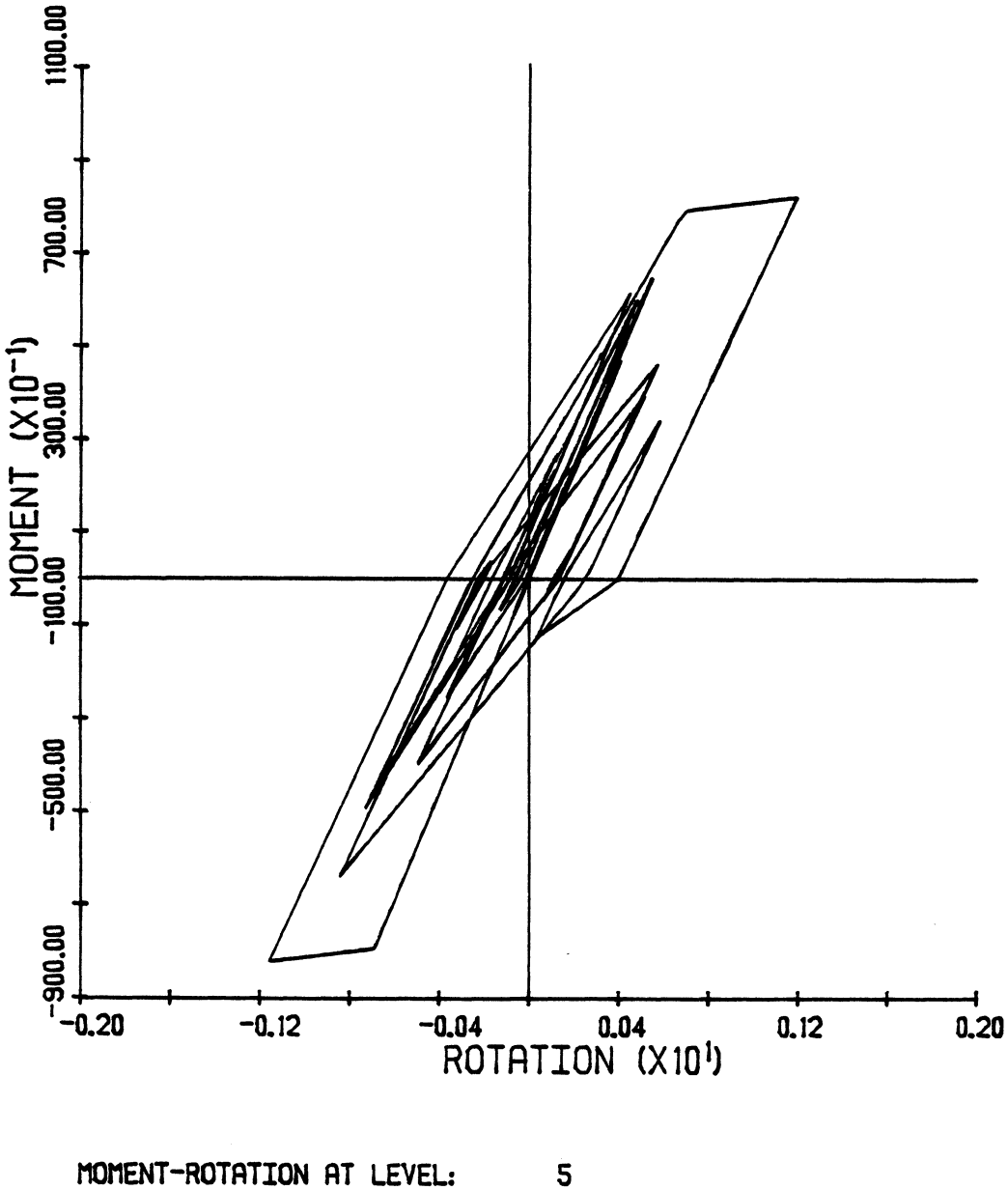

Fig. 6.6 Hysteretic Response of Beam to Column Joint at Level Five of MRF2

APPENDICES

APPENDIX A

SPECIMEN DESIGN

A.1 General

All specimens were designed with a specified concrete compressive strength of 4000 psi. The yield strength of the reinforcing steel used in design was based on the actual yield strength observed during the tests on steel coupons. Grade 40 steel was used for the beam main reinforcement and the beam and column shear reinforcement. An average value of 48 ksi for Grade 40 steel was adopted for design. The column main reinforcement for all specimens consisted of Grade 60 steel only. The Grade 60 steel was observed to have an average yield strength close to 60 ksi and hence, this value was used in the design of columns. Beam and column sections were designed using a computer program for the analysis of reinforced concrete sections. The strain hardening effect of steel was ignored for the design of members.

The overall dimensions of specimens were dictated by the size of the testing frame. All specimens had the same height of column (96 in.) and length of beams (114 in.). The member sizes were in general determined by the loading capacity of the test set up. Beam and column cross sections

were also kept constant for all specimens. The width of the slab (39-1/2 in.) in the S-series specimens was the maximum width permitted by the testing frame.

A.2 Design of subassemblages

The flexural design of beams and columns was determined by two factors. Firstly, the column to beam flexural strength ratio, which was kept constant at 1.5 for all specimens. Secondly, the joint shear stress, which was one of the variables in the experimental study. Two ranges of joint shear stress values (12-14 $\sqrt{f'_c}$ psi units and 16-18 $\sqrt{f'_c}$), based on the nominal concrete and steel strengths discussed in the previous section, were aimed at in the design of subassemblages. The column and beam main reinforcements were selected by trial and error to approximately yield the targeted values for the flexural strength ratio and the joint shear stress simultaneously. The shear reinforcement in beams and columns was designed according to Appendix A provisions of ACI Code (14). Its primary objective was to insure that no shear failure occurred in the column or in the beam. Typical beam and column shear reinforcement is shown in Fig. A.1.

For specimens with transverse beams and slab, a slab width of one-fourth the span (24 in.) was considered effective in flexural strength computations. Cross sections and reinforcement details of all specimens are given in Fig. A.2. Column axial loads for all specimens varied between twenty to thirty percent of the balanced axial load.

A typical moment vs. curvature diagram for the beam section of specimen X1 and the moment vs. axial load interaction diagram of the column for the same specimen are shown in Fig. A.3 and A.4 respectively.

The joint shear stress calculations in the design of the specimen were based on the joint shear area made up of the width of column (b) and the effective depth of column (d_{col}) in Eq. (4.1). However, during analysis of experimental results the joint shear stress calculations were revised on the basis of latest draft recommendations of ASCE-ACI Committee 352 (46) which uses total width (b) and the total depth (h) of the column. The joint shear stress values given in Table 3.3 were determined using the actual material properties for each of the specimen. The observed concrete and steel strengths were generally higher than the specified values. Correspondingly, the column to beam flexural strength ratios given in Table 2.3 were also based on the actual flexural capacities of beam and column sections.

Sample calculations for joint shear stress based on the nominal design values for specimen X1 are given below:

For the main beam

top steel, $A'_s = 2.4\ in^2$

bottom steel, $A_s = 1.76\ in^2$

For a concrete comressive strength of

$$f'_c = 4000 \text{ psi}$$

and steel yield strength of

$$f_y = 48000 \text{ psi}$$

and ignoring the strain hardening effect, the positive moment capacity of the beam is

$$M^+ = 1107 \text{ K-in}$$

and the negative moment capacity is

$$M^- = 1467 \text{ K-in}$$

Then sum of the beam positive and negative moment capacities is

$$\Sigma M_{beams} = 2574 \text{ K-in}$$

and the column shear is

$$V_{col} = 2574/88$$
$$= 29.25 \text{ K}$$

The joint shear force is

$$V_j=(A'_s+A_s)48x1.1-V_{col}$$
$$=190.4\ K$$

where the factor (1.1) accounts for strain hardening in the beam
reinforcement.
The joint shear stress is

$$v_j=V_j/(bd)_{col}$$
$$=190.4x1000/(14.25x11.83)$$
$$=1136psi$$
$$=18\sqrt{f'_c}\ \text{for}\ f'_c=4000\ psi$$

The column flexural capacity for an axial load of 55 kip (20% of the balanced axial load) is 2060 k-in. Then the column to beam flexural strength ratio becomes

$$\Sigma M_{col}/\Sigma M_{beams} = 2x2060/2574$$
$$= 1.60$$

The joint shear reinforcement consisted of either two or three layers of a set of a square and a diamond shape hoop. The hoop configuration and their spacing in the joint are shown in Fig. A.5. For joint hoops, No. 4 steel of Grade 40 was used for all specimens. The effective area of hoops for shear resistance is

$$=2x0.2+2x0.2x0.707$$
$$=0.683\ in^2$$

The percentage of transverse hoop reinforcement for two layers of hoop reinforcement is

$$\rho_t=A_{sj}/(b(d-d'))$$
$$=1.366x100/(14.25x12.5)$$
$$=0.76\%$$

where A_{sj} is the effective hoop area, b is the width of the column and $(d-d')$ is the distance between the top and bottom reinforcement of the beam.

For a joint with three layers of hoop reinforcement, the percentage of transverse reinforcement was

$$\rho_t=1.15\%$$

The slab thickness and reinforcement was determined based on typical loading on a floor level. The transverse beams used in the S-series specimens were not based on any particular design consideration. Their sizes were selected as typical sections. Because the specimens X3 and S3 had lower reinforcement in the main beam to achieve a lower joint shear stress value, the transverse beam reinforcement

in specimen S3 was also reduced.

APPENDIX B

MATERIAL PROPERTIES.

B.1 Concrete

The X-series specimens and the columns of the S-series specimens were cast using hand mixed concrete prepared in the laboratory. The slab and the beams of the S-series specimens were cast using ready mixed concrete because of the large volume of concrete involved. The concrete mix was designed according to the Recommended Practice for Selecting Proportions for Normal and Heavy Weight Concrete (ACI 211.1-74). To achieve a 28 day compressive strength of 4000 psi, several trial batches were tested before the final proportions of concrete mix were decided. The mix was designed using Type I portland cement and a well graded gravel of one inch maximum aggregate size. Quantities for one cubic yard of concrete for a design slump of 4 to 5 inches are as follows:

Cement	= 667 lbs
Fine Aggregate	= 1154 lbs
Coarse Aggregate	= 1809 lbs
Water/cement ratio	= 0.57
Water	= 380 lbs

The amount of water was adjusted to give a slump of 4 to 5 inches to facilitate proper placement of concrete in the joint. At least three 6in. x 12in. cylinders for each mix used in casting the specimens were capped and tested for compressive strength at 28 days. Other cylinders were tested on the day the specimens were tested. For stress vs. strain relationship of concrete, cylinders of 4in. x 8in. size were also prepared for each mix. All cylinders were cast in disposable moulds which were stripped after twenty four hours and cured along with their parent specimens. Table B.1 gives the casting and testing schedule and the average compressive strength of concrete at the testing date of specimens. Although the specimens were cast in three stages spread over a period of one week, the casting date given in the Table B.1 is for the day the beams and joints were cast.

B.2 Reinforcng Steel

A minimum of three coupons of each bar size were tested in tension for the stress vs. strain relationship of steel. Representative coupons were selected from each batch of reinforcing bars. Each coupon was punched for a standard gage length of 8 in. and a mehanical extensiometer was attached to the bar at these points. Strain readings were taken at a larger interval in the elastic range and the

TABLE B.1 SPECIMEN CASTING AND TESTING SCHEDULE

Specimen	Casting date	Testing date	Concrete Strength, psi		
			Bottom Column	Beam/ Slab	Top Column
X1	4.19.80	8.13.80	4245	4980	4715
X2	5.16.80	8.18.80	4475	4880	5235
X3	2.12.81	4.1.81	4790	4500	3910
S1	10.20.80	12.13.80	4320	6030	4323
S2	11.18.80	1.22.81	4100	4456	3600
S3	2.12.81	3.19.81	4230	4100	3700

interval was reduced near the yield load to locate the yield strain and the strain at the onset of strain hardening. The extensiometer was detached from the bar shortly before the ultimate load was reached and the load was increased to cause fracture in the bar. Typical stress vs. strain curves are given in Fig. 2.7. Average properties of all sizes of bars used in the tests are presented in Table 2.5.

APPENDIX C

CONSTRUCTION OF SPECIMENS

C.1 Formwork

One of the reasons for keeping the same sizes of members and the overall dimensions of both the X-series and S-series specimens was to be able to use the same form repeatedly for all specimens of a particular series. The forms were fabricated from 3/4 in. thick exterior grade plywood which was reinforced with 1-1/2 in. square fir wales. Because the specimens were cast in stages, the forms were designed to permit partial assembly without obstructing the placement of reinforcement or placing of concrete. Individual form sections were joined together by 1/4 in. machine bolts with wing nuts. To prevent warping the forms were waterproofed with orange shellac. Before placing concrete the forms were caulked at all joints with oil base clay to prevent any leakage of mortar. The inside of the forms was coated with motor oil to facilitate an easy removal of forms from the finished specimens. For the pin connection close to the beam ends, 2 in. diameter holes were made in the forms at predetermined locations for insertion of steel pipes, as shown in Fig. C.1. In the S-series specimens, slabs were stiffened externally over the pin

connections in the beams. For this purpose four wooden dollies of 1in. diameter x 4in. were placed vertically at each end of the slab form to leave holes in the slab for bolts used in stiffening of slabs. Cables from the gages attached to the reinforcing bars were taken out of the form through the holes drilled in the forms at the closest convenient location. Cross ties were place across the beam forms to prevent bulging of forms under the lateral pressure of freshly placed concrete.

C.2 Preparation of Reinforcement

The main reinforcing bars in beams and columns were straight sections and required only cutting of bars to the appropriate length. The stirrup ties, however, were bent manually to the right size and shape using a Hossfield reinforcing bar bender. The tie ends had an overlap of 2 in. to permit welding them together. This ensured closed ties with welded ends stronger than the bar tensile strength. Shear reinforcement in beams consisted of No. 3 Grade 40 hoops while in the columns, hoops were made of No. 4 bars.

The hoops and bars were then prepared for strain gage application. At the selected locations on bars, a 1/2 in. x 2 in. area was filed to remove surface deformations without cutting into the bar diameter. The prepared surface was then smoothed of any sharp ridges by a fine emery cloth. Finally the surface was cleaned by an acid cleaner, followed by a neutralizer. Strain gages and

the application accessories were manufactured by Micro-Measurement Corporation. For the gages to remain effective through yielding of the bars, type EP-08-250BG gages with a gage factor of 2.07±0.15% and resistance of 120±0.15%Ω were selected. The standard procedure recommended by the manufacturer was used for affixing the gages to the bar surface. Belden #22 AWG three lead cables were used to connect the gages with the recording device. Two leads of the cable were attached to a common terminal to compensate for any errors due to the lead wire length. All gages were then protected by a series of protective coats suggested by the manufacturer. This treatment protected the gages against water, impact or abrasions. The cables were tied to the bar close to the gage terminals to prevent any accidental pull on the gages. After installation of gages, the resistance was checked to determine proper functioning of all the gages. Any gage found defective was replaced.

C.3 Assembly of Reinforcement

The same fabrication procedure was followed for all specimens. The column reinforcing cage was assembled first using eighteen gage tie wire. The main bars were held at proper spacing by square plywood templates at each end of column. Hoop stirrups were then tied along the length at appropriate spacing. The gaged joint hoops were carefully positioned in the joint section of the column with gaged bars facing the front of the specimens. The beam and slab reinforcement was assembled in the formwork after the bottom

column had been cast.

C.4 Placing of Concrete

All specimens were cast vertically in three stages to follow the actual construction sequence of a building. The column reinforcing cage was first positioned vertically in the bottom column form and adjusted for proper concrete cover using concrete blocks of appropriate thickness. It was then checked for verticallity using a theodolite and secured in this position. Concrete was placed manually through a steel chute held inside the column reinforcement cage to prevent segregation of concrete from a drop through the height of the column. A hand held internal vibrator was employed for proper compaction.

After the concrete had set in the bottom column, the reinforcement for beams or beams and slab was placed in position and formwork assembled for the second stage of casting. Figures C.2 and C.3 show an X-series and a S-series specimen ready for this stage. The second stage usually occurred two days after the bottom column was cast. Excess concrete was struck off with wooden screeds and then the surface was smoothed with a metal float. In the last stage, the formwork for the top column was assembled and checked for proper alignment with the bottom column before placing concrete. For each batch of concrete mix used in the casting of specimens, slump was checked for proper workability.

After the concrete had attained its initial set, it

was covered with burlap and plastic sheeting to prevent any premature loss of moisture. After about three to five days, the specimens were stripped of their forms and kept covered with wet burlap for seven days. Two X-series specimens after wet curing are shown in Fig. C.4.

APPENDIX D

EXPERIMENTAL TEST SET UP

D.1 Testing Frame

The structural testing frame in the G.G. Brown Laboratory of The University of Michigan was used for the experimental study. Shown in Fig. 2.8, it essentially consists of an outer frame, which is 18 feet high, and an inner four-hinged frame. The inner frame can be displaced horizontally by a 250 kip actuator mounted on the reaction frame and attached to the top of the inner four-hinged frame. To be able to secure the test specimen with proper supports vertically inside the inner frame, the testing frame was modified to suit the purpose. Two pairs of steel brackets made out of 1-1/4 in. thick steel plate were designed and built in the laboratory and bolted to the top and bottom beams of the inner frame. These brackets were further tied together by a pair of tie rods in front and at the back. Two rollers were placed between the column face and the brackets and one plate each with cylindrical surface was placed between the column ends and the frame beams to simulate hinged supports.

The ends of the beams were tied to the bottom beam through two two-hinged links. These links provided a roller

support action to the beam ends and were also instrumented by two sets of strain gage bridges to also act as load cells. The capacity of the force links and the attached yoke assembly was carefully checked for an elastic behavior. Another testing frame with a smaller actuator was used to calibrate these force links before the tests. The test assembly was capable of a lateral displacement at the top of column of six inches in one direction and ten inches in the other direction.

D.2 Recording Devices

The instrumentation of the specimen has been described in Chapter II. The different type of control devices used in the experiments with their technical data are given in Table D.1. Data from the load cell and the displacement transducer attached to the actuator, from LVDTs placed on the beam to column joint and from the electrical resistance strain gages were recorded by Teletype terminal on paper tape as well as in printed form. A Honeywell 530 X-Y plotter continuously plotted the lateral load applied by the actuator (vertical axis) vs. the column load point displacement (horizontal axis) during the test. The technical information for different types of recording equipment used during the tests is listed in Table D.2.

D.3 Loading Procedure

The column axial load for the test specimen was applied at the bottom through a manual hydraulic jack.

TABLE D.1 HYDRAULIC SYSTEM AND CONTROL DEVICES

Type	Manufacturer	Model	Capacity
Hydraulic Actuator	MTS	207.16A	+246 K tension -328K Compression 16 in. stroke
Hydraulic power Unit	VICKERS	T40-VB20C-10	15 gpm @ 3000 psi
Servovalve	MTS	252.23	5 gpm
Controller	MTS	406.11	-
Pump Controller	GILMOR	435	-

TABLE D.2 RECORDING EQUIPMENT

Type	Manufacturer	Model
X-Y Recorder	HONEYWELL	530
Digital Voltmeter	HP	3440A
Digital Data Acquisition System	VIDAR	Autodata 5404
Terminal and Paper Tape Punch	TELETYPE	ASR33

Twenty four hours before the test, the specimen was placed in position in the frame and the column ends were secured properly. The column axial load was then applied and maintained for a day to offset any creep effects. The following day, beam ends were attached to the force links and the yoke assembly tightened without applying any

excessive load on the beams. In the case of S-series specimens, a pair of channels were bolted to the slab at each end to prevent any premature failure in the slab. Such a slab stiffening assembly is shown in Fig. D.1. Before the test was started, all strain gages were zeroed. Initially a small load was applied to check the instrumentation and the test assembly. Subsequently, the specimen was loaded through a predefined loading routine.

APPENDIX E

STRAIN GAGE LOCATIONS

Electrical strain gages were attached to the reinforcement in the joint and its vicinity. Strain data from the gages provides strain history in the reinforcing bar at a particular location. The load vs. strain plots or displacement vs. strain plots are valuable in ascertaining the effectiveness of reinforcement and the slippage of bars.

In the X-series specimens, all gages were placed at identical locations as shown in Fig. E.1. Each of the joint hoops were gaged irrespective of the number of layers of hoops in the joint. Because most of the inelastic action takes place in the beams close to the joint, more gages were attached to the beam longitudinal and shear reinforcement. In the S-series specimens focus was shifted to the effectiveness of transverse beams and slab. As such, the longitudinal and shear reinforcement of transverse beams was gaged to determine the mechanism of load transfer to the transverse beams. Due to the limited number of channels available in the scanning unit, gages could only be placed at a selected number of locations particularly in the S-series specimens. Gage locations, for the S-series specimens are shown in Fig. E.2.

APPENDIX F

HYSTERESIS MODEL

F.1 General

The proposed hysteesis model consists of six primary and five secondary rules. The secondary rules define load reversals within an outer loop. Figures F.1(a), (b), and (c) illustrate various rules of the model. The break points of the hysteresis model are determined from the section properties of the beams. Because the top and bottom reinforcement in beams are generally not the same, the moment capacity and the cracked moment of inertia are calculated both for positive and negative bending directions. This model takes into account the pinching of hysteresis loops and defines the end of pinching at a point corresponding to the cracking moment on the elastic branch. Because both beams have the same cracking moment, the total cracking moment is then twice that of a single beam. During cyclic loading, one beam undergoes positive bending while the other is subjected to negative bending. The total moment required to cause yielding in both beams is then the sum of their positve and negative yield moment capacities.

The rotation of the joint due to the flexiblity of beams at the yield level is calculated by

$$\theta'_y = M_y L/(6.0E_c(I^+_{cr}+I^-_{cr})) \qquad (F.1)$$

where θ' is the rotation of the joint due to the yielding of beams, M_y is the yield moment of the subassembly defined above, L is the span, E_c is the modulus of Elasticity of concrete and I^+_{cr}, I^-_{cr} are the cracked positive and negative moment of inertia of the beam.

The joint rotation due to the slippage of the beam bars is given by (25)

$$\theta_{slip} = (1/8)(\phi_{bar}/E_s\sigma_{bond}))(f_y/M_y)^2M^2(1/(d-d')) \qquad (F.2)$$

where ϕ_{bar} is the diameter of beam bar, E_s is the modulus of elasticity of steel, σ_{bond} is the bond stress, f_y is the yield strength of steel, M_y is the yield moment of beam, M is the moment at which rotation is desired and (d-d') is the distance between the top and bottom reinforcement of the beam.

Then the total rotation of the joint at the yield point is

$$\theta_y = \theta'_y + \theta_{slip} \qquad (F.3)$$

and the corresponding slope of the elastic branch is

$$K_1 = M_y/\theta_y \qquad (F.4)$$

The rotation corresponding to the cracking moment on the elastic branch is then

$$\theta_{cr} = M_{cr}/K_y \qquad (F.5)$$

F.2 Hysteresis Rules

Each branch of the model is referred to with the related rule number (e.g. branch 7). The terms loading, unloading and load reversal imply increasing load or rotaion in one direction, decreasing load or rotation in one direction, and the change in moment and its sign respectively. The slope of each branch is subscripted by its rule number (e.g. K_5).

RULE 1: Elastic Branch 1

1.1 Loading:

$\theta \leq \theta_y$, $K=K_1$, go to rule 1

$\theta > \theta_y$, $K=K_2$, go to rule 2

$K_2=0.05K_1$

1.2 Unloading and load reversal

$K=K_1$, go to rule 1

RULE 2: Post-yield branch 2

2.1 Loading:

$K=K_3$, go to rule 3

$=K_1(\theta_y/\theta_{max})^{\beta=0.20}$

where θ_{max} is the maximum

rotation reached in the
loading direction

RULE 3: Unloading Branch 2

3.1 Loading:

$\theta \leq \theta_{max}$, $K=K_3$, go to rule 3

$\theta > \theta_{max}$, $K=K_2$, go to rule 2

3.2 Unloading:

$K=K_3$, go to rule 3

3.3 Load reversal

1. if not yielded previously

$K=K_4$, go to rule 4

2. if yielded previously

$K=K_5$, go to rule 5

RULE 4: Crack Closing Branch 4 (no previous yielding)

4.1 Loading:

$\theta \leq \theta_y$, $K=K_4$, go to rule 4

$\theta > \theta_y$, $K=K_2$, go to rule 2

4.2 Unloading:

$K=K_3$, go to rule 7

4.3 Load reversal

$K=K_{10}$, go to rule 10

RULE 5: Crack Closing Branch 5 (previously yielded)

5.1 Loading:

$\theta \leq \theta_{cr}$, $K=K_5$, go to rule 5

$\theta > \theta_{cr}$, $K=K_6$, go to rule 6

5.2 Unloading:

$K=K_8$, go to rule 8

RULE 6: Stiffening branch 6

6.1 Loading:

$\theta \leq \theta_{max}$, $K=K_6$, go to rule 6

$\theta > \theta_{max}$, $K=K_2$, go to rule 2

6.2 Unloading:

$K=K_3$, go to rule 9

RULE 7: Unloading from Crack Closing Branch 4

7.1 Loading:

$\theta \leq \theta_r$, $K=K_3$, go to rule 7

$\theta > \theta_r$, $K=K_4$, go to rule 4

where θ_r is the rotation at which reversal of rotation occurs occurs

7.2 Unloading:

$K=K_7$, go to rule 7

7.3 Load reversal:

$K=K_{10}$, go to rule 10

RULE 8: Unloading from Crack Closing Branch 5

8.1 Loading:

$\theta \leq \theta_r$, $K=K_8$, go to rule 8

$\theta > \theta_r$, $K=K_5$, go to rule 5

8.2 Unloading:

$K=K_3$, go to rule 8

8.3 Load reversal

$K=K_{10}$, go to rule 10

RULE 9: Unloading from Branch 6

9.1 Loading:

$\theta \leq \theta_r$, $K=K_3$, go to rule 9

$\theta > \theta_r$, $K=K_6$, go to rule 6

9.2 Unloading:

$K=K_9$, go to rule 9

9.3 Load reversal

$K=K_{10}$, go to rule 10

RULE 10: Stiffening Branch for Inner Loop

10.1 Loading

$\theta \leq \theta_{max}$, $K=K_{10}$, go to rule 10

$\theta > \theta_{max}$, $K=K_2$, go to rule 2

10.2 Unloading:

$K=K_3$, go to rule 11

10.3 Load reversal:

$K=K_10$, go to rule 10

RULE 11: Unloading in the Inner Loop

11.1 Loading:

$\theta \leq \theta_r$, $K=K_{11}$, go to rule 11

$\theta > \theta_r$, $K=K_{10}$, go to rule 10

11.2 Unloading:

$K=K_{11}$, go to rule 11

11.3 Load reversal

$K=K_{10}$, go to rule 10

FIGURES

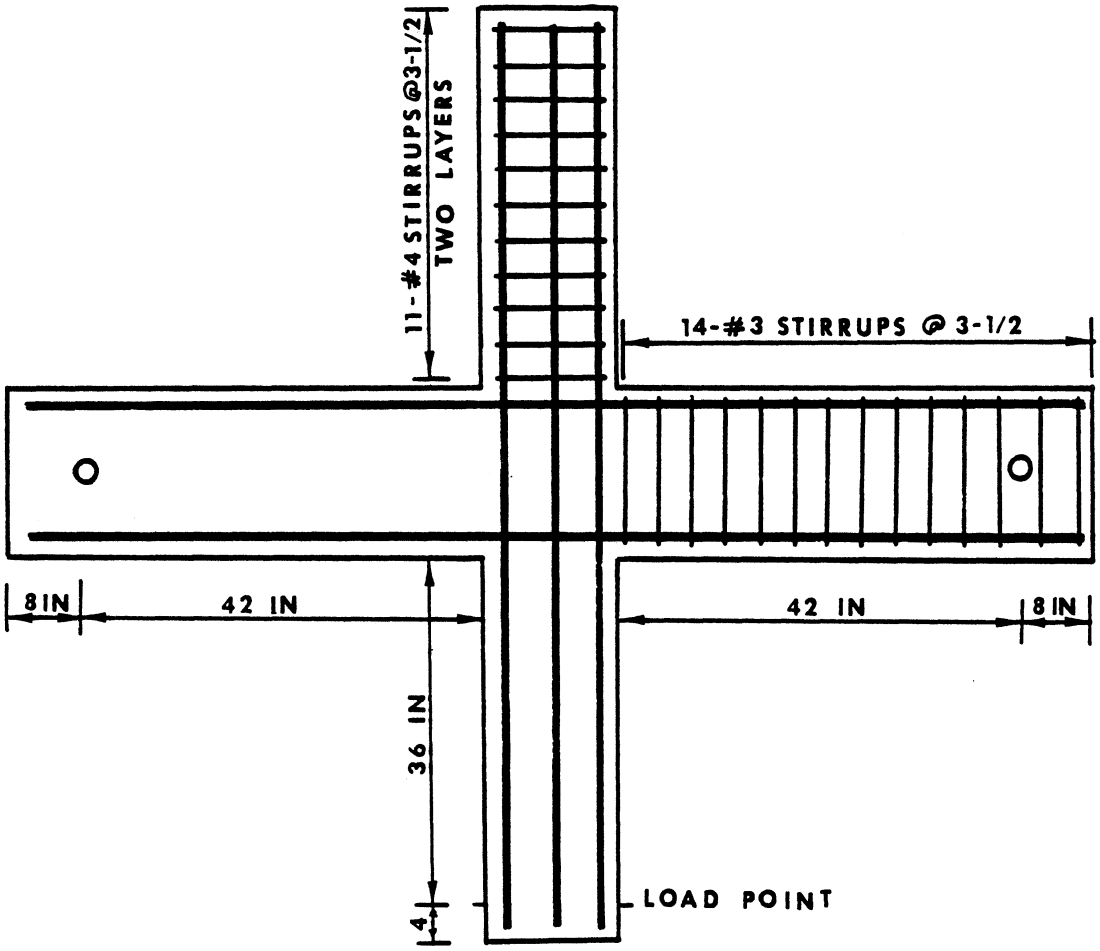

Fig. A.1 Typical Beam and Column Shear Reinforcement

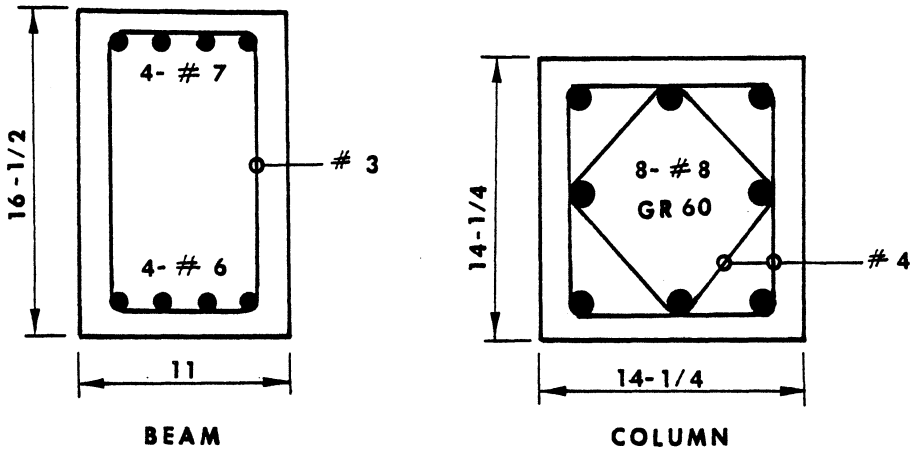

SPECIMENS X1, X2

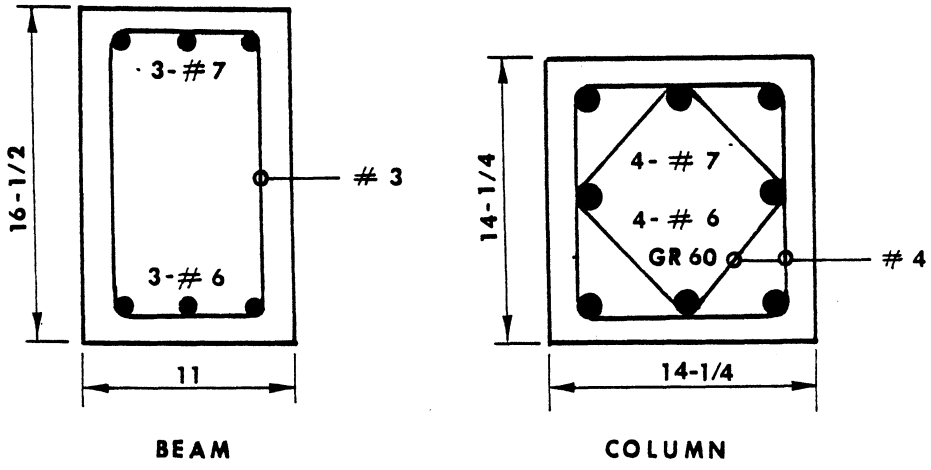

SPECIMEN X3

Fig. A.2 Beam and Column Cross Sections and Reinforcement Details

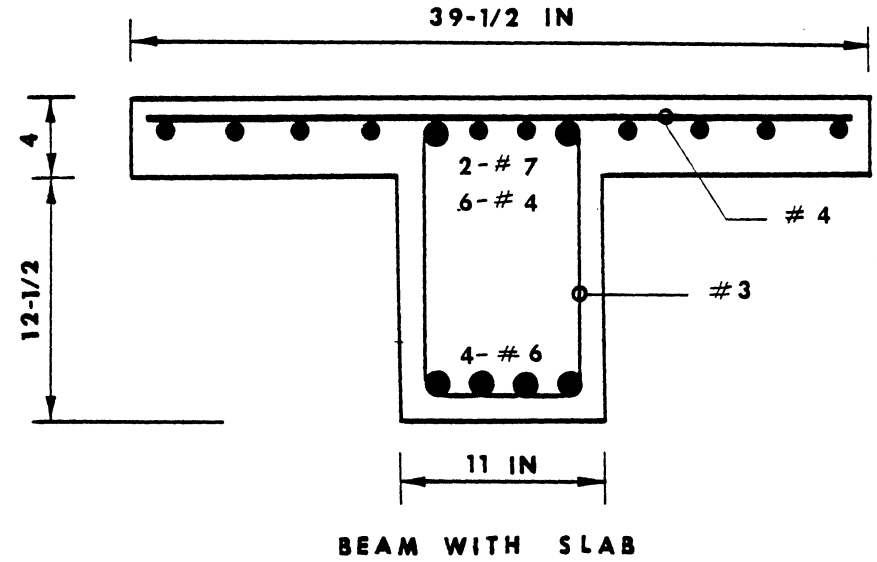

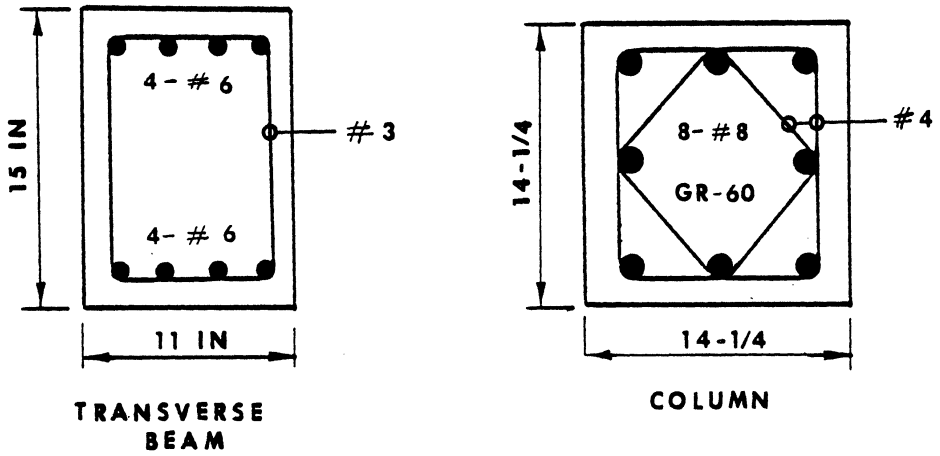

SPECIMENS S1, S2

Fig. A.2(contd.) Beam and Column Cross Sections and Reinforcement Details

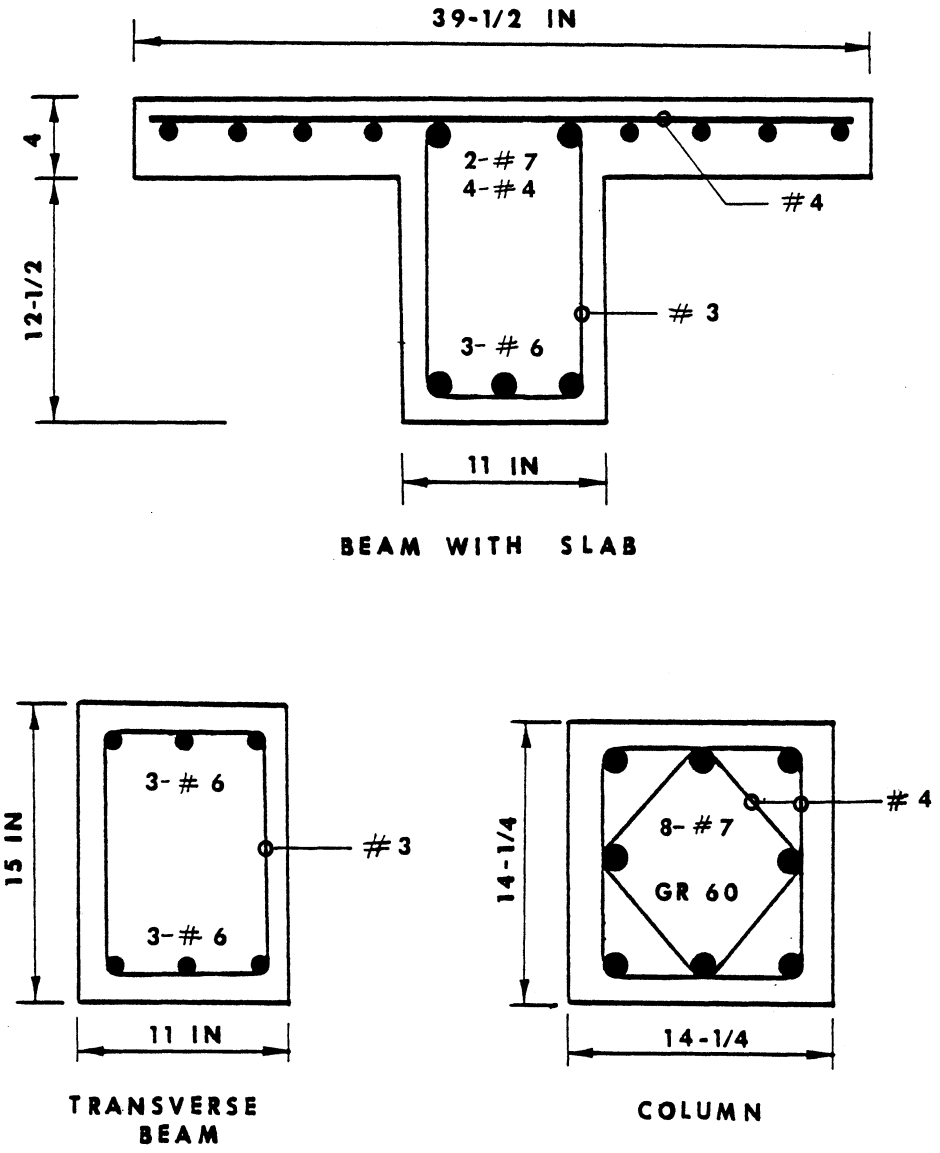

SPECIMEN S3

Fig. A.2(contd.) Beam and Column Cross Sections and Reinforcement Details

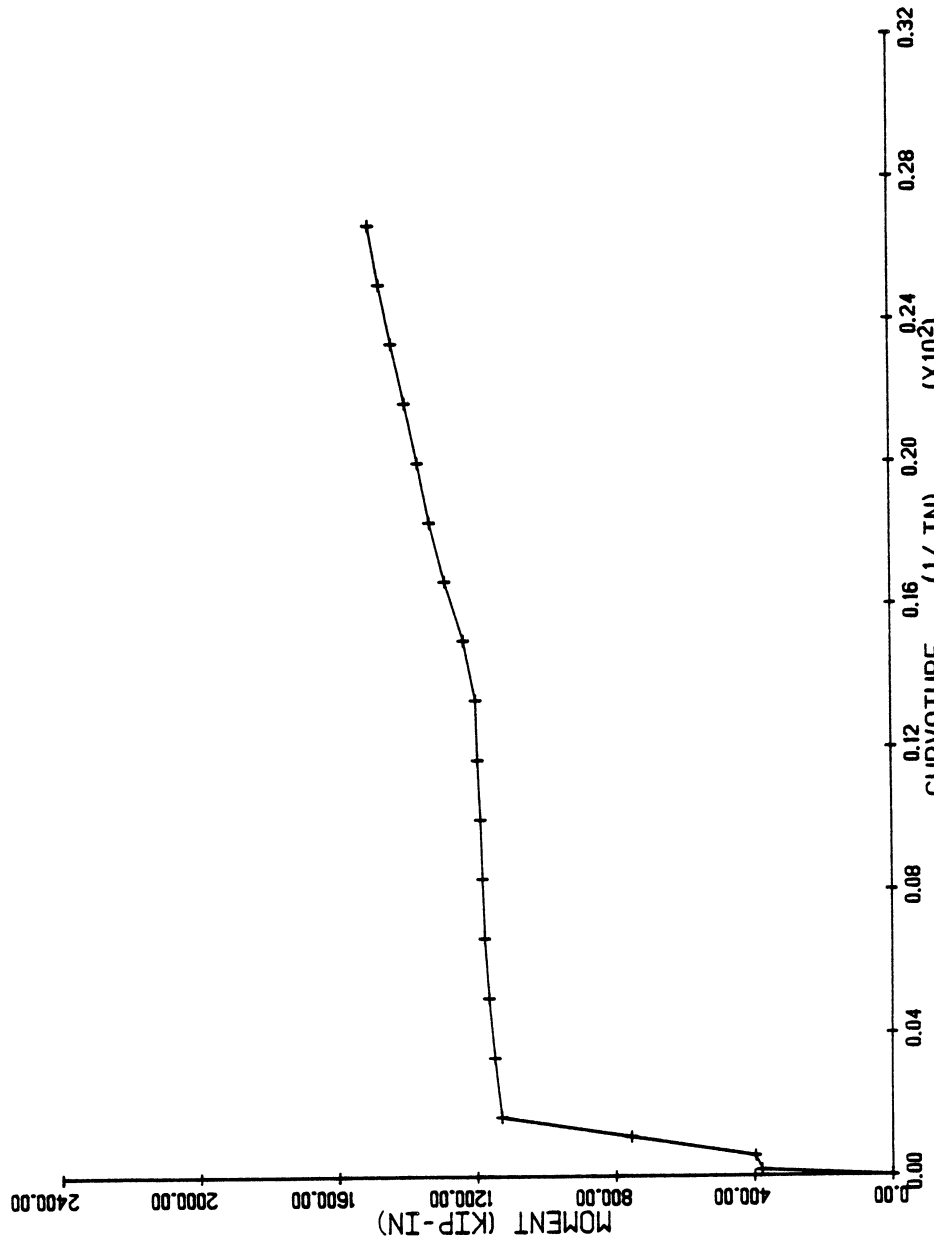

Fig. A.3 Moment-Curvature Diagram of Beam of Specimen X1

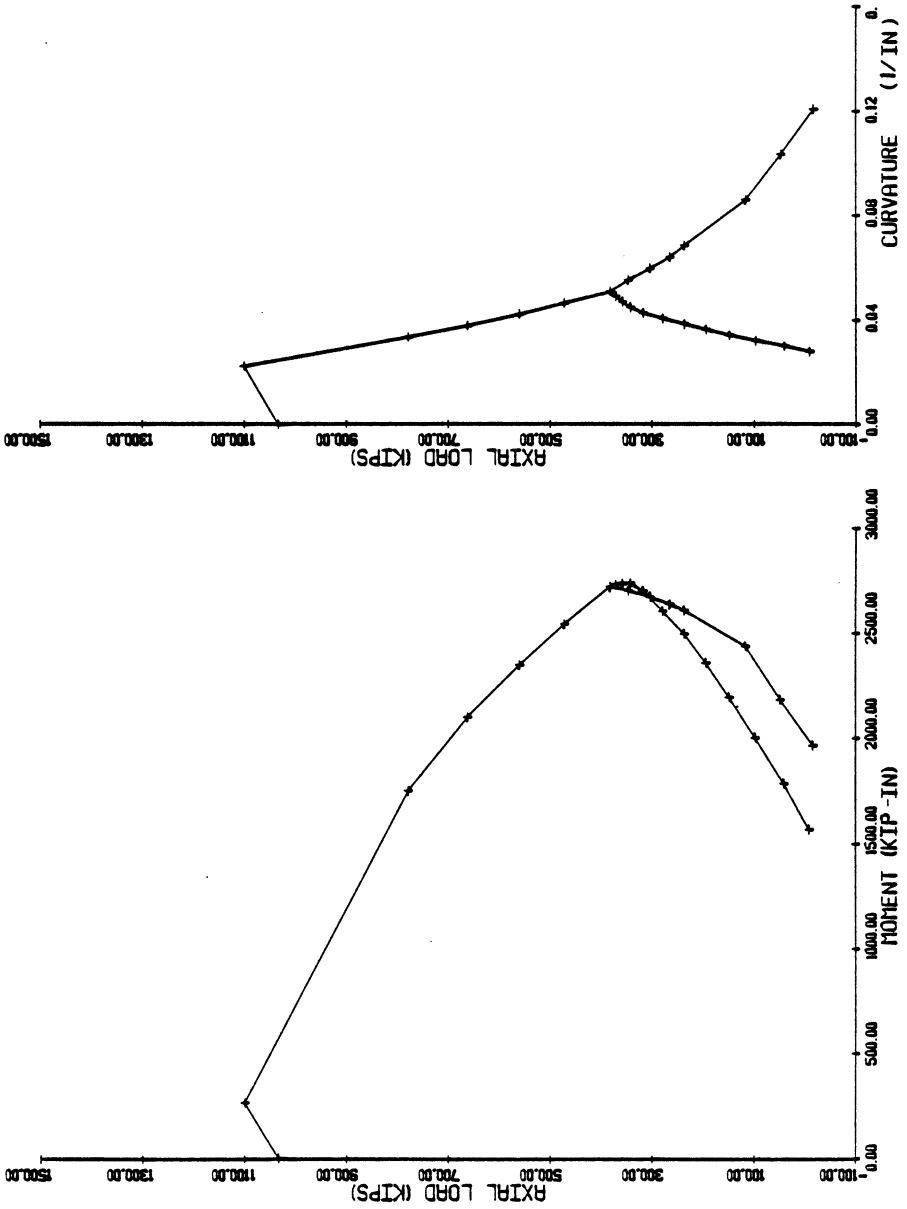

Fig. A.4 Moment-Axial Load Interaction Diagram of Column of Specimen X1

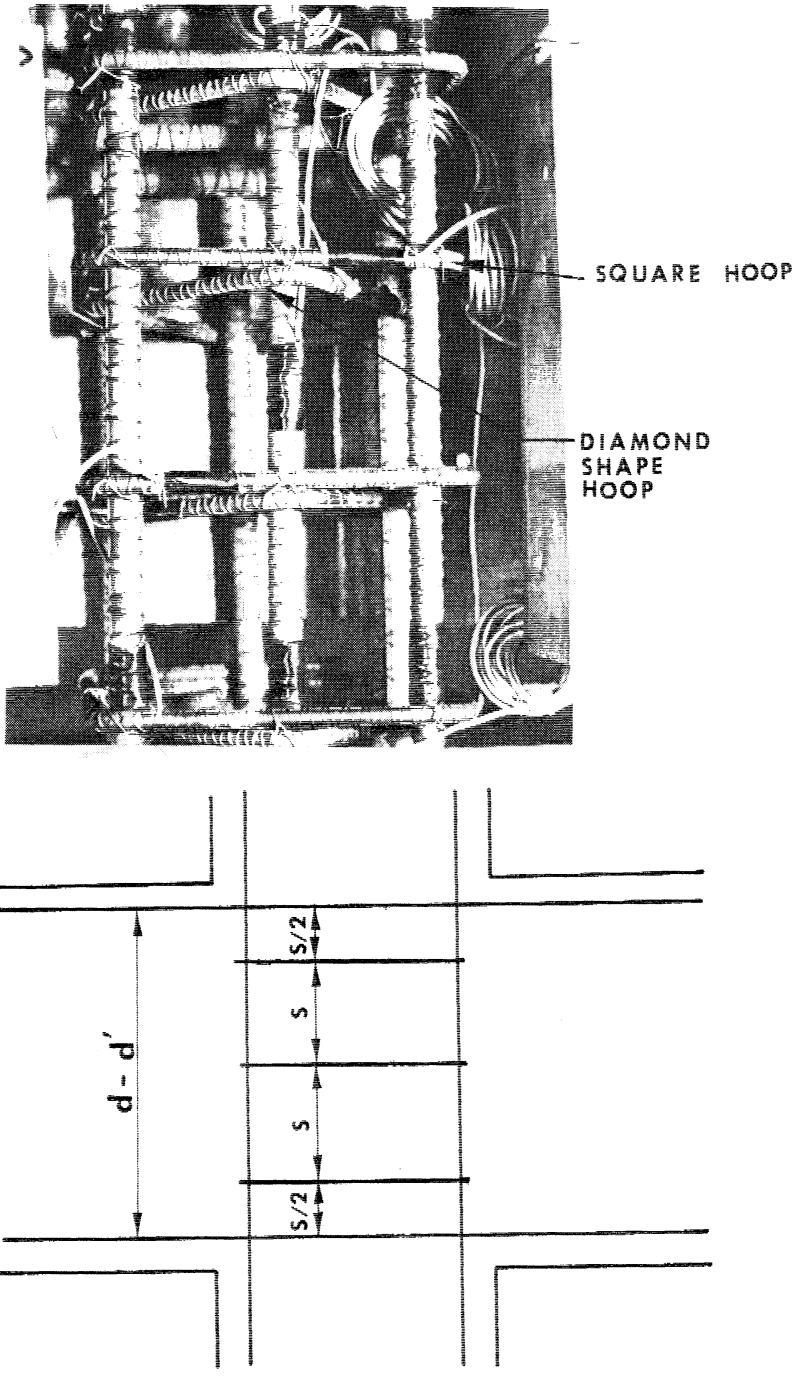

Fig. A.5 Joint Hoop Reinforcement and their Spacing

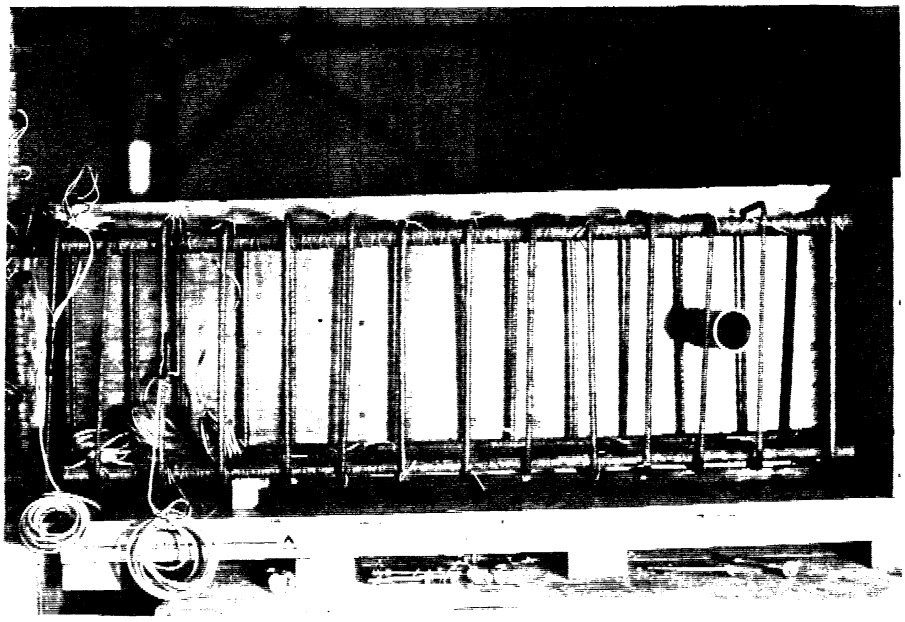

Fig. C.1 Location of Steel Pipe in the Beam Forms for Pin Connection

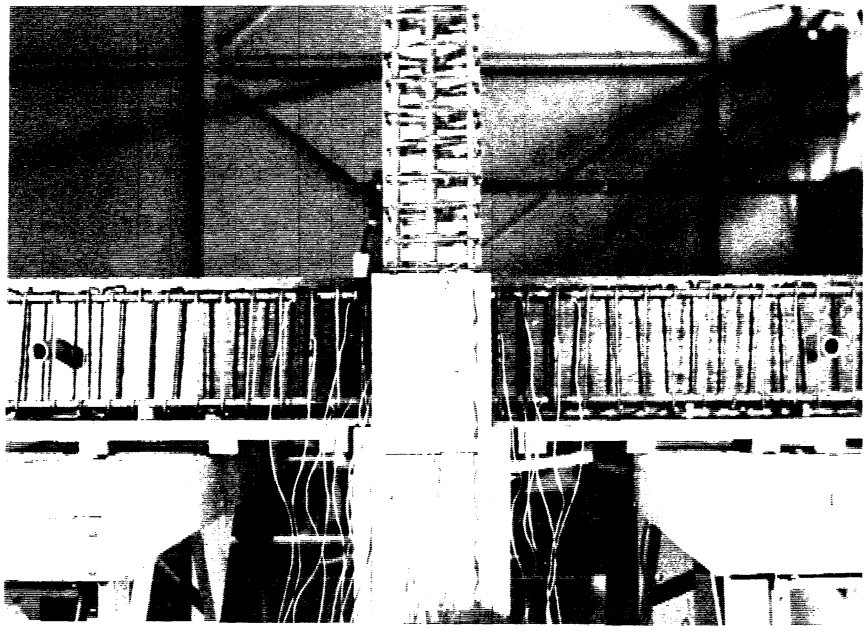

Fig. C.2 Beams of a X-Series Specimen Ready for Casting

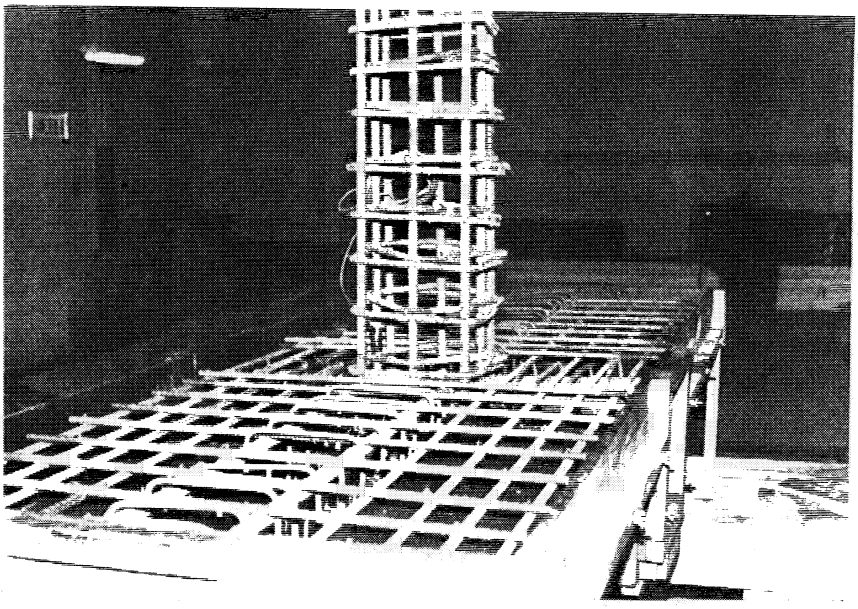

Fig. C.3 Beams and Slab of a S-Series Specimen Ready for Casting

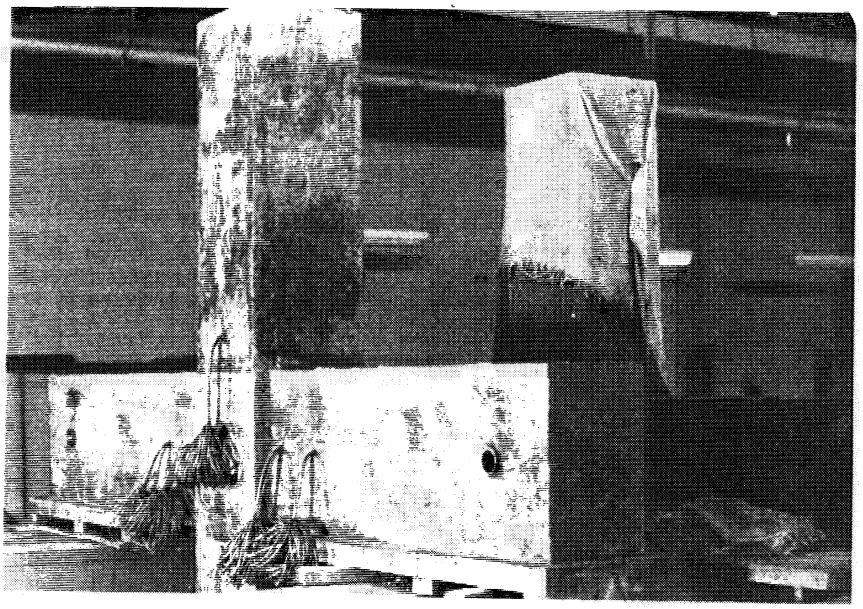

Fig. C.4 A Pair of X-Series Specimens after curing

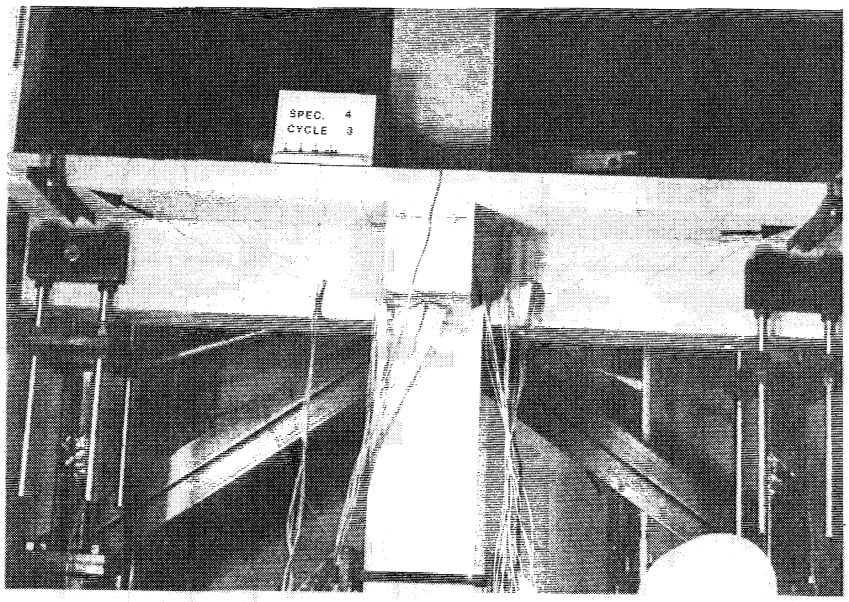

Fig. D.1 Slab End Stiffening Assembly

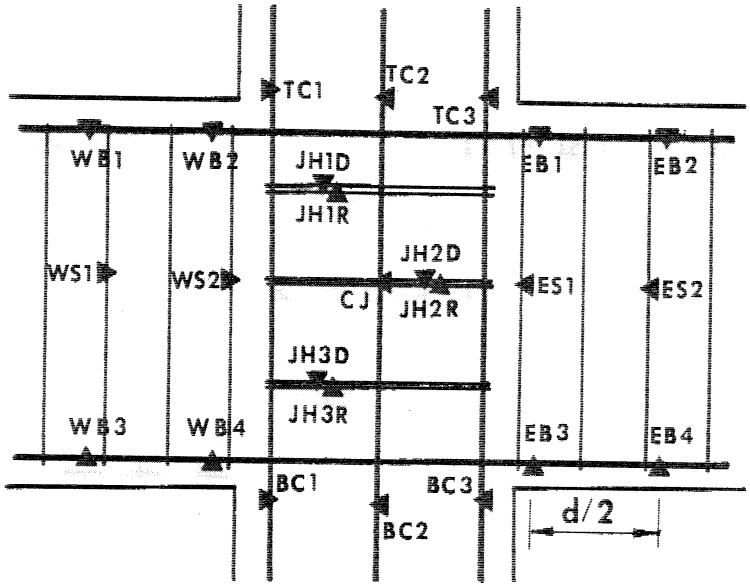

Fig. E.1 Gage Locations in X-series Specimens

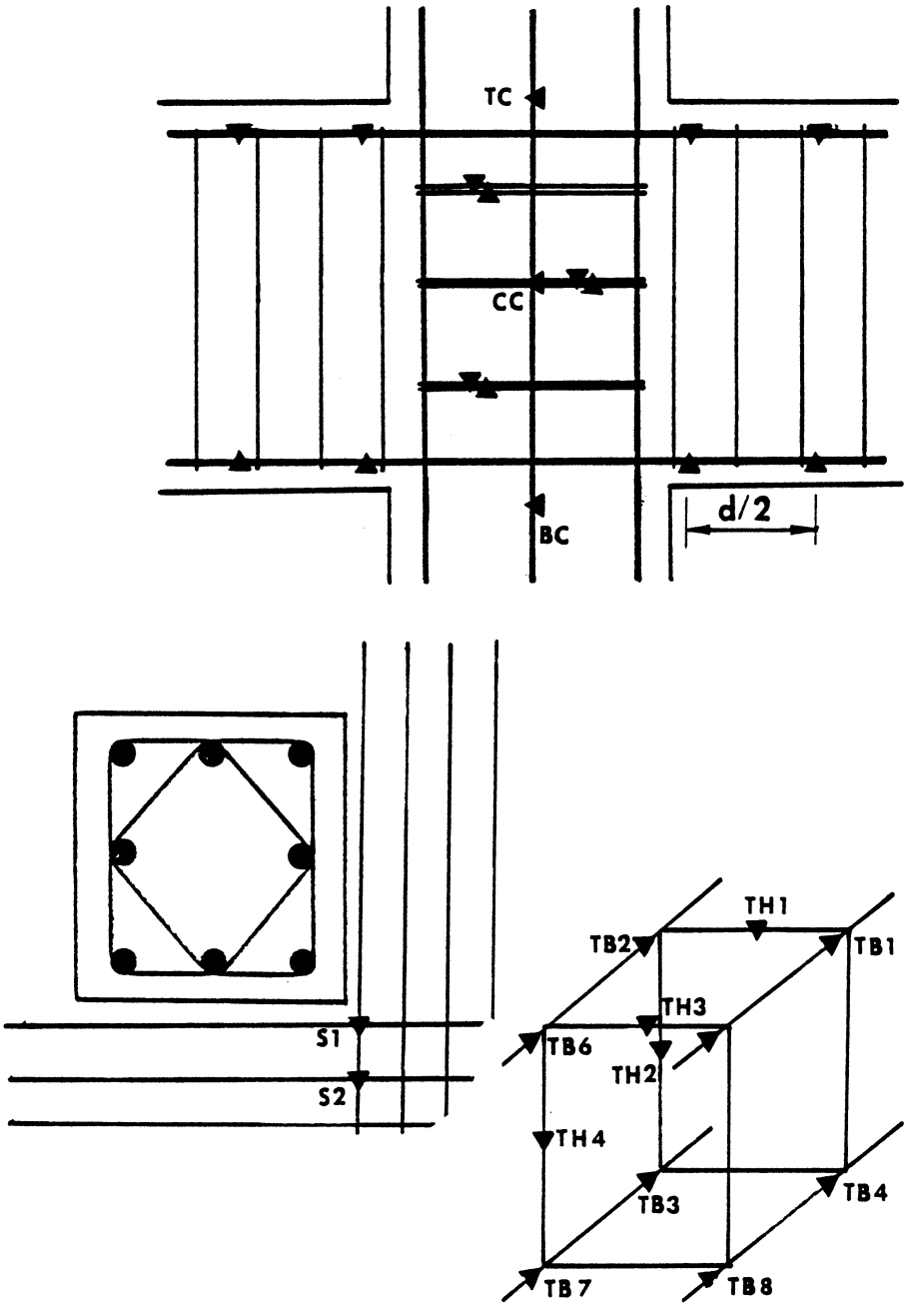

Fig. E.2 Gage Locations in S-series Specimens

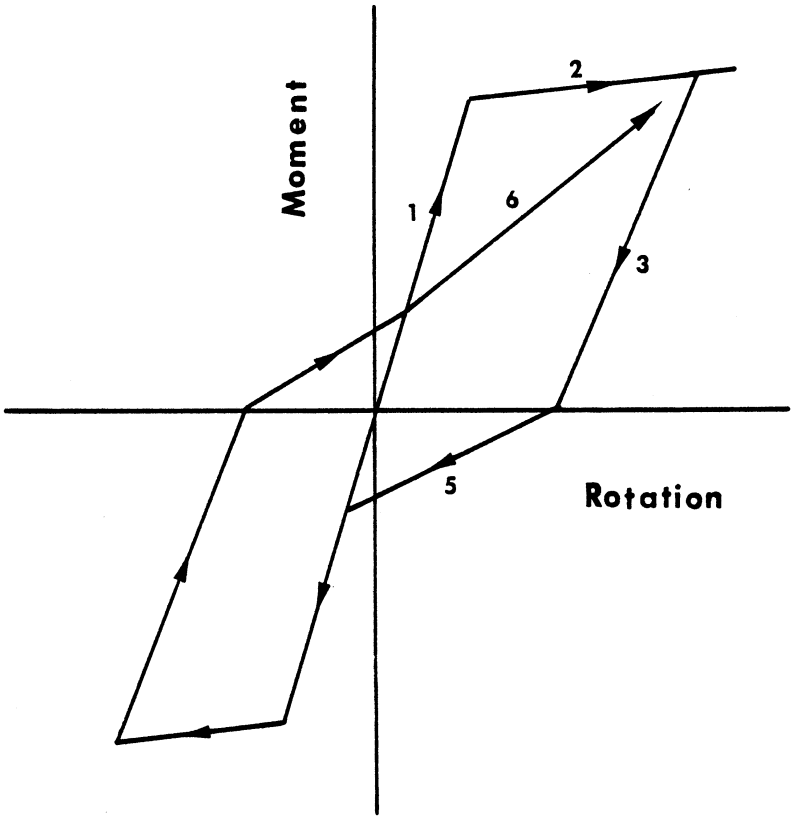

Fig. F.1(a) Hysteresis Model

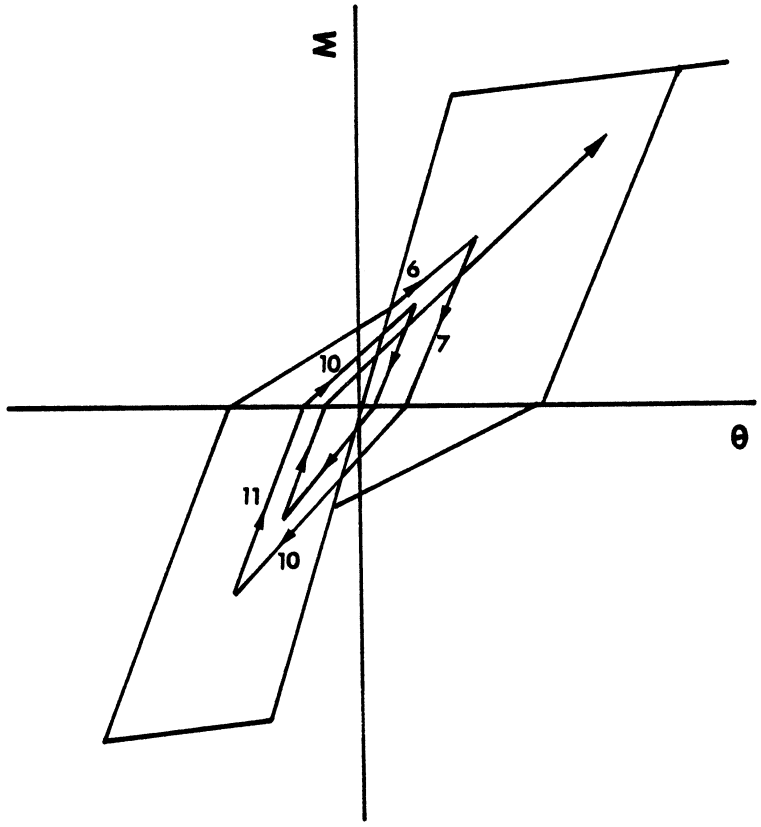

Fig. F.1(b) Hysteresis Model

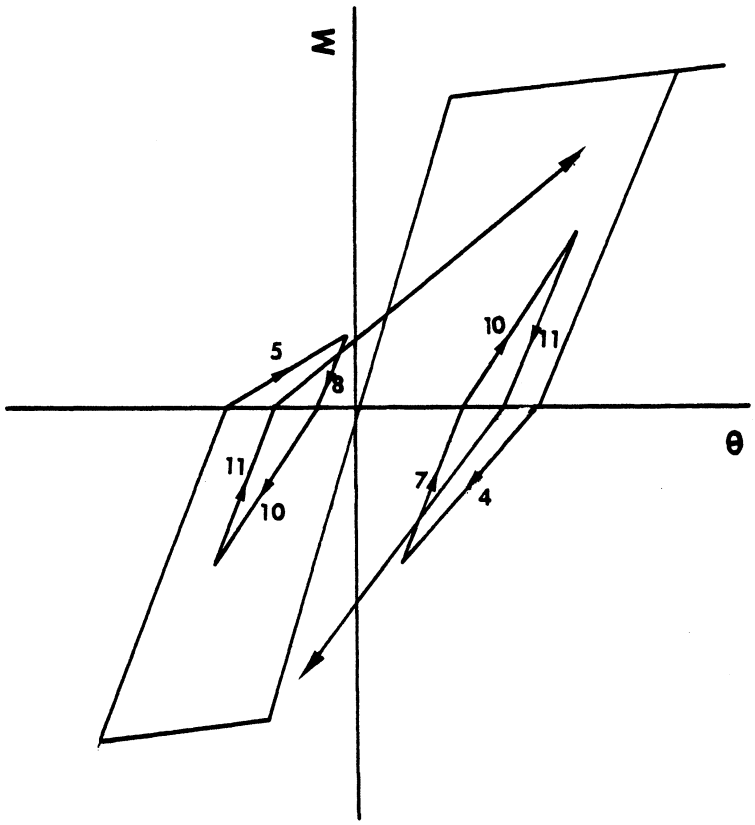

Fig. F.1(c) Hysteresis Model